SPECTRAL STOCHASTIC ISOGEOMETRIC ANALYSIS

By

KEYAN LI

A thesis in fulfilment of the requirements for the degree of

Doctor of Philosophy

School of Civil and Environmental Engineering

The University of New South Wales

Sydney, Australia

July 2019

Thesis/Dissertation Sheet

Surname/Family Name	:	**Li**
Given Name/s	:	**Keyan**
Abbreviation for degree as give in the University calendar	:	**PhD**
Faculty	:	**Faculty of Engineering**
School	:	**School of Civil and Environmental Engineering**
Thesis Title	:	**Spectral Stochastic Isogeometric Analysis**

Abstract 350 words maximum: (PLEASE TYPE)

The traditional stochastic analysis methods are becoming increasingly unappreciated for modern engineering practices. The inconsistency between intentionally designed CAD model and the traditional stochastic analysis model inevitably obstructs the accuracy, efficiency, and applicability of the traditional stochastic analysis methods. However, these requirements are becoming increasingly significant in contemporary engineering practices. Therefore, it is requisite to develop a new stochastic analysis framework complied with the requirements of modern engineering practices.

This dissertation presents a CAD-CAE integrated spectral stochastic isogeometric analysis (SSIGA) framework. And a series of structural analysis problems with uncertainties are investigated within the proposed framework. Firstly, the SSIGA is developed and investigated for the stochastic linear elasticity problem. Then, the SSIGA is further developed for the stochastic linear elasticity problem of composite plates. Moreover, the SSIGA is extended for the structural free vibration problem, namely, the stochastic eigenvalue problem. After that, the extended support vector regression (X-SVR) method is adopted within SSIGA framework for the stochastic linear stability analysis of plates. The accuracy, efficiency, and applicability of the proposed SSIGA framework for different structural problems are comprehensively investigated and verified through several elaborately selected numerical examples.

The proposed SSIGA framework provides a CAD-CAE integrated stochastic analysis framework for the modern engineering practices. By meticulously adopting the basis functions within CAD system, the SSIGA framework can maintain the exact geometries of the structures and the random fields between the CAD model and the SSIGA stochastic analysis model, even for those complex geometries inspired from real-life engineering practices. Such rigor can thoroughly eliminate the geometric errors that permanently embedded in traditional approaches. The stochastic analysis by SSIGA framework will be assuredly implemented on the intentionally designed model in CAD system. Moreover, basis functions within CAD system are always higher-order continuous over the whole physical domain. Therefore, the novel SSIGA approach can guarantee a globally smooth random field modelling and finally a globally smooth stochastic analysis result. Additionally, by implementing stochastic analysis directly on the CAD model and avoiding the mesh process in traditional stochastic analysis routines, SSIGA framework will promise an efficient stochastic analysis method for real-life engineering practices.

FOR OFFICE USE ONLY Date of completion of requirements for Award:

INCLUSION OF PUBLICATIONS STATEMENT

UNSW is supportive of candidates publishing their research results during their candidature as detailed in the UNSW Thesis Examination Procedure.

Publications can be used in their thesis in lieu of a Chapter if:

- The student contributed greater than 50% of the content in the publication and is the "primary author", ie. the student was responsible primarily for the planning, execution and preparation of the work for publication
- The student has approval to include the publication in their thesis in lieu of a Chapter from their supervisor and Postgraduate Coordinator.
- The publication is not subject to any obligations or contractual agreements with a third party that would constrain its inclusion in the thesis

Please indicate whether this thesis contains published material or not.

☐ *This thesis contains no publications, either published or submitted for publication (if this box is checked, you may delete all the material on page 2)*

☐ *Some of the work described in this thesis has been published and it has been documented in the relevant Chapters with acknowledgement (if this box is checked, you may delete all the material on page 2)*

☒ *This thesis has publications (either published or submitted for publication) incorporated into it in lieu of a chapter and the details are presented below*

CANDIDATE'S DECLARATION

I declare that:

- I have complied with the Thesis Examination Procedure
- where I have used a publication in lieu of a Chapter, the listed publication(s) below meet(s) the requirements to be included in the thesis.

Name	**Signature**	**Date (dd/mm/yy)**
Keyan Li		

Postgraduate Coordinator's Declaration (to be filled in where publications are used in lieu of Chapters)

I declare that:

- the information below is accurate
- where listed publication(s) have been used in lieu of Chapter(s), their use complies with the Thesis Examination Procedure
- the minimum requirements for the format of the thesis have been met.

PGC's Name	**PGC's Signature**	**Date (dd/mm/yy)**
Hamid Vali Pour Goudarzi		

For each publication incorporated into the thesis in lieu of a Chapter, provide all of the requested details and signatures required

Details of publication #1:
Full title: Spectral stochastic isogeometric analysis of linear elasticity
Authors: Keyan Li, Wei Gao, Di Wu, Chongmin Song, Taicong Chen
Journal or book name: Computer Methods in Applied Mechanics and Engineering
Volume/page numbers: 2018; 332: 157-190
Date accepted/ published: 19 December 2017

Status	*Published*	☒	*Accepted and In press*		*In progress (submitted)*	

The Candidate's Contribution to the Work
Keyan Li did more than 50% of the work, which includes proposing the conception and design of the work, performing analysis, collecting data and finally writing the manuscript.

Location of the work in the thesis and/or how the work is incorporated in the thesis:
The corresponding work locates in Chapter 3.

Primary Supervisor's Declaration
I declare that:
- the information above is accurate
- this has been discussed with the PGC and it is agreed that this publication can be included in this thesis in lieu of a Chapter
- All of the co-authors of the publication have reviewed the above information and have agreed to its veracity by signing a 'Co-Author Authorisation' form.

Supervisor's name	*Supervisor's signature*	*Date (dd/mm/yy)*
Wei Gao		

Co-author's Declaration
I authorise the inclusion of this publication in the student's thesis and certify that:
- the declaration made by the student on the declaration for a thesis with publication form correctly reflects the extents of the student's contribution to this work;
- the student contributed greater than 50% of the content of the publication and is the "primary author" ie. the student was responsible primarily for the planning, execution and preparation of the work for publication.

Co-author's name	*Co-author's signature*	*Date (dd/mm/yy)*
Wei Gao		
Di Wu		
Chongmin Song		
Taicong Chen		

Details of publication #2:
Full title: Spectral stochastic isogeometric analysis for static response of FGM plate with material uncertainty
Authors: Keyan Li, Di Wu, Wei Gao
Journal or book name: Thin-Walled Structures
Volume/page numbers: 2018; 132: 504-521
Date accepted/ published: 15 September 2018

Status	*Published*	☒	*Accepted and In press*		*In progress (submitted)*	

The Candidate's Contribution to the Work
Keyan Li did more than 50% of the work, which includes proposing the conception and design of the work, performing analysis, collecting data and finally writing the manuscript.

Location of the work in the thesis and/or how the work is incorporated in the thesis:
The corresponding work locates in Chapter 4.

Primary Supervisor's Declaration
I declare that:
- the information above is accurate
- this has been discussed with the PGC and it is agreed that this publication can be included in this thesis in lieu of a Chapter
- All of the co-authors of the publication have reviewed the above information and have agreed to its veracity by signing a 'Co-Author Authorisation' form.

Supervisor's name	*Supervisor's signature*	*Date (dd/mm/yy)*
Wei Gao		

Co-author's Declaration
I authorise the inclusion of this publication in the student's thesis and certify that:
- the declaration made by the student on the declaration for a thesis with publication form correctly reflects the extents of the student's contribution to this work;
- the student contributed greater than 50% of the content of the publication and is the "primary author" ie. the student was responsible primarily for the planning, execution and preparation of the work for publication.

Co-author's name	*Co-author's signature*	*Date (dd/mm/yy)*
Di Wu		
Wei Gao		

Details of publication #3:
Full title: Spectral stochastic isogeometric analysis of free vibration
Authors: Keyan Li, Di Wu, Wei Gao, Chongmin Song
Journal or book name: Computer Methods in Applied Mechanics and Engineering
Volume/page numbers: 2019; 350: 1-27
Date accepted/ published: 9 March 2019

Status	*Published*	☒	*Accepted and In press*		*In progress (submitted)*	

The Candidate's Contribution to the Work
Keyan Li did more than 50% of the work, which includes proposing the conception and design of the work, performing analysis, collecting data and finally writing the manuscript.

Location of the work in the thesis and/or how the work is incorporated in the thesis:
The corresponding work locates in Chapter 5.

Primary Supervisor's Declaration
I declare that:
- the information above is accurate
- this has been discussed with the PGC and it is agreed that this publication can be included in this thesis in lieu of a Chapter
- All of the co-authors of the publication have reviewed the above information and have agreed to its veracity by signing a 'Co-Author Authorisation' form.

Supervisor's name	*Supervisor's signature*	*Date (dd/mm/yy)*
Wei Gao		

Co-author's Declaration
I authorise the inclusion of this publication in the student's thesis and certify that:
- the declaration made by the student on the declaration for a thesis with publication form correctly reflects the extents of the student's contribution to this work;
- the student contributed greater than 50% of the content of the publication and is the "primary author" ie. the student was responsible primarily for the planning, execution and preparation of the work for publication.

Co-author's name	*Co-author's signature*	*Date (dd/mm/yy)*
Di Wu		
Wei Gao		
Chongmin Song		

Details of publication #4:
Full title: Spectral Stochastic Isogeometric Analysis for Linear Stability Analysis of Plate
Authors: Keyan Li, Di Wu, Wei Gao
Journal or book name: Computer Methods in Applied Mechanics and Engineering
Volume/page numbers: 2018; 352: 1-31
Date accepted/ published: 25 April 2019

Status	*Published*	☒	*Accepted and In press*		*In progress (submitted)*	

The Candidate's Contribution to the Work
Keyan Li did more than 50% of the work, which includes proposing the conception and design of the work, performing analysis, collecting data and finally writing the manuscript.

Location of the work in the thesis and/or how the work is incorporated in the thesis:
The corresponding work locates in Chapter 6.

Primary Supervisor's Declaration
I declare that:
- the information above is accurate
- this has been discussed with the PGC and it is agreed that this publication can be included in this thesis in lieu of a Chapter
- All of the co-authors of the publication have reviewed the above information and have agreed to its veracity by signing a 'Co-Author Authorisation' form.

Supervisor's name	*Supervisor's signature*	*Date (dd/mm/yy)*
Wei Gao		

Co-author's Declaration
I authorise the inclusion of this publication in the student's thesis and certify that:
- the declaration made by the student on the declaration for a thesis with publication form correctly reflects the extents of the student's contribution to this work;
- the student contributed greater than 50% of the content of the publication and is the "primary author" ie. the student was responsible primarily for the planning, execution and preparation of the work for publication.

Co-author's name	*Co-author's signature*	*Date (dd/mm/yy)*
Di Wu		
Wei Gao		

COPYRIGHT STATEMENT

Signed

Date

AUTHENTICITY STATEMENT

‘I certify that the Library deposit digital copy is a direct equivalent of the final officially approved version of my thesis. No emendation of content has occurred and if there are any minor variations in formatting, they are the result of the conversion to digital format.’

Signed

Date

ORIGINALITY STATEMENT

‘I hereby declare that this submission is my own work and to the best of my knowledge it contains no materials previously published or written by another person, or substantial proportions of material which have been accepted for the award of any other degree or diploma at UNSW or any other educational institution, except where due acknowledgement is made in the thesis. Any contribution made to the research by others, with whom I have worked at UNSW or elsewhere, is explicitly acknowledged in the thesis. I also declare that the intellectual content of this thesis is the product of my own work, except to the extent that assistance from others in the project's design and conception or in style, presentation and linguistic expression is acknowledged.’

Signed

Date

ABSTRACT

The traditional stochastic analysis methods are becoming increasingly unappreciated for modern engineering practices. The inconsistency between intentionally designed CAD model and the traditional stochastic analysis model inevitably obstructs the accuracy, efficiency, and applicability of the traditional stochastic analysis methods. However, these requirements are becoming increasingly significant in contemporary engineering practices. Therefore, it is requisite to develop a new stochastic analysis framework complied with the requirements of modern engineering practices.

This dissertation presents a CAD-CAE integrated spectral stochastic isogeometric analysis (SSIGA) framework. And a series of structural analysis problems with uncertainties are investigated within the proposed framework. Firstly, the SSIGA is developed and investigated for the stochastic linear elasticity problem. Then, the SSIGA is further developed for the stochastic linear elasticity problem of composite plates. Moreover, the SSIGA is extended for the structural free vibration problem, namely, the stochastic eigenvalue problem. After that, the extended support vector regression (X-SVR) method is adopted within SSIGA framework for the stochastic linear stability analysis of plates. The accuracy, efficiency, and applicability of the proposed SSIGA framework for different structural problems are comprehensively investigated and verified through several elaborately selected numerical examples.

The proposed SSIGA framework provides a CAD-CAE integrated stochastic analysis framework for the modern engineering practices. By meticulously adopting the basis functions within CAD system, the SSIGA framework can maintain the exact geometries of the structures and the random fields between the CAD model and the SSIGA stochastic

analysis model, even for those complex geometries inspired from real-life engineering practices. Such rigor can thoroughly eliminate the geometric errors that permanently embedded in traditional approaches. The stochastic analysis by SSIGA framework will be assuredly implemented on the intentionally designed model in CAD system. Moreover, basis functions within CAD system are always higher-order continuous over the whole physical domain. Therefore, the novel SSIGA approach can guarantee a globally smooth random field modelling and finally a globally smooth stochastic analysis result. Additionally, by implementing stochastic analysis directly on the CAD model and avoiding the mesh process in traditional stochastic analysis routines, SSIGA framework will promise an efficient stochastic analysis method for real-life engineering practices.

ACKNOWLEDGEMENTS

First of all, I would like to express my sincere gratitude to my supervisor Professor Wei Gao for the chance of and the continuous support to my PhD study, for his patience, encouragement, and immense knowledge. His personality and philosophy in work and life will influence me for the rest of my life. At the same time, my genuine appreciation goes to my co-supervisor, Dr. Di Wu, who is my tough “Coach Carter” pushing me to confront and overcome the deepest fear in my heart. The toughness learned from him encourages me to go beyond the measure. I would also like to deeply thank my co-supervisor, Professor Chongmin Song. Without all three of my supervisors, I could not complete this thesis.

Also, I would like to thank my beloved families: my parents and girlfriend, my uncle and aunt for their unconditional and endless support throughout the whole study period and my life. Without them, I would not be able to be here and achieve everything and words can’t express how grateful I am.

Finally, I would like to deeply thank my old friends, as well as my new friends for their accompany and encouragement. All the things with them are memorable, and the friendships with them are invaluable treasures in my life.

TABLE OF CONTENTS

LIST OF PUBLICATIONS

All the work contained in this thesis has been conducted for 3 years at The University of New South Wales Australia. By the time of completion of this thesis, there have been number of journal papers which have been published and submitted for publication. The details of the papers are:

Journal publications:

Li, K., Gao, W., Wu, D., Song, C. and Chen, T., 2018. Spectral stochastic isogeometric analysis of linear elasticity. *Computer Methods in Applied Mechanics and Engineering*, 332, pp.157-190.

Li, K., Wu, D., Gao, W. and Song, C., 2019. Spectral stochastic isogeometric analysis of free vibration. *Computer Methods in Applied Mechanics and Engineering*. 350, pp.1-27.

Li, K., Wu, D. and Gao, W., 2019. Spectral stochastic isogeometric analysis for linear stability analysis of plate. *Computer Methods in Applied Mechanics and Engineering*. 352, pp.1-31.

Li, K., Wu, D., Chen, X., Cheng, J., Liu, Z., Gao, W. and Liu, M., 2018. Isogeometric Analysis of functionally graded porous plates reinforced by graphene platelets. Composite *Structures*, 204, pp.114-130.

Li, K., Wu, D. and Gao, W., 2018. Spectral stochastic isogeometric analysis for static response of FGM plate with material uncertainty. *Thin-Walled Structures*, 132, pp.504-521.

LIST OF FIGURES

LIST OF TABLES

NOMENCLATURE

Greek Letter

$\bar{\boldsymbol{\beta}} = (\beta_x, \beta_y)$	Rotations in the *x*-*z*, *y*-*z* planes
$\boldsymbol{\beta}, \hat{\boldsymbol{\beta}} \in \Re^m$	Non-negative slack variable vectors
Γ_p	Hermite polynomial
Γ_{D_i}	Dirichlet boundary conditions domain
Γ_{N_i}	Neumann boundary conditions domain
$\boldsymbol{\gamma} = (\gamma_{xz}, \gamma_{yz})^T$	Transverse shear strains
δ_{ij}	Kronecker symbol
$\boldsymbol{\varepsilon}(\mathbf{x}, \theta)$	Stochastic strain vector
$\boldsymbol{\varepsilon}_j(\mathbf{x})$	Coefficient of stochastic strain vector
$\boldsymbol{\varepsilon}(\mathbf{x}, z, \theta)$	Stochastic in-plane strain of FGM plate
$\boldsymbol{\gamma}(\mathbf{x}, \theta)$	Stochastic shear strain FGM plate
ε_{xi}	Strain
ε_z^b	Bending strain
$\boldsymbol{\varepsilon} = (\varepsilon_{xx}, \varepsilon_{yy}, \varepsilon_{xy})^T$	In-plane strains

$\boldsymbol{\varepsilon}_i$	In-plane strains
$\boldsymbol{\varepsilon}_i^L$	Linear part of in-plane strains
$\boldsymbol{\varepsilon}_i^{NL}$	Non-linear part of in-plane strains
$\boldsymbol{\varepsilon}_b$	Bending strains
$\boldsymbol{\varepsilon}_s$	Shear strains
$\delta\boldsymbol{\varepsilon}_i^L$	Variation of linear part of in-plane strains
$\delta\boldsymbol{\varepsilon}_i^{NL}$	Variation of non-linear part of in-plane strains
$\delta\boldsymbol{\varepsilon}_b$	Variation of bending strains
$\delta\boldsymbol{\varepsilon}_s$	Variation of Shear strains
$\Delta\boldsymbol{\varepsilon}_i^L$	Increment of linear part of in-plane strains
$\Delta\boldsymbol{\varepsilon}_i^{NL}$	Increment of non-linear part of in-plane strains
$\Delta\boldsymbol{\varepsilon}_b$	Increment of bending strains
$\Delta\boldsymbol{\varepsilon}_s$	Variation of Shear strains
$\zeta_i(\theta)$	Random variables
${}^{n}\zeta$	Load factor
${}^{cr}\zeta$	Critical load factor
H	Knot vector

η_i	Random variables
$\Theta_{\mathbf{IJ}}$	Element of matrix
θ_{xi}	Rotation
θ_{yi}	Rotation
$\theta_0, \theta_1, \theta_2, \theta_3, \theta_4, \theta_5$	Experiment result
$\mathbf{\Lambda_{IJ}}$	Element of matrix
λ_i	Eigenvalue
$\lambda(\theta)$	Stochastic eigenvalue
$\hat{\lambda}(\theta)$	Approximation of stochastic eigenvalue
$\hat{\lambda}_1, \hat{\lambda}_2$	Toning parameters
$\mu, \mu_{\mathbf{I}}$	Mean value
$\mu_{E^G(\mathbf{x}_0,\theta)}, \mu_{E^L(\mathbf{x}_0,\theta)}$	Mean value
$\mu_{\rho^G(\mathbf{x}_0,\theta)}, \mu_{\rho^L(\mathbf{x}_0,\theta)}$	Mean value
$\mu(\mathbf{x})$	Mean function of random field
Ξ	Knot vector
ξ_i	Knot element
$\rho(z)$	Functionally graded density

ρ_m	Density of metal
ρ_c	Density of ceramic
$\rho^G(\mathbf{x},\theta)$	Gaussian random field of material density
$\hat{\rho}^G(\mathbf{x},\theta)$	Approximation of random field $\rho^G(\mathbf{x},\theta)$
$\rho^L(\mathbf{x},\theta)$	Lognormal random field of material density
$\hat{\rho}^L(\mathbf{x},\theta)$	Approximation of random field $\rho^L(\mathbf{x},\theta)$
$\rho_m^L(\mathbf{x})$	Coefficient of PCE/aPC for random field $\rho^L(\mathbf{x},\theta)$
Σ	σ-algebra
$\boldsymbol{\sigma}(\mathbf{x},\theta)$	Stochastic stress vector
$\boldsymbol{\sigma}_{ij}(\mathbf{x})$	Coefficient of stochastic stress vector
$\boldsymbol{\sigma}(\mathbf{x},z,\theta)$	Stochastic in-plane stress vector of FGM plate
$\hat{\boldsymbol{\sigma}}_i$	In-plane stress resultants
$\overline{\boldsymbol{\sigma}}$	Coefficient matrix
σ,σ_H	Standard deviation
$\sigma_{E^G(\mathbf{x}_0,\theta)},\sigma_{E^L(\mathbf{x}_0,\theta)}$	Standard deviation
$\sigma_{\rho^G(\mathbf{x}_0,\theta)},\sigma_{\rho^L(\mathbf{x}_0,\theta)}$	Standard deviation
σ_{ij}	Stress tensor

σ_{xi}	Stress
$\boldsymbol{\tau}(\mathbf{x}, z, \theta)$	Stochastic shear stress vector of FGM plate
$\nu(z)$	Functionally graded Poisson's ratio
ν_m	Poisson's ratio of metal
ν_c	Poisson's ratio of ceramic
$\nu(\mathbf{x}, z, \theta)$	Random field of FGM Poisson's ratio
$\hat{\nu}(\mathbf{x}, z, \theta)$	Approximation of random field $\nu(\mathbf{x}, z, \theta)$
$\mathcal{G}_{\mathbf{I}}^{\mathbf{J}}$	Coefficient
$\zeta_{i_2}(\theta)$	Random variable
$\boldsymbol{\Phi}$	Eigenvector
$\boldsymbol{\Phi}(\theta)$	Stochastic eigenvector
$\hat{\boldsymbol{\Phi}}(\theta)$	Approximation of stochastic eigenvector
$\bar{\boldsymbol{\Phi}}(\mathbf{x}_i)$	Appropriate mapping function mapping *i*th input data.
$\boldsymbol{\varphi}_i, \boldsymbol{\varphi}_m$	Expansion terms
$\varphi_i(\mathbf{x})$	Eigenfunction
$\phi_{\mathbf{I}}^{i_2}$	Coefficient
$\boldsymbol{\Psi}_j(\theta)$	Hermite polynomial, Arbitrary polynomial

Ω	Sample space
ω_i	Deflection

English Letter

$\mathbf{A}$	Coefficient matrix
$\hat{\mathbf{A}}, \hat{\mathbf{A}}_k$	Coefficient matrix
$\hat{\mathbf{A}}(\mathbf{x}, \theta)$	Stochastic coefficient matrix
$A(\bullet)$	Coefficient matrix
$a_{i_1}, a_{i_1 i_2}, a_{i_1 i_2 i_3}, \ldots$	Coefficient
a_k	Coefficient
$a^*(\bullet)$	Coefficient matrix
$\mathbf{B}, \mathbf{B}^m, \mathbf{B}^b, \mathbf{B}^s, \mathbf{B}_i^L, \mathbf{B}_i^{NL}$	Kinematics matrices
$\bar{\mathbf{B}}$	Coefficient matrix
$\hat{\mathbf{B}}(\mathbf{x}, \theta)$	Stochastic coefficient matrix
$\mathbf{B_{IJ}}$	Element of matrix
$B_{\mathbf{I}}$	**I** th control points
B_i	Control points
$\mathbf{b}, \mathbf{b}_k$	Coefficient vector

b_0, b_k	Coefficients
$\mathbf{C_{IJ}}$	Element of matrix
$\hat{\mathbf{C}}, \hat{\mathbf{C}}_k$	Coefficient matrix
Cov[•,•]	Covariance
$C_{HH}(\mathbf{x}, \mathbf{x}')$	Covariance functions
$C(\xi)$	Splines curve
c_{ijk}	Coefficient
c_{ijkl}	Coefficient
$\mathbf{D}$	Elasticity matrix
$\mathbf{D}_0$	Deterministic elasticity matrix
$\mathbf{D}(\mathbf{x}, \theta)$	Stochastic elasticity matrix
$\mathbf{D}_b$	Coefficient matrix
$\hat{\mathbf{D}}_b(\mathbf{x}, \theta)$	Stochastic coefficient matrix
$\mathbf{D}_s$	Coefficient matrix
$\hat{\mathbf{D}}_s(\mathbf{x}, \theta)$	Stochastic coefficient matrix
D	Physical domain
D_e	Elemental physical domain

$\hat{\mathbf{d}}, \hat{\mathbf{d}}_k$	Coefficient vector
E[•]	Expectation
$E^G(\mathbf{x}, \theta)$	Gaussian random field of Young's modulus
$\hat{E}^G(\mathbf{x}, \theta)$	Approximation of random field $E^G(\mathbf{x}, \theta)$
$E^G(\mathbf{x}, z, \theta)$	Gaussian random field of FGM Young's modulus
$\hat{E}^G(\mathbf{x}, z, \theta)$	Approximation of random field $E^G(\mathbf{x}, z, \theta)$
$E^L(\mathbf{x}, \theta)$	Lognormal random field of Young's modulus
$\hat{E}^L(\mathbf{x}, \theta)$	Approximation of random field $E^L(\mathbf{x}, \theta)$
$E_i^L(\mathbf{x})$	Coefficient of PCE/aPC for random field $E^L(\mathbf{x}, \theta)$
$E(z)$	Functionally graded Young's modulus
E_m	Young's modulus of metal
E_c	Young's modulus of ceramic
$\mathbf{e}_m = [1,1,...,1]^{\mathrm{T}}$	Unit vector
$\hat{\mathbf{e}}, \hat{\mathbf{e}}_k$	Coefficient vector
$e(\mathbf{x})$	Truncating error
$e_{M,P-1}$	Truncating error
$e_j(\eta)$	polynomials of exact degree j

$err(\boldsymbol{x})$	Point-wise estimator of the error variance
$\mathbf{F}$	Force vector
$\mathbf{F}_k$	Expanded force vector
F	Probability measure
$\hat{f}(\mathbf{x}), \hat{f}_k(\mathbf{x})$	Regression function
$f_{H(\mathbf{x}_0,\theta)}(r)$	PDF of random variable of $H(\mathbf{x}_0,\theta)$ at $\mathbf{x}_0$
$\mathbf{G}(z)$	Constitutive matrices
$\hat{\mathbf{G}}(\mathbf{x}, z, \theta)$	Stochastic constitutive matrix
$\hat{\mathbf{G}}, \hat{\mathbf{G}}_k$	Coefficient matrix
G_1	Coefficient matrix
$H(\mathbf{x},\theta)$	Random field
$H^G(\mathbf{x},\theta)$	Gaussian random field
$H^L(\mathbf{x},\theta)$	Lognormal random field
$\bar{H}(\mathbf{x}), \bar{H}^G(\mathbf{x})$	Mean field
$\tilde{H}(\mathbf{x},\theta), \tilde{H}^G(\mathbf{x},\theta)$	Random field with zero mean value
$H(\mathbf{x}_0,\theta)$	Random variable at $\mathbf{x}_0$
$H(\mathbf{x},\theta_0)$	Realization of the random field $H(\mathbf{x},\theta)$

$\hat{H}(\mathbf{x},\theta)$	Approximation of random field $H(\mathbf{x},\theta)$
$\hat{H}^G(\mathbf{x},\theta)$	Approximation of Gaussian random field $H^G(\mathbf{x},\theta)$
$\hat{H}^L(\mathbf{x},\theta)$	Approximation of lognormal random field $H^L(\mathbf{x},\theta)$
h	Thickness of the plate
$\mathbf{I}_{n\times n}$	Identity matrix with size $n\times n$
$\mathbf{J}$	Jacobian matrix
$\mathbf{K}$	Global stiffness matrix
$\mathbf{K}^e$	Elemental stiffness matrix
$\mathbf{K}(\theta)$	Global stochastic stiffness matrix
$\mathbf{K}^e(\theta)$	Elemental stiffness matrix
$\mathbf{K}_0^e$	Elemental mean stiffness matrix
$\mathbf{K}_i^e, \mathbf{K}_{i_1}^e$	Elemental deterministic stiffness matrix
$\mathbf{K}_{jk}$	Simplified stochastic stiffness matrix
$\mathbf{K}_{ib}$	Linear in-plane-bending stiffness matrix
$\mathbf{K}_s$	Shear stiffness matrix
$\mathbf{K}_i^{NL}$	Nonlinear in-plane stiffness matrix
$\mathbf{K}_\sigma$	Initial stress matrix

$\mathbf{K}_{ib}(\theta)$	Stochastic linear in-plane-bending stiffness matrix
$\mathbf{K}_{s}(\theta)$	Stochastic shear stiffness matrix
$\mathbf{K}_{i}^{NL}(\theta)$	Stochastic nonlinear in-plane stiffness matrix
$\mathbf{K}_{\sigma}(\theta)$	Stochastic initial stress matrix
$\mathbf{K}_{train}$	Kernel matrix
$K_{GGK}(\mathbf{x}_i, \mathbf{x}_j)$	*n*th order generalized Gegenbauer kernel function
$\hat{\mathbf{k}}(\mathbf{x}_i)$	*i*th empirical feature vector
$L_i(\mathbf{x})$	Coefficient of lognormal PCE/aPC expansion
l_x, l_y, l_z	Correlation lengths in *x*-, *y*-, and *z*-axis
l_2^{ε}	Quadratic ε-insensitive loss function
$\mathbf{M}$	Global mass matrix
$\mathbf{M}^e$	Elemental mass matrix
$\mathbf{M}(\theta)$	Global stochastic mass matrix
$\mathbf{M}^e(\theta)$	Elemental stochastic mass matrix
$\mathbf{M}_0^e$	Elemental mean mass matrix
$\mathbf{M}_{i_2}^e$	Elemental deterministic mass matrix
$M_{j,q}$	B-spline basis functions

M, M_1, M_2	Number of terms
$\mathbf{m}, \mathbf{m}_k$	Coefficient vector
m_z	Moment
$\mathbf{N}_{cp}$	Number of the control points
$N_{i,p}$	B-spline basis functions
P	Number of terms
$P_d^{\alpha}(\mathbf{x})$	Generalized Gegenbauer polynomial
$\mathbf{p}, \mathbf{p}_k$	Non-negative variables
$\mathbf{Q}(z)$	Constitutive matrices
$\hat{\mathbf{Q}}(\mathbf{x}, z, \theta)$	Stochastic constitutive matrix
$\mathbf{Q}, \mathbf{Q}_k$	Coefficient vector
$\mathbf{q}, \mathbf{q}_k$	Non-negative variables
$\Re$	Real number
$\Re^d$	Real number vector with size d
$\Re^+$	Positive real number
$\Re^{m \times n}$	Real number matrix with size $n \times m$
$\mathbf{R}(\mathbf{x}) = 0$	System of equations

$\mathbf{R}_k$	kth equations of $\mathbf{R}(\mathbf{x}) = 0$
$\frac{\partial \mathbf{R}_k}{\partial \lambda_j}$	Derivative of $\mathbf{R}_k$ with respect to λ_j
$\frac{\partial \mathbf{R}_k}{\partial \mathbf{\Phi}_{jl}}$	Derivative of $\mathbf{R}_k$ with respect to $\mathbf{\Phi}_{jl}$
R_i^p	NURBS basis functions
$R_{\mathbf{I}}^{\mathbf{P}}(\boldsymbol{\xi})$	**I**th basis function
$R_{\mathbf{I},x}^{\mathbf{P}},\ R_{\mathbf{I},y}^{\mathbf{P}}$	Derivative along x-axis and y-axis of the **I**th basis function
$\mathbf{S}$	Coefficient matrix
S_{ξ}	Support of random vector $\boldsymbol{\xi}$
$S(\xi,\eta)$	Splines surface
$S(\boldsymbol{\xi})$	General expression for T-spline and NURBS surface
t_n	nth load step
$\mathbf{U}$	Displacement vector
$\mathbf{U}(\theta)$	Stochastic displacement vector
$\mathbf{U}_j$	Coefficient of stochastic displacement vector
$\bar{\mathbf{u}} = (u_0, v_0)^T$	membrane displacement of the mid-plane
$\mathbf{u}_{\mathbf{I}}$	Degree of freedom with respect to **I**th control point

$\mathbf{u}(t)$	Displacement vector
$\ddot{\mathbf{u}}(t)$	Acceleration vector
$\mathbf{u}, \mathbf{u}_k$	Lagrange multiplier vector
$\mathbf{u}^*$	Solution of the X-SVR
u_z	Displacement
$u(x, y, z)$	Displacement field
$v(x, y, z)$	Displacement field
$\mathbf{W}(\zeta)$	Weight function
$\mathbf{w}$	Normal vector of te hyperplane
$w(x, y, z)$	Displacement field
w_0	Membrane displacement of the mid-plane
$X(\theta)$	Random variable
X_j	Coefficient of PCE
X_{mijk}	Coefficient
$\mathbf{x}_{new}, \mathbf{x}_{old}$	New, old version of $\mathbf{x}$
$\Delta\mathbf{x}$	Increasement of $\mathbf{x}$
$\mathbf{x}_{train}$	Training dataset input

$\mathbf{y}_{train}$	Training dataset output
$\mathbf{y}$	Degree of freedom vector
$\mathbf{y}(\theta)$	Stochastic degree of freedom vector
$\delta\mathbf{y}$	Variation of the degree of freedom vector
$\mathbf{z}, \mathbf{z}_k$	Coefficient vector
$\mathbf{0}_n = [0, 0, ..., 0]^T$	Zero vector

Chapter 1

INTRODUCTION

1.1 Summary

An introductory chapter is presented which outlines the necessity, contribution as well as the layout of this dissertation. Thus, Chapter 1 is properly organized as follows. Section 1.2 introduces the motivation of the research work. Section 1.3 states the research objective and scopes. Then in Section 1.4, a comprehensive dissertation layout is presented, and finally, all research supports from organizations have been acknowledged in Section 1.5.

1.2 Motivation of research

The finite element method (FEM) is a traditional numerical method for solving problems of engineering and mathematical physics. These problems include structural analysis, fluid flow, heat transfer, etc., and are usually modelled as boundary value problems, or in general, partial differential equations. The finite element method can approximate their results by formulating these problems into a system of algebraic equations. Originated at the 1950s and 1960s, the finite element method spreads quickly into other scientific and engineering disciplines, and now with many commercial programs are available, finite element method is widespread.

However, the deterministic FEM analysis gradually becomes less appreciate for the engineering practices, because the existences, and more significantly, the influences of

inevitable uncertainties in real-life engineering applications have been widely admitted. The incompetence of deterministic FEM on quantitatively assessing the effect of these intrinsic uncertainties has restrained its applicability. Such restriction has stimulated the studies on stochastic analysis to critically assess the safety of real-life engineering practices against various complications. As a result, considerable numerical methods have been developed for the stochastic analysis of real-life engineering applications. These developed stochastic analysis methods meticulously integrate uncertainty quantification within the deterministic FEM analysis framework. Such integration of uncertain quantification into FEM has significantly promoted the applicability of these traditional stochastic analysis methods by completely inheriting the characteristics of FEM. However, it is reminded that such adoption is always a double-edged sword which possesses both favourable advantages and inevitable limitations.

Despite of the remarkable advantages and benefits of what FEM has brought to modern engineering applications, there are still some inadequacies associated with this masterpiece. One inevitable, yet critical, issue exists in the Computer-Aided Design-Computer-Aided Engineering (CAD-CAE) work routine of FEM. That is, the FEM usually is conducted by firstly transferring the geometric information in the CAD system into the CAE system. Subsequently, the relevant analysis by FEM will be executed within the CAE system. Such conventional FEM analysis routine results some issues obstructing the accuracy, efficiency and applicability of FEM. One primary issue associated with the FEM routine is the geometric inconsistency between the design models in CAD system and the analysis models in CAE systems. The two separate environments are tenuously linked by the mesh process in FEM. Such process will construct an analysis model by approximate the intentionally designed model. Consequently, geometric error will inevitably be introduced into the analysis model and permanently exist in the FEM routine,

especially when the physical geometry of engineering applications is complex. Unsurprisingly, such inherent defect of the FEM also exists in the whole process of traditional stochastic analysis methods. The direct consequence of this intrinsic defect is that regardless how accurate the stochastic analysis is, the results are always incorrect simply because the investigated model is not the intentionally designed one. Such effect would be specifically magnified for stochastic analysis of modern engineering practices, which are usually involved with complex physical geometries and are also sensitive to the geometric inaccuracy.

Another issue of FEM is on the computational efficiency. It is reported that 80% of the time of whole FEM analysis is spent on the communication between two separate environments (Cottrell, Hughes and Bazilevs, 2009). Traditional FEM based stochastic analysis is usually involved with a fair amount of repetitive communications between two distinctive environments. This will certainly increase the computational time for the uncertainty analysis at each uncertain-analysis-to-design cycle, and consequently, the overall turnaround time for the real practices is incapable of fulfilling the efficiency requirement of modern engineering practices.

Moreover, the higher accuracy requirement in both modelling and analysis in modern engineering practices can’t be achieved by the FEM, which mainly adopts lower order polynomial basis functions. Undoubtedly, the traditional FEM based stochastic analysis methods cannot satisfy such higher accuracy requirements of contemporary engineering practices as well.

Clearly, the traditional FEM based stochastic analysis method is incapable of handling the new challenges. Meanwhile, these challenges are becoming increasingly significant as the development of modern society. Therefore, it is requisite to develop a new

stochastic analysis framework complied with the developments and requirements of modern engineering practices.

1.3 Objective and scope

The inspiration of this study comes from the increasingly significant challenges in accuracy and efficiency of stochastic analysis for modern engineering practices. Therefore, the main purpose of this thesis is to propose a CAD-CAE integrated stochastic analysis framework which can efficiently handle aforementioned challenges. More explicitly, this thesis has developed the following areas.

Firstly, an accurate, efficient, and applicable CAD-CAE integrated stochastic analysis framework is proposed for the structural linear elasticity analysis. The random field is firstly modelled within CAD system. Thus, a consistency between the intentionally design model and stochastic analysis model can be achieved for the modern engineering structures.

Then, such freshly proposed modern stochastic analysis framework is extended to the composite structures, which has been successfully implemented across a wide range of engineering disciplines including automotive, civil, military, biomedical, electrical, etc.

Secondly, such CAD-CAE integrated stochastic analysis framework is meticulously developed for the structural free vibration problem, namely, the generalized stochastic eigenvalue problem. Globally smooth estimations for stochastic eigenvalues and eigenvectors can be achieved.

Finally, the stochastic linear stability analysis for plate is developed within the CAD-CAE integrated stochastic analysis framework. A semi-sampling method is adopted for the stochastic eigenvalue problem coupled with a stochastic linear elasticity problem.

In order to achieve all the goals of this thesis, the following individual tasks have been thoroughly developed and implemented:

1) Random field modelling within CAD system is developed such that the spatially dependent uncertainties can be accurately applied on the intentionally designed CAD model.
2) The CAD basis function based Karhunen-Loève (K-L) expansion is proposed and formulated. The accuracy and the influence of h- and k- refinement of the CAD basis function on K-L expansion is comprehensively investigated and compared with available analytical results.
3) The polynomial chaos expansion (PCE) is developed and implemented for the representation of the stochastic responses such that these responses can be properly represented even without the knowledge of the corresponding covariance relationship.
4) A stochastic Galerkin based method is proposed and developed within the CAD-CAE integrated stochastic analysis framework, namely, spectral stochastic isogeometric analysis (SSIGA) for the stochastic linear elasticity problems.
5) The SSIGA is formulated for two fundamental engineering structures, Mindlin plate and Kirchhoff-Love shell. Different orders of statistical moments (i.e., mean value and standard deviation), probability density function (PDF), and cumulative distribution function (CDF) of concerned stochastic responses (i.e., displacement, strain, and stress) are obtained and verified with large cycle Monte Carlo Simulation (MCS) method.
6) The novel SSIGA framework is extended to estimate the performance of the composite material plate with uncertain material property under static load. Both

spatially dependent and independent uncertainties are involved within the framework.

7) The random field with non-Gaussian (lognormal) distribution is developed and incorporated into the proposed framework, and proper formulation is proposed for practical application.
8) Arbitrary polynomial chaos (aPC) is firstly introduced into the framework to provide a more flexible and practical method to model the stochastic responses of modern engineering practices against various complications.
9) The SSIGA framework is proposed for the stochastic structural free vibration problem, namely, the stochastic eigenvalue problem. A stochastic Galerkin approach is proposed to formulate the problem into a system of nonlinear equations. The Newton-Raphson approach is adopted to solve the nonlinear system.
10) Such approach is formulated and implemented for structural free vibration analysis of the Mindlin plate and Kirchhoff-Love shell. The stochastic eigenvalue and eigenvectors are calculated, and corresponding statistical information are obtained. The accuracy and efficiency of the proposed method is partially verified through Monte Carlo Simulation (MCS) method.
11) The SSIGA framework is proposed for the stochastic linear stability analysis of plates. An extend support vector regression (X-SVR) is adopted within the framework. And a sampling method is developed, and corresponding sampling method is proposed to calculate the stochastic critical load. Similarly, Monte Carlo Simulation (MCS) method is adopted for the verifications.

The abovementioned tasks have outlined the contribution of this thesis, and the SSIGA framework can be easily implemented and extended for the modern engineering practices.

1.4 Layout of thesis

This study proposed and developed a novel CAD-CAE integrated stochastic analysis framework, i.e., Spectral Stochastic Isogeometric Analysis (SSIGA), for modern engineering practices. The accuracy, efficiency, and applicability of the proposed framework has been comprehensively investigated and thoroughly demonstrated through series of works in this thesis.

Firstly, the Spectral Stochastic Isogeometric Analysis (SSIGA) is freshly proposed in Chapter 3. By meticulously adopting the basis functions within CAD system (i.e. NURBS and T-splines), the SSIGA framework can maintain the exact geometries of the structures and random fields between the CAD model and SSIGA stochastic analysis model, even for those complex geometries inspired from real-life engineering practices. Such rigor can thoroughly eliminate the geometric errors that permanently embedded in traditional approaches. The stochastic analysis by SSIGA framework will be assuredly implemented on the intentionally designed model in CAD system. Moreover, basis functions within CAD system are always higher-order continuous over the whole physical domain. Therefore, the novel SSIGA approach can guarantee a globally smooth random field modelling and finally a globally smooth stochastic analysis result. Additionally, by implementing stochastic analysis directly on the CAD model and avoiding the mesh process in traditional stochastic analysis methods, SSIGA framework will promise an efficient stochastic analysis method for real-life engineering practices. The proposed framework is formulated for the stochastic linear elasticity of Mindlin plate and Kirchhoff-Love shell involved with complex geometry. And, the accuracy and efficiency of the proposed framework for each case is comprehensive investigated and demonstrated

by comparing with Monte Carlo Simulation (MCS) method with significantly large number of cycles.

In Chapter 4, the SSIGA framework is presented for quantitatively assessing the performance of functionally graded materials (FGM) plate with uncertain material properties under static load. The SSIGA framework can maintain the exact geometries of both FGM plate and random field acting on the plate between the design model and stochastic analysis model. Thus, the stochastic analysis is surely implemented on the intentionally designed CAD model of FGM plate. That is, the consistency of the geometry of an FGM plate in CAD model, deterministic Computer-Aided Engineering (CAE) model, and structural safety assessment model can be exactly maintained. This unique feature is extremely important for practically stimulated FGM plates with complex geometries and spatially dependent uncertain system parameters.

Moreover, in Chapter 5, the SSIGA framework is proposed for structural free vibration analysis, namely, the generalized stochastic eigenvalue problems. Within this chapter, the modelling of random field with non-Gaussian distribution and the arbitrary polynomial chaos (aPC) are freshly introduced into the SSIGA framework. Then, a Galerkin-based method is proposed for the generalized stochastic eigenvalue problem. Such approach can circumvent the dependence of the statistical solution on the quality and quantity of the underlying random number generator, and provides an approximation to the complete probabilistic description of the eigensolutions. In the end, the stochastic generalized eigenvalue problem is formulated as a group of deterministic non-linear equations, and can be easily solved by the Newton-Raphson method. Since the closed-form solutions for the stochastic eigenvalue problems are usually unavailable, thus, the Monte Carlo Simulation (MCS) method is also adopted for partially verifying the proposed method.

Then, in Chapter 6, the SSIGA framework is freshly proposed for the stochastic linear stability analysis of plates with uncertain material properties and complex geometries. The proposed SSIGA framework is applicable to different material models, i.e., homogeneous material, functionally graded material, and functionally graded porous material, etc. An extended support vector regression (X-SVR) with a generalized Gegenbauer polynomial kernel is developed, and then, implemented within the SSIGA framework for establishing the statistical characteristics (e.g., mean and standard deviation etc.) of the structural buckling load. Such semi-sampling scheme can also effectively establish the PDF and CDF of the critical buckling load of the FGM plate with relatively small sampling size. As a result, the computational efficiency will be significantly reduced when comparing with the full-scale Monte-Carlo simulation (MCS) technique.

Finally, the overall conclusions of this thesis are drawn in Chapter 7, accompanied with some recommendation analysis on uncertain analysis as well as suggestions for future researches.

1.5 Acknowledgement

All research work involved in this thesis was supported by Australian Research Council through several Discovery and Linkage projects. Moreover, the computational work involved herein was undertaken with the assistance of resources and services from the National Computational Infrastructure (NCI), which is supported by the Australian Government.

Chapter 2

LITERATURE REVIEW

2.1 Summary

This chapter reviews the existing studies about the isogeometric analysis (IGA) and spectral finite element method (SFEM). The research works about IGA are summarized in Section 2.2. Particularly, an introduction about the development and related techniques of IGA is presented in the Subsection 2.2.1. Some of the mechanics problems that are investigated under IGA framework are categorized in Subsection 2.2.2. Most importantly, IGA for structural analysis is summarized in Subsection 2.2.3. The relevant works for the SFEM is presented in Section 2.3. A general introduction about stochastic analysis is presented in Subsection 2.3.1. The uncertainty modelling and uncertainty quantification under the SFEM are presented in Subsection 2.3.2 and 2.3.3 respectively.

2.2 Isogeometric analysis (IGA)

2.2.1 Introduction

In the last century, computer is not as powerful and popular as it is today. All the drawing work of engineering projects was done manually. Then, the development of computers and computer aided design (CAD) saved engineers from the repetitive labour work, and those drawings could be done on computers accurately and efficiently. Nowadays, most engineering and architectural designs are highly relied on CAD (Rogers, 2001). Since 1972, the B-splines have been widely applied to represent the curves by the

designers (Cottrell, Hughes and Bazilevs, 2009). Then, the non-uniform rational B-splines (NURBS) is further developed as a generalization of B-splines, which has been used in CAD programs since 1975 (Cottrell, Hughes and Bazilevs, 2009). As a commonly used modelling technique in computer graphics for generating and representing curves and surfaces, NURBS offer great flexibility and precision for handling both analytic and modelled shapes (Rogers, 2001). In particular, NURBS can represent conic sections, like circles, cylinders and spheres exactly. Although NURBS were only used in proprietary codes of some car companies at early stage, today they are used in all standard CAD packages (Rogers, 2001). More importantly, many efficient stable numerical algorithms have been well-developed to generate NURBS objects (Piegl and Tiller, 1997).

Besides the CAD system, Computer Aided Engineering (CAE) is to use computer technology with programmed codes to solve problems in engineering analysis. Originating in 1950s and 1960s, the finite element method (FEM) is the most widely used method in CAE (Hughes, Cottrell and Bazilevs, 2005). It numerically solves the partial differential equations, which are used for modelling the real engineering problems by approximating their results through lower order Lagrange polynomials. (Cottrell, Hughes and Bazilevs, 2009). After the launch of the first commercial computer programs, FEM becomes widely spread in different engineering and scientific disciplines. And, new techniques, formulations, basis functions, and applications, are developed in the followed decades. However, when it comes to the higher order partial differential problems, which require higher order basis functions, FEM met challenge in accuracy and efficiency. Moreover, for modern engineering analysis, CAD and CAE systems are closely related. However, they are not related directly. Instead, communication processes are necessary for the two separating systems. As the advent of modern society and modern engineering, the requirement for more accurate and efficient analysis method has been emerged due to

the increasing complexity involved in the engineering applications. With such gaps between two separating systems, traditional FEM cannot always provide a satisfactory analysis result with desirable efficiency and accuracy. In order to properly integrate CAD and CAE systems, Isogeometric Analysis (IGA) was firstly proposed by Hughes et al. (Hughes, Cottrell and Bazilevs, 2005), and a monograph of the isogeometric analysis has been published entirely on the subject (Cottrell, Hughes and Bazilevs, 2009). Isogeometric analysis is developed by following the concept of isoparametric analysis but in a reverse direction. The NURBS basis functions, representing geometries in CAD system, are directly employed to represent partial differential equation unknowns. By doing so, problem domain with conic sections geometry, e.g. circles, cylinders, spheres etc. can be represented exactly, and problems with complex geometry can be represented more properly Moreover, NURBS basis function can achieve C^{p-1} continuity with pth order NURBS, even across the boundaries of elements. Isogeometric analysis has analogues of *h*-, *p*- and *hp*-refinement strategies as FEM. In addition to them, a new higher-order methodology, *k*-refinement, is freshly developed, and provides IGA with advantages of efficiency and robustness over traditional *p*-refinement. (Hughes, Cottrell and Bazilevs, 2005).

After the successful launch of such innovation, IGA has attracted a lot of attentions from academic communities. Firstly, mathematical studies and engineering investigation would necessary for a new numerical method. Bezilevs et al. (BAZILEVS *et al.*, 2006) initiated a mathematical study of IGA based on NURBS, and studied the approximation and stability properties in the context of *h*-refinement. Cottrell et al. (Cottrell, Hughes and Reali, 2007) then investigated the effects of smoothness of basis functions on solution accuracy within IGA framework through two simple one-dimensional structural eigenvalue problems and two static shell boundary value problems modelled with

trivariate NURBS solids. In this work, they also developed a *k*-method, a local refinement strategy. Hughes et al. (Hughes, Reali and Sangalli, 2008) compared the approximation properties of standard C^0 continuous finite elements with NURBS on problems of structural vibrations and wave propagation, and NURBS presented the possibility of higher order accuracy and robustness. Evans et al. (Evans *et al.*, 2009) conducted a mathematical study of the *k*-method utilizing results in approximation theory. Theoretical results indicate that, for many function spaces, higher-order splines with maximal continuity are optimal approximants with respect to the number of degrees of freedom, and numerical studies have validated and improved these results. Beirão da Veiga et al. (Beirão da Veiga *et al.*, 2011) presented a result on error estimates for NURBS approximation of smooth functions, explicit in the mesh-size *h*, degrees *p*, space regularities $\boldsymbol{k}_1$, $\boldsymbol{k}_2$, that determine the approximation. Hughes et al. (Hughes, Evans and Reali, 2014) studied the accuracy of finite elements and NURBS approximations to the elliptic eigenvalue problem, and the implications of these results to the corresponding elliptic boundary-value problem and the parabolic and hyperbolic initial-value problems. Meanwhile, many other researchers also did contribution to the error estimation of IGA for different engineering or mathematical problems (Akkerman *et al.*, 2007; van der Zee and Verhoosel, 2011; Xu *et al.*, 2012; Beirão da Veiga, Cho and Sangalli, 2012; Dedè and Santos, 2012; Hassani, Ganjali and Tavakkoli, 2012; da Veiga *et al.*, 2014; Tagliabue, Dedè and Quarteroni, 2014; Bartezzaghi, Dedè and Quarteroni, 2015; Kleiss and Tomar, 2015; Kumar, Kvamsdal and Johannessen, 2017).

Since the NURBS basis functions generally are not interpolatory functions, special treatments are necessary for imposing essential boundary condition. Bazilevs and Hughes (Bazilevs and Hughes, 2007) proposed a Weakly enforced Dirichlet boundary conditions are compared with strongly enforced conditions for boundary layer solutions of the

advection–diffusion equation and incompressible Navier–Stokes equations. Then, they (Bazilevs, Michler, *et al.*, 2007) proposed a modification of the original weak boundary condition formulation that consistently incorporates the well-known ‘‘law of the wall’’. Apart from the abovementioned methods, transformation method (Wang and Xuan, 2010), Nitsche's method (Embar, Dolbow and Harari, 2010), quasi Interpolation (Costantini *et al.*, 2010), Lagrange multiplier method (Shojaee, Izadpenah and Haeri, 2012), blending method (Lu, Yang and Ge, 2013; Ge *et al.*, 2016) are also have been investigated to solve this problem.

In addition to the NURBS, new splines techniques are developed and incorporated into IGA. T-splines (Sederberg *et al.*, 2003), as a generalization of NURBS, is one of the most important techniques. Bazilevs et al. (Bazilevs, Calo, *et al.*, 2010) explored T-splines, a generalization of NURBS enabling local refinement, as a basis for isogeometric analysis. They test T-splines on some elementary two-dimensional and three-dimensional fluid and structural analysis problems and attain good results in all cases. Scott et al. (Scott *et al.*, 2012) developed a local refinement algorithm for analysis-suitable T-splines which does not produce excessive propagation of control points. They then demonstrated its use as an adaptive framework for isogeometric analysis. Evans et al. (Evans *et al.*, 2015) developed hierarchical-analysis-suitable T-splines (HASTS), and the resulting spaces are a superset of both analysis-suitable T-splines and hierarchical B-splines. The additional flexibility provided by the hierarchy of T-spline spaces results in simple, highly localized refinement algorithms which can be utilized in a design or analysis context. Except for T-splines, many other techniques, for example, B-splines (Costantini *et al.*, 2010; Manni, Pelosi and Lucia Sampoli, 2011; Bornemann and Cirak, 2013; Y.-W. Wang *et al.*, 2013; Johannessen, Kvamsdal and Dokken, 2014; Berdinsky *et al.*, 2015; Jiang and Dolbow, 2015; Johannessen, Remonato and Kvamsdal, 2015), PHT-splines (Nguyen-Thanh *et al.*,

2011; P. Wang *et al.*, 2011), THB-splines (Giannelli, Jüttler and Speleers, 2012; Giannelli *et al.*, 2016), are also developed and applied for different engineering problems under IGA framework.

Apart from the basic mathematical error estimations and splines techniques, numerous engineering techniques are developed to handle the complex geometries and problems inspired from the real-life engineering techniques, for example, trimmed surface (Kim, Seo and Youn, 2009, 2010; Seo, Kim and Youn, 2010a; Schmidt, Wüchner and Bletzinger, 2012; Ruess *et al.*, 2014; Beer, Marussig and Zechner, 2015; Kang and Youn, 2015; Nagy and Benson, 2015; Marussig and Hughes, 2018), volumetric parameterization (Martin, Cohen and Kirby, 2009; Martin and Cohen, 2010; W. Wang *et al.*, 2011, 2013; Zhang, Wang and Hughes, 2013, 2012; Evans and Thomas J. R. Hughes, 2013; Xu *et al.*, 2013b, 2013c, 2013a; Liu *et al.*, 2014), Bézier extraction (Borden *et al.*, 2011; Scott *et al.*, 2011; Irzal *et al.*, 2014; Evans *et al.*, 2015; Thomas *et al.*, 2015; Hennig, Müller and Kästner, 2016), quadrature (Schellekens and De Borst, 1993; Auricchio *et al.*, 2012; Schillinger, Hossain and Hughes, 2014; Adam, Bouabdallah, *et al.*, 2015; Adam, Hughes, *et al.*, 2015; Hillman, Chen and Bazilevs, 2015; Nagy and Benson, 2015), multi-patch (Hesch and Betsch, 2012; Kleiss *et al.*, 2012; Apostolatos *et al.*, 2014; V. P. Nguyen *et al.*, 2014; Greco and Cuomo, 2014; Breitenberger *et al.*, 2015; Dornisch, Vitucci and Klinkel, 2015; Du, Zhao and Wang, 2015; Guo and Ruess, 2015; Kapl *et al.*, 2015; Buchegger, Jüttler and Mantzaflaris, 2016).

Also, a lot of excellent researchers elaborately designed and developed programming packages, which not only provides convenience for further researches on IGA but also explore the possibility of commercialization of this technique. De Falco et al. (de Falco, Reali and Vázquez, 2011) developed a suite of free software tools for applications on Isogeometric Analysis (IGA). They focused on providing a common framework for the

implementation of the many IGA methods for the discretization of partial differential equations currently studied, mainly based on B-Splines and NURBS, while being flexible enough to allow users to implement new and more general methods with a relatively small effort. Rypl and Patzák (Rypl and Patzák, 2012) presented how the isogeometric analysis can be integrated within an object oriented finite element environment so that most of the existing functionality of the finite element code is reused. Hsu et al. (Hsu *et al.*, 2015) proposed an interactive parametric design-through-analysis platform to help design engineers and analysts make more effective use of Isogeometric Analysis (IGA) to improve their product design and performance. Pauletti et al. (Pauletti *et al.*, 2015) presented the design of an object-oriented general purpose library for isogeometric analysis, where the mathematical concepts of the isogeometric method and their relationships are directly mapped into classes and their interactions. Nguyen et al. (V. P. Nguyen *et al.*, 2015) presented an introduction to IGA applied to simple analysis problems and the related computer implementation aspects. Dalcin et al. (Dalcin *et al.*, 2016) developed a high-performance IGA analysis framework based on PETSc, a high-performance library for the scalable solution of partial differential equations, which simplifies the development of large-scale scientific codes, provides a rich environment for prototyping, and separates parallelism from algorithm choice. They name the framework PetIGA.

2.2.2 Mechanics problems

Due to its well-demonstrated advantages over traditional FEM, IGA has been applied to a wide range of mechanics problems. The exact geometry representation, globally smoothness, and inherent higher continuity of basis function within IGA is attractive to a numerous engineering and scientific problems.

The IGA can exactly and smoothly represents the physical domains. Such rigor provides evident benefits in biomechanics. Zhang et al. (Zhang *et al.*, 2006) described an approach to construct hexahedral solid NURBS meshes for patient-specific vascular geometric models from imaging data for use in IGA. Due to studies of the impact of LVADs on thermodynamics are notably lacking, Bazilevs et al. (Bazilevs *et al.*, 2009) initiated a computational study of the Jarvik 2000 LVAD model employing isogeometric fluid-structure interaction analysis. They focused on a patient-specific configuration in which the LVAD is implanted in the descending thoracic aorta, performed computations for three pump settings, and reported their observations for several quantities of hemodynamic interest.

The aforementioned advantage is also attractive for the analysis of fluids and fluid-structures interaction. Bazilevs and Hughes (Bazilevs and Hughes, 2007) applied IGA to solve the advection-diffusion equation and incompressible Navier-Stokes equations. Bazilevs et al. (Bazilevs, Calo, *et al.*, 2007) successfully applied the YZβ approach to the simulation of drug delivery in patient-specific coronary arteries under IGA framework. Bazilevs and Akkerman (Bazilevs and Akkerman, 2010) presented an application of the residual-based variational multiscale turbulence modelling (RBVMS) methodology to the computation of turbulent Taylor-Couette flow at high Reynolds number under IGA framework. Bazilevs et al. (Bazilevs, Michler, *et al.*, 2010) combined (i) NURBS-based IGA, (ii) residual-driven turbulence modelling and (iii) weak imposition of no-slip and no-penetration Dirichlet boundary conditions on unstretched meshes to compute wall-bounded turbulent flows. Bazilevs et al. (Bazilevs *et al.*, 2013) proposed IGA of Lagrangian shock hydrodynamics, and extended it to 3D axisymmetric case (Bazilevs *et al.*, 2014). Evans and Hughes (Evans and Thomas J.R. Hughes, 2013) developed divergence-conforming B-splines for application to the incompressible Navier-Stokes

equations on geometrically mapped domains. Ghaffari Motlagh et al. (Ghaffari Motlagh *et al.*, 2013) presented an application of the residual-based variational multiscale modelling methodology within IGA to the computation of laminar and turbulent concentric annular pipe flows.

Moreover, in contact problem, IGA can provide a smooth contact surface and then lead to more physically accurate contact stresses. De Lorenzis et al. (De Lorenzis *et al.*, 2011) applied NURBS-based IGA to Coulomb frictional contact problems between deformable bodies, in the context of large deformations and the numerical examples show that the proposed contact formulation in conjunction with the NURBS discretization delivers accurate and robust predictions. Temizer et al. (Temizer, Wriggers and Hughes, 2011) studied NURBS-based IGA of contact problems and compare with standard C^0-continuous Lagrange finite elements and concluded that NURBS-based IGA is a viable technology for contact problems and offers potential accuracy as well as convergence improvements over C^0-continuous finite elements. De Lorenzis (De Lorenzis, Wriggers and Zavarise, 2012) applied NURBS-based IGA to 3D frictionless large deformation contact problems. Temizer et al. (Temizer, Wriggers and Hughes, 2012) presented a three-dimensional mortar-based frictional contact treatment in IGA with NURBS under the finite deformation regime. Dimitri et al. (Dimitri *et al.*, 2014) applied IGA with T-splines to frictionless contact problems between deformable bodies in the context of large deformations. Also, a comprehensive review about isogeometric contact can be found in De Lorenzis et al. (De Lorenzis, Wriggers and Hughes, 2014).

Structural dynamics problem is also a mechanics problem that can benefit from the global smoothness and higher order basis function of IGA. Cottrell et al. (Cottrell *et al.*, 2006) applied IGA to several structural models, including rods, thin beams, membranes, and thin plates. Rotationless beam and plate models are utilized as well as three-

dimensional solid models. More significantly, a geometrically exact model of the NASA Aluminium Testbed Cylinder is constructed, and frequencies and mode shapes are computed and shown to compare favourably with experimental results. Willberg et al. (Willberg *et al.*, 2012) developed a higher order schemes and verified their capabilities with respect to accuracy and numerical performance on Lamb wave propagation in Structural Health Monitoring (SHM) applications. Coox et al. (Coox *et al.*, 2016) evaluated the performance of a NURBS-based isogeometric finite element formulation for solving stationary acoustic problems in two dimensions. In addition to above applications, IGA is also applied to Crack (D. J. Benson *et al.*, 2010; De Luycker *et al.*, 2011), Electromagnetics(Buffa, Sangalli and Vázquez, 2010, 2014; Ratnani and Sonnendrücker, 2012), topology optimization (Seo, Kim and Youn, 2010b), and etc.

2.2.3 Structural analysis

The IGA methodology aims to improve the interoperability between numerical simulation and the geometry modelling. Namely, IGA is designed to properly integrate the CAE and the CAD systems. Such masterpiece not only drastically reduces the geometry error in the meshing process of traditional FEM routine, but also offers a flexible and efficient framework for refinement, de-refinement, degree-elevation, and re-modelling. In addition, the basis functions within IGA framework are globally smooth beyond the classical C^0 continuity of traditional FEM. These features evidently provide IGA advantages in structural analysis, especially for plates and shell structures with complex geometries, which are commonly used in real-life engineering applications.

For plate structures, traditional plate theories and new plate theories are proposed, developed, or reinforced by incorporating IGA. The first one is classical plate theory (CPT), also known as thin plate theory. S. Shojaee et al. (Shojaee *et al.*, 2012) presented

an isogeometric finite element method for natural frequencies analysis of thin plate problems of various geometries. They designed several numerical examples, and demonstrated the effectiveness, robustness and accuracy of proposed method by comparing with the theoretical solutions and other numerical methods. Then, S. Shojaee et al. (Shojaee *et al.*, 2012) further developed the IGA based CPT for natural frequencies and buckling analysis of thin symmetrically laminated composite plates. They compared the numerical results with either the analytical solutions or other available numerical methods, and excellent agreements are found. Also, VALIZADEH et al. (VALIZADEH *et al.*, 2013) investigated the buckling, free and forced vibration behaviours of orthotropic plates through the IGA based CPT. Yin et al. (Yin, Yu and Liu, 2013) applied the IGA based CPT to functionally graded material plates, and investigated their free vibration behaviour. Excellent agreement with exist analytical or numerical solutions can be observed.

The Reissner–Mindlin plate theory, also known as first-order shear deformation theory (FSDT), is another important plate theory beside the classical plate theory (CPT). Beirão da Veiga et al. (Beirão da Veiga *et al.*, 2012) presented an isogeometric method for the discretization of the Reissner–Mindlin plate bending problem. Their new formulation is locking-free by construction and is natural from the theoretical/mechanical viewpoint. Moreover, they proved that the method is uniformly stable and satisfies optimal convergence estimates, and the theoretical results are fully supported by numerical tests. After that, they also studied a reformulated version of Reissner–Mindlin plate theory in which rotation variables are eliminated in favour of transverse shear strains. This theory has the advantage that the "shear locking" phenomenon is completely precluded, independent of the basis functions used for displacement and shear strains (Beirão Da Veiga *et al.*, 2015). The IGA based FSDT is also developed for functionally graded

material (FGM) plates, laminated composite and sandwich plates, and other composite plates. Valizadeh et al. (Valizadeh *et al.*, 2013) studied the static and dynamic characteristics of FGM plates through IGA. Yin et al. (Yin *et al.*, 2014) developed an effective, simple, robust and locking-free simple first-order shear deformation plate theory (S-FSDT) under the IGA framework, and analysed the static bending, buckling, and free vibration of homogeneous and functionally graded plates. Then, Yu et al. (Yu *et al.*, 2015) developed S-FSDT for geometrically nonlinear analysis of homogeneous and non-homogeneous FGM plates. The accuracy and the effectiveness of the presented approach is illustrated by comparing the obtained results with reference solutions. Also, Yu et al. (Yu *et al.*, 2016) combined the IGA, the level set and the S-FSDT to form a new effective and accurate approach for simulating free vibration and buckling problems of laminated composite plates with cutouts. In this work, they investigated the effects of different boundary conditions, gradient index, length-to-thickness ratio, geometric shape, etc. on the geometrically nonlinear mechanical responses of FGM plates. Thai et al. (Thai *et al.*, 2012) presented IGA based FSDT for static, free vibration, and buckling analysis of laminated composite plate. Kapoor and Kapania (Kapoor and Kapania, 2012) developed IGA based geometrically nonlinear analysis for laminated composite plates using FSDT. Kapoor et al. (Kapoor, Kapania and Soni, 2013) further did post-processor for interlaminar stress calculation in composite and sandwich plates under the IGA based FSDT. Thai et al. (Thai *et al.*, 2013) investigated static, free vibration and buckling analysis of laminated composite and sandwich plates. Le-Manh and Lee (Le-Manh and Lee, 2014) investigated the post-buckling behaviour of laminated composite plates using NURBS-based IGA. Mirzaei and Kiani (Mirzaei and Kiani, 2017) analysed the thermal buckling response of composite laminated plates reinforced with graphene sheets through IGA. Huang et al. (Huang, Nguyen-Thanh and Zhou, 2017) investigated the buckling

analysis for the Mindlin–Reissner cracked plates by applying the extended isogeometric analysis (XIGA) coupled with Bézier extraction operator. Li et al. (Li, Wu, *et al.*, 2018) investigated the static linear elasticity, natural frequency, and buckling behaviour of functionally graded porous plates reinforced by graphene platelets (GPLs). Both first- and third-order shear deformation plate theories are incorporated within the IGA. Nguyen et al. (Nguyen *et al.*, 2019) presented an isogeometric Bézier finite element formulation for bending and transient analysis of functionally graded porous (FGP) plates reinforced by graphene platelets (GPLs) embedded in piezoelectric layers. In addition, Dornisch, Klinkel and B. Simeon (Dornisch, Klinkel and B. Simeon, 2013) proposed a new Reissner–Mindlin plate formulation with exactly calculated director.

Higher-order shear deformation plate theory (HSDT) is also a well-developed and widely applied plate theory. Particularly, third-order shear deformation plate theory (TSDT) belongs to HSDT. Nguyen-Xuan et al. (Nguyen-Xuan, Thai and Nguyen-Thoi, 2013) presented a simple and effective formulation based on a fifth-order shear deformation theory (FiSDT) in combination with IGA for composite sandwich plates. Tran et al. (Tran, Ferreira and Nguyen-Xuan, 2013) studied the static, dynamic, and buckling behaviour of FGM through the IGA based TSDT. Tran et al. (Tran, Thai and Nguyen-Xuan, 2013) studied the thermal buckling behaviour of FGM plates through the IGA based TSDT. Jari et al. (Jari, Atri and Shojaee, 2015) investigated the static, thermo-mechanical buckling and free vibration analysis of FGM by the IGA based TSDT. Tran et al. (Tran, Ly, *et al.*, 2015) combined extended isogeometric analysis (XIGA) and HSDT to study the free vibration of cracked FGM plates. Tran et al. (Tran, Lee, *et al.*, 2015) implemented geometrically nonlinear analysis of laminated composite plates by combining IGA and HSDT. Phung-Van et al. (Phung-Van, Abdel-Wahab, *et al.*, 2015) investigated the static and dynamic behaviour of FG carbon nano-reinforced composite

plates. Phung-Van et al. (Phung-Van, De Lorenzis, *et al.*, 2015) investigated static, free vibration and dynamic control of piezoelectric composite plates integrated with sensors and actuators. Thai et al. (Thai *et al.*, 2015) investigated the suitability of NURBS-based IGA within a third-order shear deformation theory for the simulation of the static, dynamic, and buckling response of laminated composite plates. Tran and Kim (Tran and Kim, 2018) studied static and free vibration of multilayered plates based on isogeometric analysis (IGA) and higher-order shear and normal deformation theory.

Except for classical plate theory (CPT), first-order shear deformation theory (FSDT), and high-order shear deformation theory (HSDT), other new plate theories are also developed under the IGA framework, for example, the inverse trigonometric shear deformation theory (V.-H. Nguyen *et al.*, 2014), the inverse tangent shear deformation theory (ITSDT) (Thai *et al.*, 2014), the refined plate theory (RPT) (Nguyen-Xuan *et al.*, 2014; Tran *et al.*, 2014; N.-T. Nguyen *et al.*, 2015; Nguyen *et al.*, 2017; Tan, Nguyen-Thanh and Zhou, 2017; Tran and Kim, 2018).

For shell structures, shell theories under different kinematics assumptions are developed by taking the advantages of IGA. Kiendl et al. (Kiendl *et al.*, 2009) developed one important shell model, the Kirchhoff-Love shell, on the basis of the isogeometric approach. Then, they (Kiendl *et al.*, 2010) investigated shell structures comprised of multiple patches. Nguyen-Thanh et al. (Nguyen-Thanh *et al.*, 2011) presented a novel approach for isogeometric analysis of thin shells using PHT-splines. Sauer et al. (Sauer, Duong and Corbett, 2014) proposed a geometrically exact membrane formulation based on curvilinear coordinates and IGA, and is suitable for both solid and liquid membranes. Chen et al. (Chen *et al.*, 2014) extended NURBS-based IGA to thin shell/membrane structures which allows for finite membrane stretching as well as large deflection and bending strain. In their work, the assumed non-linear kinematics employs the Kirchhoff-

Love shell theory to describe the mechanical behaviour of thin to ultra-thin structures. Tepole et al. (Tepole *et al.*, 2015) investigated computational modelling of thin biological membranes, for example, skin, alveoli, blood vessels, and heart valves, through Kirchhoff-Love shell under IGA. Kiendl et al. (Kiendl *et al.*, 2015) presented formulations for compressible and incompressible hyperelastic thin shells which can use general 3D constitutive models. Nguyen-Thanh et al. (Nguyen-Thanh *et al.*, 2015) developed an extended isogeometric element (XIGA) formulation for analysis of through-the-thickness cracks in thin shell structures. Riffnaller-Schiefer et al. (Riffnaller-Schiefer, Augsdörfer and Fellner, 2016) presented a discretisation of Kirchhoff–Love thin shells based on a subdivision algorithm that generalises NURBS to arbitrary topology. Goyal and Simeon (Goyal and Simeon, 2017) developed an alternative formulation for multi-patch isogeometric Kirchhoff-Love shell that improves the condition number of the system and removes the penalty parameter dependence. Casquero et al. (Casquero *et al.*, 2017) employed analysis-suitable T-spline surfaces of arbitrary degree for performing structural analysis of fully nonlinear thin shells. Maurin et al. (Maurin *et al.*, 2018) proposed an isogeometric collection method for Kirchhoff-Love shell. Zareh and Qian (Zareh and Qian, 2019) presented application of rational triangular Bézier splines (rTBS) for developing Kirchhoff–Love shell elements in the context of IGA. Balobanov et al. (Balobanov *et al.*, 2019) derived a strain gradient elasticity model for Kirchhoff-Love shells of arbitrary geometry. Pigazzini et al. (Pigazzini *et al.*, 2019) extended a recently-developed framework for isogeometric analysis of composite Kirchhoff-Love shells to drive material damage evolution with a smoothed strain field.

Except for the Kirchhoff-Love shell theory for thin shell structures, there is also a corresponding Reissner-Mindlin shell theory for thick shell structures. D.J. Benson et al. (D.J. Benson *et al.*, 2010) developed Reissner-Mindlin shell formulation based on a

degenerated solid and implemented it for NURBS-based IGA. Casanova and Gallego (Casanova and Gallego, 2013) introduced a third-order shear deformation theory (TSDT) shell theory for a composite shell. Benson et al. (Benson *et al.*, 2013) propose a new isogeometric shell formulation that blends Kirchhoff-Love theory with Reissner–Mindlin theory. Dornisch, Klinkel and Bernd Simeon (Dornisch, Klinkel and Bernd Simeon, 2013) presented an isogeometric Reissner-Mindlin shell derived from the continuum theory. Dornisch and Klinkel (Dornisch and Klinkel, 2014) presented a framework for the computation of complex geometries containing intersections of multiple patches with Reissner-Mindlin shell elements. Kiendl et al. (Kiendl, Marino and De Lorenzis, 2017) presented an isogeometric collocation formulation for the Reissner–Mindlin shell problem. Zou et al. (Zou *et al.*, 2017) presented a geometrically exact isogeometric blended shell formulation.

2.3 Stochastic finite element method (SFEM)

2.3.1 Introduction

The random nature of many features of physical events is widely recognized by industry and researchers. More importantly, the effects of intrinsic randomness of system parameters acting on the outputs of the system have been extensively acknowledged. However, the natural stimuli that activate physical systems may be completely unpredictable by deterministic models. As a result, the characterizations provided by deterministic models is less satisfactory with respect to their predictive capabilities (Oden *et al.*, 2003).

As for the computational mechanics, numerous methodologies of stochastic analysis have been extensively proposed and investigated, also implemented in different

engineering applications. Generally, there are three categories of methodologies can be classified based on the uncertainty modelling techniques. The first main class is the probabilistic approach, also known as stochastic approach, and it has been developed in many different engineering disciplines (Papadrakakis, Papadopoulos and Lagaros, 1996; Papadopoulos and Papadrakakis, 2005; Sudret, Defaux and Pendola, 2005; Falsone and Ferro, 2007; Long *et al.*, 2015). This approach employs well-developed statistical techniques to construct the probabilistic profiles of system outputs (Gao and Kessissoglou, 2007). Then, based on the obtained probabilistic information, subsequent works such as safety assessment, reliability analysis, as well as reliability-based engineering designs can be performed (Gao, 2007; Hurtado and Alvarez, 2012).

However, the probabilistic approach is unsuitable and less confident for engineering situations where the availabilities of information on the uncertain parameters are restricted due to both predictable and unpredictable reasons (Gao *et al.*, 2011; Zhang, 2012). Therefore, in order to fulfil the uncertainty analysis for situations with insufficiency of data, the non-probabilistic uncertainty analysis scheme has been developed. It includes fuzzy analysis (Elishakoff, 1997; Wu, Gao, Wang, *et al.*, 2016), interval analysis (Wu, Gao, Song, *et al.*, 2016; Wu, Gao, Tin-Loi, *et al.*, 2016; Wu *et al.*, 2017; Wu, Gao and Tangaramvong, 2017), info-gap model(Ben-Haim, 1996, 2006; Ben-Haim and Ben-Haim, 2016) and as well as others (Kang and Luo, 2009; Kang, Luo and Li, 2011; Jiang, Bi, *et al.*, 2013).

Nowadays, due to the increasing complexity and disparate availability of information observed in modern engineering applications, it gradually becomes inadequate to model all the uncertain system inputs by utilizing single uncertainty modelling technique. Consequently, the realization of such engineering demand has stimulated the development of the third type of uncertainty analysis, known as the hybrid approach. The

hybrid method provides a more flexible uncertainty analysis to situations where more than one type of uncertainty exists. Some examples of the hybrid approach are including the stochastic interval analysis (Gao, Song and Tin-Loi, 2010; Wang *et al.*, 2014; Wu, Gao, Song, *et al.*, 2016; Wu, Gao, Tin-Loi, *et al.*, 2016), hybrid reliability analysis (Du, Sudjianto and Huang, 2005; Jiang, Long, *et al.*, 2013), interval random analysis (Guo and Du, 2009; Xia, Yu and Liu, 2013; Wu, Gao, Song, *et al.*, 2016; Wu, Gao, Tin-Loi, *et al.*, 2016; Wu and Gao, 2017a, 2017b), as well as random fuzzy analysis (Haldar and Reddy, 1992; Möller *et al.*, 2009).

This review will mainly focus on the probabilistic/stochastic approach, more specifically, the stochastic finite element method (SFEM).

2.3.2 Uncertainty modelling

The stochastic structural analysis must start with the modelling of uncertainties, which are the inputs the stochastic system and usually are related with the mechanical, geometric, and the external loading conditions (Stefanou, 2009). Usually, uncertainties can be divided into two categories, spatially independent and spatially dependent. The first type includes random variables or random vectors with specific distribution type. However, some characteristic uncertainties, for example, the Young's modulus, the Poisson's ratio, and the density, are spatially dependent so that they can be physically compatible. A single value or several values are incapable of considering this characteristic. Therefore, a more realistic way to describe these uncertainties is stochastic/random processes or fields. Rationally, the probability distributions and correlation structures of these stochastic processes or fields should be defined through experimental measurements. Unfortunately, in most cases, due to the lack of relevant experimental data, assumptions are made regarding these probabilistic characteristics. Two main categories of stochastic

processes and fields can be defined based on their probability distribution: Gaussian and non-Gaussian (Stefanou, 2009).

2.3.2.1 Gaussian distribution

Gaussian random field is widely applied in engineering disciplines, not only due to its simplicity, but also because of the computability with the central limit theorem (Spanos and Zeldin, 1998). Numerous methods are developed for the simulation of Gaussian random fields. Among these methods, the Karhunen–Loève (K–L) expansion method (Ghanem and Spanos, 1991) and the spectral representation method are two most used in applications (Shinozuka and Deodatis, 1991, 1996).

The K-L expansion is used to represent both stationary and non-stationary stochastic processes. Ghanem and Spanos (Ghanem and Spanos, 1991) dealt with the K-L expansion in the context of spectral stochastic finite elements. Huang et al. (Huang, Quek and Phoon, 2001a) analysed the K-L expansion as a simulation tool for both stationary and non-stationary Gaussian processes focusing on convergence and accuracy. Phoon et al. (K. . Phoon, Huang and Quek, 2002) presented a simple wavelet-Galerkin approach to solve the Fredholm integral equation for K–L simulation. K. K. Phoon et al. (K. K. Phoon, Huang and Quek, 2002) developed a unified and practical framework for generating second-order stationary and non-stationary, Gaussian and non-Gaussian processes with a specified marginal distribution function and covariance function. Later, they improved the simulation technique by prescribing a fractile covariance function (Phoon, Quek and Huang, 2004). Then, in the work of Grigoriu (Grigoriu, 2006), the Karhunen–Loève, spectral, and sampling representations, referred to as the KL, SP, and SA representations, are defined and some features/limitations of KL-, SP-, and SA-based approximations commonly used in applications are stated. Stefanou and Papadrakakis (Stefanou and Papadrakakis, 2007) did an in-depth assessment on the capabilities of the two commonly

used method, namely, the spectral representation method and the K-L expansion, in the simulation of Gaussian stochastic processes and fields. Liu et al. (Liu, Liu and Peng, 2017) proposed a random function embedded K-L expansion method to break through the barrier that conventional K-L expansions for simulation of stochastic processes often encounter the challenge of dealing with hundreds of random variables. Zheng and Dai (Zheng and Dai, 2017) developed a consistent generalization of K–L expansion for multi-dimensional random field simulation.

The spectral representation method originates from the simulation of a one-dimensional stochastic process using harmonic wave superposition method (Rice, 1945). Then, the concept of spectral representation method and the corresponding principle for applications are defined and proposed in the works of Shinozuka (Shinozuka, 1971; Shinozuka and Jan, 1972). After that, Shinozuka and Deodatis (Shinozuka and Deodatis, 1991) derived the theoretical formulation for the one-dimensional stochastic processes with single variables (Shinozuka and Deodatis, 1991). Then, they extended the formulations to the multi-dimensional Gaussian random fields (Shinozuka and Deodatis, 1996). Meanwhile, Deodatis (Deodatis, 1996b) investigated an analogous method for the multi-variant stationary process featuring the ergodic behaviours. At the same, he also suggested the spectral representation-based simulation algorithm to generate sample functions of a non-stationary, multi-variate stochastic process with evolutionary power spectral (Deodatis, 1996a). Spanos and Zeldin (Spanos and Zeldin, 1998) investigated the characteristics of sample functions of spectral representation scheme, including computational efficiency and applicability. Also, Li and Kareem (Li and Kareem, 1991) utilized the fast Fourier transform (FFT) technique to simulate a multivariate nonstationary Gaussian random process with prescribed evolutionary spectral description. Di Paola (Di Paola, 1998) discussed some computational aspects on the generation

procedure of n-variate wind velocity vectors in detail. Katafygiotis et al. (Katafygiotis, Zerva and Malyarenko, 1999) introduced a rigorous methodology for the simulation of homogeneous and partially isotropic multidimensional random fields. Di Paola and Gullo (Di Paola and Gullo, 2001) proposed a very efficient procedure for the generation of multivariate wind velocity stochastic processes by wave superposition as well as autoregressive time series is proposed. Cacciola and Deodatis (Cacciola and Deodatis, 2011) proposed a spectral-representation-based methodology for generating fully non-stationary and spectrum-compatible ground motion vector processes at a number of locations on the ground surface. Liu et al. (Liu, Liu and Peng, 2016) proposed a family of renewed spectral representation schemes in conjunction with the formulation of random functions, which are served as a random constraint correlating the random variables included in the spectral representation schemes. Shields and Kim (Shields and Kim, 2017) generalized the Spectral Representation Method for simulation of asymmetrically nonlinear (skewed higher-order) stochastic processes. Peng et al. (Peng *et al.*, 2017) introduced a stochastic wave-based simulation scheme for the multivariate nonstationary random process along a straight line in conjunction with either a direct summation of cosine functions or the application of a two-dimensional (2D) FFT. J. Chen et al. (Chen, Kong and Peng, 2017) extended the stochastic harmonic function (SHF) representation originally to evolutionary non-stationary processes, where the time-domain representation of non-stationary stochastic processes is expressed as the linear combination of a series of stochastic harmonic components. Liu et al. (Liu, Liu and Peng, 2018) deduced an unified formulation accommodating spectral representation method (SRM) and proper orthogonal decomposition (POD).

Except for the K-L expansion and spectral representation methods, some other methods are also available for the simulation of Gaussian random fields. Zhang and

Ellingwood (Zhang and Ellingwood, 1994) derived a general continuous orthogonal series expansion of the random field, and examined its relationship with the K-L expansion used in recent stochastic finite-element studies. Li and Der Kiureghian (Li and Der Kiureghian, 1993) proposed a more efficient method called optimal linear estimation (OLE) for the approximation of Gaussian random field. It is sometimes referred to as the Kriging method. The expansion optimal linear estimation (EOLE) is an expansion method of OLE. A comprehensive comparison between the K–L expansion and the EOLE method can be found in (Sudret and Kiureghian, 2000). Zhang et al. (Zhang, Liu and Huang, 2019) presented a high-order polynomial based Ritz–Galerkin approach. In their work, the Legendre, the Chebyshev, and the Gegenbauer orthogonal polynomials are used to realize the Ritz–Galerkin approximation.

2.3.2.2 Non-Gaussian distribution

The most commonly used probability distribution to model the stochastic processes and fields is certainly the Gaussian, however, such choice is made mostly for convenience rather than for mathematical or physical reasons. In fact, various material properties and external load conditions are intrinsically bounded for physical reasons. That is, they usually display strong non-Gaussian characteristics. Therefore, the simulation of non-Gaussian stochastic/random processes and fields is significant for stochastic structural analysis.

In 1988, based on spectral representation method (SRM),Yamazaki and Shinozuka (Yamazaki and Shinozuka, 1988) proposed an iterative methodology to simulate a non-Gaussian stochastic field according to a target non-Gaussian SDF and a target non-Gaussian marginal CDF, with zero mean and variance σ^2 compatible with that of the target SDF. This method is based on the work of Grigoriu (Grigoriu, 1984, 1995). Gurley et al. (Gurley, Kareem and Tognarelli, 1996) addressed the simulation of a class of non-

normal processes based on measured samples and sample characteristics of the system input and output. Gurley et al. (Gurley, Tognarelli and Kareem, 1997) examined state-of-the-art analysis and simulation tools for applications to wind engineering, introduced improvements recently developed by the authors, and directions for future work at that time. Then, Grigoriu (Grigoriu, 1998) addressed the available methods at that time is cannot be extended to generate realizations of non-Gaussian processes, and developed a simulation algorithm for generating realizations of non-Gaussian stationary translation processes with a specified marginal distribution and covariance function, called translation process. Also, Deodatis and Micaletti (Deodatis and Micaletti, 2001) have identified that Yamazaki and Shinozuka's algorithm cannot match accurately the prescribed non-Gaussian marginal CDF when it deviates significantly from the Gaussian, and explained in detail the theoretical reasons for this problem. Shi and Koutsourelakis (Shi and Koutsourelakis, 2006) have developed a methodology with similar accuracy to the Deodatis and Micaletti algorithm, but without the drawback of generating non-Gaussian fields that are not translation ones according to Grigoriu's classic definition (Grigoriu, 1984, 1995). Puig et al. (Puig, Poirion and Soize, 2002) gave a mathematical justifications for a Monte Carlo simulation technique based on memoryless transformations of Gaussian processes. Their method is based Hermite polynomial expansion. Sakamoto and Ghanem (Sakamoto and Ghanem, 2002) developed a method for representing and synthesizing random processes that have been specified by their two-point correlation function and their nonstationary marginal probability density functions. The target process is represented as a transformation based on polynomial chaos expansion of an appropriate Gaussian process. Must of abovementioned methods are based on translation process. Since a translation process is characterized by the covariance of the underlying Gaussian process, efforts have been devoted to determining the

unknown underlying Gaussian covariance function from the known non-Gaussian target. Most of the work assumes that correlation in the non-Gaussian process can be specified using a suitably correlated Gaussian process. However, this is not always possible. For an arbitrarily prescribed marginal distribution function and an arbitrarily prescribed covariance function (or equivalently, spectral density function), the underlying Gaussian process which would yield the target covariance function after transform may not exist. Therefore, Phoon et al. (Phoon, Huang and Quek, 2005) proposed a K-L expansion based method for non-stationary and multi-dimensional non-Gaussian stochastic processes. Then, Li et al. (Li, Phoon and Quek, 2007) demonstrated that K–L expansion can be used to address the situation with incompatible target functions where the commonly used translation approach may not be applicable. It is therefore a more robust method for simulation of non-Gaussian processes because it can generate different processes satisfying the same target spectral density function and the same target marginal distribution function regardless of their compatibility. Graham-Brady and Xu (Graham-Brady and Xu, 2008) introduced a short-range-correlation (SRC) model in the framework of Markov/Gibbs random field theory to characterize and simulate random media. Zentner et al. (Zentner *et al.*, 2016) proposed a new method for the identification and simulation of non-Gaussian and non-stationary stochastic fields given a database. Dai et al. (Dai, Zheng and Ma, 2019) developed a new method for explicitly representing and synthesizing non-Gaussian and non-stationary stochastic processes that have been specified by their covariance function and marginal cumulative distribution function. The target process is firstly represented in the Karhunen-Loève (K-L) series form, the random coefficients in the K-L series is subsequently decomposed using one-dimensional polynomial chaos (PC) expansion. Zhang's method can also be applied for non-stationary non-Gaussian stochastic processes and fields (Zhang, Liu and Huang, 2019).

2.3.3 Uncertainty quantification

After successfully modelled the stochastic/random processes and fields, the uncertainty should be propagated through the investigated system, and the stochastic responses of the system should be assessed. Thus, uncertainty quantification is another significant component should be addressed. The SFEM is an extension of the classical deterministic FEM approach for the stochastic engineering problems. From a mathematical point of view, SFEM is a powerful tool for the solution of stochastic partial differential equations (PDEs). The SFEM has been successfully applied to different engineering disciplines with satisfactory results.

One of the most popular method is the straight Monte Carlo Simulation (MCS) method. By adopting MCS method, a deterministic problem is solved numerous times (usually large than 1 million), and for each time, the uncertainty is sampled by elaborated designed algorithm. After that, the response variability can be easily calculated using simple statistical method. Due to its robustness and simplicity. MCS is often used in many researches as a reference method in order to check the accuracy of other approaches. However, a large number of circles of deterministic analysis usually means a significant computational cost especially for large-scale systems with considerable stochastic dimension. The basic direct MCS method is inefficient, thus, many other variants haven developed to address such issue (Kardara, Bucher and Shinozuka, 1989; Papadopoulos, Deodatis and Papadrakakis, 2005; Schuëller, 2006). Nowadays, the development of efficient and robust algorithm and the powerful computers made the direct MCS a powerful tool for complex SFEM problems. Thus, it is often used as a reference approach for validating the results of the other methods now (Papadrakakis and Papadopoulos,

1996; Elishakoff and Ren, 1999; Argyris, Papadrakakis and Stefanou, 2002; Bielewicz and Górski, 2002; Stefanou and Papadrakakis, 2004; Tartakovsky and Xiu, 2006).

Perturbation method is also a popular method under SFEM. It is based on a Taylor series expansion of the response vector of a physical system. Vanmarcke and Grigoriu (Vanmarcke and Grigoriu, 1983) developed a method for solving a variety of engineering mechanics problems in which physical properties exhibit one-dimensional spatial random variation. Liu et al. (Liu, Belytschko and Mani, 1986) developed a perturbation approach for the determination of the probabilistic distribution of the dynamic response of truss structures. Kleiber and Hien (Kleiber. and Hien, 1994) provided a comprehensive monograph about the perturbation method in SFEM. Matthies et al. (Matthies *et al.*, 1997) presented an perturbation approach for uncertainties in probabilistic numerical analysis of structures and solids. Cavadar et al. (Cavdar *et al.*, 2008) developed perturbation method based SFEM for the structures with composite sections under earthquake forces. Under the framework of IGA, perturbation method is also paid attention by some researchers. Hien and Noh (Hien and Noh, 2017) developed stochastic isogeometric analysis for the free vibration of functionally graded plates with spatially varying random material properties in conjugation with perturbation method. Ding et al. (Ding *et al.*, 2018) proposed a novel generalized *n*th order perturbation isogeometric method (GNP-IGA) for efficient steady heat transfer stochastic analysis with material uncertainty. Then, Ding et al. (Ding *et al.*, 2019) developed this method for exactly modelling/representing composite structures comprising of different materials with particular attention to both static and dynamic analysis of structures with random material characteristics.

Stochastic Galerkin (SG) is another important uncertain quantification method under SFEM framework. It is introduced in the work of Ghanem and Spanos(Ghanem and Spanos, 1990, 1991), spectral stochastic finite element method (SSFEM), which extended

deterministic FEM for the solution of boundary value problems with random material properties (Sudret and Kiureghian, 2000; Stefanou, 2009). Ghanem and Kruger (Ghanem and Kruger, 1996a) addresses the issues involved in solving systems of linear equations which arise in the context of the spectral stochastic finite element (SSFEM) formulation. Two efficient solution procedures are presented that dramatically reduce the amount of computations involved in numerically solving these problems. Anders and Hori (Anders and Hori, 2001) applied it for the problem of three-dimensional softening elasto-plastic bodies with random material properties. Ngah and Young (Ngah and Young, 2007) demonstrated an application of the spectral stochastic finite element method (SSFEM) for predicting the performance of a composite structure with variable material constitutive properties. Ghosh and Farhat (Ghosh and Farhat, 2008) focused on the computation of statistical moments of strains and stresses in a random system model where uncertainty is modelled by a stochastic finite element method based on the polynomial chaos expansion. Aahikari (Adhikari, 2011) combined the spectral finite element and SSFEM for the linear structural dynamics problems. Giovanis et al. (Giovanis, Papadopoulos and Stavroulakis, 2015) proposed a methodology to construct an adaptive sparse polynomial chaos (PC) expansion of the response of stochastic systems whose input parameters are independent random variables modelled as random fields. Do et al. (Do, Gao and Song, 2016) presented a study on non-deterministic problems in the presence of the multiple imprecise-random-field uncertainties by extending the spectral stochastic finite element framework. Do et al. (Do *et al.*, 2016) described a method for discretising planar C2-regular domains immersed in non-conforming triangulations. Do et al. (Do *et al.*, 2017) extended the scaled boundary finite element method (SBFEM) to non-deterministic framework defined on random domain wherein random behaviour is exhibited in the presence of the random-field uncertainties.

The computation through the SG method is always involved with a large system of equations. When direct solution techniques are used for this purpose, the required computing time is prohibitive and impractical. In order to solve this disadvantage, Krylov-type iterative techniques like preconditioned conjugate gradient method (PCG) are developed. leading to a substantial reduction of the number of iterations irrespectively of the coefficient of variation of the input random field and thus the convergence behaviour of the iterative algorithms (Ghanem and Kruger, 1996b; Pellissetti and Ghanem, 2000; Chung *et al.*, 2005; Eiermann, Ernst and Ullmann, 2007; Chen and Guedes Soares, 2008). Also, in order to solve this problem, a stochastic reduced basis method (SRBM) is developed (Nair and Keane, 2002; Sachdeva, Nair and Keane, 2006; Doostan, Ghanem and Red-Horse, 2007; Surya Mohan, Nair and Keane, 2008). Recently, Stavroulakis et al. (Stavroulakis *et al.*, 2017) explored the applicability of modern GPU for this problem, and the benefits achieved with the exploitation of the GPU capabilities are demonstrated.

Usually, the SG method is used in the conjugation with the K-L expansion of Gaussian random fields. For non-Gaussian random fields, PCE can be used to represent the stochastic input (Ghanem and Kruger, 1996a; R. Ghanem, 1999a; Roger Ghanem, 1999). In particular, the use of PCE for a lognormal random field can lead to a closed-form expression since a lognormal random field can be defined by a simple transformation of Gaussian field. However, the application of PCE for both input and output can lead to a loss of accuracy (Sudret and Kiureghian, 2000; Sudret and Der Kiureghian, 2002). Then, the use of generalized polynomial chaos expansion (gPCE) is more suitable for the general non-Gaussian random fields. (Xiu and Karniadakis, 2003; Lucor, Su and Karniadakis, 2004; Foo, Yosibash and Karniadakis, 2007).

Chapter 3

SPECTRAL STOCHASTIC ISOGEOMETRIC ANALYSIS OF LINEAR ELASTICITY

3.1 Summary

This chapter presents a novel stochastic analysis framework for the linear elasticity problem. The spectral stochastic analysis is introduced into isogeometric analysis (IGA), and a novel, yet robust, stochastic analysis framework, namely the spectral stochastic isogeometric analysis (SSIGA), is freshly proposed.

Chapter 3 is organized as follows. The concept of IGA is briefly introduced in Section 3.3. Subsequently, the proposed SSIGA approach is presented in Section 3.4. Particularly, the concept of random field, the SSIGA spectral decomposition of the random field, as well as the concept of polynomial chaos are presented in subsections 3.4.1, 3.4.2 and 3.4.3, respectively. Consequently, the proposed SSIGA approach for linear elasticity problem is formulated in Subsection 3.4.4. In order to illustrate the effectiveness and efficiency of the proposed method, three distinctive numerical examples are thoroughly explored in Section 3.5. Finally, conclusions are drawn in Section 3.6.

The research work developed in Chapter 3 has produced one journal paper which has been published in *Computer Methods in Applied Mechanics and Engineering*, detailed as:

Li, K., Gao, W., Wu, D., Song, C. and Chen, T., 2018. Spectral stochastic isogeometric analysis of linear elasticity. *Computer Methods in Applied Mechanics and Engineering*, 332, pp.157-190.

3.2 Introduction

A new stochastic computational analysis framework, namely the spectral stochastic isogeometric analysis (SSIGA), is introduced. According to the authors' best knowledge, the presented work herein is the first reported work to integrate the spectral stochastic computational scheme into the isogeometric analysis. Unlike traditional numerical solutions of the Karhunen-Loève (K-L) expansion, the non-uniform rational B-spline (NURBS) and T-spline basis functions are employed within the proposed framework of SSIGA, so the random fields acting on a continuous physical medium with complex geometry can be handled in an appropriate, physically feasible and efficient fashion. The polynomials chaos expansion (PCE) is implemented to represent the stochastic structural response (e.g., displacement, strain and stress), such that all corresponding statistical characteristics (e.g., mean and standard deviation) can be robustly acquired. Furthermore, by utilizing the nonparametric statistical analysis (Silverman, 2018), both probability density functions (PDFs) and cumulative distribution functions (CDFs) of concerned structural displacements and stresses can be effectively established. Within the framework of IGA, by meticulously implementing the concept of the higher-order k-refinement, the proposed SSIGA provides a more legitimate and efficient stochastic computational approach for modern engineering structures which are complicated by both spatially dependent uncertainties and complex geometries. The accuracy, the efficiency, and the applicability of SSIGA for linear elasticity are comprehensively investigated and demonstrated through three numerical examples.

By succeeding the advantage of IGA, the proposed SSIGA provides a novel, yet effective, stochastic computational approach with several unique superiorities. First of all, the proposed SSIGA approach is applicable to situations where the physical domains of the random fields are possessing complex geometries. In particular, the proposed SSIGA can exactly represent commonly encountered shapes such as, ellipse, circles, spheres and cylinders. That is, exact geometries of the physical domains can be promised even at a relatively coarse level of discretization and consequently, the corresponding geometrical errors can be significantly diminished. Secondly, by freshly adopting NURBS and T-spline based isogeometric basis functions within the scheme of the K-L expansion, a more appropriate, smoother and effective spectral decomposition of the covariance function of the random field can be accomplished. The homogeneous nature of the NURBS and T-spline based isogeometric basis functions can improve the quality of the approximation of the covariance function of the random field, thus the entire stochastic analysis can be upgraded into a new level in which a reliable and meaningful results can be anticipated. Finally, the proposed SSIGA can also inherit the efficiency of IGA in real-life engineering projects by integrating the Computer-Aided Engineering (CAE) into the Computer-Aided Design (CAD).

3.3 Isogeometric analysis (IGA)

3.3.1 The knot vector and basis function

The one-dimensional knot vector is a non-decreasing set of coordinates in the parameter space, which can be denoted as $\Xi = \{\xi_1, \xi_2, \ldots, \xi_{n_{cp}+p+1}\}$, where $\xi_i \in \Re$ is the ith knot; i is the knot index, such that $i = 1,2,\ldots,\mathbf{N}_{cp} + p + 1$; p denotes the polynomial order; and $\mathbf{N}_{cp}$ denotes the number of the B-spline basis functions.

For a given knot vector, the B-spline basis functions are defined recursively by the Cox-de Boor recursion formula, starting with piecewise constants ($p = 0$):

$$N_{i,0}(\xi) = \begin{cases} 1 & \text{if } \xi_i \le \xi \le \xi_{i+1} \\ 0 & \text{otherwises} \end{cases} \tag{3.1}$$

For $p = 1,2,3,\ldots$ the B-spline basis functions are defined as:

$$N_{i,p}(\xi) = \frac{\xi - \xi_i}{\xi_{i+p} - \xi_i} N_{i,p-1}(\xi) + \frac{\xi_{i+p+1} - \xi}{\xi_{i+p+1} - \xi_{i+1}} N_{i+1,p-1}(\xi) \tag{3.2}$$

3.3.2 The B-spline curves and surfaces

The B-spline curve is defined as the sum over the n basis functions with polynomial order p , i.e., $N_{i,p}, i = 1,2,\ldots,n$ and the corresponding control points $B_i \in \Re^d, i = 1, 2, \ldots, n$, where $d = 1, 2, 3$ is the dimensionality of space.

$$C(\xi) = \sum_{i=1}^{n} N_{i,p}(\xi) B_i \tag{3.3}$$

Moreover, a B-spline surface is defined as a tensor product of two one-dimensional parametric B-spline bases with a generic control net $\{B_{i,j}\}, i = 1, 2, \ldots, n,\ j = 1, 2, \ldots, m$, which can be expressed as follows:

$$S(\xi, \eta) = \sum_{i=1}^{n} \sum_{j=1}^{m} N_{i,p}(\xi) M_{j,q}(\eta) B_{i,j} \tag{3.4}$$

where $N_{i,p}(\xi)$ and $M_{j,q}(\eta)$ are the B-spline basis functions of order p and q , which are corresponding to the knot vectors $\Xi = \{\xi_1, \xi_2, \ldots, \xi_{n+p+1}\}$ and $\mathrm{H} = \{\eta_1, \eta_2, \ldots, \eta_{n+p+1}\}$, respectively.

3.3.3 The non-uniform rational B-spline (NURBS) curves and surfaces

The one-dimensional NURBS basis functions can be built from the B-spline basis functions as:

$$R_i^p(\xi) = \frac{N_{i,p}(\xi)w_i}{\sum_{i=1}^{n} N_{i,p}(\xi)w_i} = \frac{N_{i,p}(\xi)w_i}{W(\xi)} \tag{3.5}$$

where R_i^p denotes the *i*th NURBS basis function with *p*th order ; $N_{i,p}$ denotes the *i*th B-spline basis function with *p*th order; w_i denotes a set of positive weights corresponding to each NURBS basis function.

Therefore, for a given set of control points $\{B_i\}$ with size n, the NURBS curve can be defined as:

$$C(\xi) = \sum_{i=1}^{n} R_i^p(\xi)B_i \tag{3.6}$$

Similarly, the two-dimensional NURBS basis functions can be defined as:

$$R_{i,j}^{p,q}(\xi,\eta) = \frac{N_{i,p}(\xi)M_{j,q}(\eta)w_{i,j}}{\sum_{i=1}^{n}\sum_{j=1}^{m} N_{i,p}(\xi)M_{j,q}(\eta)w_i} = \frac{N_{i,p}(\xi)M_{j,q}(\eta)w_{i,j}}{W(\xi,\eta)} \tag{3.7}$$

Consequently, for a given control net $\{B_{i,j}\}$, the NURBS surface can be defined as:

$$S(\xi,\eta) = \sum_{i=1}^{n}\sum_{j=1}^{m} R_{i,j}^{p,q}(\xi,\eta)B_{i,j} \tag{3.8}$$

Furthermore, a generalization of the NURBS, also known as T-spline, is proposed in (Sederberg *et al.*, 2003), and has already been applied to IGA in (Bazilevs, Calo, *et al.*,

2010). Some related evaluation techniques can be found in (Borden *et al.*, 2011; Scott *et al.*, 2011)

Without loss of generality, the following alternative notation is adopted in this study for both T-spline and the NURBS surface.

$$S(\xi) = \sum_{\mathbf{I}}^{\mathbf{N}_{cp}} R_{\mathbf{I}}^{\mathbf{P}}(\xi) B_{\mathbf{I}} \tag{3.9}$$

where ξ denotes the parameters of each dimension; $\mathbf{I}$ denotes the global basis function index; $\mathbf{P}$ denotes the degree of basis function of each dimension; $\mathbf{N}_{cp} = m \times n$ denotes the total number of control points. By representing in such alternative fashion, a generalized formulation can be accomplished for one-, two- and three-dimensional T-spline and NURBS geometries.

3.3.4 Isogeometric analysis for linear elasticity problem

Generally, the strong form of the linear elasticity problem can be illustrated as a boundary value problem (Hughes, 2012). That is,

Given $f_i : D \to \Re$, $\mathrm{g}_i : \Gamma_{\mathrm{D}_i} \to \Re$, and $\mathrm{h}_i : \Gamma_{\mathrm{N}_i} \to \Re$ such that

$$\sigma_{ij,j} + f_i = 0 \qquad \text{in } D \tag{3.10}$$

$$u_i = g_i \qquad \text{on } \Gamma_{D_i} \tag{3.11}$$

$$\sigma_{ij} n_j = h_i \qquad \text{on } \Gamma_{N_i} \tag{3.12}$$

where D denotes the physical domain; σ_{ij} denotes stress tensor; Eq.(3.10) denotes the governing partial differential equations; Eqs.(3.11) and (3.12) respectively denote the Dirichlet and Neumann boundary conditions, which are applied in each direction

independently, namely, $\overline{\Gamma_{D_i} \cup \Gamma_{N_i}} = \Gamma$ and $\Gamma_{D_i} \cap \Gamma_{N_i} = \varnothing$ for $i = 1,\ldots,d$; g_i denotes the prescribed boundary displacements; h_i denotes tractions.

By combining with the Galerkin's method, the strong form of the linear elasticity problem finally can be expressed in matrix form with size $N \times N$, where N is the number of degrees of freedom of the system, as follows,

$$\mathbf{KU} = \mathbf{F} \tag{3.13}$$

where $\mathbf{U} \in \Re^N$ is the displacement vector; $\mathbf{F} \in \Re^N$ is the force vector; $\mathbf{K} \in \Re^{N \times N}$ is the global stiffness matrix, which can be obtained from assembling the elemental stiffness matrices, $\mathbf{K} = \sum_e \mathbf{K}^e$, where

$$\mathbf{K}^e = \int_{D_e} \mathbf{B}^T \mathbf{D} \mathbf{B} \mathrm{d} D_e \tag{3.14}$$

where $\mathbf{B}$ denotes the matrix relates strain vector to the displacement of elemental control points; $\mathbf{D}$ denotes the elasticity matrix; D_e denotes the physical domain of the *e*th element.

3.4 Spectral stochastic isogeometric analysis (SSIGA)

3.4.1 Preliminary

Regarding a probability space (Ω, Σ, F), Ω denotes the sample space; Σ denotes the σ-algebra, and F denotes the probability measure which is a function on Σ such that $F : \Sigma \to [0,\ 1]$.

A random field $H(\mathbf{x}, \theta)$ is a collection of continuously indexed random variable, and the continuous parameter $\mathbf{x} \in \Re^d$. For a given parameter $\mathbf{x}_0$, $H(\mathbf{x}_0, \theta)$ denotes a random

variable, such that, $\forall \mathbf{x}_0 \in \Re^d$, $H(\mathbf{x}_0, \theta) \sim f_{H(\mathbf{x}_0,\theta)}(r)$, where $f_{H(\mathbf{x}_0,\theta)}(r)$ denotes the corresponding probability density function (PDF) of the random variable. On the other hand, for a given outcome θ_0 , $H(\mathbf{x}, \theta_0)$ denotes a realization of the random field.

Based on the data obtained from engineering projects, various types of random fields have been adapted for different engineering applications. Among all available random fields, the homogeneous Gaussian random field $H^G(\mathbf{x}, \theta)$ has been prevalently implemented in numerous engineering analyses to model the spatially dependent uncertain parameters. Therefore, in order to effectively illustrate the proposed SSIGA approach, this study selects the homogeneous Gaussian random field as a representative to model the spatially dependent uncertainties.

Regarding the homogeneous Gaussian random field, the random variable at an arbitrary point $\mathbf{x}_0$, which is located at any position within the domain of the random field, follows a Gaussian distribution. That is, $H(\mathbf{x}_0, \theta) \sim N(\mu_{H(\mathbf{x}_0,\theta)}, \sigma_{H(\mathbf{x}_0,\theta)})$, $\forall \mathbf{x}_0 \in \Re^d$, where $\mu_{H(\mathbf{x}_0,\theta)}$, $\sigma_{H(\mathbf{x}_0,\theta)} \in \Re$ denote the corresponding mean and standard deviation of the random variable at $\mathbf{x}_0$, respectively; $N(\bullet)$ denotes the probability density function (PDF) of the Gaussian random variable at $\mathbf{x}_0$.

In addition to the adoption of the underpinned distribution type for the random field, the frequently implemented exponential covariance function, which is also motivated from realistic engineering applications, is adopted to model the dependency of the uncertain parameters in this study. The incorporated exponential covariance functions have generalized forms as follows:

$$C_{HH}(\mathbf{x},\mathbf{x}') = \begin{cases} \sigma_H^2 \cdot e^{-\frac{|x-x'|}{l_x}} & \text{for } 1-\text{D fields} \\ \sigma_H^2 \cdot e^{-\frac{|x-x'|}{l_x}} \cdot e^{-\frac{|y-y'|}{l_y}} & \text{for } 2-\text{D fields} \\ \sigma_H^2 \cdot e^{-\frac{|x-x'|}{l_x}} \cdot e^{-\frac{|y-y'|}{l_y}} \cdot e^{-\frac{|z-z'|}{l_z}} & \text{for } 3-\text{D fields} \end{cases} \tag{3.15}$$

where $\sigma_H \in \Re^+$ denotes the standard deviation of the random field; $l_x, l_y, l_z \in \Re^+$ denote the correlation lengths in *x*-axis and *y*-axis, respectively.

3.4.2 Generalized isogeometric basis function based Karhunen-Loève expansion

After the successful establishment of the random field, the next step involved is the random field discretization. The K-L expansion is one type of series expansion methods which has been prevalently implemented for random field discretization. The K-L expansion is based on the spectral decomposition of the covariance function $C_{HH}(\mathbf{x},\mathbf{x}')$, which is bounded, symmetric and positive definite. It has the following spectral or eigen-decomposition:

$$C_{HH}(\mathbf{x},\mathbf{x}') = \sum_{i=1}^{\infty} \lambda_i \varphi_i(\mathbf{x}) \varphi_i(\mathbf{x}') \tag{3.16}$$

and its eigenvalues and eigenfunctions are the solutions of the homogeneous Fredholm integral equation of second kind given by:

$$\forall i = 1,\ldots,n \quad \int_D C_{HH}(\mathbf{x},\mathbf{x}') \varphi_i(\mathbf{x}') dD_{x'} = \lambda_i \varphi_i(\mathbf{x}) \tag{3.17}$$

where λ_i denotes the *i*th eigenvalue and $\varphi_i(\mathbf{x})$ denotes the corresponding eigenfunction. Eq.(3.17) arises from the fact that the eigenfunctions form a complete orthogonal set satisfying the equation:

$$\int_D \varphi_i(\mathbf{x})\varphi_j(\mathbf{x})dD = \delta_{ij} \tag{3.18}$$

where δ_{ij} is the Kronecker symbol.

Consequently, by implementing the K-L expansion, the random field $H(\mathbf{x},\theta)$, can be explicitly discretised as:

$$H(\mathbf{x},\theta) = \mu(\mathbf{x}) + \sum_{i=1}^{\infty}\sqrt{\lambda_i}\zeta_i(\theta)\varphi_i(\mathbf{x}) \tag{3.19}$$

where $\mu(\mathbf{x})$ denotes the mean function of the random field; $\{\zeta_i(\theta), i = 1,\ldots\}$ denotes a set of random variables; $\{\varphi_i(\mathbf{x}), i = 1,\ldots\}$ denotes the set of eigenfunctions corresponding to $\{\zeta_i(\theta), i = 1,\ldots\}$; and λ_i denotes the corresponding eigenvalue.

Based on the orthonormality of the eigenfunctions presented in Eq.(3.16), each random variable in the K-L expansion can be easily expressed as the following closed form:

$$\zeta_i(\theta) = \frac{1}{\sqrt{\lambda_i}}\int_D [H(\mathbf{x},\theta) - \mu(\mathbf{x})]\varphi_i(\mathbf{x})dD \tag{3.20}$$

According to Eq.(3.18), $\{\zeta_i(\theta), i = 1,\ldots\}$ is a set of uncorrelated random variables, with mean $\mathrm{E}(\zeta_i(\theta)) = 0$ and covariance. $\mathrm{E}(\zeta_i(\theta)\zeta_j(\theta)) = \delta_{ij}$ (Kronecker Symbol) It is highlighted that for the case of Gaussian random field, $\{\zeta_i(\theta), i = 1,\ldots\}$ becomes a collection of mutually independent standard Gaussian random variables. Furthermore, the

well-preserved convergence of a Gaussian random field represented by the K-L expansion has been theoretically proved (Michel, 1977).

When it comes to the SSIGA decomposition of the random field, both the geometry representation and the K-L expansion should be simultaneously considered. The geometry representation of a two-dimensional random field can be formulated generally as:

$$S(\xi) = \sum_{\mathbf{I}}^{\mathbf{N}_{cp}} R_{\mathbf{I}}^{\mathbf{P}}(\xi) B_{\mathbf{I}} \tag{3.21}$$

where ξ denotes the parameters of each dimension; $\mathbf{I}$ denotes the global basis function index; $\mathbf{P}$ denotes the degree of basis function of each dimension; $\mathbf{N}_{cp}$ denotes the total number of control points. $B_{\mathbf{I}}$ denotes the $\mathbf{I}$th control points coordinate.

According to the K-L expansion presented in Eq.(3.19) , the random field can be divided into two parts as follows:

$$H(\mathbf{x},\theta) = \bar{H}(\mathbf{x}) + \tilde{H}(\mathbf{x},\theta) \tag{3.22}$$

where $\bar{H}(\mathbf{x})$ denotes the mean field; $\tilde{H}(\mathbf{x},\theta)$ denotes a random field with zero mean value and covariance function $C_{HH}(\mathbf{x},\mathbf{x}')$.

Without loss of generality, the mean field $\bar{H}(\mathbf{x})$ of a Gaussian random field can be represented by the generalized isogeometric basis function as:

$$\bar{H}(\mathbf{x}) = \mu(\mathbf{x}) = \sum_{\mathbf{I}}^{\mathbf{N}_{cp}} \mu_{\mathbf{I}} R_{\mathbf{I}}^{\mathbf{P}}(\xi) \tag{3.23}$$

where, $\mu_{\mathbf{I}}$ denotes the mean corresponding to the **I**th control point; For homogeneous Gaussian random field, $\mu_{\mathbf{I}}$ possesses a constant value μ for each index **I**, so μ.

The essence of the K-L expansion of $\tilde{H}(\mathbf{x},\theta)$ is mainly hinged on the solving of the homogeneous Fredholm integral equation of the second kind as expressed in Eq.(3.17). However, the analytical solution of Eq.(3.17) can only be easily accessible to the problems with simple geometry and special forms of the covariance function. Therefore, in order to extend the applicability of such analytical tool over situations involving random fields acting on physical domain with complex geometries, a new numerical method, namely the generalized isogeometric basis functions (i.e., NURBS and T-spline based isogeometric basis functions) based Galerkin type approach, is proposed for solving the Fredholm equation.

Since the generalized isogeometric basis functions are a complete basis of the Hilbert space $L^2(\Omega)$, each eigenfunction of $C_{HH}(\mathbf{x},\mathbf{x}')$ may be represented by its expansion over this basis as follows:

$$\varphi_k(\mathbf{x}) = \sum_{\mathbf{I}}^{\mathbf{N}_{cp}} \vartheta_{\mathbf{I}}^k R_{\mathbf{I}}^{\mathbf{P}}(\xi) \tag{3.24}$$

where $\varphi_k(\mathbf{x})$ denotes the *k*th eigenfunction; $\vartheta_{\mathbf{I}}^k$ are the unknown coefficients corresponding to the **I**th generalized isogeometric basis function $R_{\mathbf{I}}^{\mathbf{P}}(\xi)$. Thus, $C_{HH}(\mathbf{x},\mathbf{x}')$ can be reformulated as:

$$C_{HH}(\mathbf{x},\mathbf{x}') = \sum_{i=1}^{\infty} \lambda_i \left(\sum_{\mathbf{I}}^{\mathbf{N}_{cp}} \vartheta_{\mathbf{I}}^i R_{\mathbf{I}}^{\mathbf{P}}(\xi) \right) \left(\sum_{\mathbf{I}}^{\mathbf{N}_{cp}} \vartheta_{\mathbf{I}}^i R_{\mathbf{I}}^{\mathbf{P}}(\xi') \right) \tag{3.25}$$

For practical implementation, the series is approximated by a finite number of terms, that is

$$C_{HH}(\mathbf{x},\mathbf{x}') \approx \hat{C}_{HH}(\mathbf{x},\mathbf{x}')_M = \sum_{i=1}^{M} \lambda_i \left(\sum_{\mathbf{I}}^{\mathbf{N}_{cp}} \vartheta_{\mathbf{I}}^i R_{\mathbf{I}}^{\mathbf{P}}(\xi) \right) \left(\sum_{\mathbf{I}}^{\mathbf{N}_{cp}} \vartheta_{\mathbf{I}}^i R_{\mathbf{I}}^{\mathbf{P}}(\xi') \right) \tag{3.26}$$

where $\hat{C}_{HH}(\mathbf{x},\mathbf{x}')_M$ denotes the spectral approximation of $C_{HH}(\mathbf{x},\mathbf{x}')$ with *M*-terms, That is, $\forall a > 0, \exists N(a) \in \aleph$ s.t. if $M \geq N, |\hat{C}_{HH}(\mathbf{x},\mathbf{x}')_M - C_{HH}(\mathbf{x},\mathbf{x}')| < a$.

The Galerkin type method aims at obtaining the best approximation of a function when truncating the infinite series after specific terms. Generally, this process is accomplished by projecting the function onto the space spanned by the adopted basis functions. Therefore, the truncating error $e(\mathbf{x})$ introduced by the Galerkin procedure formulated in Eq.(3.17) can be determined as:

$$e(\mathbf{x}) = \sum_{\mathbf{I}}^{\mathbf{N}_{cp}} \vartheta_{\mathbf{I}}^k \left[\int_D C_{HH}(\mathbf{x},\mathbf{x}') R_{\mathbf{I}}^{\mathbf{P}}(\xi) dD_{\mathbf{x}'} - \lambda_k R_{\mathbf{I}}^{\mathbf{P}}(\xi) \right] \tag{3.27}$$

Requiring the truncated series being the projection of φ_k onto the space $\mathrm{H}_{\mathbf{N}}$ spanned by $\{R_{\mathbf{I}}^{\mathbf{P}}(\xi)\}$ indicates that the residual should be orthogonal to $\mathrm{H}_{\mathbf{N}}$ in $L^2(\mathrm{D})$, that is

$$\left\langle e, R_{\mathbf{I}}^{\mathbf{P}} \right\rangle \equiv \int_{\mathrm{D}} e(\mathbf{x}) R_{\mathbf{I}}^{\mathbf{P}}(\xi) dD = 0 \tag{3.28}$$

Through mathematical transformation, Eq.(3.28) can be further simplified as follows:

$$\mathbf{C}\Theta = \Lambda \mathbf{B}\Theta \tag{3.29}$$

where $\mathbf{C}$, $\mathbf{B}$ and Θ are $\mathbf{N}_{cp} \times \mathbf{N}_{cp}$ matrices, which are defined as:

$$\begin{aligned}
\mathbf{B}_{\mathbf{IJ}} &= \int_D R_{\mathbf{I}}(\xi) R_{\mathbf{J}}(\xi) dD_{\mathbf{x}} \\
\mathbf{C}_{\mathbf{IJ}} &= \int_D \int_D R_{\mathbf{I}}(\xi) R_{\mathbf{J}}(\xi) dD_{\mathbf{x}} dD_{\mathbf{x}'} \\
\Theta_{\mathbf{IJ}} &= \vartheta_{\mathbf{I}}^{\mathbf{J}} \\
\mathbf{\Lambda}_{\mathbf{IJ}} &= \delta_{\mathbf{IJ}} \lambda_{\mathbf{J}}
\end{aligned} \tag{3.30}$$

where $\mathbf{I} = 1, ..., \mathbf{N}_{cp}$, and $\mathbf{J} = 1, ..., \mathbf{N}_{cp}$.

By implementing the proposed Galerkin approach, the eigenvectors Θ and eigenvalues λ_i of the Fredholm integral equation can be robustly determined even the physical domain is irregular. Consequently, the generalized isogeometric basis functions based K-L expansion of a generic random field $H(\mathbf{x}, \theta)$ can be formally expressed as:

$$H(\mathbf{x}, \theta) = \bar{H}(\mathbf{x}) + \tilde{H}(\mathbf{x}, \theta) \approx \sum_{\mathbf{I}}^{\mathbf{N}_{cp}} \mu_{\mathbf{I}} R_{\mathbf{I}}^{\mathbf{p}}(\xi) + \sum_{i=1}^{M} \sqrt{\lambda_i} \zeta_i(\theta) \left(\sum_{\mathbf{I}}^{\mathbf{N}_{cp}} \vartheta_{\mathbf{I}}^{i} R_{\mathbf{I}}^{\mathbf{p}}(\xi) \right) \tag{3.31}$$

In order to evidently illustrate the applicability and accuracy of such novel computational procedure, the first numerical example presented in Section 4 is dedicated to such purpose.

In the proposed K-L expansion, the generalized isogeometric basis functions (NURBS and T-spline) are adopted to represent the eigenfunction of Fredholm integral equation. The benefits of such adoption can be reflected in the following areas:

1. The generalized isogeometric basis functions can achieve higher order continuity within the entire physical domain, even at the boundary of the element. Generally, the random field is defined upon a continuous physical medium, which intrinsically requires not only continuity but also smoothness within the physical domain, namely, more than C^0 continuity in mathematical model. Such intrinsic physical requirement of random field can be easily achieved by the generalized isogeometric basis functions;

2. With the application of Bézier extraction technique, global basis information can be localized to local element. It is possible to improve numerical calculation efficiency for subsequent calculation when the order of basis function for each local element is the same. What's more, the localization mechanism can be easily incorporated into the existing finite element codes, which means the proposed K-L expansion can be easily integrated into the existing application.

Therefore, the proposed K-L expansion provides an appropriate, physically feasible and efficient way to discretise random field.

3.4.3 The polynomial chaos expansion (PCE)

Since the information regarding the covariance functions of the structural responses is unknown, the polynomial chaos expansion (PCE) is implemented to quantify the evolution of the considered uncertainties in the linear elastic analysis through SSIGA. The following presents a brief introduction on PCE. Interested readers can refer to (Ghanem and Spanos, 1991; Sudret and Kiureghian, 2000) for detailed explanation of the theory of PCE.

In order to achieve a more effective illustration, a random variable, $X(\theta):\Omega\to\Re$ is considered. Based on the concept of PCE, the random variable $X(\theta)$ can be alternatively represented as:

$$
\begin{aligned}
X(\theta) = a_0\Gamma_0 &+ \sum_{i_1=1}^{\infty} a_{i_1}\Gamma_1(\zeta_{i_1}(\theta)) \\
&+ \sum_{i_1}^{\infty}\sum_{i_2=1}^{i_1} a_{i_1 i_2}\Gamma_2(\zeta_{i_1}(\theta),\zeta_{i_2}(\theta)) \\
&+ \sum_{i_1}^{\infty}\sum_{i_2=1}^{i_1}\sum_{i_3=1}^{i_2} a_{i_1 i_2 i_3}\Gamma_3(\zeta_{i_1}(\theta),\zeta_{i_2}(\theta),\zeta_{i_3}(\theta)) \\
&+ \sum_{i_1}^{\infty}\sum_{i_2=1}^{i_1}\sum_{i_3=1}^{i_2}\sum_{i_4=1}^{i_3} a_{i_1 i_2 i_3 i_4}\Gamma_4(\zeta_{i_1}(\theta),\zeta_{i_2}(\theta),\zeta_{i_3}(\theta),\zeta_{i_4}(\theta)) + \cdots,
\end{aligned}
\tag{3.32}
$$

where $\{\zeta_{i_k}(\theta)\}_{k=1}^{\infty}$ denotes a set of orthogonal Gaussian random variables; $\hat{\Gamma}_p$ denotes all the polynomials in $\{\zeta_{i_k}(\theta)\}_{k=1}^{\infty}$ of degree not exceeding p; Γ_p denotes the collection of all polynomials in $\hat{\Gamma}_p$ orthogonal to $\hat{\Gamma}_{p-1}$; $a_{i_1}, a_{i_1 i_2}, a_{i_1 i_2 i_3}, a_{i_1 i_2 i_3 i_4}, \ldots$ denote the corresponding coefficient of each polynomial. Detailed evaluation on the coefficient of the polynomials can be refereed to (Ghanem and Spanos, 1991; Sudret and Kiureghian, 2000).

The Gaussian random field is implemented in this study to represent spatially dependent uncertainties, and the generalized isogeometric basis functions based K-L expansion proposed in Section 3.4.2 is adopted to discretise the input Gaussian random field. As mentioned previously, $\{\zeta_{i_k}(\theta)\}_{k=1}^{\infty}$ is a collection of orthogonal Gaussian random variables. Consequently, the Hermite polynomials of Gaussian random variable set $\{\zeta_{i_k}(\theta)\}_{k=1}^{\infty}$ are selected to construct the PCE, which can be described as:

$$
\Gamma_p(\zeta_{i_1}(\theta),\ldots,\zeta_{i_\infty}(\theta)) = e^{\frac{1}{2}\prod_{k=1}^{p}\zeta_{i_k}^2}\prod_{k=1}^{p}\left(-\frac{\partial}{\partial\zeta_{i_k}(\theta)}\right) e^{\frac{1}{2}\prod_{k=1}^{p}\zeta_{i_k}^2}
\tag{3.33}
$$

For the purpose of achieving a more effective notations, Eq.(3.32) can be alternatively expressed as follows:

$$X(\theta) = X_0 \boldsymbol{\Psi}_0(\theta) + X_1 \boldsymbol{\Psi}_1(\theta) + X_2 \boldsymbol{\Psi}_2(\theta) + X_3 \boldsymbol{\Psi}_3(\theta) + \cdots = \sum_{j=0}^{\infty} X_j \boldsymbol{\Psi}_j(\theta) \tag{3.34}$$

where $\{\boldsymbol{\Psi}_j(\theta)\}_{j=1}^{\infty}$ denotes the series of the Hermite polynomials of a set of random variables $\{\zeta_i(\theta)\}_{i=1}^{\infty}$. In addition, $\{\boldsymbol{\Psi}_j(\theta)\}_{j=1}^{\infty}$ is a collection of orthogonal polynomials which satisfies

$$\left\langle \boldsymbol{\Psi}_j(\theta), \boldsymbol{\Psi}_k(\theta) \right\rangle = \left\langle \boldsymbol{\Psi}_j^2(\theta) \right\rangle \delta_{jk} \tag{3.35}$$

where δ_{jk} is the Kronecker delta and $\langle \bullet \rangle$ defines the inner product in the Hilbert space, that is:

$$\langle \bullet \rangle = \int_{S_\zeta} (\bullet) \mathbf{W}(\boldsymbol{\zeta}) d\boldsymbol{\zeta} \tag{3.36}$$

The weight function $\mathbf{W}(\boldsymbol{\zeta})$ adopts the product of PDF of each Gaussian random variable in the set $\{\zeta_i(\theta)\}_{i=1}^{\infty}$ as follows:

$$\mathbf{W}(\boldsymbol{\zeta}) = \prod_{i=1}^{\infty} f_{\zeta_i} = \frac{1}{\sqrt{(2\pi)^p}} \cdot e^{-\frac{1}{2\zeta(\theta)^T \zeta(\theta)}} \tag{3.37}$$

3.4.4 SSIGA for linear elasticity problems

With the consideration of the uncertain Young's modulus, the stochastic linear elasticity problem formulated within the analysis framework of SSIGA can be formulated as:

$$\mathbf{K}(\theta)\mathbf{U}(\theta) = \mathbf{F} \tag{3.38}$$

and the global stochastic stiffness matrix $\mathbf{K}(\theta)$ is assembled from element stochastic stiffness matrices $\mathbf{K}^e(\theta)$, where:

$$\mathbf{K}^e(\theta) = \int_{D_e} \mathbf{B}^T \mathbf{D}(\mathbf{x},\theta)\mathbf{B} dD_e \tag{3.39}$$

Since the **B** matrix of Eq.(3.39) is constant, the only source of uncertainty of the stochastic linear elasticity problem is reflected by the stochastic elasticity matrix:

$$\mathbf{D}(\mathbf{x},\theta) \equiv E^G(\mathbf{x},\theta)\mathbf{D}_0 \tag{3.40}$$

where $\mathbf{D}_0$ denotes the deterministic elasticity matrix; $E^G(\mathbf{x},\theta)$ denotes the Young's modulus of the material that is modelled as homogeneous Gaussian random field.

Subsequently, the random field $E^G(\mathbf{x},\theta)$ can be discretised by the proposed generalized isogeometric basis functions based K-L expansion as:

$$E^G(\mathbf{x},\theta) = \sum_{\mathbf{I}}^{\mathbf{N}_{cp}} \mu_{\mathbf{I}} R_{\mathbf{I}}^{\mathbf{P}}(\xi) + \sum_{i=1}^{\infty} \sqrt{\lambda_i}\zeta_i(\theta)\left(\sum_{\mathbf{I}}^{\mathbf{N}_{cp}} \vartheta_{\mathbf{I}}^i R_{\mathbf{I}}^{\mathbf{P}}(\xi) \right) \tag{3.41}$$

By substituting Eq. (3.41) into Eq.(3.40), the stochastic **D** matrix can be reformulated as:

$$\begin{aligned} \mathbf{D}(\mathbf{x},\theta) &\equiv E^G(\mathbf{x},\theta)\cdot\mathbf{D}_0 \\ &= \sum_{\mathbf{I}}^{\mathbf{N}_{cp}} \mu_{\mathbf{I}} R_{\mathbf{I}}^{\mathbf{P}}(\xi)\mathbf{D}_0 + \sum_{i=1}^{\infty} \sqrt{\lambda_i}\zeta_i(\theta)\left(\sum_{\mathbf{I}}^{\mathbf{N}_{cp}} \vartheta_{\mathbf{I}}^i R_{\mathbf{I}}^{\mathbf{P}}(\xi) \right)\mathbf{D}_0 \end{aligned} \tag{3.42}$$

Moreover, by substituting Eq.(3.42) into Eq.(3.39), the elemental stiffness matrix can be transformed into:

$$\mathbf{K}^e(\theta) = \mathbf{K}_0^e + \sum_{i=1}^{\infty} \mathbf{K}_i^e \zeta_i(\theta) \tag{3.43}$$

where $\mathbf{K}_0^e$ denotes the mean element stiffness matrix and $\mathbf{K}_i^e$ denotes deterministic element stiffness matrix corresponding to each Gaussian random variable $\zeta_i(\theta)$. Specifically:

$$\mathbf{K}_0^e = \int_{D_e} \sum_{\mathbf{I}}^{\mathbf{N}_{cp}} \mu_{\mathbf{I}} R_{\mathbf{I}}^{\mathbf{P}}(\boldsymbol{\xi}) \cdot \mathbf{B}^T \mathbf{D}_0 \mathbf{B} dD_e \tag{3.44}$$

$$\mathbf{K}_i^e = \sqrt{\lambda_i} \int_{D_e} \left(\sum_{\mathbf{I}}^{\mathbf{N}_{cp}} \vartheta_{\mathbf{I}}^i R_{\mathbf{I}}^{\mathbf{P}}(\boldsymbol{\xi}) \right) \cdot \mathbf{B}^T \mathbf{D}_0 \mathbf{B} dD_e \tag{3.45}$$

Consequently, by assembling across entire structural domain, the governing equation of the stochastic linear elasticity problem through the analysis framework of SSIGA can be reformulated as:

$$\left(\mathbf{K}_0 + \sum_{i=1}^{\infty} \mathbf{K}_i \zeta_i(\theta) \right) \cdot \mathbf{U}(\theta) = \mathbf{F} \tag{3.46}$$

Without loss of generality, let $\zeta_0(\theta) \equiv 1$, Eq.(3.46) can be simplified as follows

$$\left(\sum_{i=0}^{\infty} \mathbf{K}_i \zeta_i(\theta) \right) \cdot \mathbf{U}(\theta) = \mathbf{F} \tag{3.47}$$

Furthermore, by implementing the PCE, the structural displacement of the stochastic linear system can be expanded as:

$$\begin{aligned} \mathbf{U}(\theta) &= \mathbf{U}_0 \boldsymbol{\Psi}_0(\theta) + \mathbf{U}_1 \boldsymbol{\Psi}_1(\theta) + \mathbf{U}_2 \boldsymbol{\Psi}_2(\theta) + \mathbf{U}_3 \boldsymbol{\Psi}_3(\theta) + \cdots \\ &= \sum_{j=0}^{\infty} \mathbf{U}_j \boldsymbol{\Psi}_j(\theta) \end{aligned} \tag{3.48}$$

By substituting Eq.(3.48) into Eq.(3.47), the governing equation of the stochastic linear system can be further reformulated as:

$$\left(\sum_{i=0}^{\infty}\mathbf{K}_i\zeta_i(\theta)\right)\cdot\left(\sum_{j=0}^{\infty}\mathbf{U}_j\boldsymbol{\Psi}_j(\theta)\right)=\mathbf{F} \tag{3.49}$$

For practical implementation, the series involved in Eq.(49) should be truncated at finite number of terms. In particular, by truncating the generalized isogeometric basis functions based K-L expansion at the *M*th terms and the PCE at *Pth* terms, Eq.(3.49) can be alternatively expressed as:

$$\left(\sum_{i=0}^{M}\mathbf{K}_i\zeta_i(\theta)\right)\cdot\left(\sum_{j=0}^{P-1}\mathbf{U}_j\boldsymbol{\Psi}_j(\theta)\right)=\mathbf{F} \tag{3.50}$$

where the number of terms P of the PCE can be evaluated by the truncation order M of the K-L expansion and the polynomial order *p* as follows:

$$P=\begin{pmatrix}M+p\\M\end{pmatrix} \tag{3.51}$$

As a result, the residual produced by the truncating process can be defined as:

$$e_{M,P-1}=\left(\sum_{i=0}^{M}\mathbf{K}_i\zeta_i(\theta)\right)\cdot\left(\sum_{j=0}^{P-1}\mathbf{U}_j\boldsymbol{\Psi}_j(\theta)\right)-\mathbf{F} \tag{3.52}$$

Minimizing the residual formulated in Eq.(3.52) in the sense of mean square to obtain the optional approximation of the space spanned by $\{\boldsymbol{\Psi}_j(\theta)\}_{k=0}^{P-1}$ yields:

$$\left\langle\sum_{i=0}^{M}\sum_{j=0}^{P-1}\mathbf{K}_i\mathbf{U}_j\zeta_i(\theta)\boldsymbol{\Psi}_j(\theta),\boldsymbol{\Psi}_k(\theta)\right\rangle=\left\langle\mathbf{F},\boldsymbol{\Psi}_k(\theta)\right\rangle,\quad k=0,\ldots,P-1 \tag{3.53}$$

By introducing the following notations:

$$c_{ijk}=\left\langle\zeta_i(\theta)\boldsymbol{\Psi}_j(\theta)\boldsymbol{\Psi}_k(\theta)\right\rangle \tag{3.54}$$

$$\mathbf{F}_k = \left\langle \mathbf{F}, \boldsymbol{\Psi}_k(\theta) \right\rangle \tag{3.55}$$

Eq.(3.53) can be alternatively expressed as:

$$\sum_{i=0}^{M} \sum_{j=0}^{P-1} c_{ijk} \mathbf{K}_i \mathbf{U}_j = \mathbf{F}_k \tag{3.56}$$

For the purpose of simplicity, introducing

$$\mathbf{K}_{jk} = \sum_{i=0}^{M} c_{ijk} \mathbf{K}_i \tag{3.57}$$

Then, Eq.(3.56) can be reformulated as:

$$\sum_{j=0}^{P-1} \mathbf{K}_{jk} \cdot \mathbf{U}_j = \mathbf{F}_k, \quad k = 0, \ldots, P-1 \tag{3.58}$$

After solving the above stochastic system presented in Eq.(3.58), the stochastic structural displacement $\mathbf{U}(\theta)$ can be adequately approximated as:

$$\mathbf{U}(\theta) = \sum_{j=0}^{P-1} \mathbf{U}_j \boldsymbol{\Psi}_j(\theta) \tag{3.59}$$

Consequently, the related statistical characteristics of the stochastic structural response $\mathbf{U}(\theta)$, namely the mean vector and covariance matrix, can be explicitly determined as:

$$\mathrm{E}(\mathbf{U}(\theta)) = \sum_{j=0}^{P-1} \left\langle \mathbf{U}_j \boldsymbol{\Psi}_j(\theta) \right\rangle = \mathbf{U}_0 \tag{3.60}$$

$$\begin{aligned} \mathrm{Cov}(\mathbf{U}(\theta), \mathbf{U}(\theta)) &= \left\langle \mathbf{U}(\theta) - \mathbf{U}_0, \mathbf{U}(\theta) - \mathbf{U}_0 \right\rangle \\ &= \left\langle \sum_{j=0}^{P-1} \mathbf{U}_j \boldsymbol{\Psi}_j(\theta) - \mathbf{U}_0, \sum_{j=0}^{P-1} \mathbf{U}_j \boldsymbol{\Psi}_j(\theta) - \mathbf{U}_0 \right\rangle \\ &= \sum_{j=0}^{P-1} \left\langle \boldsymbol{\Psi}_j^2 \right\rangle \mathbf{U}_i \cdot \mathbf{U}_i^T \end{aligned} \tag{3.61}$$

By taking a step further, the stochastic strain, at location $\mathbf{x}$ within a generic structural element, can also be formulated through the PCE as:

$$\boldsymbol{\varepsilon}(\mathbf{x},\theta)=\sum_{j=0}^{P-1}\boldsymbol{\Psi}_j(\theta)\boldsymbol{\varepsilon}_j(\mathbf{x}) \tag{3.62}$$

where $\boldsymbol{\varepsilon}_j(x)=\mathbf{B}^T\{\mathbf{U}_j\}^e$ denotes the polynomial chaos coefficient of the strain vector corresponding to a specific element.

Thus, the mean vector and covariance matrix of the stochastic strain can be determined as:

$$\mathrm{E}[\boldsymbol{\varepsilon}(\mathbf{x},\theta)]=\boldsymbol{\varepsilon}_0 \tag{3.63}$$

$$\mathrm{Cov}[\boldsymbol{\varepsilon}(\mathbf{x},\theta)]=\sum_{i=0}^{P-1}\left\langle\boldsymbol{\Psi}_j^2\right\rangle\boldsymbol{\varepsilon}_i\cdot\boldsymbol{\varepsilon}_i^T \tag{3.64}$$

From the Hooke's law, the stochastic stress, at location x within a generic structural element, can be also formulated through the PCE as:

$$\begin{aligned}\boldsymbol{\sigma}(\mathbf{x},\theta)&=\mathbf{D}(\mathbf{x},\theta)\cdot\boldsymbol{\varepsilon}(\mathbf{x},\theta)\\&=\zeta_0(\theta)\cdot\sum_{\mathbf{I}}^{\mathbf{N}_{cp}}\mu_{\mathbf{I}}R_{\mathbf{I}}^{\mathbf{P}}(\boldsymbol{\xi})\cdot\sum_{j=0}^{P-1}\boldsymbol{\Psi}_j(\theta)\cdot\mathbf{D}_0\boldsymbol{\varepsilon}_j(\mathbf{x})\\&\quad+\sum_{i=i}^{M}\sum_{j=0}^{P-1}\zeta_i(\theta)\boldsymbol{\Psi}_j(\theta)\cdot\sqrt{\lambda_i}\cdot\left(\sum_{\mathbf{I}}^{\mathbf{N}_{cp}}\vartheta_{\mathbf{I}}^iR_{\mathbf{I}}^{\mathbf{P}}(\boldsymbol{\xi})\right)\cdot\mathbf{D}_0\boldsymbol{\varepsilon}_j(\mathbf{x})\\&=\sum_{\mathbf{I}}^{\mathbf{N}}\mu_{\mathbf{I}}R_{\mathbf{I}}^{\mathbf{P}}(\boldsymbol{\xi})\sum_{j=0}^{P-1}\boldsymbol{\Psi}_j(\theta)\cdot\boldsymbol{\sigma}_{0j}(\mathbf{x})\\&\quad+\sum_{i=i}^{M}\sum_{j=0}^{P-1}\zeta_i(\theta)\boldsymbol{\Psi}_j(\theta)\cdot\boldsymbol{\sigma}_{ij}(\mathbf{x})\end{aligned} \tag{3.65}$$

Consequently, the mean vector and covariance matrix of the stochastic stress at location $\mathbf{x}$ within a generic structural element can be calculated as:

$$
\begin{aligned}
\mathrm{E}[\boldsymbol{\sigma}(\mathbf{x},\theta)] &= \sum_{\mathbf{I}}^{\mathbf{N}_{cp}} \mu_{\mathbf{I}} R_{\mathbf{I}}^{\mathbf{P}}(\boldsymbol{\xi}) \cdot \sum_{j=0}^{P-1} \left\langle \boldsymbol{\Psi}_j(\theta) \right\rangle \cdot \boldsymbol{\sigma}_{0j}(\mathbf{x}) \\
&\quad + \sum_{i=i}^{M} \sum_{j=0}^{P-1} \left\langle \zeta_i(\theta), \boldsymbol{\Psi}_j(\theta) \right\rangle \cdot \boldsymbol{\sigma}_{ij}(\mathbf{x}) \\
&= \sum_{\mathbf{I}}^{\mathbf{N}_{cp}} \mu_{\mathbf{I}} R_{\mathbf{I}}^{\mathbf{P}}(\boldsymbol{\xi}) \cdot \boldsymbol{\sigma}_{00}(\mathbf{x}) + \sum_{i=i}^{M} \sum_{j=0}^{P-1} \left\langle \zeta_i(\theta), \boldsymbol{\Psi}_j(\theta) \right\rangle \cdot \boldsymbol{\sigma}_{ij}(\mathbf{x})
\end{aligned}
\tag{3.66}
$$

$$
\begin{aligned}
\mathrm{Cov}[\boldsymbol{\sigma}(\mathbf{x},\theta), \boldsymbol{\sigma}(\mathbf{x},\theta)] &= \sum_{k=0}^{P-1} \sum_{j=0}^{P-1} \sum_{l=0}^{M} \sum_{i=0}^{M} c_{iljk} \boldsymbol{\sigma}_{ij}(\mathbf{x}) \cdot \boldsymbol{\sigma}_{lk}^{T}(\mathbf{x}) \\
&\quad - E[\boldsymbol{\sigma}(\mathbf{x},\theta)] \cdot E^{T}[\boldsymbol{\sigma}(\mathbf{x},\theta)]
\end{aligned}
\tag{3.67}
$$

where $c_{ijkl} = \left\langle \zeta_i(\theta)\zeta_l(\theta)\boldsymbol{\Psi}_j(\theta)\boldsymbol{\Psi}_k(\theta) \right\rangle$ can be solved similarly as Eq.(3.54).

To achieve a more effective communication on the proposed SSIGA, a flowchart on the entire process of the proposed spectral stochastic isogeometric analysis is presented.

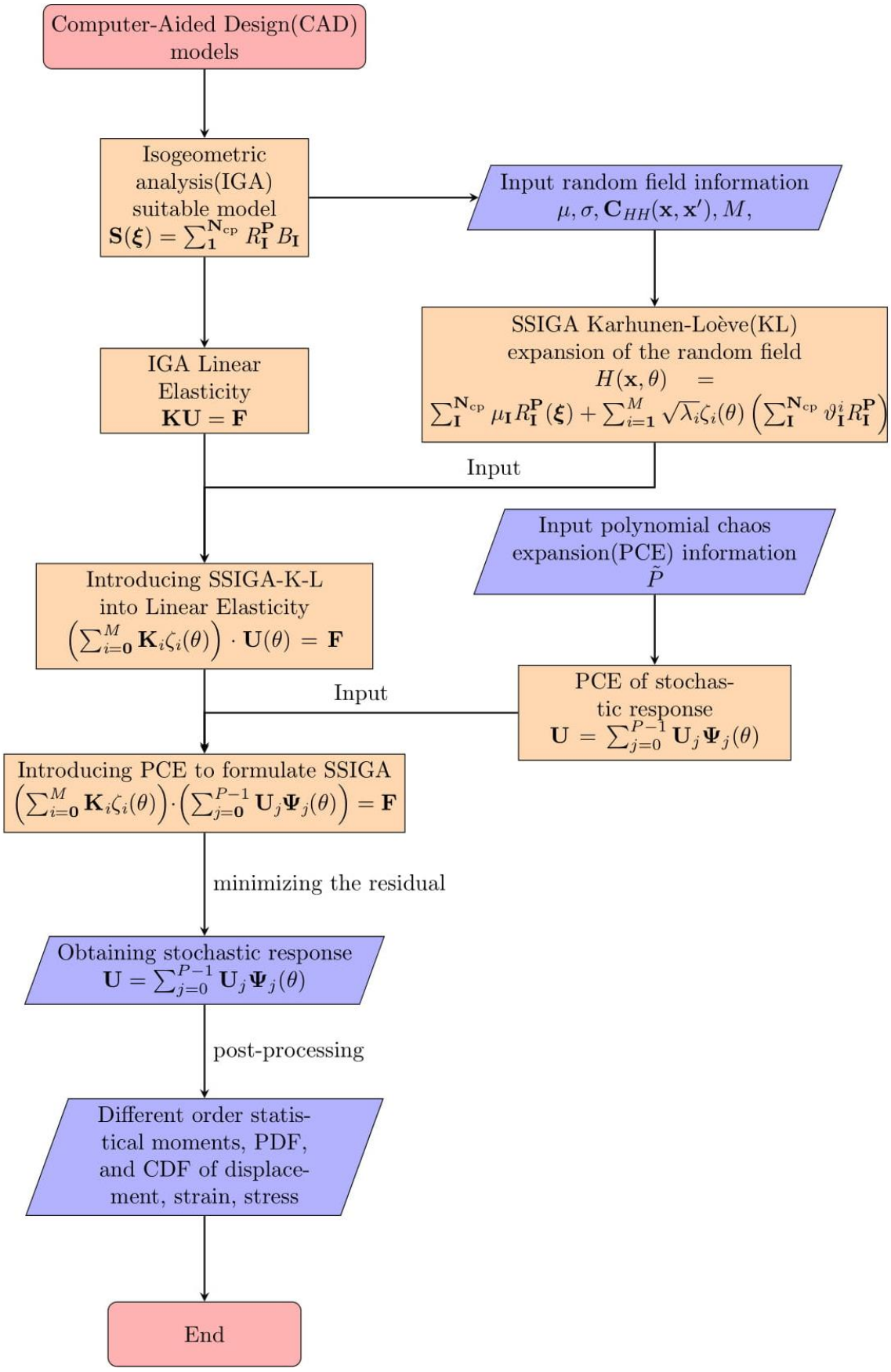

Figure 3.1 Flowchart of the proposed SSIGA analysis framework for linear elasticity

3.5 Numerical examples

In order to demonstrate the applicability, accuracy and effectiveness of the proposed SSIGA analysis scheme, three numerical examples are thoroughly explored within this section. For the first numerical example, the freshly proposed generalized isogeometric basis functions based K-L expansion approach is rigorously verified against the well-established theoretical results. Subsequently, the proposed SSIGA analysis framework is further implemented for the stochastic static analysis of a circular Mindlin plates in the second example, and a torpedo-shape Kirchhoff-Love shell in the third example. Moreover, for the last two examples where analytical solutions are absent, the accuracy of the results obtained by the SSIGA is partially verified by the Monte Carlo simulation method with large simulation cycles. The Monte-Carlo Simulation adopted herein is achieved by repeatedly executing the deterministic IGA with one possible realization of the random field at each cycle until the predefined total number of simulations is reached. Within the context of the presented numerical examples, all random numbers are generated by employing the Statistics toolbox of MATLAB R2016b, also the evaluation of IGA basis functions is based on the technique presented in (V. P. Nguyen *et al.*, 2015).

3.5.1 Numerical example: generalized isogeometric basis functions based Karhunen-Loève expansion

In order to rigorously verify the accuracy and the applicability of the freshly proposed generalized isogeometric basis functions based K-L expansion approach, a two-dimensional square Gaussian random field, with mean $\mu = 1$, standard deviation $\sigma = 0.2$, and side length $l = 2$ is considered. Since T-spline are defined locally, whereas NURBS are defined globally, the proposed K-L expansion is implemented by NURBS to achieve a globally conclusion. The considered covariance function of the Gaussian random field

is the typical two-dimensional exponential function, that is, $C_{HH}(\mathbf{x},\mathbf{x}') = \sigma^2 \exp(-\frac{|x_1 - x_2|}{l_x} - \frac{|y_1 - y_2|}{l_y})$, where the correlation lengths are $l_x = l_y = 2$. The general layout and three possible normalized realizations of the two-dimensional Gaussian random field are showed in Figure 3.2. For this particular example, exact solutions of the eigenvalues and eigenfunctions of the spectrum decomposition are achievable by taking the tensor product of two one-dimensional Gaussian random fields (Ghanem and Spanos, 1991; Sudret and Kiureghian, 2000).

For the two parametric directions, ξ and η, a second order basis functions in each direction is adopted. The corresponding polynomial orders and knot vector of the coarse mesh of the geometry are given in Table 3.1, and the control points are also presented in Table 3.2. The h- and k-refinements are employed to further refine the mesh of the geometry of the random field.

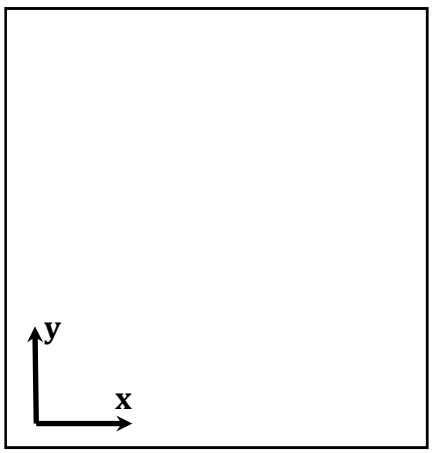

(a)

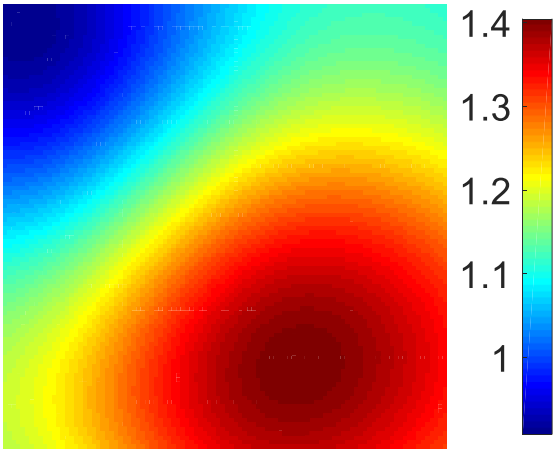

(b)

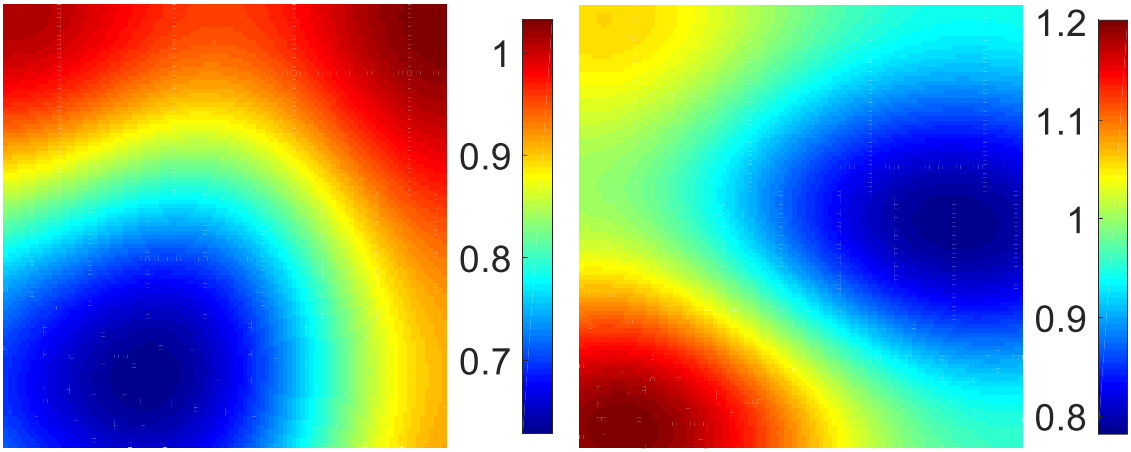

(c) (d)

Figure 3.2 (a) Physical domain and (b)-(d) possible normalized realizations of random field with square geometry

Table 3.1 Polynomial orders and knot vectors for square random field

Direction	Order	Knot Vector
ξ	$p = 2$	$\Xi = \{0,0,0,1,1,1\}$
η	$q = 2$	$\mathrm{H} = \{0,0,0,1,1,1\}$

Table 3.2 Control points for square random field

i	j	$B_{i,j}$	$w_{i,j}$
1	1	(0, 0)	1
1	2	(0, 1)	1
1	3	(0, 2)	1
2	1	(1, 0)	1
2	2	(1, 1)	1

2	3	(1, 2)	1
3	1	(2, 0)	1
3	2	(2, 1)	1
3	3	(2, 2)	1

Firstly, the influence of the h-refinement is investigated. Given the coarsest mesh information presented in Tables 1 and 2 with basis order $p = q = 2$, the h-refinement with order 2, 3, 4 and 5 are applied respectively to both directions as illustrated in Figure 3.3. By implementing the proposed K-L expansion, the first six eigenvalues in Eq.(3.31) of the different h-refinement meshes are calculated based on Eq.(3.30) and then reported in Table 3.3 and Figure 3.4. In addition, the analytical solutions of the eigenvalues are also presented in Table 3.3 and Figure 3.4 for the purpose of result verification. Moreover, the covariance function obtained from the proposed K-L expansion with 6 terms for each considered mesh is constructed in Figure 3.5. To illustrate the applicability and accuracy of the proposed K-L expansion, the target covariance function is also presented in Figure 3.5.

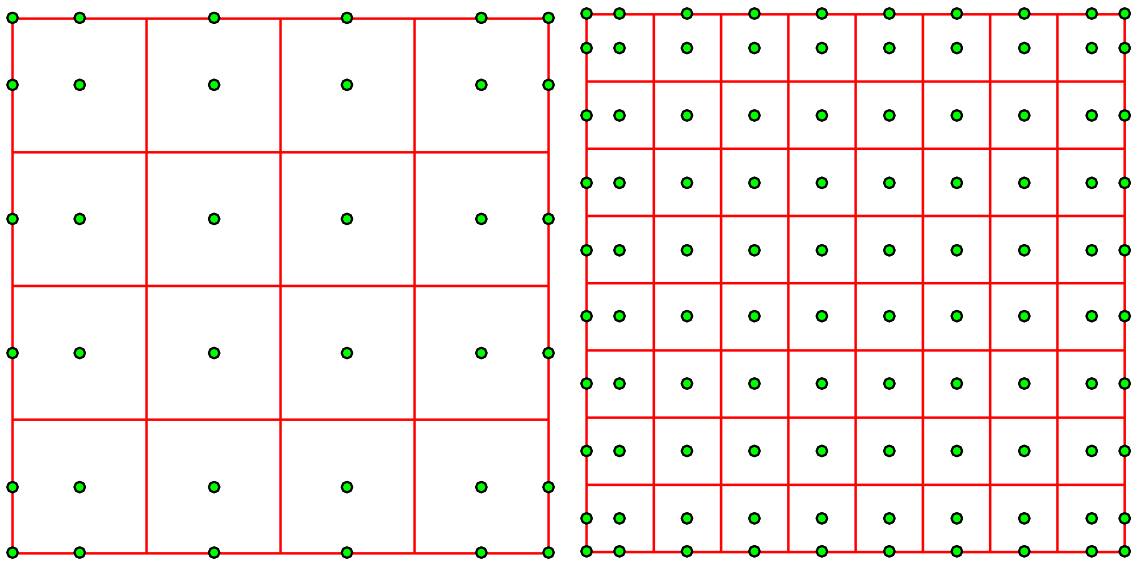

(a) (b)

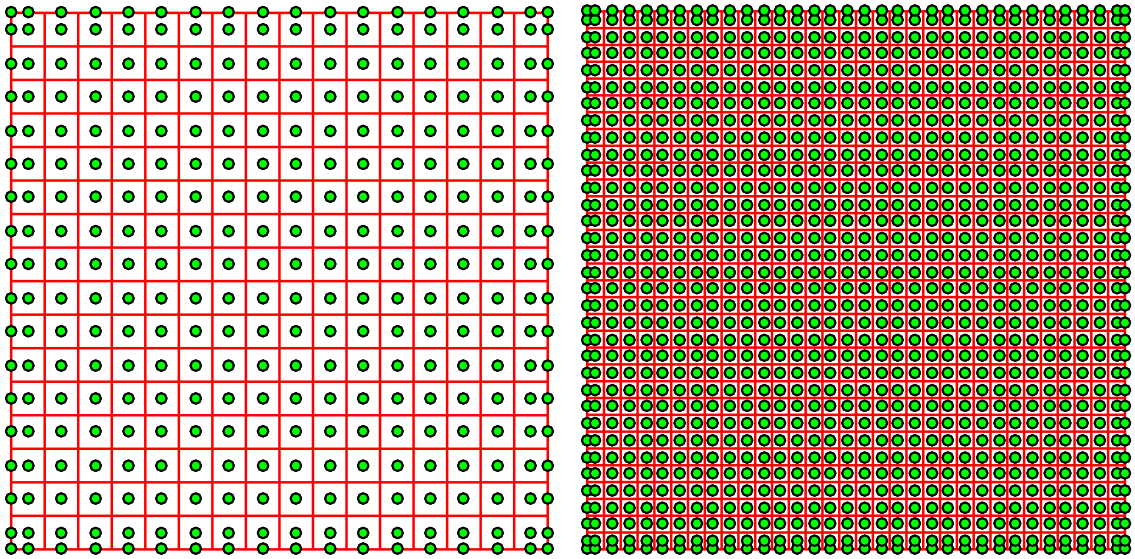

(c) (d)

Figure 3.3 The (a) 2-, (b) 3-, (c) 4-, and (d) 5-order of the h-refinement

Table 3.3 Eigenvalues of the different order of the h-refinement

	Generalized isogeometric basis functions based K-L expansion				Analytical (Ana)
The order of the h-refinement	2	3	4	5	-
λ_1	2.19173	2.18545	2.18389	2.18350	2.18337
λ_2	0.41285	0.40907	0.40814	0.40791	0.40783
λ_3	0.41285	0.40907	0.40814	0.40791	0.40783
λ_4	0.13775	0.13436	0.13352	0.13332	0.13325
λ_5	0.13775	0.13436	0.13352	0.13332	0.13325
λ_6	0.07777	0.07657	0.07628	0.07620	0.07618

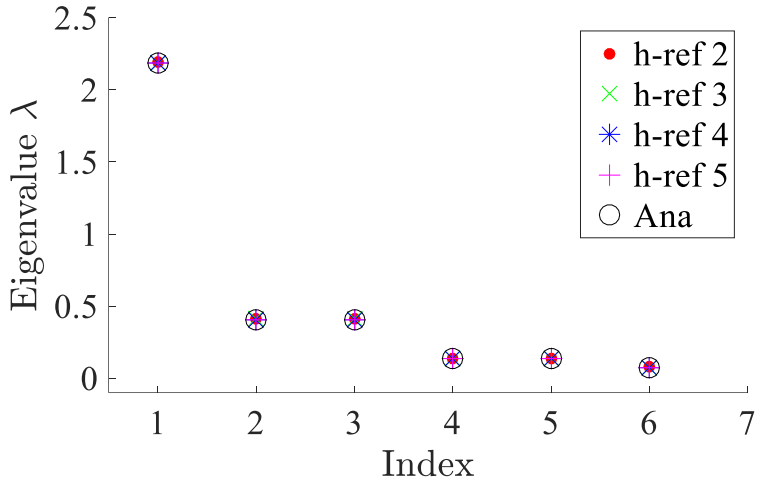

Figure 3.4 Eigenvalues of the different order of the h-refinement

As illustrated in both Table 3.3 and Figure 3.4, by increasing the order of the h-refinement, the considered eigenvalues converge to the analytical solutions. In particular, a relative error of 0.01% can be achieved when the 4-order h-refinement is implemented. Also, the convergent trend of using different order of the h-refinement is illustrated in Figure 3.5. Therefore, the convergence of the covariance function of the random field estimated by the proposed K-L expansion using the h-refinement can be confirmed when higher orders are implemented.

Subsequently, the influence of the k-refinement on the proposed K-L expansion is investigated. Similarly, given the coarsest mesh information as Table 3.1 and Table 3.2 with basis order $p = q = 2$, the "pure" k-refinement (Cottrell, Hughes and Reali, 2007) with an increasing order of the basis function from 2 to 5 are applied as shown in Figure 3.6. In order to minimize the influence of the h-refinement, each "pure" k-refined mesh in Figure 3.6 with different order of basis functions is the 4-order h-refined as shown in Figure 3.7. In this way, although different meshes have different number of control points, the same number of elements can be anticipated. The eigenvalues corresponding to different meshes with different basis orders are listed in Table 3.4 and plotted in Figure

3.8. Moreover, the corresponding covariance functions are also plotted in Figure 3.9. It is noticed that the exponential covariance function of Gaussian random field under consideration is non-differentiable at the four edges of the physical domain, so the relative errors at origin and points along the edges are larger than other parts (Huang, Quek and Phoon, 2001b). To further elaborate this point, considering a one-dimensional Gaussian random field with exponential covariance function with a unit correlation length, that is, $C_{HH}(x,x') = \sigma_H^2 \cdot e^{-|x-x'|} = \sigma_H^2 \cdot e^{-|lagx|}$. The function $e^{-|lagx|}$ is C^0 continuous at $lagx = 0$, namely, its derivative is discontinuous at $lagx = 0$. However, the spectral expansion process is based on continuous functions, which can't represent the discontinuity properly even no derivative terms exist in the spectral expansion process. Therefore, the C^0 continuity results the inaccurate approximation at $lagx = 0$ within in the K-L expansion.

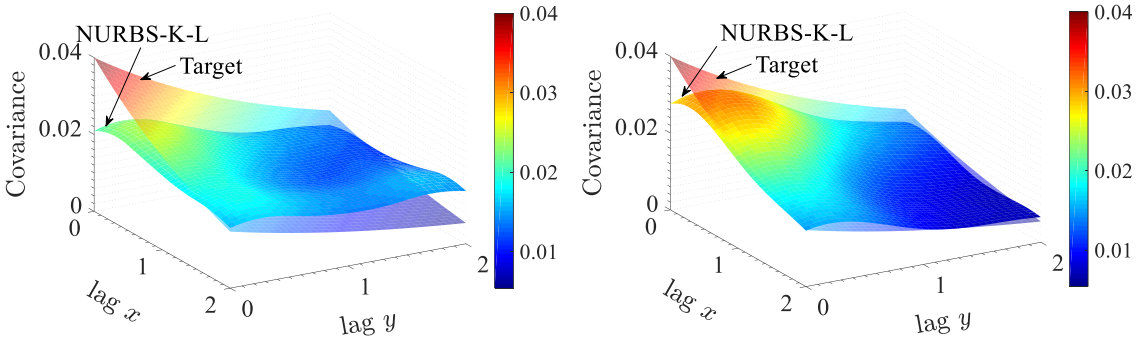

(a)

(b)

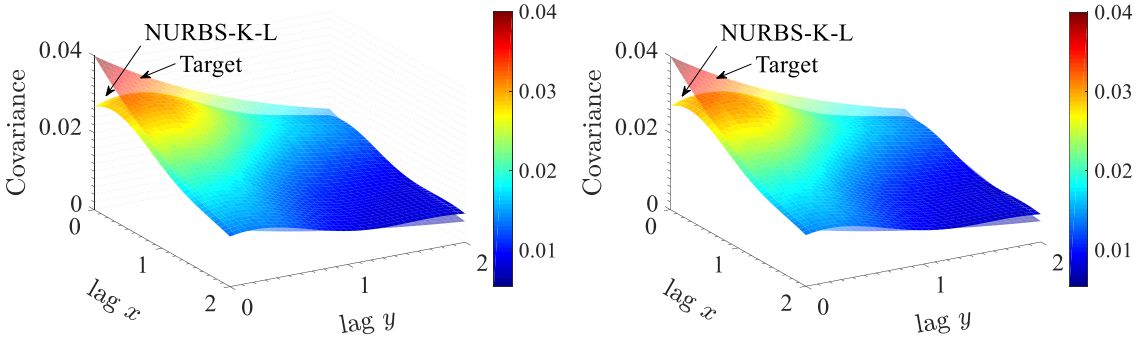

(c)

(d)

Figure 3.5 Covariance function estimated by the proposed K-L expansion of (a) 2-, (b) 3-, (c) 4-, and (d) 5-order h-refinement.

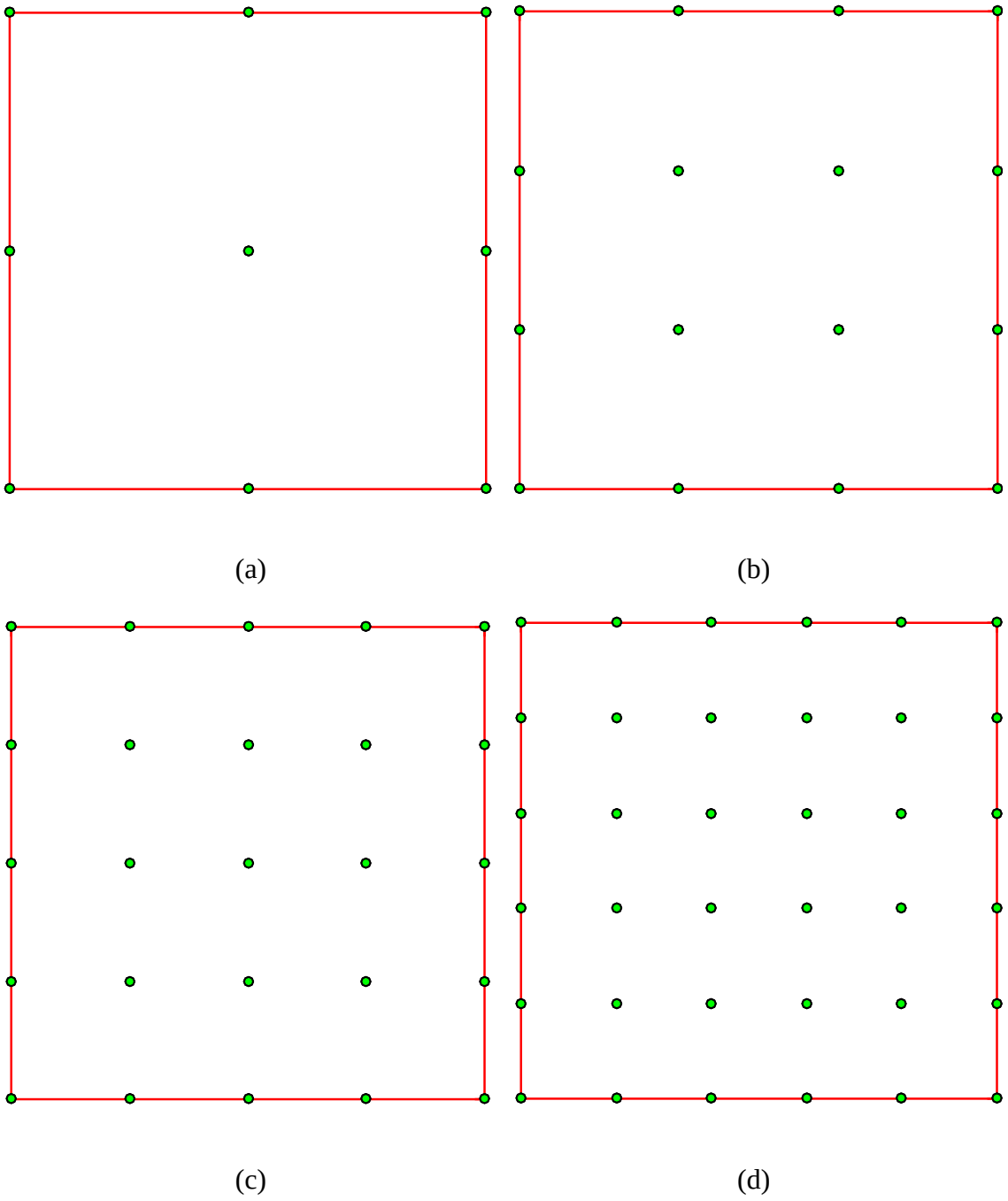

Figure 3.6 Mesh of the “pure” k-refinement for different orders of the basis function (a) $p = q = 2$; (b) $p = q = 3$; (c) $p = q = 4$; (d) $p = q = 5$.

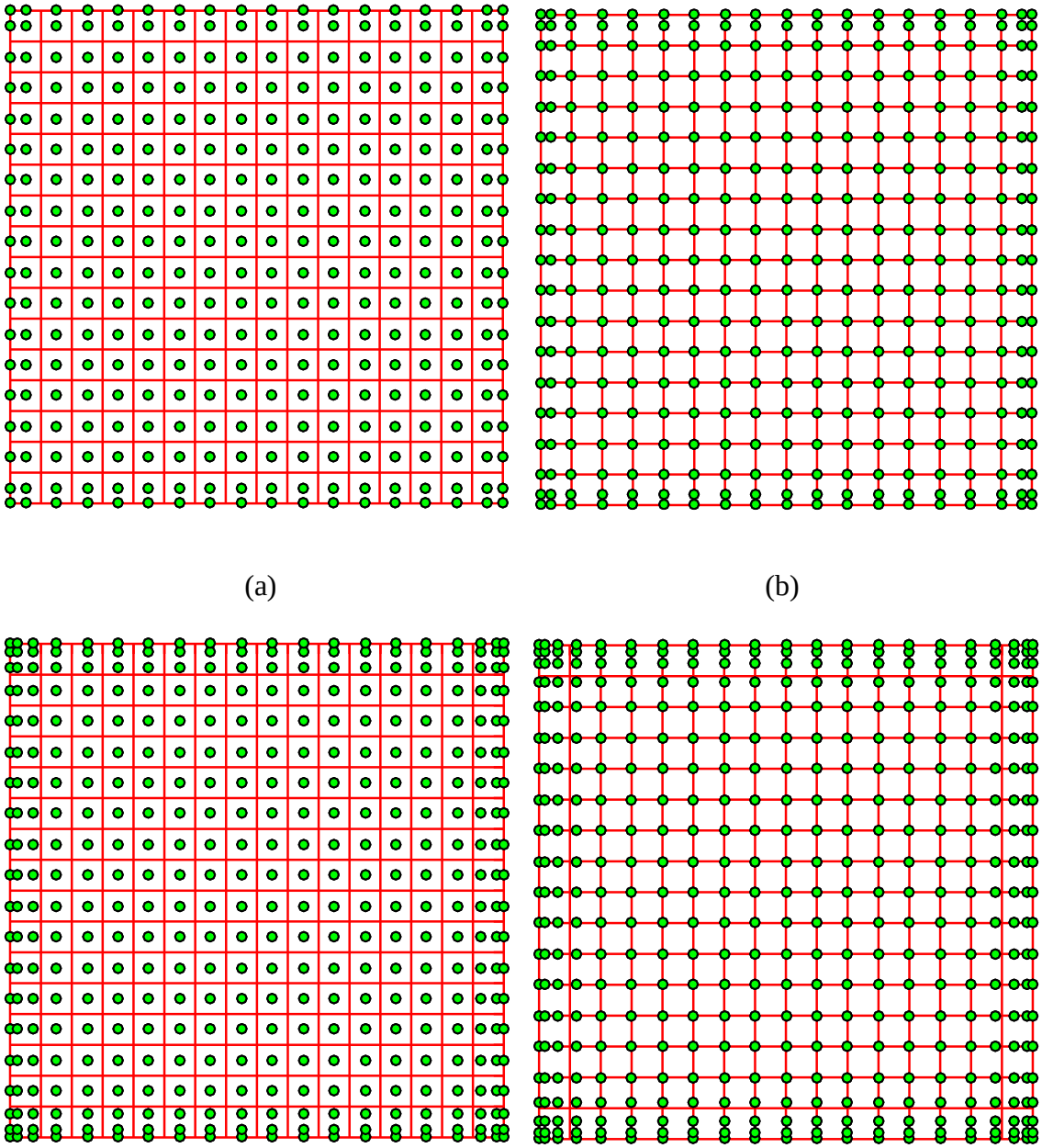

(a) (b)

(c) (d)

Figure 3.7 Mesh of different basis order of the k-refinement (a) $p = q = 2$; (b) $p = q = 3$; (c) $p = q = 4$; (d) $p = q = 5$

Table 3.4 Eigenvalues of different basis order with order 4 h-refinement

	Generalized isogeometric basis functions based K-L expansion	Analytical (Ana)

The basis order of the k-refinement	2	3	4	5	-
λ_1	2.18389	2.18368	2.18358	2.18352	2.18337
λ_2	0.40814	0.40802	0.40796	0.40792	0.40783
λ_3	0.40814	0.40802	0.40796	0.40792	0.40783
λ_4	0.13352	0.13341	0.13336	0.13333	0.13325
λ_5	0.13352	0.13341	0.13336	0.13333	0.13325
λ_6	0.07628	0.07623	0.07622	0.07621	0.07618

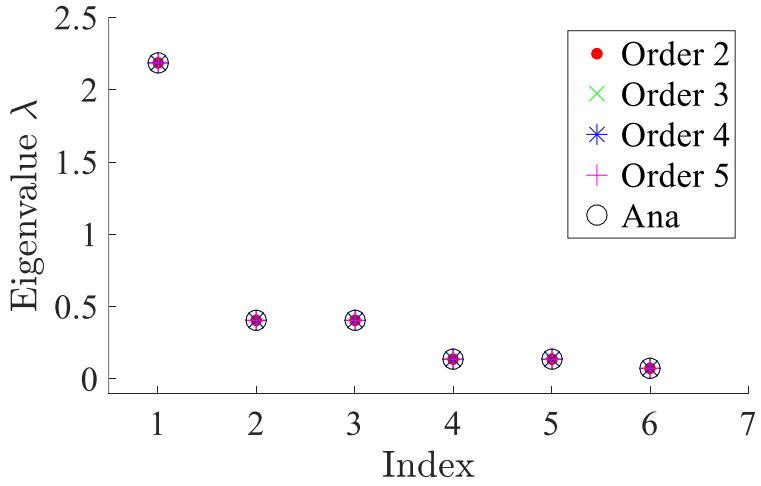

Figure 3.8 Eigenvalues of different basis order with order of the k-refinement

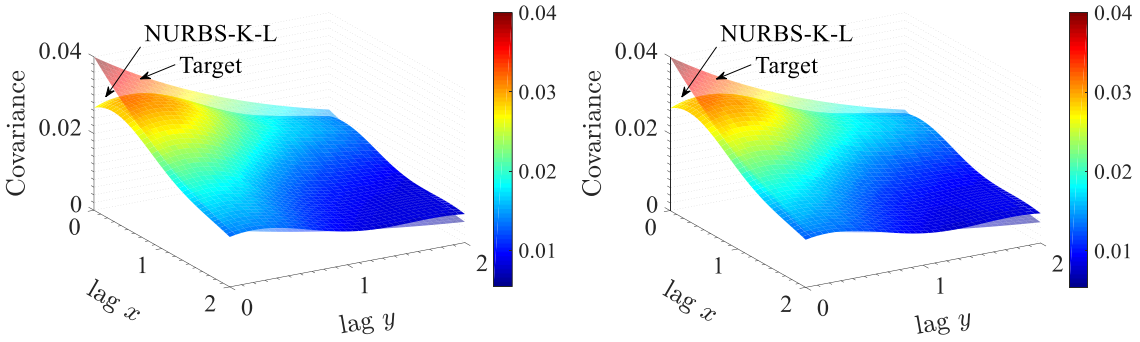

(a) (b)

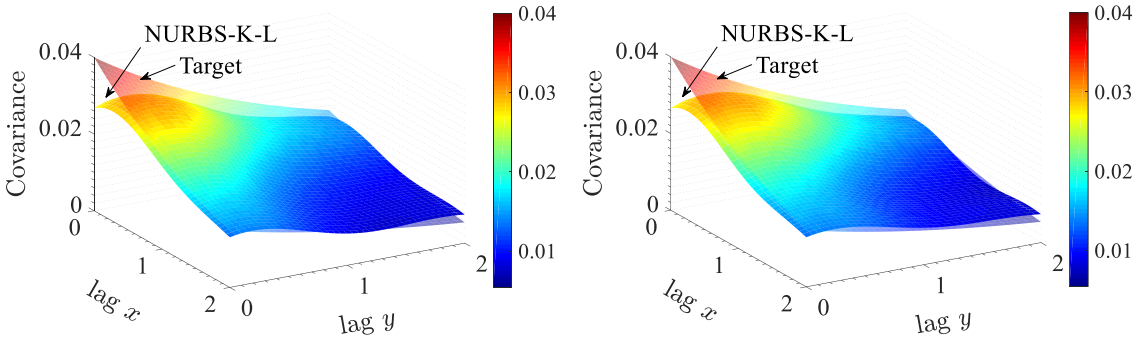

(c) (d)

Figure 3.9 Covariance function estimated by the proposed K-L expansion with 6 terms based on (a) $p = q = 2$; (b) $p = q = 3$; (c) $p = q = 4$; (d) $p = q = 5$ order of the k-refinement $lag(x) = | x_1 - x_2 |, lag(y) = | y_1 - y_2 |$

From Table 3.4, Figures 3.8 and Figure 3.9, it is evidently demonstrated that the convergence of the freshly proposed K-L expansion with 6 terms by using the k-refinement can be anticipated when the higher order basis functions are implemented.

Finally, the accuracy of the proposed K-L expansion is investigated. The analysis is based on the NURBS basis functions with order $p = q = 2$ and 5-order h-refinement. Different numbers of the proposed K-L expansion term are adopted to represent the random field. Also, the corresponding point-wise error estimator and mean variances are employed to epitomize the accuracy as shown in Figure 3.10. The point-wise estimator of the error variance is:

$$err(\boldsymbol{x}) = \frac{\mathrm{Var}[H(\boldsymbol{x},\theta) - H(\boldsymbol{x},\theta)]}{\mathrm{Var}[H(\boldsymbol{x})]} \tag{3.68}$$

and the mean variance (MV) can be formulated as:

$$\text{Mean variance} = \frac{\int_D err(\boldsymbol{x}) dD}{\int_D 1 dD} \tag{3.69}$$

From Figure 3.10, it can be observed that by increasing the number of terms used in the proposed K-L expansion, the point-wise error is also decreasing.

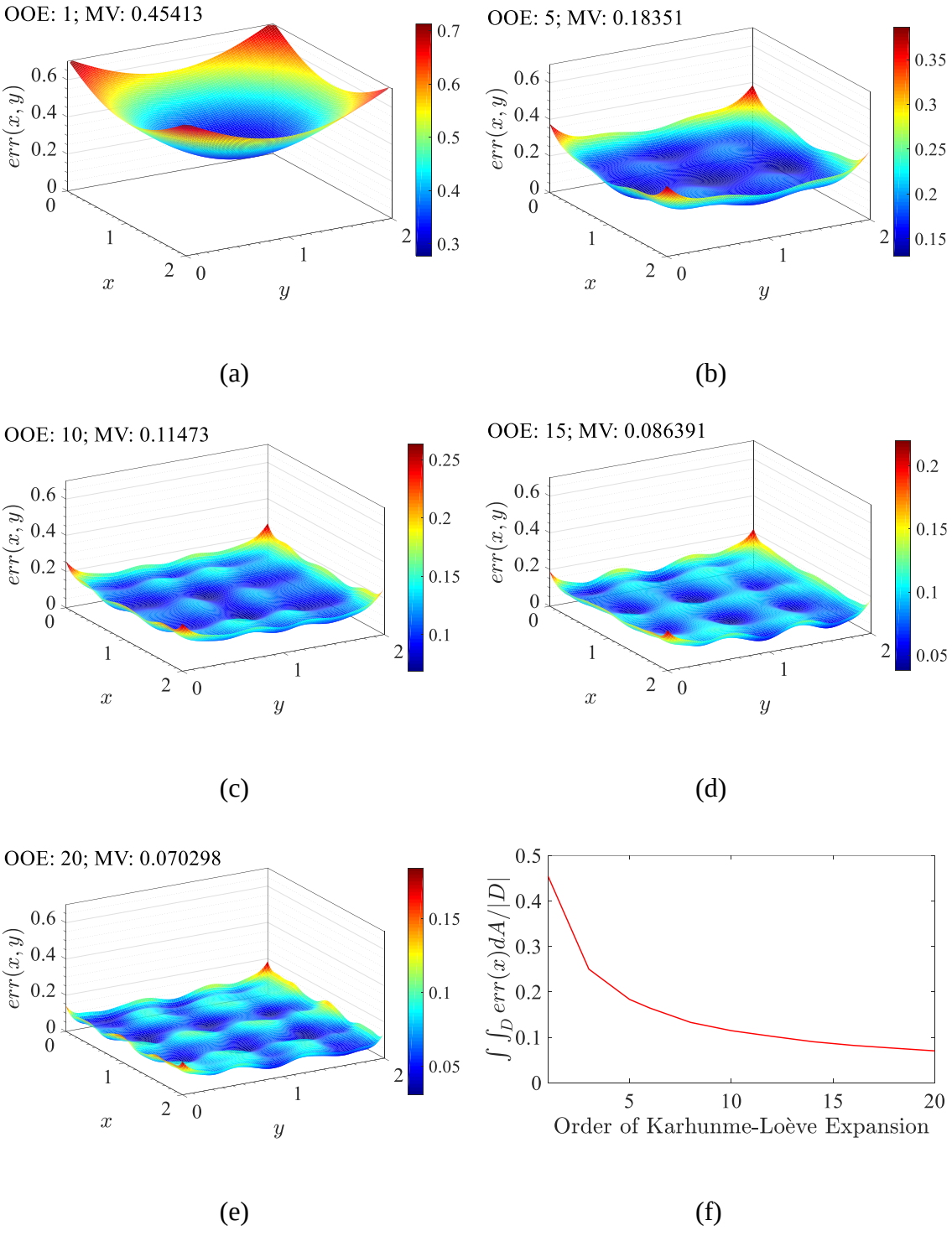

(a) (b)

(c) (d)

(e) (f)

Figure 3.10 (a)-(e) Point-wise estimator for variance error, represented for different number of SSIGA-K-L expansion terms; (f) Mean variance corresponding to different proposed K-L expansion terms.

The proposed generalized isogeometric basis functions based K-L expansion can represent random field geometry in a more proper way, and for some conic geometry (e.g., a random field with the geometry as shown in Figure 3.11), exact representations are accessible. Therefore, insufficient consideration of the stochastic parameter caused by the approximation of geometry can be eliminated at the coarsest level of geometry representation, and further the h- or k- refinement will not change the geometry anymore. Moreover, by increasing the order of the h- and k- refinement, all considered eigenvalues are converging to analytical solutions. In particular, the k-refinement can improve the accuracy of the eigenvalues when higher order basis function is adopted. The decomposition of the random field is hinged on the choice of the basis functions. The proposed K-L expansion can provide a higher continuity of the covariance function, so a smoother, yet adequate, representation of the random field can be accomplished.

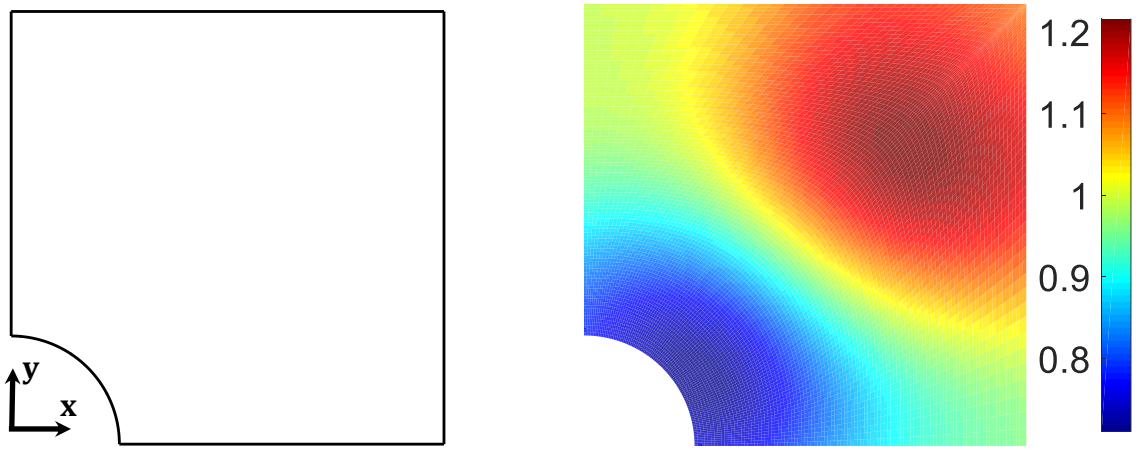

(a) (b)

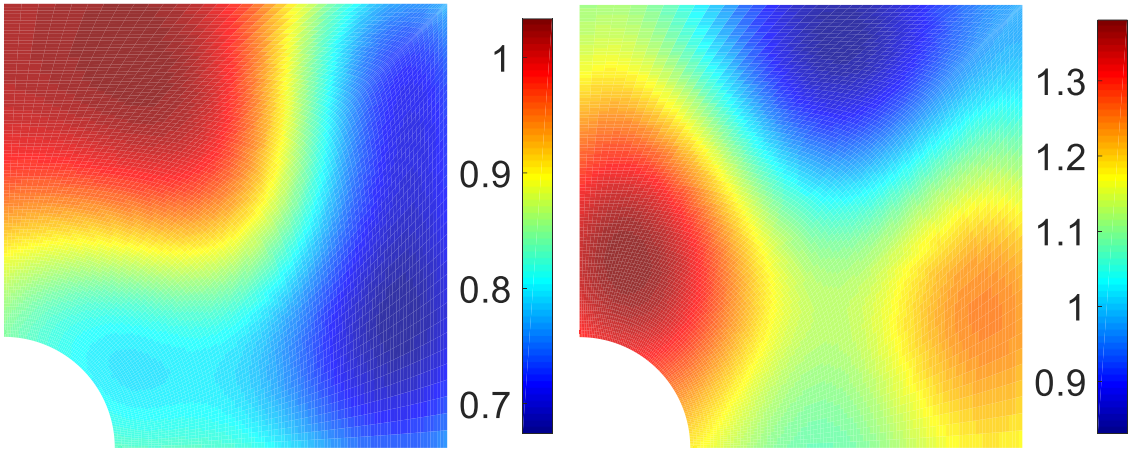

(c) (d)

Figure 3.11 (a) Physical domain and (b)-(d) possible normalized realizations of the random field of a square domain with a curved corner

3.5.2 Numerical example: circular ring Mindlin–Reissner plate

In the second numerical example, a circular ring-shape Mindlin-Reissner plate involving spatially dependent uncertain Young's modulus is investigated. As aforementioned, the Young's modulus is modelled as a Gaussian random field, with mean $\mu = 3\times10^7$, standard deviation $\sigma = 3\times10^6$. An exponential function is employed to describe the covariance of the Young's modulus,

$$C_{HH}(\mathbf{x},\mathbf{x}') = \sigma^2 \exp\left(-\frac{|x_1 - x_2|}{l_x} - \frac{|y_1 - y_2|}{l_y}\right) \tag{3.70}$$

where $l_x = l_y = 2$ denote the correlation lengths in the *x*- and *y*-direction respectively. The general structural layout of the investigated circular ring plate is presented in Figure 3.12 and a normalized possible realization of the random field is presented in Figure 3.13.

For the structure member shown in Figure 3.12, the thickness of the plate is 1.2, the inner radius is 2 and the outer radius is 4. The plate is subjected to a uniformly distributed

load with magnitude of $q = 1 \times 10^3$ and both left and right edges of the plate, as indicated in Figure 3.12(a), are clamped. In this example, a two-dimensional NURBS basis functions is implemented. The two parametric directions, ξ and η, are selected which are corresponding to the radial and circumferential directions, respectively. The corresponding polynomial orders and knot vector of the initial geometry are given in Table 5, and the control points are presented in Table 3.6

The coarsest mesh is plotted as Figure 3.14(a). In this case, in order to obtain a mesh with sufficient convergence for further analysis, the coarsest mesh is h-refined with order 3, 4, 5 for both directions as shown in Figure 3.14 (b)-(d). Meanwhile, ABAQUS based finite element analysis with different structural meshes are also implemented as comparisons, whose meshes are plotted in Figure 3.15.

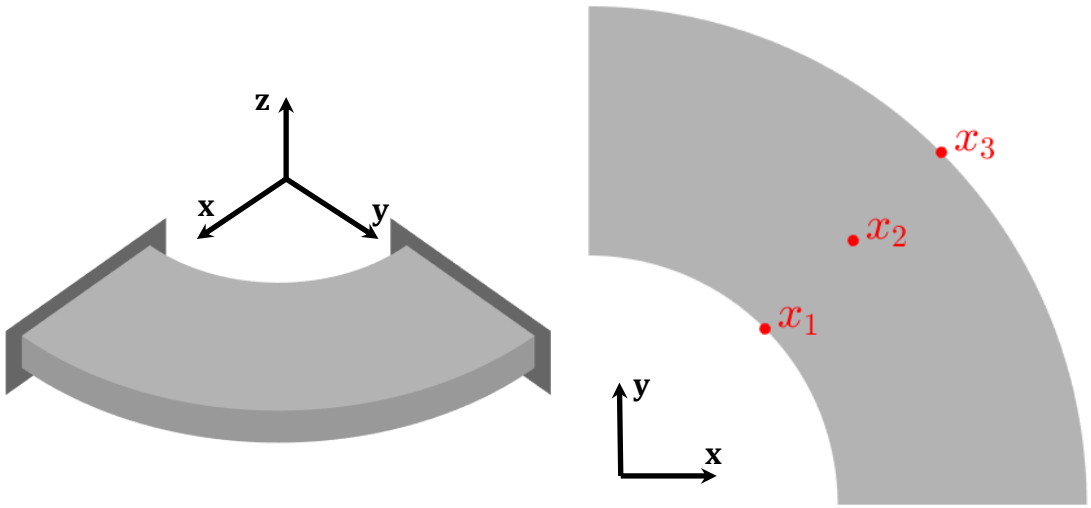

(a) (b)

Figure 3.12 Circular ring plate structural layout (a) three-dimensional view; (b) top View;

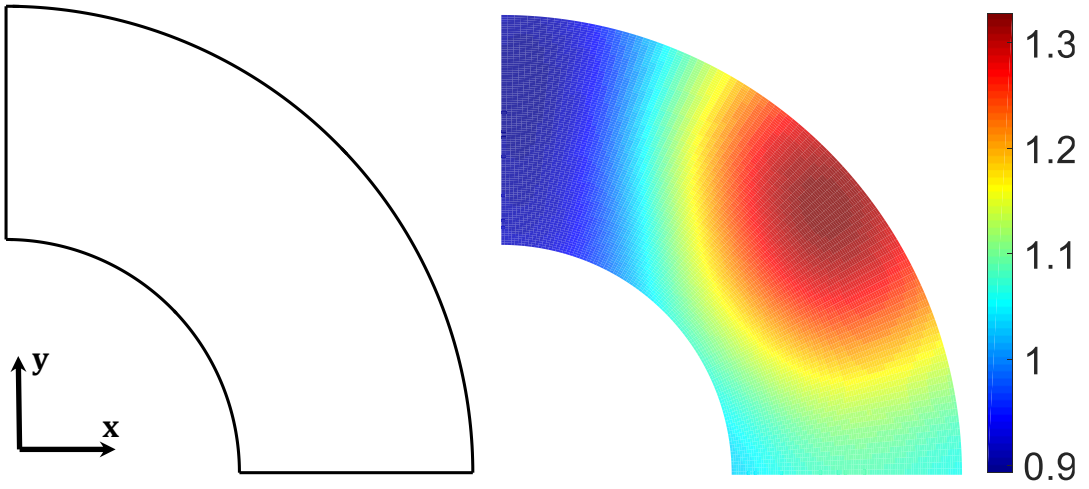

(a) (b)

Figure 3.13 (a) Physical domain and (b) a possible normalized realization of random field with circular ring geometry

Table 3.5 The polynomial orders and knot vectors of the circular ring plate

Direction	Order	Knot Vector
ξ	$p=2$	$\Xi=\{0,0,0,1,1,1\}$
η	$q=2$	$\mathrm{H}=\{0,0,0,1,1,1\}$

Table 3.6 The control points of the circular ring plate

i	j	$B_{i,j}$	$w_{i,j}$
1	1	(2, 0)	1
1	2	(2, 2)	$1/\sqrt{2}$
1	3	(0, 2)	1
2	1	(3, 0)	1
2	2	(3, 3)	$1/\sqrt{2}$

2	3	(0, 3)	1
3	1	(4, 0)	1
3	2	(4, 4)	$1/\sqrt{2}$
3	3	(0, 4)	1

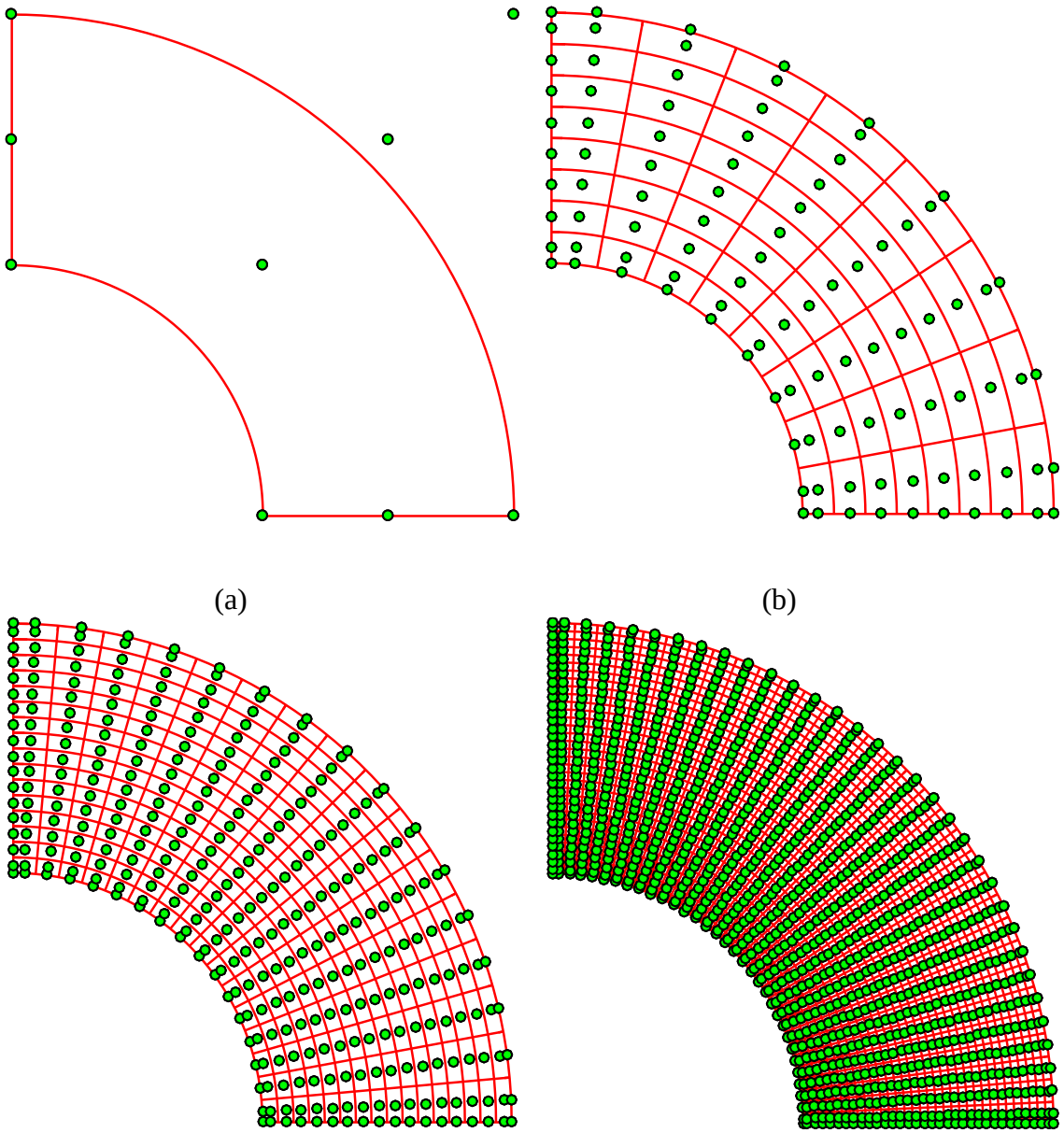

Figure 3.14 Circular ring plate meshes. (a) Coarsest mesh; (b) 3-order h-refinement mesh; (c) 4-order h-refinement mesh; (d) 5-order h-refinement mesh.

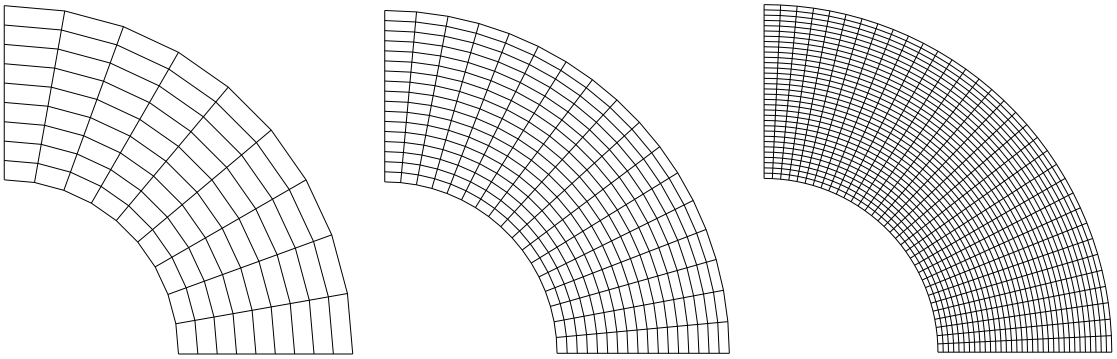

(a) (b) (c)

Figure 3.15 ABAQUS based FEM meshes with (a) 10×10; (b) 18×18; (c) 34×34 control number

Table 3.7 compares the displacement of the point $x_3\,(4/\sqrt{2},4/\sqrt{2})$, which is the midpoint at outer edge, obtained from different meshes of IGA and FEM with corresponding control points (nodes) and knot spans (elements) information being outlined in Table 3.7.

Table 3.7 Comparisons of deflection ω at point x_3 between IGA and FEM

Method	Number of Control Points/Nodes	Number of Knot Spans/Elements	Deflection ω at point x_3
IGA	100	64	9.19267e-04
	324	256	9.20752e-04
	1156	1024	9.20939e-04
FEM	100	81	8.90099e-04
	324	289	9.12210e-04
	1156	1089	9.18648e-04
	1002001	1000000	9.21002e-04

According to Table 3.7, IGA based Mindlin plate analysis is applicable and shows good convergence rate when comparing with the FEM. Within the analysis framework of IGA, relatively fewer amounts of control points are possible to adequately solve a linear system to satisfy specific precision requirement so the size of the stiffness matrix of IGA will also be relatively smaller. Generally, the polynomial chaos expansion based stochastic analysis framework enlarges the deterministic stiffness matrix significantly. For example, when adopting four terms in the traditional K-L expansion and 4-order PCE, the stiffness matrix will be enlarged by 70 times along each dimension. Since IGA is possible to result a deterministic stiffness matrix with relatively smaller size in this particular example, the computational tractability of SSIGA can be further maintained after the Galerkin process. In this example, a 5-order h-refinement is adopted for the generalized isogeometric basis functions based K-L expansion in both directions.

Within the proposed SSIGA analysis framework, the Gaussian random field is decomposed by the proposed K-L expansion with four terms and all concerned structural responses are estimated by three types of PCE, namely 2-order PCE, 3-order PCE, and 4-order PCE. Moreover, due to the unavailability of analytical solutions of the statistical characteristics of the concerned structural responses, the Monte-Carlo Simulation (MCS) with 100,000 simulation cycles were adopted for partially verifying the results of SSIGA.

Figure 3.16-3.18 show the means and standard deviations of U_i, θ_{xi}, θ_{yi} of all presented control points determined by both the SSIGA with different PCE orders and MCS approaches. By closely examining Figures 3.16-3.18, a fairly well agreement between the proposed SSIGA and MCS approaches can be observed for both the means and standard deviations of the structural deformations of all control points.

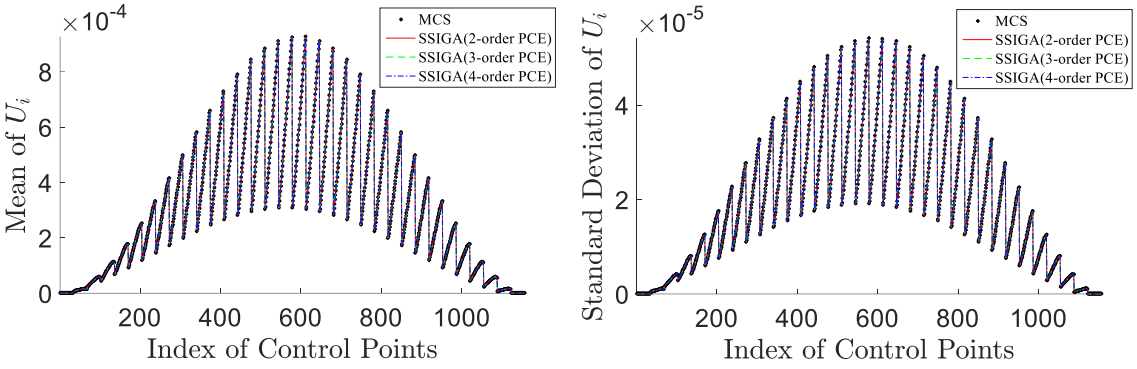

(a) (b)

Figure 3.16 Comparison of (a) means and (b) standard deviations of U_i of control points between SSIGA and MCS approaches

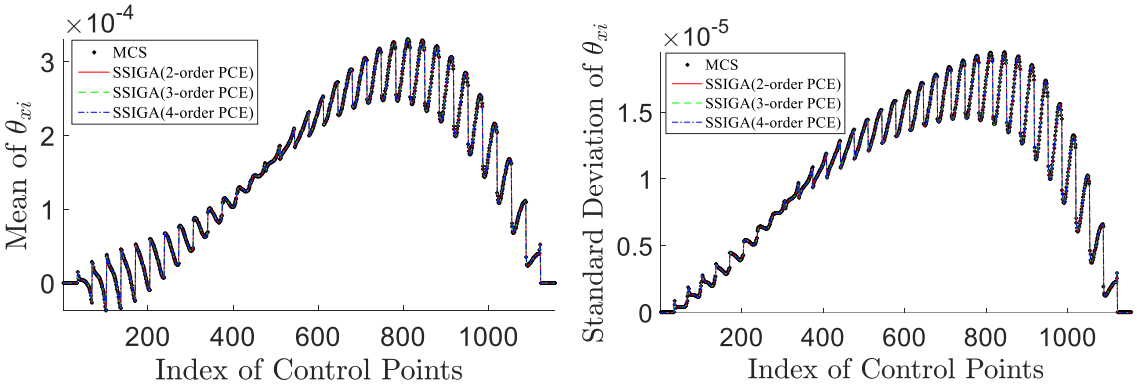

(a) (b)

Figure 3.17 Comparison of (a) means and (b) standard deviations of θ_{xi} of control points between SSIGA and MCS approaches

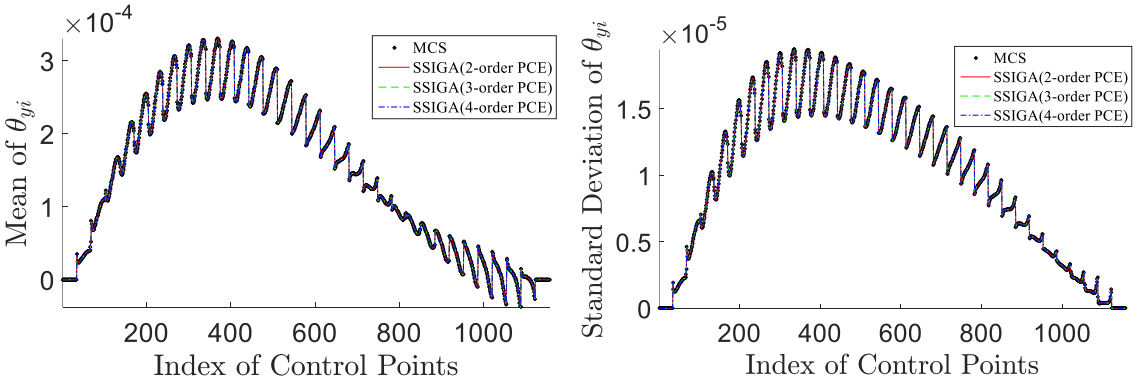

(a) (b)

Figure 3.18 Comparison of (a) means and (b) standard deviations of θ_{yi} of control points between SSIGA and MCS approaches

Moreover, since the control points are not interpolated on the plate, three physical points on the plate with coordinates, $x_1(2/\sqrt{2}, 2/\sqrt{2})$, $x_2(3/\sqrt{2}, 3/\sqrt{2})$ and $x_3(4/\sqrt{2}, 4/\sqrt{2})$, are selected for further investigation.

Once again, by implementing the SSIGA and MCS with 100,000 simulations, the means and standard deviations of the concerned structural responses (i.e., deflection ω_i, rotation θ_{xi}, strain ε_{xi}, stress σ_{xi}, i = 1, 2, 3) of the three selected physical points are calculated and the corresponding results are shown in Figures 3.19-3.22. Furthermore, Table 3.8-3.11 report the maximum and minimum relative errors of the means and standard deviations of the considered structural responses of the three selected physical points between the SSIGA and MCS approaches. From both illustrative figures and numeric tables, excellent agreements of the means and standard deviations of the three selected points between SSIGA and MCS approaches can be clearly observed. Therefore, the accuracy of the proposed SSIGA on the determination of the first two moments of statistics of the structural responses is evidently demonstrated.

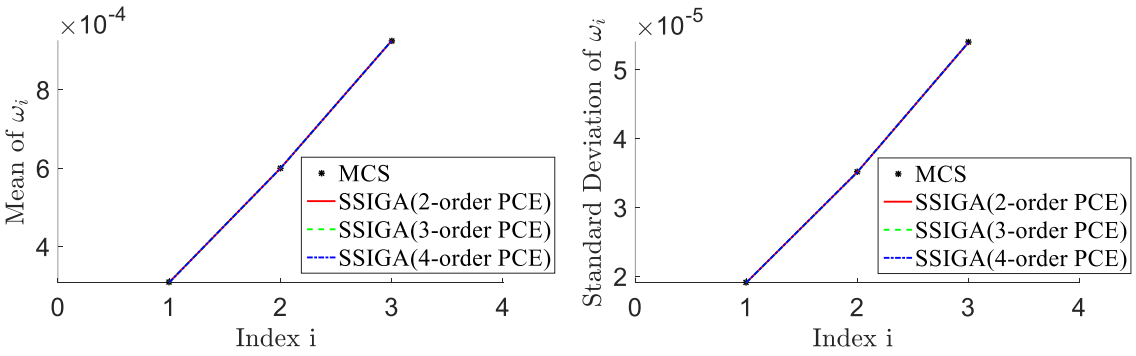

(a) (b)

Figure 3.19 Comparison of (a) means and (b) standard deviations of the deflection ω_i between SSIGA and MCS approaches

Table 3.8 Relative difference of the means and standard deviations of the deflection ω_i between SSIGA and MCS approaches

Relative Difference of ω_i	Mean		Standard deviation	
	Max (%)	Min (%)	Max (%)	Min (%)
SSIGA(2-order PCE)	2.9309604e-02	2.4825263e-02	3.3606602e-01	3.1238819e-01
SSIGA(3-order PCE)	2.9309604e-02	2.4825263e-02	2.9947100e-01	2.8464993e-01
SSIGA(4-order PCE)	2.9309604e-02	2.4825263e-02	2.9947100e-01	2.8464993e-01

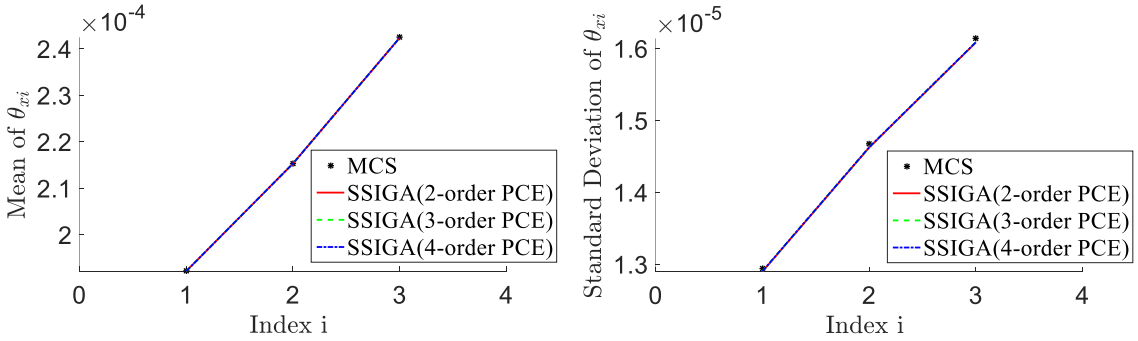

(a) (b)

Figure 3.20 Comparison of (a) means and (b) standard deviations of rotation θ_{xi} between SSIGA and MCS approaches

Table 3.9 Relative difference of the means and standard deviations of the rotation θ_{xi} between SSIGA and MCS approaches

Relative Difference of θ_{xi}	Mean		Standard deviation	
	Max (%)	Min (%)	Max (%)	Min (%)
SSIGA(2-order PCE)	2.3829029e-02	2.1380565e-02	3.2917076e-01	3.2475204e-01
SSIGA(3-order PCE)	2.3829029e-02	2.1380565e-02	2.9818244e-01	2.9575506e-01
SSIGA(4-order PCE)	2.3829029e-02	2.1380565e-02	2.9818244e-01	2.9575506e-01

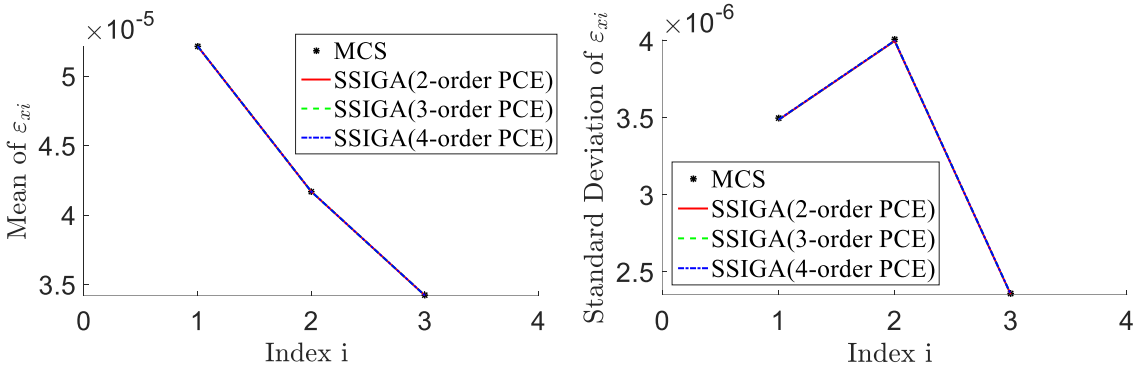

(a) (b)

Figure 3.21 Comparison of (a) means and (b) standard deviations of the strain ε_{xi} between SSIGA and MCS approaches

Table 3.10 Relative difference of the means and standard deviations of the strain ε_{xi} between SSIGA and MCS approaches

Relative Difference of ε_{xi}	Mean		Standard deviation	
	Max (%)	Min (%)	Max (%)	Min (%)
SSIGA(2-order PCE)	3.0644336e-02	2.5289660e-02	2.9219806e-01	1.9574417e-01
SSIGA(3-order PCE)	3.0644336e-02	2.5289660e-02	2.5788016e-01	1.4832411e-01
SSIGA(4-order PCE)	3.0644336e-02	2.5289660e-02	2.5788016e-01	1.4832411e-01

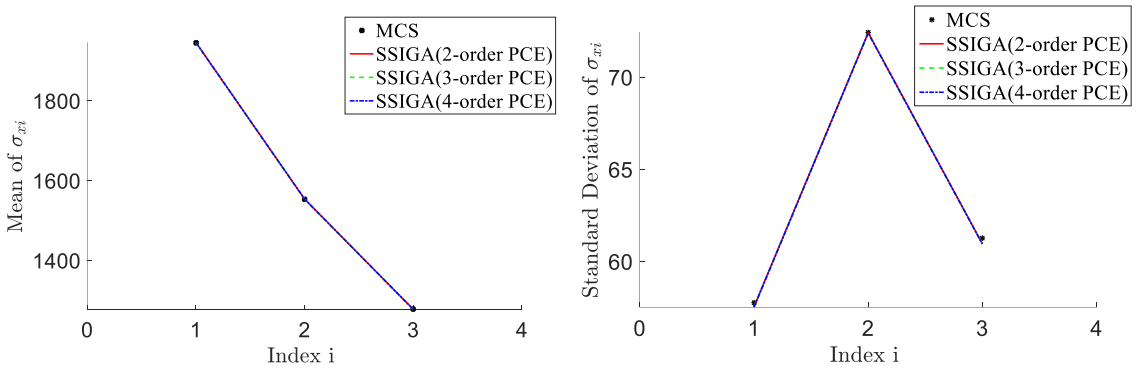

(a) (b)

Figure 3.22 Comparison of (a) means and (b) standard deviations of the stress σ_{xi} between SSIGA and MCS approaches

Table 3.11 Relative difference of the means and standard deviations of the stress σ_{xi} between SSIGA and MCS approaches

Relative Difference of σ_{xi}	Mean		Standard deviation	
	Max (%)	Min (%)	Max (%)	Min (%)
SSIGA(2-order PCE)	6.3440741e-03	2.2965962e-04	4.9125830e-01	3.6745915e-02
SSIGA(3-order PCE)	6.3440741e-03	2.2965962e-04	5.0268595e-01	6.2972845e-02
SSIGA(4-order PCE)	6.3440741e-03	2.2965962e-04	5.0268595e-01	6.2972845e-02

In addition to the validation of the proposed SSIGA approach on the determination of the first two statistical moments of some selected structural responses, the SSIGA approach is further implemented for estimating the PDFs and CDFs of the structural responses. Within the scheme of the proposed SSIGA, 100,000 samples were generated after applying the proposed K-L expansion on the inputs and the PCE on the outputs to effectively establish the PDFs and CDFs. Once again, the MCS approach is employed for verification purposes. With this part of investigation, all PDFs and CDFs of the concerned structural responses were established by implementing a non-parametric statistical inference technique known as the kernel density estimation approach. For this particular part of investigation, the physical point $\mathrm{x}_2(3/\sqrt{2},3/\sqrt{2})$ is selected again, and the PDFs and CDFs of the deflection ω, rotation θ_x, strain ε_x, and stress σ_x at point x_2 are established and reported in Figures 3.23, 3.25, 3.27, and 3.29, respectively. Moreover, in

order to quantitatively measure the differences of CDFs between the SSIGA approach and MCS with 100,000 calculations, the relative errors between the two computational methods of each considered structural responses are also presented in Figures 3.24, 3.26, 3.28, and 3.30. From the information presented in Figures 3.23-3.30, it is evidently illustrated that the proposed SSIGA approach is adequate for establishing the PDF and CDF of any concerned structural response. Also, another important point can be realized from this exercise is that when the order of the PCE is increased, the relative errors are also reduced.

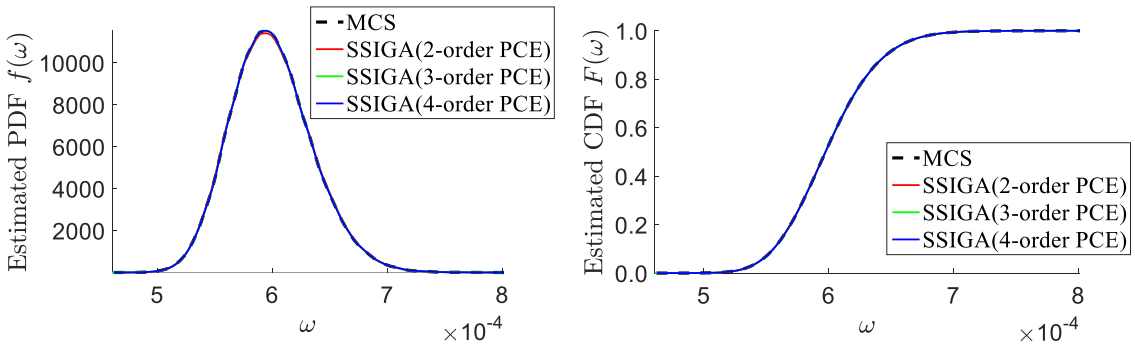

(a) (b)

Figure 3.23 Estimated (a) PDF and (b) CDF of the deflection ω at point x_2

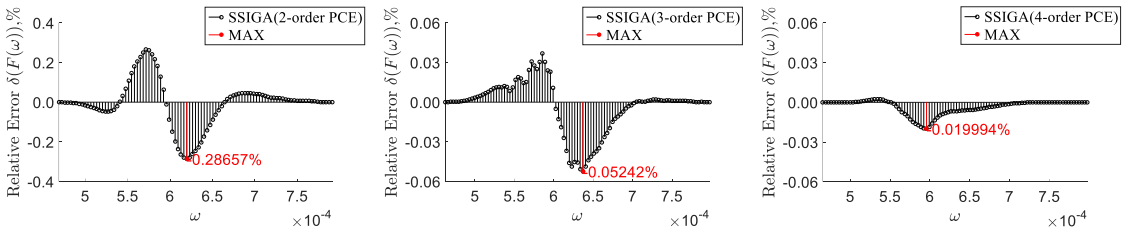

(a) (b) (c)

Figure 3.24 Relative error of the estimated CDF of ω between SSIGA and MCS (a) 2-order PCE (b) 3-order PCE and (c) 4-order PCE

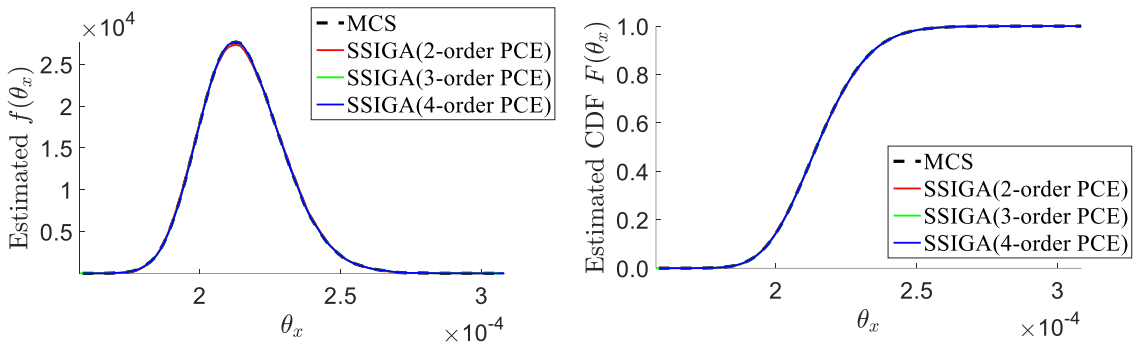

(a) (b)

Figure 3.25 Estimated (a) PDF and (b) CDF of the rotation θ_x at point x_2

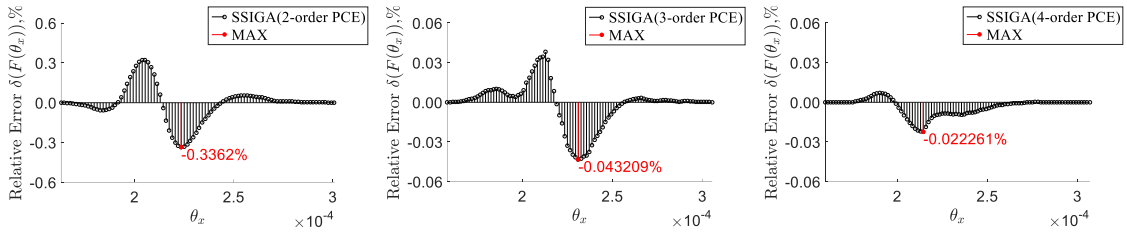

(a) (b) (c)

Figure 3.26 Relative error of the estimated CDF of θ_x between SSIGA and MCS (a) 2-order PCE (b) 3-order PCE and (c) 4-order PCE

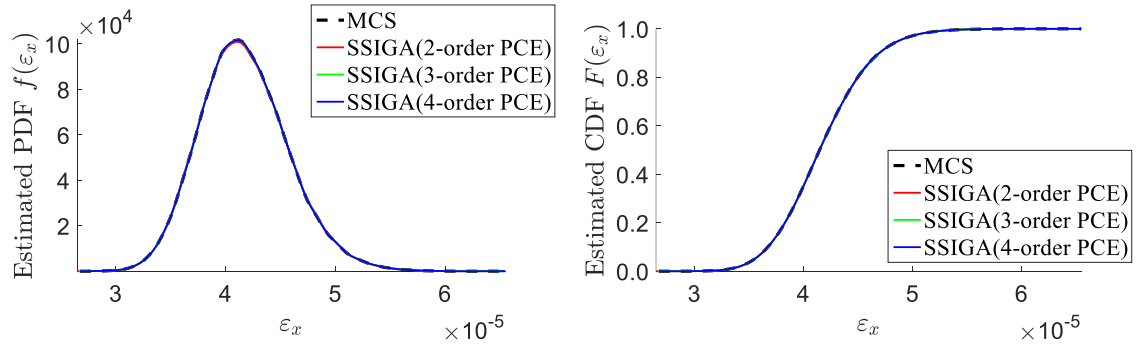

(a) (b)

Figure 3.27 Estimated (a) PDF and (b) CDF of the strain ε_x s at point x_2

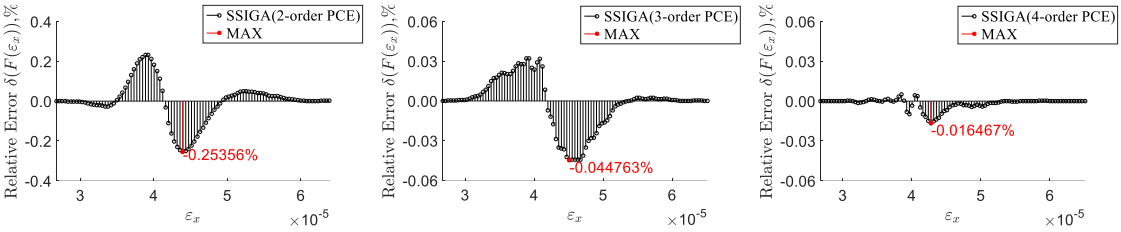

(a) (b) (c)

Figure 3.28 Relative error of the estimated CDF of ε_x between SSIGA and MCS (a) 2-order PCE (b) 3-order PCE and (c) 4-order PCE

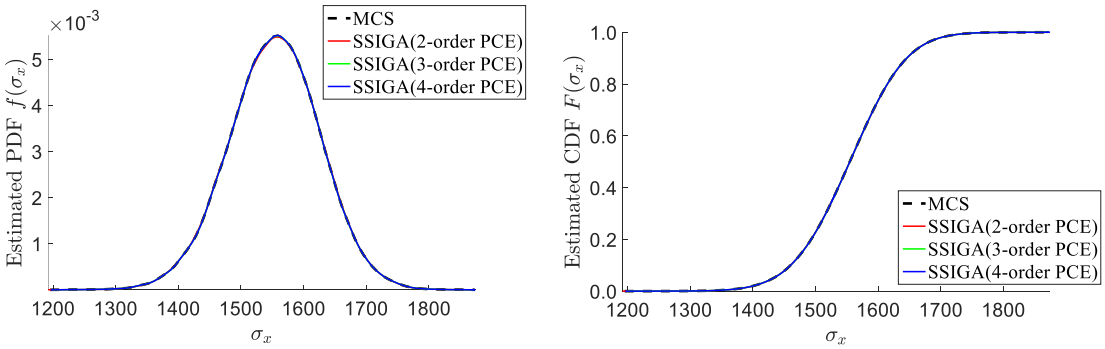

(a) (b)

Figure 3.29 Estimated (a) PDF and (b) CDF of the stress σ_x at point x_2

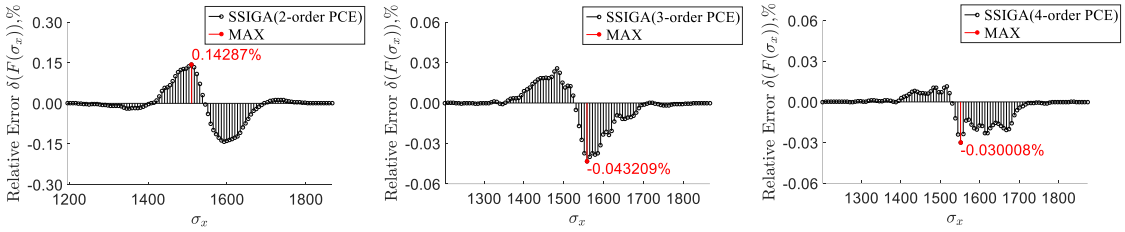

(a) (b) (c)

Figure 3.30 Relative error of the estimated CDF of σ_x between SSIGA and MCS (a) 2-order PCE (b) 3-order PCE and (c) 4-order PCE

3.5.3 Numerical example: torpedo-shape Kirchhoff-Love shell

In order to further explore the applicability of the proposed SSIGA approach for stochastic system with complex geometry, a torpedo-shape shell is investigated. The general structural layout is depicted in Figure 3.31. The spatially dependent uncertain Young's modulus of the shell is modelled as a Gaussian random field, which has mean $\mu = 3\times10^7$, standard deviation $\sigma = 3\times10^6$ and the covariance function as:

$$C_{HH}(\mathbf{x},\mathbf{x}') = \sigma^2 \cdot e^{-\frac{|x-x'|}{l_x}} \cdot e^{-\frac{|y-y'|}{l_y}} \cdot e^{-\frac{|z-z'|}{l_z}} \tag{3.71}$$

where $l_x = l_y = l_z = 50$ denote the correlation lengths in *x*-, y-, and *z*-direction respectively.

The structure showed in Figure 3.31 is modelled by T-spline, and it is investigated underneath the Kirchhoff-Love shell theory (Kiendl *et al.*, 2009). Without loss of generality, a unit thickness is assumed in this particular example. A uniformly distributed load with magnitude of $q = 1\times10^3$ is applied on the structure surface along the positive direction of z-axis.

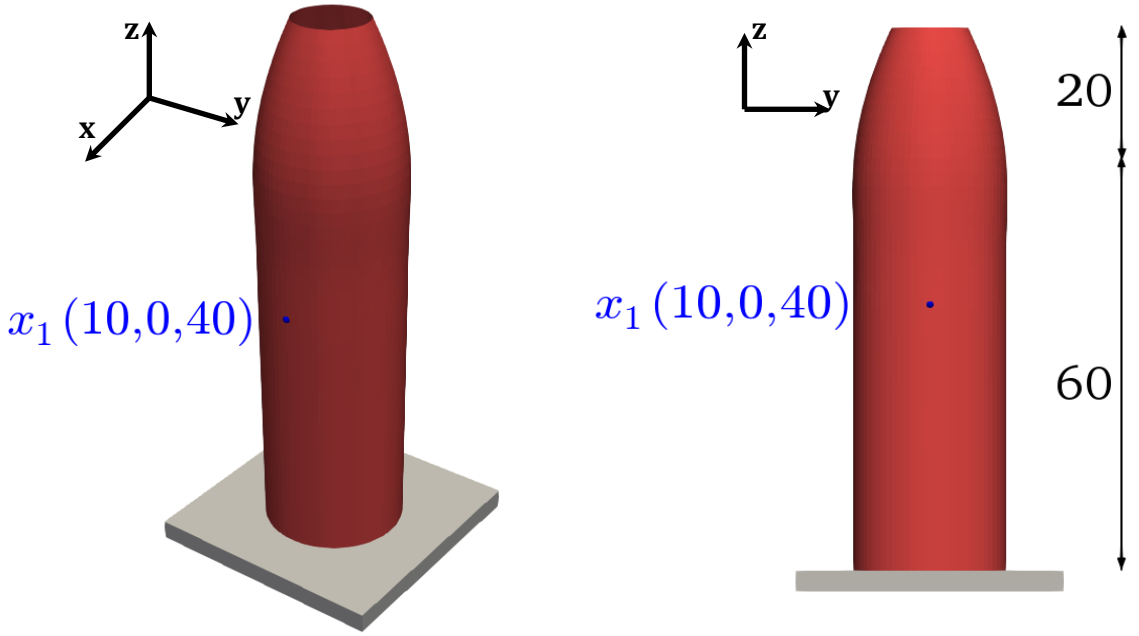

(a) (b)

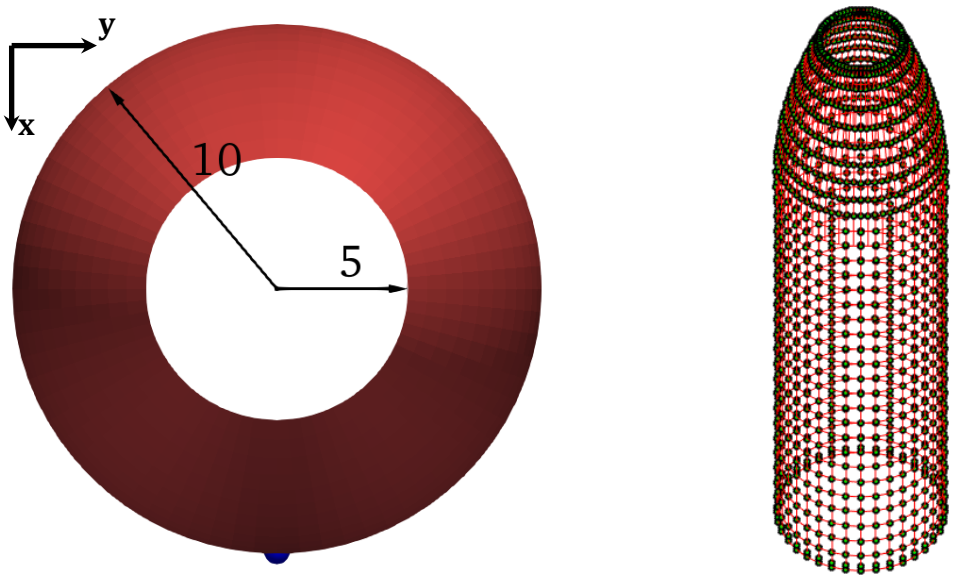

(c) (d)

Figure 3.31 Structural layout of torpedo-shape shell (a) 3D view, (b) front view, (c) top view, (d) T-Splines Mesh

Within the analysis framework offered by the SSIGA, the Gaussian random field of the Young's modulus is decomposed by the 4-term generalized isogeometric basis functions based K-L expansion, and a 5-order PCE is implemented for estimating all concerned stochastic structural responses in this case. Once again, the MCS with 100,000 simulations is employed for the purpose of partial result verification.

In this example, a physical point $x_1(10,0,40)$ on the shell is analysed directly. By utilizing the SSIGA and MCS with 100,000 simulations, the first two statistical moments of u_z, ε_z^b and m_z of the considered physical point is determined and the results are reported in Table 3.12-3.14, respectively. In order to quantitatively assess the performance of the SSIGA approach, absolute relative errors, which are compared with the results of the MCS with 100,000 simulations, are also calculated and reported in each table for u_z, ε_z^b, and m_z. As evidently illustrated in Tables 3.12-3.14, the means and

standard deviations of the considered physical point obtained by the SSIGA are having excellent agreement with the MCS approach.

Table 3.12 Means, standard deviations and absolute relative error of u_z between MCS and SSIGA

u_z	Mean	Standard deviation
SSIGA (5-order PCE)	7.6150000e-02	6.3825000e-03
MCS	7.6143375e-02	6.3533808e-03
Absolute Relative Error (%)	8.6997718e-03	4.5832494e-01

Table 3.13 Relative difference of the means and standard deviations of ε_z^b between MCS and SSIGA

ε_z^b	Mean	Standard deviation
SSIGA (5-order PCE)	-3.4540000e-05	6.4657000e-06
MCS	-3.4534706e-05	6.4712063e-06
Absolute Relative Error (%)	1.5327267e-02	8.5090745e-02

Table 3.14 Relative difference of the means and standard deviations of m_z between MCS and SSIGA

m_z	Mean	Standard deviation
SSIGA (5-order PCE)	-45.3080000	6.9262000
MCS	-45.3025557	6.9278478
Absolute Relative Error (%)	1.2017569e-02	2.3786305e-02

In addition to the determinations of the means and standard deviations of the concerned structural responses, the PDFs and CDFs of the structural responses at point $x_1(10,0,40)$ is established by utilizing the SSIGA and the results are also verified by comparing with the MCS with 100,000 simulations. The PDFs and CDFs of the concerned structural responses at point $x_1(10,0,40)$ are systematically established as shown in Figures 31-33. Particularly, the relative errors of the CDFs of the concerned structural responses are also reported in Figures 3.32-3.34.

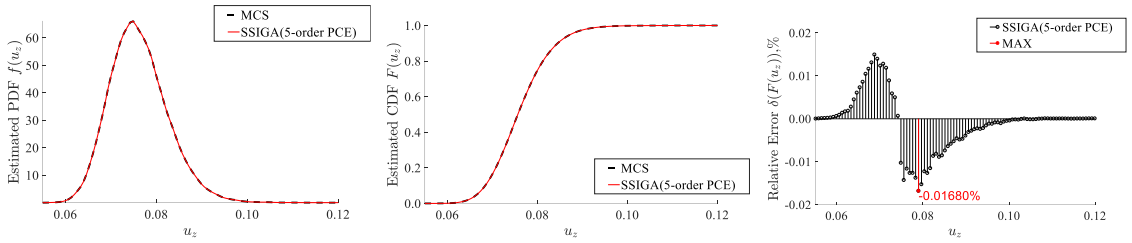

(a) (b) (c)

Figure 3.32 Estimated (a) PDF, (b) CDF and (c) relative errors of CDF of u_z at point x_1

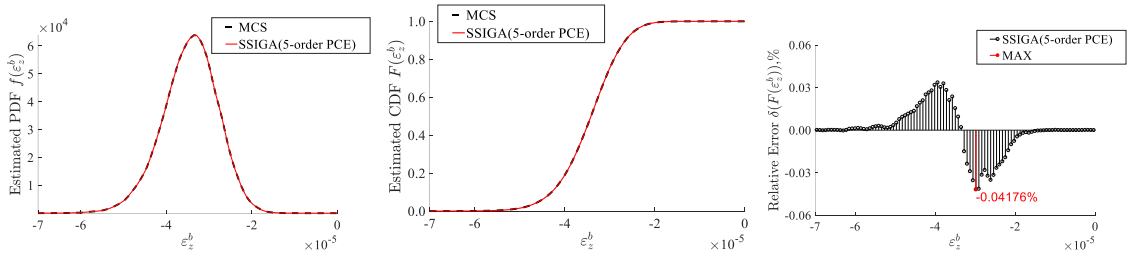

(a) (b) (c)

Figure 3.33 Estimated (a) PDF, (b) CDF and (c) relative errors of CDF of ε_z^b at point x_1

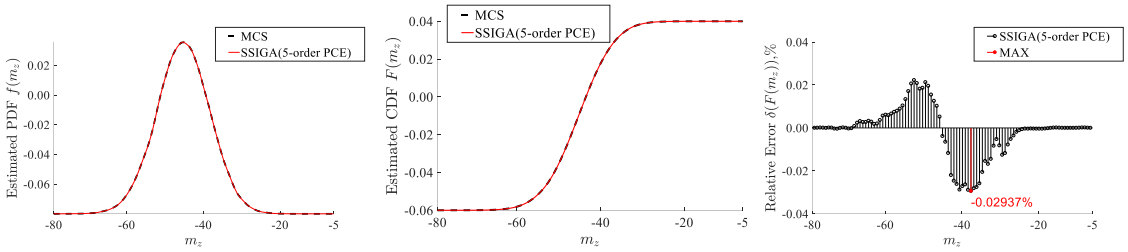

(a) (b) (c)

Figure 3.34 Estimated (a) PDF, (b) CDF and (c) relative errors of CDF of m_z at point x_1

From the quantitative assessment on the relative errors between the SSIGA and MCS approaches, the maximum relative errors between SSIGA results and MCS results are less than 0.05%, which is small enough to prove the accuracy and applicability of the proposed SSIGA scheme for stochastic analysis of engineering structures with irregular geometries.

Furthermore, the results of the MCS approach was obtained by running at ten nodes on a cluster, with each nodes has 2×8 cores (Intel Xeon E5-2670 (Sandy Bridge) 2.6GHz), namely 160 cores in total. The MCS with 100,000 simulations were executed by parallel computing with 160 workers on MATLAB 2016b at the cluster and costed 7 hours 7 mins 50 seconds. On the other hand, all results of the SSIGA approach was obtained by running at a node on a cluster with 2×14 cores (Intel Xeon Broadwell technology, 2.6 GHz). However, parallel computing was not implemented in the calculation of the SSIGA approach. The total computational time of SSIGA approach, which includes both the determinations of the means and standard deviations of the structural responses of the selected point and the establishments of the PDFs and CDFs presented in Figures 3.32-3.34, was 5 hours 43 mins 0 seconds. Therefore, based on the reported technical information, the proposed SSIGA approach certainly shows superior

computational efficiency over the exhaustively simulative MCS approach for a torpedo-shape shell structure which suffers from both spatially dependent uncertainties and irregular geometry.

3.6 Conclusion

Spectral Stochastic Isogeometric Analysis (SSIGA), as a significant extension of the Spectral Stochastic Analysis, is thoroughly investigated in this paper for the first time. Within the proposed SSIGA analysis framework, a generalized isogeometric basis functions based Karhunen-Loève expansion approach is firstly proposed to spectrally decompose the input random fields. Subsequently, by employing the polynomial chaos expansion, the statistical characteristics of any concerned structural responses can be adequately estimated. In addition, by combining with the non-parametric statistical inference techniques (e.g., the kernel density estimation approach), the PDFs and CDFs of any concerned structural responses can be robustly established. Consequently, the proposed SSIGA approach provides an integrated, yet physically valid, stochastic analysis framework for engineering structures that are suffering from both inevitable spatially dependent uncertainties and complex geometries. By comprehensively investigating three distinctive numerical examples, the applicability, accuracy, and efficiency of the SSIGA approach are evidently illustrated.

Chapter 4

SPECTRAL STOCHASTIC STOCAHSTIC ISOGEOMETRIC ANALYSIS FOR STATIC RESPONSE OF FGM PLATE

4.1 Summary

In this chapter, the nondeterministic structural responses of functionally graded material (FGM) plates under static loads with uncertain material property is investigated. The considered spatially dependent uncertainties are modelled as random fields with Gaussian distribution. A novel spectral stochastic isogeometric analysis (SSIGA) framework is proposed for such uncertainty quantification through the first-order shear deformation theory.

The Chapter 4 is structured as follows. The deterministic static analysis of FGM plate through IGA is presented in Section 4.3. After that, the proposed SSIGA approach is introduced in Section 4.4. Subsequently, two numerical examples are investigated in Section 4.5 to illustrate the effectiveness and efficiency of the SSIGA approach. Finally, the conclusion is drawn in Section 4.6.

The research work developed in Chapter 4 has produced one journal paper which has been published in *Thin-Walled Structures*, detailed as:

Li, K., Wu, D. and Gao, W., 2018. Spectral stochastic isogeometric analysis for static response of FGM plate with material uncertainty. *Thin-Walled Structures*, 132, pp.504-521.

4.2 Introduction

A novel computational stochastic analysis framework, namely the spectral stochastic isogeometric analysis (SSIGA) (Li, Gao, *et al.*, 2018), is presented for quantitatively assessing the performance of FGM plates with uncertain material properties under static load. Unlike traditional stochastic analysis methods, the SSIGA approach introduced herein is capable of handling uncertainty analysis involving both spatially independent (i.e., random variables) and dependent (i.e., random fields) uncertain parameters. By implementing the NURBS as the basis functions for the Karhunen-Loève (K-L) expansion, a new, yet practical, random field discretization technique is forged. The benefit of such novel technique is that the random field of uncertain parameter that is acting on complex physical domain can be more systematically and effectively handled. By further implementing the polynomial chaos expansion (PCE) approach, explicit formulations on the first two statistical moments (i.e., means and standard deviations) of any concerned structural responses (i.e., displacements, strain, and stress) of the FGM plate can be expressed. In addition to the estimations on the means and standard deviations of the structural responses, the proposed SSIGA approach can also adequately establish the probability density functions (PDFs) and cumulative distribution functions (CDFs) of the concerned structural responses through the kernel density estimation approach. Consequently, such critical information provides a quantitative measure of

performance, which is known as the structural reliability, of FGM plate. Yet, such competence on offering PDFs and CDFs has distinguished the proposed method from the previously developed first-order perturbation based stochastic analysis framework. Two numerical examples are thoroughly investigated to illustrate the applicability, effectiveness and efficiency of the proposed computational approach.

In addition to the superiority on the uncertainty quantification, the proposed SSIGA analysis framework also possesses some unique advantages. By developing the stochastic analysis grounding on the success of the deterministic IGA, the introduced SSIGA framework can maintain the exact geometries of both FGM plate and random field acting on the plate between the design model and stochastic analysis model. Such rigor can eliminate the modelling errors that often occur during the model transformation in practical engineering. That is, by establishing a stochastic analysis in Computer-Aided Design (CAD) framework, the consistency of the geometry of an FGM plate in CAD model, deterministic Computer-Aided Engineering (CAE) model, and structural safety assessment model can be exactly maintained. In fact, the proposed SSIGA meticulously combines the CAD, CAE as well as structural safety assessment into a unified framework. This unique feature is extremely important for practically stimulated FGM plates with complex geometries and spatially dependent uncertain system parameters. Without a consistent geometry of an FGM plate between the CAD model and the stochastic analysis model, the outcome of the stochastic analysis would become meaningless which could potentially jeopardize the safety of the FGM plate. In such cases, the SSIGA approach can certainly bring ease of modelling with desirable level of accuracy.

4.3 Isogeometric static analysis of FGM plate

4.3.1 The material properties of the FGM plate

For this paper, the top and bottom surfaces of the considered ceramic-metal FGM plate with thickness h are assumed to be purely ceramic and metallic respectively. The mid-plane of the plate is the *x*-*y* plane, and the positive *z*-axis is perpendicularly upward from the mid-plane. For the considered FGM plate, the Young's modulus E, mass density ρ, and Poisson's ratio ν vary along the thickness direction with a power law distribution as following

$$E(z) = E_m + (E_c - E_m)(\frac{1}{2} + \frac{z}{h})^n \tag{4.1}$$

$$\rho(z) = \rho_m + (\rho_c - \rho_m)(\frac{1}{2} + \frac{z}{h})^n \tag{4.2}$$

$$\nu(z) = \nu_m + (\nu_c - \nu_m)(\frac{1}{2} + \frac{z}{h})^n \tag{4.3}$$

where n denotes the gradient index; z denotes the thickness coordinate within $[-h/2, h/2]$; and the subscripts m and c represent the metal and ceramic constituents, respectively. The material properties of some common FGM components are presented in Table 4.1.

Table 4.1 Functionally graded material properties

Property	Aluminium Al	Zirconia-1 ZrO_2-1	Zirconia-2 ZrO_2-2	Alumina Al_2O_3
$E(GPa)$	70	200	151	380
ν	0.3	0.3	0.3	0.3
$\rho(\mathrm{kg/m^3})$	2707	5700	3000	3800

4.3.2 First-order shear deformation theory of plate

In this subsection, the formulation of first-order shear deformation theory (FSDT) of plate is briefly presented. Let D be the domain in $\Re^2$ occupied by the mid-plane of the plate. Within the analysis framework of the FSDT, the displacement fields $u(x, y, z)$, $v(x, y, z)$, and $w(x, y, z)$ are defined as:

$$\begin{aligned} u(x, y, z) &= u_0(x, y) + z\beta_x(x, y) \\ v(x, y, z) &= v_0(x, y) + z\beta_y(x, y), \qquad -\frac{h}{2} \le z \le \frac{h}{2} \\ w(x, y.z) &= w_0(x, y) \end{aligned} \tag{4.4}$$

where $\bar{\mathbf{u}} = (u_0, v_0)^T$, w_0 and $\bar{\boldsymbol{\beta}} = (\beta_x, \beta_y)$ denote the membrane displacements, the deflection of the mid-plane and the rotations in the *x*-*z*, *y*-*z* planes, respectively.

Adopting the small strain assumption, the relationship between in-plane strain $\boldsymbol{\varepsilon} = (\varepsilon_{xx}, \varepsilon_{yy}, \varepsilon_{xy})^T$ and displacement can be established as:

$$\boldsymbol{\varepsilon} = \begin{Bmatrix} u_{0,x} \\ u_{0,y} \\ u_{0,y} + v_{0,x} \end{Bmatrix} + z \begin{Bmatrix} \beta_{x,x} \\ \beta_{y,y} \\ \beta_{x,y} + \beta_{y,x} \end{Bmatrix} = \boldsymbol{\varepsilon}_0 + z\boldsymbol{\varepsilon}_b \tag{4.5}$$

The transverse shear strain $\boldsymbol{\gamma} = (\gamma_{xz}, \gamma_{yz})^T$ can be defined as:

$$\boldsymbol{\gamma} = \begin{Bmatrix} w_{0,x} + \beta_x \\ w_{0,y} + \beta_y \end{Bmatrix} \tag{4.6}$$

The weak form of the static problem of FGM plates within the FSDT can be formulated as following

$$\int_D \delta\boldsymbol{\varepsilon}^T \bar{\mathbf{D}}\boldsymbol{\varepsilon} dD + \int_D \delta\boldsymbol{\gamma}^T \bar{\mathbf{D}}_s \boldsymbol{\gamma} dD = \int_D \delta w q_0 dD \tag{4.7}$$

where q_0 denotes the transverse loading per unit area, and

$$\bar{\mathbf{D}} = \begin{bmatrix} \mathbf{A} & \bar{\mathbf{B}} \\ \bar{\mathbf{B}} & \mathbf{D}_b \end{bmatrix} \quad \bar{\mathbf{D}}_s = [\mathbf{D}_s] \tag{4.8}$$

with

$$(\mathbf{A}, \bar{\mathbf{B}}, \mathbf{D}_b) = \int_{-h/2}^{h/2} (1, z, z^2)\mathbf{Q}(z)dz \tag{4.9}$$

$$\mathbf{D}_s = \int_{-h/2}^{h/2} \mathbf{G}(z)dz \tag{4.10}$$

where $\mathbf{Q}(z)$ and $\mathbf{G}(z)$ denote the constitutive matrices, which can be explicitly expressed as:

$$\mathbf{Q}(z) = \frac{E(z)}{1-\nu^2(z)} \begin{bmatrix} 1 & \nu(z) & 0 \\ \nu(z) & 1 & 0 \\ 0 & 0 & [1-\nu(z)]/2 \end{bmatrix} \tag{4.11}$$

$$\mathbf{G}(z) = \frac{kE(z)}{2[1+\nu(z)]} \begin{bmatrix} 1 & 0 \\ 0 & 1 \end{bmatrix} \tag{4.12}$$

where $k = 5/6$ denotes the shear correction factor; $E(z)$, $\nu(z)$ are formulated as Eq.(4.1) and Eq.(4.3) respectively.

4.3.3 Isogeometric analysis of FGM plate

By implementing the two-dimensional NURBS basis functions presented in Eq.(3.9), the displacement field can be interpolated as

$$\mathbf{u}(\xi) = \sum_{\mathbf{I}}^{\mathbf{N}_{cp}} R_{\mathbf{I}}^{\mathbf{P}}(\xi)\mathbf{u}_{\mathbf{I}} \tag{4.13}$$

where $R_{\mathbf{I}}^{\mathbf{P}}$ denotes the two-dimensional NURBS basis function; $\mathbf{u}_{\mathbf{I}} = (u_{\mathbf{I}}, v_{\mathbf{I}}, w_{\mathbf{I}}, \beta_{x\mathbf{I}}, \beta_{y\mathbf{I}})^T$ and $\mathbf{u} = (u, v, w, \beta_x, \beta_y)^T$.

Therefore, the membrane, bending, and the shear strains can be explicitly expressed as follows:

$$\boldsymbol{\varepsilon}_0 = \sum_{\mathbf{I}}^{\mathbf{N}_{cp}} \mathbf{B}_{\mathbf{I}}^m(\boldsymbol{\xi})\mathbf{u}_{\mathbf{I}}, \quad \boldsymbol{\varepsilon}_b = \sum_{\mathbf{I}}^{\mathbf{N}_{cp}} \mathbf{B}_{\mathbf{I}}^b(\boldsymbol{\xi})\mathbf{u}_{\mathbf{I}}, \quad \boldsymbol{\gamma} = \sum_{\mathbf{I}}^{\mathbf{N}_{cp}} \mathbf{B}_{\mathbf{I}}^s(\boldsymbol{\xi})\mathbf{u}_{\mathbf{I}} \tag{4.14}$$

where

$$\begin{aligned}
\mathbf{B}_{\mathbf{I}}^m &= \begin{bmatrix} R_{\mathbf{I},x}^{\mathbf{P}} & 0 & 0 & 0 & 0 \\ 0 & R_{\mathbf{I},y}^{\mathbf{P}} & 0 & 0 & 0 \\ R_{\mathbf{I},y}^{\mathbf{P}} & R_{\mathbf{I},x}^{\mathbf{P}} & 0 & 0 & 0 \end{bmatrix} \\
\mathbf{B}_{\mathbf{I}}^b &= \begin{bmatrix} 0 & 0 & 0 & R_{\mathbf{I},x}^{\mathbf{P}} & 0 \\ 0 & 0 & 0 & 0 & R_{\mathbf{I},y}^{\mathbf{P}} \\ 0 & 0 & 0 & R_{\mathbf{I},y}^{\mathbf{P}} & R_{\mathbf{I},x}^{\mathbf{P}} \end{bmatrix} \\
\mathbf{B}_{\mathbf{I}}^s &= \begin{bmatrix} 0 & 0 & R_{\mathbf{I},x}^{\mathbf{P}} & R_{\mathbf{I}}^{\mathbf{P}} & 0 \\ 0 & 0 & R_{\mathbf{I},y}^{\mathbf{P}} & 0 & R_{\mathbf{I}}^{\mathbf{P}} \end{bmatrix}
\end{aligned} \tag{4.15}$$

and $R_{\mathbf{I}}^{\mathbf{P}}$, $R_{\mathbf{I},x}^{\mathbf{P}}$, and $R_{\mathbf{I},y}^{\mathbf{P}}$ denote the function value, the derivative along x-axis, and the derivative along y-axis of the **I**th NURBS function at a specific parametric point $\boldsymbol{\xi}$.

By substituting Eq.(4.15) into Eq.(4.7), the governing equation of the static problem of the FGM plate through the FSDT can be formulated as:

$$\mathbf{KU} = \mathbf{F} \tag{4.16}$$

where $\mathbf{K}$ denotes the global stiffness matrix which has formulation as

$$\mathbf{K} = \int_D \begin{Bmatrix} \mathbf{B}^m \\ \mathbf{B}^b \end{Bmatrix}^T \begin{bmatrix} \mathbf{A} & \bar{\mathbf{B}} \\ \bar{\mathbf{B}} & \mathbf{D}_b \end{bmatrix} \begin{Bmatrix} \mathbf{B}^m \\ \mathbf{B}^b \end{Bmatrix} dD + \int_D (\mathbf{B}^s)^T \mathbf{D}_s \mathbf{B}^s dD \tag{4.17}$$

and $\mathbf{F}$ denotes the force vector which is given by

$$\mathbf{F} = \int_D q_0 \mathbf{N} dD \tag{4.18}$$

where q_0 denotes the uniformly distributed load; $\mathbf{N}$ can be expressed as follows,

$$\mathbf{N} = [R_1^{\mathbf{P}} \mathbf{I}_{5\times5} \quad R_2^{\mathbf{P}} \mathbf{I}_{5\times5} \quad \dots \quad R_{\mathbf{N}_{cp}}^{\mathbf{P}} \mathbf{I}_{5\times5}] \tag{4.19}$$

and $\mathbf{I}_{5\times5}$ is an identity matrix with size 5×5.

4.4 SSIGA for stochastic static analysis of FGM plate

By following the generalized isogeometric analysis basis function based K-L expansion in Chapter 3, the random field $H(\mathbf{x},\theta)$ can be discretised as:

$$H(\mathbf{x},\theta) = \sum_{\mathbf{I}}^{\mathbf{N}_{cp}} \mu_{\mathbf{I}} R_{\mathbf{I}}^{\mathbf{P}}(\xi) + \sum_{i=1}^{\infty} \sqrt{\lambda_i}\zeta_i(\theta) \left(\sum_{\mathbf{I}}^{\mathbf{N}_{cp}} \vartheta_{\mathbf{I}}^i R_{\mathbf{I}}^{\mathbf{P}}(\xi) \right) \tag{4.20}$$

Then, by truncating the second part with M terms, the random field $H(\mathbf{x},\theta)$ can be approximated as

$$H(\mathbf{x},\theta) \approx \hat{H}(\mathbf{x},\theta) = \sum_{\mathbf{I}}^{\mathbf{N}_{cp}} \mu_{\mathbf{I}} R_{\mathbf{I}}^{\mathbf{P}}(\xi) + \sum_{i=1}^{M} \sqrt{\lambda_i}\zeta_i(\theta) \left(\sum_{\mathbf{I}}^{\mathbf{N}_{cp}} \vartheta_{\mathbf{I}}^i R_{\mathbf{I}}^{\mathbf{P}}(\xi) \right) \tag{4.21}$$

In this paper, the Young's modulus of the FGM plate is considered as a spatially dependent uncertain parameter which is modelled as a Gaussian random field, that is $E^G(\mathbf{x},z,\theta)$, and:

$$\begin{aligned} E^G(\mathbf{x},z,\theta) &= H^G(\mathbf{x},\theta)E(z) \\ &= H^G(\mathbf{x},\theta)\left(E_m + (E_c - E_m)(\frac{1}{2}+\frac{z}{h})^n \right) \end{aligned} \tag{4.22}$$

where $H^G(\mathbf{x},\theta)$ is a homogeneous Gaussian random field with mean μ, standard deviation σ and covariance function $C_{HH}(\mathbf{x},\mathbf{x}')$.

By implementing the aforementioned K-L expansion, the discretization of the spatially dependent uncertain Young's modulus of the FGM plate with M terms, i.e., $\hat{E}^G(\mathbf{x},z,\theta)$ can be explicitly formulated as:

$$\begin{aligned}\hat{E}^G(\mathbf{x},z,\theta) &= \hat{H}^G(\mathbf{x},\theta)E(z)\\ &= \left(\bar{H}(\mathbf{x})+\tilde{H}(\mathbf{x},\theta)\right)E(z)\\ &= \left(\sum_{\mathbf{I}}^{\mathbf{N}_{cp}}\mu_{\mathbf{I}}R_{\mathbf{I}}^{\mathbf{P}}(\xi)\right)E(z)+\sum_{i=1}^{M}\sqrt{\lambda_i}\zeta_i(\theta)\left(\sum_{\mathbf{I}}^{\mathbf{N}_{cp}}\vartheta_{\mathbf{I}}^{i}R_{\mathbf{I}}^{\mathbf{P}}(\xi)\right)E(z)\end{aligned} \tag{4.23}$$

With the consideration of the uncertain Young's modulus of the FGM plate, the stochastic static analysis of FGM plates based on FSDT within the SSIGA analysis framework can be formulated as:

$$\mathbf{K}(\theta)\mathbf{U}(\theta)=\mathbf{F} \tag{4.24}$$

and the stochastic global stiffness matrix $\mathbf{K}(\theta)$ is assembled from the stochastic elemental stiffness matrices $\mathbf{K}^e(\theta)$,

$$\mathbf{K}^e(\theta)=\left(\int_{D_e}\begin{Bmatrix}\mathbf{B}^m\\ \mathbf{B}^b\end{Bmatrix}^T\begin{bmatrix}\hat{\mathbf{A}}(\mathbf{x},\theta) & \hat{\mathbf{B}}(\mathbf{x},\theta)\\ \hat{\mathbf{B}}(\mathbf{x},\theta) & \hat{\mathbf{D}}_b(\mathbf{x},\theta)\end{bmatrix}\begin{Bmatrix}\mathbf{B}^m\\ \mathbf{B}^b\end{Bmatrix}dD_e+\int_{D_e}(\mathbf{B}^s)^T\hat{\mathbf{D}}_s(\mathbf{x},\theta)\mathbf{B}^s dD_e\right) \tag{4.25}$$

Since matrices $\mathbf{B}^m$, $\mathbf{B}^b$, and $\mathbf{B}^s$ are constant, the only source of uncertainty within the stochastic static analysis of FGM plate is reflected from the stochastic elasticity matrices $\hat{\mathbf{A}}(\mathbf{x},\theta)$, $\hat{\mathbf{B}}(\mathbf{x},\theta)$, $\hat{\mathbf{D}}_b(\mathbf{x},\theta)$, and $\hat{\mathbf{D}}_s(\mathbf{x},\theta)$, that is

$$(\hat{\mathbf{A}}(\mathbf{x},\theta),\hat{\mathbf{B}}(\mathbf{x},\theta),\hat{\mathbf{D}}_b(\mathbf{x},\theta))=\int_{-h/2}^{h/2}(1,z,z^2)\hat{\mathbf{Q}}(\mathbf{x},z,\theta)dz \tag{4.26}$$

$$\hat{\mathbf{D}}_s(\mathbf{x},\theta)=\int_{-h/2}^{h/2}\hat{\mathbf{G}}(\mathbf{x},z,\theta)dz \tag{4.27}$$

where $\hat{\mathbf{Q}}(\mathbf{x},z,\theta)$ and $\hat{\mathbf{G}}(\mathbf{x},z,\theta)$ are the stochastic constitutive matrices, which can be explicitly expressed as:

$$\hat{\mathbf{Q}}(\mathbf{x},z,\theta)=\frac{\hat{E}^G(\mathbf{x},z,\theta)}{1-\nu^2(z)}\begin{bmatrix}1 & \nu(z) & 0\\ \nu(z) & 1 & 0\\ 0 & 0 & [1-\nu(z)]/2\end{bmatrix} \tag{4.28}$$

$$\hat{\mathbf{G}}(\mathbf{x},z,\theta)=\frac{k\hat{E}^G(\mathbf{x},z,\theta)}{2[1+\nu(z)]}\begin{bmatrix}1 & 0\\ 0 & 1\end{bmatrix} \tag{4.29}$$

where $\nu(z)$ is defined as Eq.(4.3).

By implementing the NURBS-based K-L expansion, $\hat{E}^G(\mathbf{x},z,\theta)$ can be expressed as Eq.(4.23), and consequently $\hat{\mathbf{Q}}(\mathbf{x},z,\theta)$ and $\hat{\mathbf{G}}(\mathbf{x},z,\theta)$ can be formulated as:

$$\begin{aligned}\hat{\mathbf{Q}}(\mathbf{x},z,\theta)&=\frac{\left(\bar{H}(\mathbf{x})+\tilde{H}(\mathbf{x},\theta)\right)E(z)}{1-\nu^2(z)}\begin{bmatrix}1 & \nu(z) & 0\\ \nu(z) & 1 & 0\\ 0 & 0 & [1-\nu(z)]/2\end{bmatrix}\\ &=\left(\bar{H}(\mathbf{x})+\tilde{H}(\mathbf{x},\theta)\right)\mathbf{Q}(z)\\ &=\sum_{\mathbf{I}}^{\mathbf{N}_{cp}}\mu_{\mathbf{I}}R_{\mathbf{I}}^{\mathbf{P}}(\boldsymbol{\xi})\mathbf{Q}(z)+\sum_{i=1}^{M}\sqrt{\lambda_i}\zeta_i(\theta)\left(\sum_{\mathbf{I}}^{\mathbf{N}_{cp}}\vartheta_{\mathbf{I}}^{i}R_{\mathbf{I}}^{\mathbf{P}}(\boldsymbol{\xi})\right)\mathbf{Q}(z)\end{aligned} \tag{4.30}$$

$$\begin{aligned}\hat{\mathbf{G}}(\mathbf{x},z,\theta)&=\frac{\left(\bar{H}(\mathbf{x})+\tilde{H}(\mathbf{x},\theta)\right)E(z)}{2[1+\nu(z)]}\begin{bmatrix}1 & 0\\ 0 & 1\end{bmatrix}\\ &=\left(\bar{H}(\mathbf{x})+\tilde{H}(\mathbf{x},\theta)\right)\mathbf{G}(z)\\ &=\sum_{\mathbf{I}}^{\mathbf{N}_{cp}}\mu_{\mathbf{I}}R_{\mathbf{I}}^{\mathbf{P}}(\boldsymbol{\xi})\mathbf{G}(z)+\sum_{i=1}^{M}\sqrt{\lambda_i}\zeta_i(\theta)\left(\sum_{\mathbf{I}}^{\mathbf{N}_{cp}}\vartheta_{\mathbf{I}}^{i}R_{\mathbf{I}}^{\mathbf{P}}(\boldsymbol{\xi})\right)\mathbf{G}(z)\end{aligned} \tag{4.31}$$

Consequently, $\hat{\mathbf{A}}(\mathbf{x},\theta)$, $\hat{\mathbf{B}}(\mathbf{x},\theta)$, $\hat{\mathbf{D}}_b(\mathbf{x},\theta)$, and $\hat{\mathbf{D}}_s(\mathbf{x},\theta)$ can be expressed as follows:

$$
\begin{aligned}
(\hat{\mathbf{A}}(\mathbf{x},\theta),\hat{\mathbf{B}}(\mathbf{x},\theta),\hat{\mathbf{D}}_b(\mathbf{x},\theta)) &= \left(\bar{H}(\mathbf{x})+\tilde{H}(\mathbf{x},\theta)\right)\int_{-h/2}^{h/2}(1,z,z^2)\mathbf{Q}(z)dz \\
&= \sum_{\mathbf{I}}^{\mathbf{N}_{cp}}\mu_{\mathbf{I}}R_{\mathbf{I}}^{\mathbf{P}}(\boldsymbol{\xi})(\mathbf{A},\bar{\mathbf{B}},\mathbf{D}_b) \\
&\quad+\sum_{i=1}^{M}\sqrt{\lambda_i}\zeta_i(\theta)\left(\sum_{\mathbf{I}}^{\mathbf{N}_{cp}}\vartheta_{\mathbf{I}}^{i}R_{\mathbf{I}}^{\mathbf{P}}(\boldsymbol{\xi})\right)(\mathbf{A},\bar{\mathbf{B}},\mathbf{D}_b)
\end{aligned}
\tag{4.32}
$$

$$
\begin{aligned}
\hat{\mathbf{D}}_s(\mathbf{x},\theta) &= \left(\bar{H}(\mathbf{x})+\tilde{H}(\mathbf{x},\theta)\right)\int_{-h/2}^{h/2}\mathbf{G}(z)dz \\
&= \sum_{\mathbf{I}}^{\mathbf{N}_{cp}}\mu_{\mathbf{I}}R_{\mathbf{I}}^{\mathbf{P}}(\boldsymbol{\xi})\mathbf{D}_s \\
&\quad+\sum_{i=1}^{M}\sqrt{\lambda_i}\zeta_i(\theta)\left(\sum_{\mathbf{I}}^{\mathbf{N}_{cp}}\vartheta_{\mathbf{I}}^{i}R_{\mathbf{I}}^{\mathbf{P}}(\boldsymbol{\xi})\right)\mathbf{D}_s
\end{aligned}
\tag{4.33}
$$

By substituting Eqs.(4.32) and (4.32) into Eq.(4.25), the stochastic elemental stiffness matrix of the FGM plate can be formulated as:

$$
\mathbf{K}^e(\theta)=\mathbf{K}_0^e+\sum_{i=1}^{M}\mathbf{K}_i^e\zeta_i(\theta) \tag{4.34}
$$

where

$$
\mathbf{K}_0^e=\sum_{\mathbf{I}}^{\mathbf{N}_{cp}}\mu_{\mathbf{I}}R_{\mathbf{I}}^{\mathbf{P}}(\boldsymbol{\xi})\left(\int_{D_e}\begin{Bmatrix}\mathbf{B}^m\\ \mathbf{B}^b\end{Bmatrix}^T\begin{bmatrix}\mathbf{A} & \bar{\mathbf{B}}\\ \bar{\mathbf{B}} & \mathbf{D}_b\end{bmatrix}\begin{Bmatrix}\mathbf{B}^m\\ \mathbf{B}^b\end{Bmatrix}dD_e+\int_{D_e}(\mathbf{B}^s)^T\mathbf{D}_s\mathbf{B}^s dD_e\right) \tag{4.35}
$$

$$
\mathbf{K}_i^e(\theta)=\sqrt{\lambda_i}\left(\sum_{\mathbf{I}}^{\mathbf{N}_{cp}}\vartheta_{\mathbf{I}}^{i}R_{\mathbf{I}}^{\mathbf{P}}(\boldsymbol{\xi})\right)\left(\int_{D_e}\begin{Bmatrix}\mathbf{B}^m\\ \mathbf{B}^b\end{Bmatrix}^T\begin{bmatrix}\mathbf{A} & \bar{\mathbf{B}}\\ \bar{\mathbf{B}} & \mathbf{D}_b\end{bmatrix}\begin{Bmatrix}\mathbf{B}^m\\ \mathbf{B}^b\end{Bmatrix}dD_e+\int_{D_e}(\mathbf{B}^s)^T\mathbf{D}_s\mathbf{B}^s dD_e\right) \tag{4.36}
$$

Finally, by assembling across entire structural domain, Eq.(4.24) can be reformulated as

$$
\left(\mathbf{K}_0+\sum_{i=1}^{M}\mathbf{K}_i\zeta_i(\theta)\right)\mathbf{U}(\theta)=\mathbf{F} \tag{4.37}
$$

Without loss of generality, let $\zeta_0(\theta) \equiv 1$, Eq.(4.37) can be simplified as follows

$$\left(\sum_{i=0}^{M} \mathbf{K}_i \zeta_i(\theta) \right) \mathbf{U}(\theta) = \mathbf{F} \tag{4.38}$$

Meanwhile, by implementing the PCE in Chapter 3, the structural displacement of the stochastic linear system associated with FGM plate can be represented as:

$$\begin{aligned} \mathbf{U}(\theta) &= \mathbf{U}_0 \boldsymbol{\psi}_0(\theta) + \mathbf{U}_1 \boldsymbol{\psi}_1(\theta) + \mathbf{U}_2 \boldsymbol{\psi}_2(\theta) + \mathbf{U}_3 \boldsymbol{\psi}_3(\theta) + \cdots \\ &= \sum_{j=0}^{\infty} \mathbf{U}_j \boldsymbol{\psi}_j(\theta) \end{aligned} \tag{4.39}$$

Substituting Eq.(4.39) into Eq.(4.38), the stochastic governing equation of the static analysis of the FGM plate can be transformed to:

$$\left(\sum_{i=0}^{M} \mathbf{K}_i \zeta_i(\theta) \right) \left(\sum_{j=0}^{\infty} \mathbf{U}_j \boldsymbol{\psi}_j(\theta) \right) = \mathbf{F} \tag{4.40}$$

For real-life engineering applications, the series involved in Eq.(4.40) should be truncated at finite number of terms. Thus, by truncating the PCE at *Pth* term, Eq.(4.40) can be alternatively expressed as:

$$\left(\sum_{i=0}^{M} \mathbf{K}_i \zeta_i(\theta) \right) \left(\sum_{j=0}^{P-1} \mathbf{U}_j \boldsymbol{\psi}_j(\theta) \right) = \mathbf{F} \tag{4.41}$$

where the number of terms P of the PCE can be evaluated by the truncation order M of the NURBS-based K-L expansion and the polynomial order *p* as follows:

$$P = \begin{pmatrix} M + p \\ M \end{pmatrix} \tag{4.42}$$

Accordingly, the residual produced by the truncating process can be defined as:

$$e_{M,P-1} = \left(\sum_{i=0}^{M} \mathbf{K}_i \zeta_i(\theta) \right) \cdot \left(\sum_{j=0}^{P-1} \mathbf{U}_j \boldsymbol{\psi}_j(\theta) \right) - \mathbf{F} \tag{4.43}$$

Minimizing the residual formulated in Eq.(4.43) in the sense of mean square to obtain the optional approximation of the space spanned by $\{\boldsymbol{\psi}_j(\theta)\}_{k=0}^{P-1}$ yields:

$$\left\langle \sum_{i=0}^{M} \sum_{j=0}^{P-1} \mathbf{K}_i \mathbf{U}_j \zeta_i(\theta) \boldsymbol{\psi}_j(\theta), \boldsymbol{\psi}_k(\theta) \right\rangle = \left\langle \mathbf{F}, \boldsymbol{\psi}_k(\theta) \right\rangle, \quad k = 0, \ldots, P-1 \tag{4.44}$$

By introducing the following notations:

$$c_{ijk} = \left\langle \zeta_i(\theta) \boldsymbol{\psi}_j(\theta) \boldsymbol{\psi}_k(\theta) \right\rangle \tag{4.45}$$

$$\mathbf{F}_k = \left\langle \mathbf{F}, \boldsymbol{\psi}_k(\theta) \right\rangle \tag{4.46}$$

Eq.(4.44) can be alternatively expressed as:

$$\sum_{i=0}^{M} \sum_{j=0}^{P-1} c_{ijk} \mathbf{K}_i \mathbf{U}_j = \mathbf{F}_k \tag{4.47}$$

By introducing

$$\mathbf{K}_{jk} = \sum_{i=0}^{M} c_{ijk} \mathbf{K}_i \tag{4.48}$$

Eq.(4.47) can be reformulated as:

$$\sum_{j=0}^{P-1} \mathbf{K}_{jk} \mathbf{U}_j = \mathbf{F}_k, \quad k = 0, \ldots, P-1 \tag{4.49}$$

After solving the above stochastic system presented in Eq.(4.49), the stochastic structural displacement $\mathbf{U}(\theta)$ can be adequately approximated as:

$$\mathbf{U}(\theta) = \sum_{j=0}^{P-1} \mathbf{U}_j \boldsymbol{\psi}_j(\theta) \tag{4.50}$$

Consequently, the related statistical characteristics of the stochastic structural response $\mathbf{U}(\theta)$, namely the mean vector and covariance matrix of the structural displacement of the FGM plate, can be directly determined as:

$$\mathrm{E}(\mathbf{U}(\theta)) = \sum_{j=0}^{P-1} \left\langle \mathbf{U}_j \boldsymbol{\psi}_j(\theta) \right\rangle = \mathbf{U}_0 \tag{4.51}$$

$$\begin{aligned} \mathrm{Cov}(\mathbf{U}(\theta), \mathbf{U}(\theta)) &= \left\langle \mathbf{U}(\theta) - \mathbf{U}_0, \mathbf{U}(\theta) - \mathbf{U}_0 \right\rangle \\ &= \left\langle \sum_{j=0}^{P-1} \mathbf{U}_j \boldsymbol{\psi}_j(\theta) - \mathbf{U}_0, \sum_{j=0}^{P-1} \mathbf{U}_j \boldsymbol{\psi}_j(\theta) - \mathbf{U}_0 \right\rangle \\ &= \sum_{j=0}^{P-1} \left\langle \boldsymbol{\psi}_j^2 \right\rangle \mathbf{U}_i \cdot \mathbf{U}_i^T \end{aligned} \tag{4.52}$$

By taking a step further, the stochastic in-plane strain $\boldsymbol{\varepsilon}(\mathbf{x}, z, \theta) = (\varepsilon_{xx}(\mathbf{x}, z, \theta), \varepsilon_{yy}(\mathbf{x}, z, \theta), \varepsilon_{xy}(\mathbf{x}, z, \theta))^T$ of the FGM plate at location $(\mathbf{x}, z)$, and shear strain $\boldsymbol{\gamma}(\mathbf{x}, \theta) = (\gamma_{xz}(\mathbf{x}, \theta), \gamma_{yz}(\mathbf{x}, \theta))^T$ of the FGM plate at location $\mathbf{x}$ can also be formulated through the PCE as follow:

$$\boldsymbol{\varepsilon}(\mathbf{x}, z, \theta) = \sum_{j=0}^{P-1} \boldsymbol{\psi}_j(\theta) \boldsymbol{\varepsilon}_j(\mathbf{x}, z) \tag{4.53}$$

$$\boldsymbol{\gamma}(\mathbf{x}, \theta) = \sum_{j=0}^{P-1} \boldsymbol{\psi}_j(\theta) \boldsymbol{\gamma}_j(\mathbf{x}) \tag{4.54}$$

where $\boldsymbol{\varepsilon}_j(\mathbf{x}, z) = (\mathbf{B}^m(\mathbf{x}))^T \{\mathbf{U}_j\}^e + z \cdot (\mathbf{B}^b(\mathbf{x}))^T \{\mathbf{U}_j\}^e$ and $\boldsymbol{\gamma}_j(\mathbf{x}) = (\mathbf{B}^s(\mathbf{x}))^T \{\mathbf{U}_j\}^e$ denote the polynomial chaos coefficient of the in-plane strain and shear strain vectors respectively.

Thus, the mean vector and covariance matrix of the stochastic in-plane strain $\boldsymbol{\varepsilon}(\mathbf{x}, z, \theta)$ and shear strain $\boldsymbol{\gamma}(\mathbf{x}, \theta)$ of the FGM plate can be determined as:

$$\mathrm{E}[\boldsymbol{\varepsilon}(\mathbf{x}, z, \theta)] = \boldsymbol{\varepsilon}_0 \tag{4.55}$$

$$\mathrm{Cov}[\boldsymbol{\varepsilon}(\mathbf{x}, z, \theta)] = \sum_{i=0}^{\tilde{P}-1} \left\langle \boldsymbol{\psi}_j^2 \right\rangle \boldsymbol{\varepsilon}_i \cdot \boldsymbol{\varepsilon}_i^T \tag{4.56}$$

$$\mathrm{E}[\boldsymbol{\gamma}(\mathbf{x}, \theta)] = \boldsymbol{\gamma}_0 \tag{4.57}$$

$$\mathrm{Cov}[\boldsymbol{\gamma}(\mathbf{x}, \theta)] = \sum_{i=0}^{\tilde{P}-1} \left\langle \boldsymbol{\psi}_j^2 \right\rangle \boldsymbol{\gamma}_i \cdot \boldsymbol{\gamma}_i^T \tag{4.58}$$

Furthermore, from the Hooke's law, the stochastic in-plane stress $\boldsymbol{\sigma}(\mathbf{x}, z, \theta)$ and shear stress $\boldsymbol{\tau}(\mathbf{x}, z, \theta)$ of the FGM plate at location $(\mathbf{x}, z)$ can also be formulated through the PCE as follows:

$$\begin{aligned}
\boldsymbol{\sigma}(\mathbf{x}, z, \theta) &= \hat{\mathbf{G}}(\mathbf{x}, z, \theta) \cdot \boldsymbol{\varepsilon}(\mathbf{x}, z, \theta) \\
&= \zeta_0(\theta) \cdot \sum_{\mathbf{I}}^{\mathbf{N}_{cp}} \mu_{\mathbf{I}} R_{\mathbf{I}}^{\mathbf{P}}(\boldsymbol{\xi}) \cdot \sum_{j=0}^{P-1} \boldsymbol{\psi}_j(\theta) \cdot \mathbf{G}(z) \boldsymbol{\varepsilon}_j(\mathbf{x}, z) \\
&\quad + \sum_{i=i}^{M} \sum_{j=0}^{P-1} \zeta_i(\theta) \boldsymbol{\psi}_j(\theta) \cdot \sqrt{\lambda_i} \cdot \left(\sum_{\mathbf{I}}^{\mathbf{N}_{cp}} \vartheta_{\mathbf{I}}^i R_{\mathbf{I}}^{\mathbf{P}}(\boldsymbol{\xi}) \right) \cdot \mathbf{G}(z) \boldsymbol{\varepsilon}_j(\mathbf{x}, z) \\
&= \sum_{\mathbf{I}}^{\mathbf{N}_{cp}} \mu_{\mathbf{I}} R_{\mathbf{I}}^{\mathbf{P}}(\boldsymbol{\xi}) \sum_{j=0}^{P-1} \boldsymbol{\psi}_j(\theta) \cdot \boldsymbol{\sigma}_{0j}(\mathbf{x}, z) \\
&\quad + \sum_{i=i}^{M} \sum_{j=0}^{P-1} \zeta_i(\theta) \boldsymbol{\psi}_j(\theta) \cdot \boldsymbol{\sigma}_{ij}(\mathbf{x}, z)
\end{aligned} \tag{4.59}$$

$$
\begin{aligned}
\boldsymbol{\tau}(\mathbf{x},z,\theta) &= \hat{\mathbf{D}}_s(\mathbf{x},z,\theta)\cdot\boldsymbol{\gamma}(\mathbf{x},\theta) \\
&= \zeta_0(\theta)\cdot\sum_{\mathbf{I}}^{\mathbf{N}_{cp}}\mu_{\mathbf{I}}R_{\mathbf{I}}^{\mathbf{P}}(\boldsymbol{\xi})\cdot\sum_{j=0}^{P-1}\boldsymbol{\psi}_j(\theta)\cdot\mathbf{D}_s(z)\boldsymbol{\gamma}_j(\mathbf{x}) \\
&\quad+\sum_{i=i}^{M}\sum_{j=0}^{P-1}\zeta_i(\theta)\boldsymbol{\psi}_j(\theta)\cdot\sqrt{\lambda_i}\cdot\left(\sum_{\mathbf{I}}^{\mathbf{N}_{cp}}\mathcal{G}_{\mathbf{I}}^{i}R_{\mathbf{I}}^{\mathbf{P}}(\boldsymbol{\xi})\right)\cdot\mathbf{D}_s(z)\boldsymbol{\gamma}_j(\mathbf{x}) \\
&= \sum_{\mathbf{I}}^{\mathbf{N}_{cp}}\mu_{\mathbf{I}}R_{\mathbf{I}}^{\mathbf{P}}(\boldsymbol{\xi})\sum_{j=0}^{P-1}\boldsymbol{\psi}_j(\theta)\cdot\boldsymbol{\tau}_{0j}(\mathbf{x},z) \\
&\quad+\sum_{i=i}^{M}\sum_{j=0}^{P-1}\zeta_i(\theta)\boldsymbol{\psi}_j(\theta)\cdot\boldsymbol{\tau}_{ij}(\mathbf{x},z)
\end{aligned}
\tag{4.60}
$$

Consequently, the mean vector and covariance matrix of the stochastic in-plane stress $\boldsymbol{\sigma}(\mathbf{x},z,\theta)$ and shear stress $\boldsymbol{\tau}(\mathbf{x},z,\theta)$ of the FGM plate at location $(\mathbf{x},z)$ can be calculated as:

$$
\begin{aligned}
\mathrm{E}[\boldsymbol{\sigma}(\mathbf{x},z,\theta)] &= \sum_{\mathbf{I}}^{\mathbf{N}_{cp}}\mu_{\mathbf{I}}R_{\mathbf{I}}^{\mathbf{P}}(\boldsymbol{\xi})\cdot\sum_{j=0}^{P-1}\left\langle\boldsymbol{\psi}_j(\theta)\right\rangle\cdot\boldsymbol{\sigma}_{0j}(\mathbf{x},z) \\
&\quad+\sum_{i=i}^{M}\sum_{j=0}^{P-1}\left\langle\zeta_i(\theta),\boldsymbol{\psi}_j(\theta)\right\rangle\cdot\boldsymbol{\sigma}_{ij}(\mathbf{x},z) \\
&= \sum_{\mathbf{I}}^{\mathbf{N}_{cp}}\mu_{\mathbf{I}}R_{\mathbf{I}}^{\mathbf{P}}(\boldsymbol{\xi})\cdot\boldsymbol{\sigma}_{00}(\mathbf{x},z)+\sum_{i=i}^{M}\sum_{j=0}^{P-1}\left\langle\zeta_i(\theta),\boldsymbol{\psi}_j(\theta)\right\rangle\cdot\boldsymbol{\sigma}_{ij}(\mathbf{x},z)
\end{aligned}
\tag{4.61}
$$

$$
\begin{aligned}
\mathrm{Cov}[\boldsymbol{\sigma}(\mathbf{x},z,\theta),\boldsymbol{\sigma}(\mathbf{x},z,\theta)] &= \sum_{k=0}^{P-1}\sum_{j=0}^{P-1}\sum_{l=0}^{M}\sum_{i=0}^{M}c_{iljk}\boldsymbol{\sigma}_{ij}(\mathbf{x},z)\cdot\boldsymbol{\sigma}_{lk}^{T}(\mathbf{x},z) \\
&\quad-\mathrm{E}[\boldsymbol{\sigma}(\mathbf{x},z,\theta)]\cdot\mathrm{E}^{T}[\boldsymbol{\sigma}(\mathbf{x},z,\theta)]
\end{aligned}
\tag{4.62}
$$

$$
\begin{aligned}
\mathrm{E}[\boldsymbol{\tau}(\mathbf{x},z,\theta)] &= \sum_{\mathbf{I}}^{\mathbf{N}_{cp}}\mu_{\mathbf{I}}R_{\mathbf{I}}^{\mathbf{P}}(\boldsymbol{\xi})\cdot\sum_{j=0}^{P-1}\left\langle\boldsymbol{\psi}_j(\theta)\right\rangle\cdot\boldsymbol{\tau}_{0j}(\mathbf{x},z) \\
&\quad+\sum_{i=i}^{M}\sum_{j=0}^{P-1}\left\langle\zeta_i(\theta),\boldsymbol{\psi}_j(\theta)\right\rangle\cdot\boldsymbol{\tau}_{ij}(\mathbf{x},z) \\
&= \sum_{\mathbf{I}}^{\mathbf{N}_{cp}}\mu_{\mathbf{I}}R_{\mathbf{I}}^{\mathbf{P}}(\boldsymbol{\xi})\cdot\boldsymbol{\tau}_{00}(\mathbf{x},z)+\sum_{i=i}^{M}\sum_{j=0}^{P-1}\left\langle\zeta_i(\theta),\boldsymbol{\psi}_j(\theta)\right\rangle\cdot\boldsymbol{\tau}_{ij}(\mathbf{x},z)
\end{aligned}
\tag{4.63}
$$

$$
\begin{aligned}
\mathrm{Cov}[\boldsymbol{\tau}(\mathbf{x},z,\theta),\boldsymbol{\tau}(\mathbf{x},z,\theta)] &= \sum_{k=0}^{P-1}\sum_{j=0}^{P-1}\sum_{l=0}^{M}\sum_{i=0}^{M}c_{iljk}\boldsymbol{\tau}_{ij}(\mathbf{x},z)\cdot\boldsymbol{\tau}_{lk}^{T}(\mathbf{x},z) \\
&\quad-\mathrm{E}[\boldsymbol{\tau}(\mathbf{x},z,\theta)]\cdot\mathrm{E}^{T}[\boldsymbol{\tau}(\mathbf{x},z,\theta)]
\end{aligned}
\tag{4.64}
$$

where $c_{ijkl} = \left\langle \zeta_i(\theta)\zeta_l(\theta)\boldsymbol{\psi}_j(\theta)\boldsymbol{\psi}_k(\theta) \right\rangle$ can be obtained through a similar fashion that is utilized in Eq.(4.45).

4.5 Numerical examples

To demonstrate the effectiveness and efficiency of the proposed SSIGA framework on stochastic static analysis of FGM plate, two numerical examples are thoroughly explored in this section. For the first numerical example, the proposed SSIGA analysis framework is implemented for the stochastic static analysis of an Al_2O_3/Al FGM dart shape plate. In addition, a ZrO_2-1/Al FGM plate with irregular curvatures is investigated in the second example. Due to the absence of analytical solutions on the statistical moments of the structural responses of the two considered FGM plates, the accuracy of the results determined by the proposed method is partially verified by the exhaustive Monte Carlo Simulation (MCS) approach with large simulations. For all numerical examples investigated in this paper, all random numbers are generated by employing the Statistics toolbox of MATLAB R2016b, and the evaluations of IGA basis functions are based on the technique presented in (V. P. Nguyen *et al.*, 2015).

4.5.1 Numerical example: dart shape FGM plate

In the first numerical example, a dart shape Al_2O_3/Al FGM plate involving spatially dependent uncertain Young's modulus is investigated. The general structural layout and the adopted IGA refinement of the investigated dart shape FGM plate are presented in Figure 1. The considered FGM plate is subjected to a uniformly distributed load with magnitude of $q = 1\times10^3 kN/m^2$ along the z-axis. The FGM plate is fully clamped by the red supports as shown in Figure 4.1. The Young's modulus of the FGM plate is modelled as a Gaussian random field as follows:

$$E^G(\mathbf{x},z,\theta)=H^G(\mathbf{x},\theta)\left(E_m+(E_c-E_m)(\frac{1}{2}+\frac{z}{h})^n\right) \tag{4.65}$$

where $H^G(\mathbf{x},\theta)$ denote a Gaussian random field with mean $\mu=1.0$, standard deviation $\sigma=0.1$, and covariance function $C_{HH}(\mathbf{x},\mathbf{x}')=\sigma^2\exp\left(-\frac{|x_1-x_2|}{2}-\frac{|y_1-y_2|}{2}\right)$; $h=0.01$ m denotes plate thickness; $n=4$ denotes volume fraction exponent; E_c denotes Young's modulus of Al_2O_3; E_m denotes Young's modulus of Al. In order to visualize the impacts of the material uncertainty, one possible realization of the random field of the Young's modulus of the FGM plate is illustrated in Figure 4.2. The values of E_m and E_c are adopted from Table 4.1.

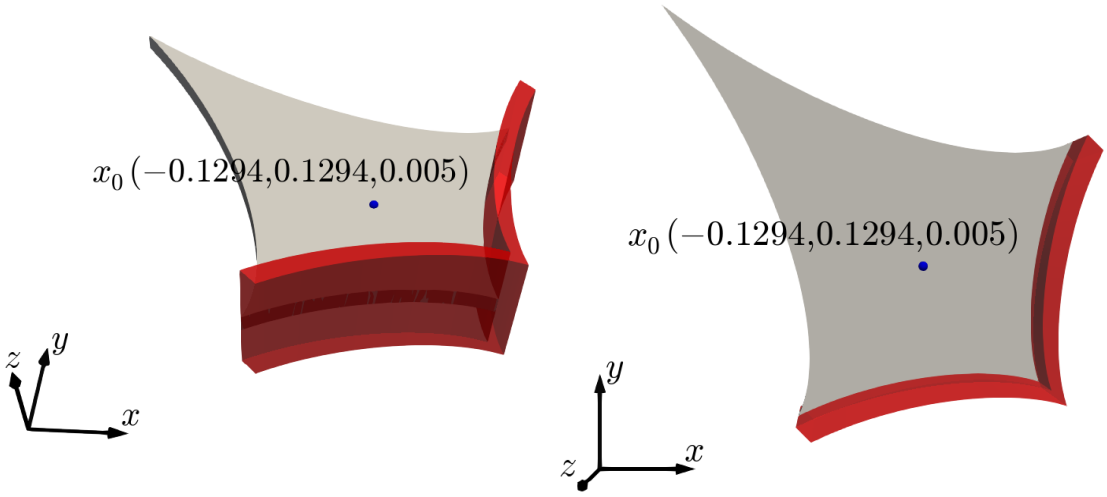

(a) (b)

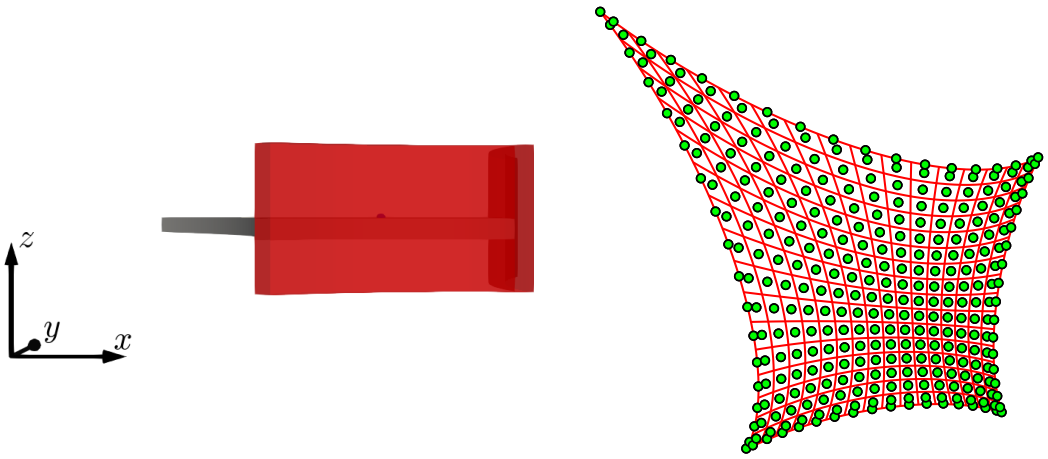

(c) (d)

Figure 4.1 Dart shape FGM plate (a) 3D view; (b) top view; (c) front view; (d) IGA refinement

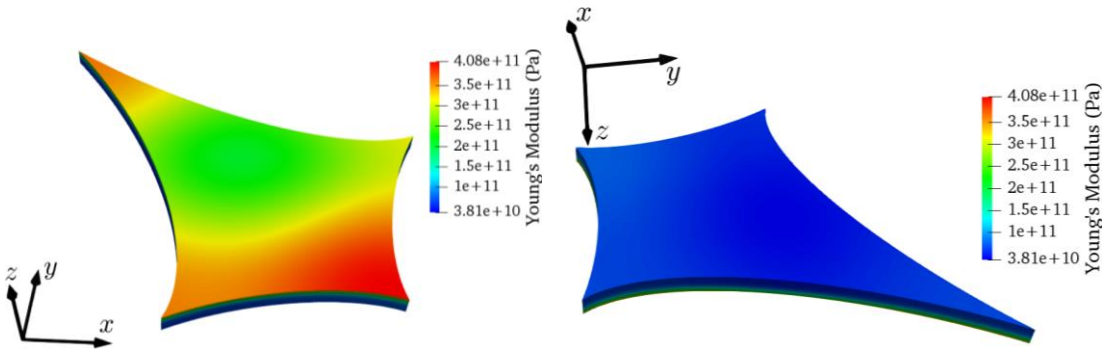

(a) (b)

Figure 4.2 Realization of the random field of the dart shape FGM plate (a) from top surface to bottom surface; (b) from bottom surface to top surface

Since the convergence study of the NURBS-based Karhunen-Loève expansion has been evidently illustrated in (Li, Gao, *et al.*, 2018; Rahman, 2018), a repeating convergence study is omitted herein. Interested readers can refer to (Li, Gao, *et al.*, 2018; Rahman, 2018) for the detailed convergence study of the NURBS-based Karhunen-Loève expansion for Gaussian random field with the considerations of different types of refinement. For this study, the Gaussian random field is decomposed by the NURBS-based K-L expansion with four terms. Moreover, all concerned structural responses are estimated by different orders of PCE, namely 1-order PCE, 2-order PCE, 3-order PCE, 4-order PCE, 5-order PCE, 6-order PCE, 7-order PCE, and 8-order PCE. Moreover, the MCS approach with 1,000,000 simulation cycles was adopted for partially verifying the results.

Table 4.2 compares the mean and standard deviations of u_z, ε_{xx}, σ_{xx}, γ_{xz}, and τ_{xz} at x_0 obtained from SSIGA and MCS approaches. By closely examining Table 4.2, a good agreement between the SSIGA and MCS approaches can be observed for both the means and standard deviations of all the concerned structural responses at x_0.

In addition to the validation of the SSIGA approach on the determination of the first two statistical moments of the concerned structural responses of the FGM plate, the SSIGA approach is further implemented for estimating the PDFs and CDFs of the structural responses. Within this part of investigation, all PDFs and CDFs of the concerned structural responses were established by implementing a non-parametric statistical inference technique known as the kernel density estimation approach. For this particular part of investigation, the point x_0 is selected again, and the PDFs and CDFs of u_z, ε_{xx}, σ_{xx}, γ_{xz}, and τ_{xz} at x_0 are established and reported in Figures 4.3-4.7, respectively. From the information presented in Figures 4.3-4.7, it is evidently illustrated that the proposed SSIGA approach is competent for establishing the PDFs and CDFs of the concerned structural responses. Also, another crucial point can be realized from this investigation is that when the order of the PCE is increased, the PDFs and CDFs estimated by the SSIGA approach would converge to the results of the MCS approach.

Table 4.2 Comparison for statistical characteristics of u_z, ε_{xx}, σ_{xx}, γ_{xz}, and τ_{xz} at x_0 between SSIGA and MCS approaches

Method	Statistical characteristics	u_z	ε_{xx}	σ_{xx}	γ_{xz}	τ_{xz}

MCS	Mean	0.0573	-1.0435e-4	-5.6291e+7	6.9452e-5	1.0090e+7
	Standard deviation	0.0037	9.1814e-6	1.6938e+6	6.7698e-6	6.7935e+5
SSIGA (1-order PCE)	Mean	0.0573	-1.0432e-4	-5.6296e+7	6.9429e-5	1.0090e+7
	Standard deviation	0.0037	8.9905e-6	1.7647e+6	6.6232e-6	6.8550e+5
SSIGA (2-order PCE)	Mean	0.0573	-1.0433e-4	-5.6293e+7	6.9433e-5	1.0090e+7
	Standard deviation	0.0037	9.1487e-6	1.6964+6	6.7409e-6	6.7987+5
SSIGA (3-order PCE)	Mean	0.0573	-1.0433e-4	-5.6293e+7	6.9434e-5	1.0090e+7
	Standard deviation	0.0037	9.1523e-6	1.6957e+6	6.7480e-6	6.7949e+5
SSIGA (4-order PCE)	Mean	0.0573	-1.0433e-4	-5.6293e+7	6.9429e-5	1.0089e+7
	Standard deviation	0.0037	9.1522e-6	1.6956e+6	6.7483e-6	6.8005e+5
SSIGA (5-order PCE)	Mean	0.0573	-1.0433e-4	-5.6293e+7	6.9437e-5	1.0091e+7
	Standard deviation	0.0037	9.1522e-6	1.6956e+6	6.7406e-6	6.8011e+5

SSIGA (6-order PCE)	Mean	0.0573	-1.0433e-4	-5.6293e+7	6.9431e-5	1.0090e+7
	Standard deviation	0.0037	9.1524e-6	1.6957e+6	6.7449e-6	6.7980e+5
SSIGA (7-order PCE)	Mean	0.0573	-1.0433e-4	-5.6293e+7	6.9431e-5	1.0090e+7
	Standard deviation	0.0037	9.1523e-6	1.6957e+6	6.7424e-6	6.7972e+5
SSIGA (8-order PCE)	Mean	0.0573	-1.0433e-4	-5.6293e+7	6.9432e-5	1.0090e+7
	Standard deviation	0.0037	9.1523e-6	1.6957e+6	6.7438e-6	6.7955e+5

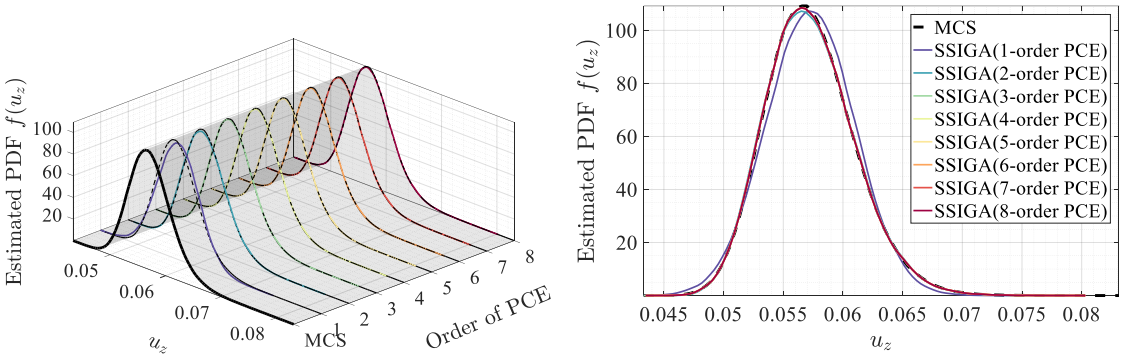

(a) (b)

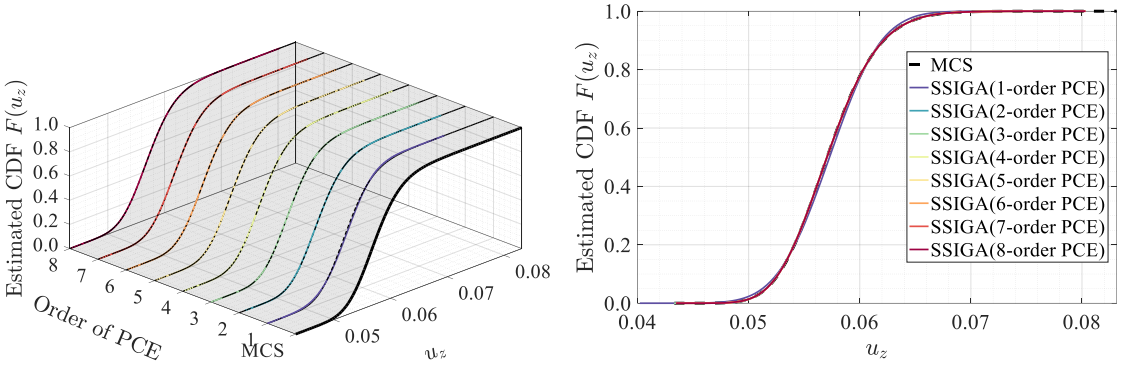

(c) (d)

Figure 4.3 Estimated (a) PDF(3D), (b) PDF(2D), (c) CDF(3D), and (d) CDF(2D) of u_z at x_0

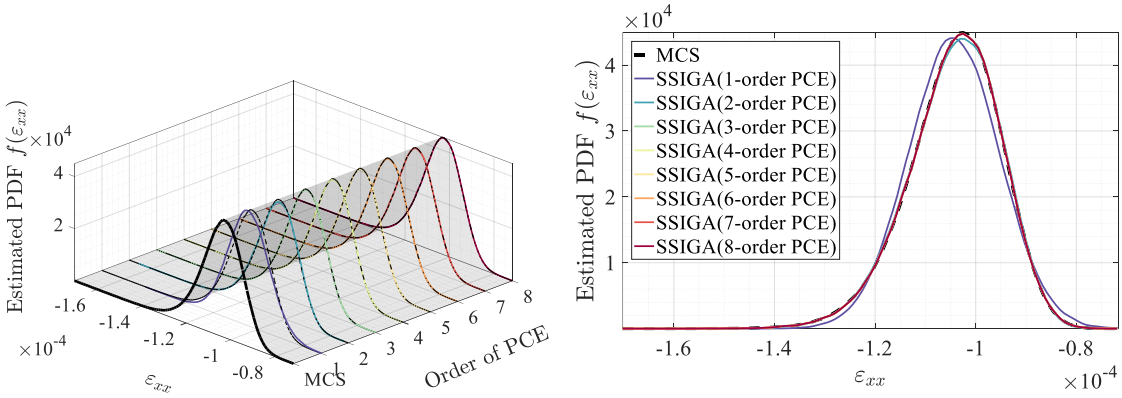

(a) (b)

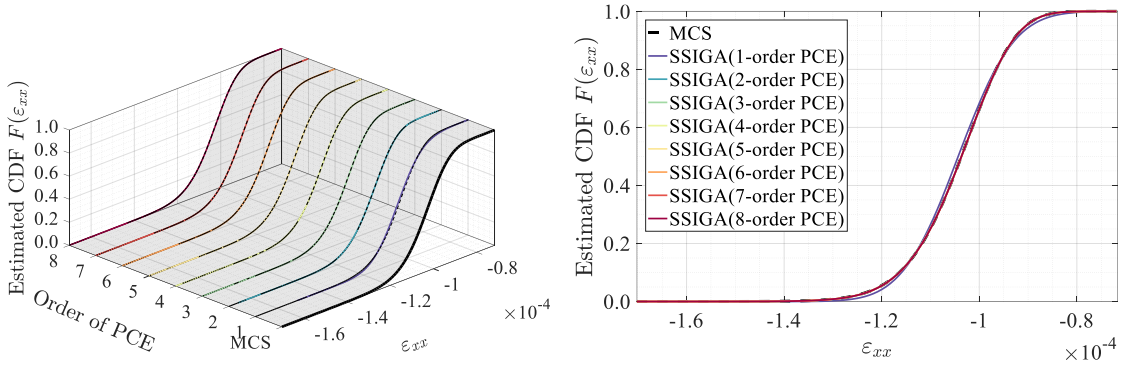

(c) (d)

Figure 4.4 Estimated (a) PDF(3D), (b) PDF(2D), (c) CDF(3D), and (d) CDF(2D) of ε_{xx} at x_0

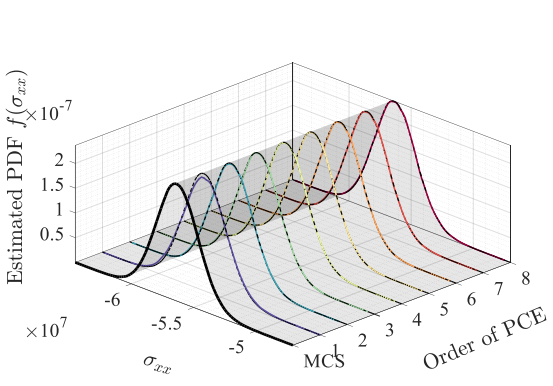

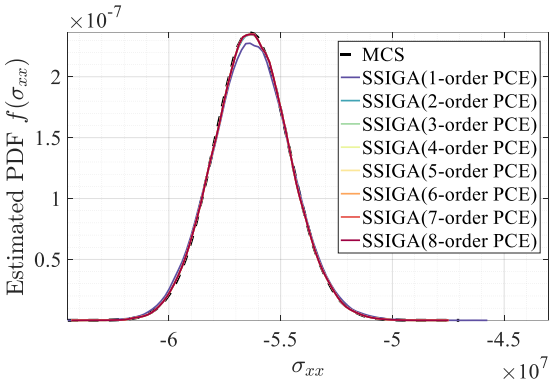

(a) (b)

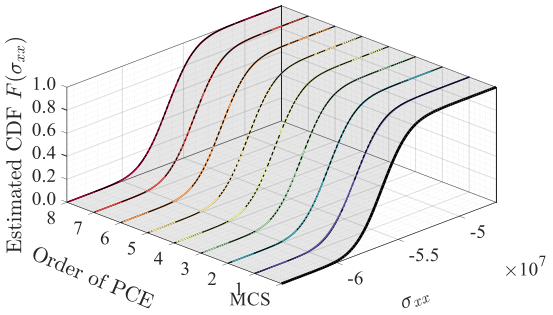

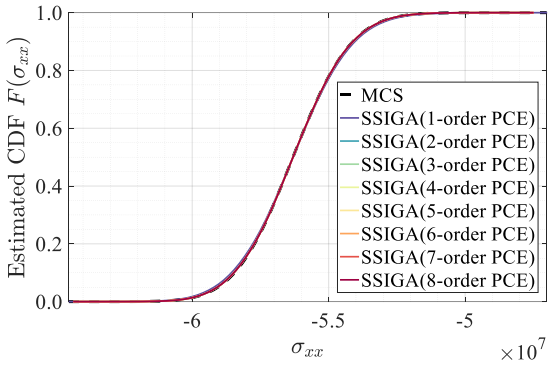

(c) (d)

Figure 4.5 Estimated (a) PDF(3D), (b) PDF(2D), (c) CDF(3D), and (d) CDF(2D) of σ_{xx} at x_0

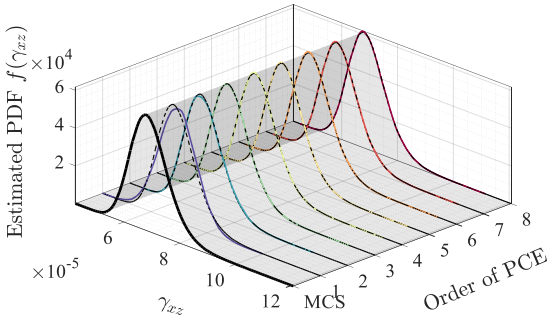

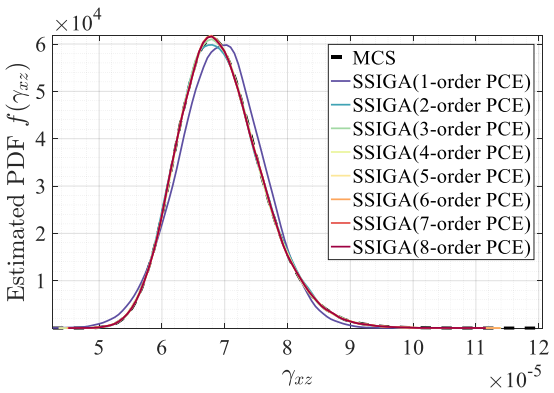

(a) (b)

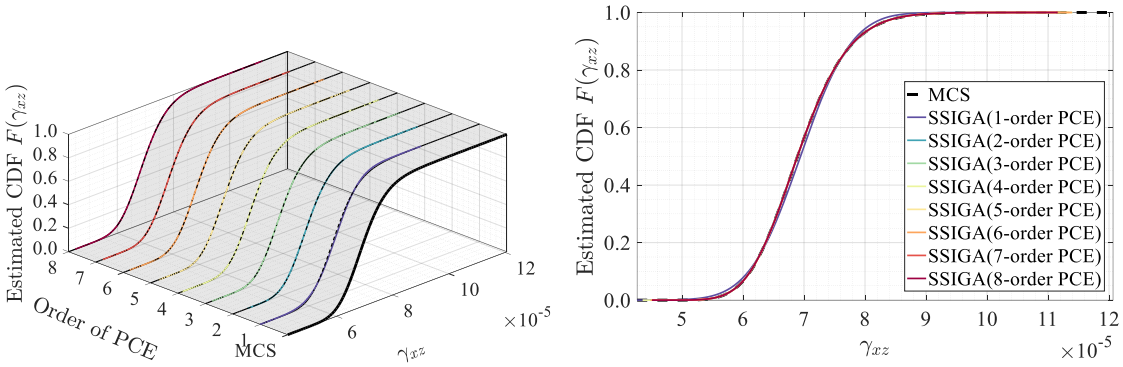

(c) (d)

Figure 4.6 Estimated (a) PDF(3D), (b) PDF(2D), (c) CDF(3D), and (d) CDF(2D) of γ_{xz} at x_0

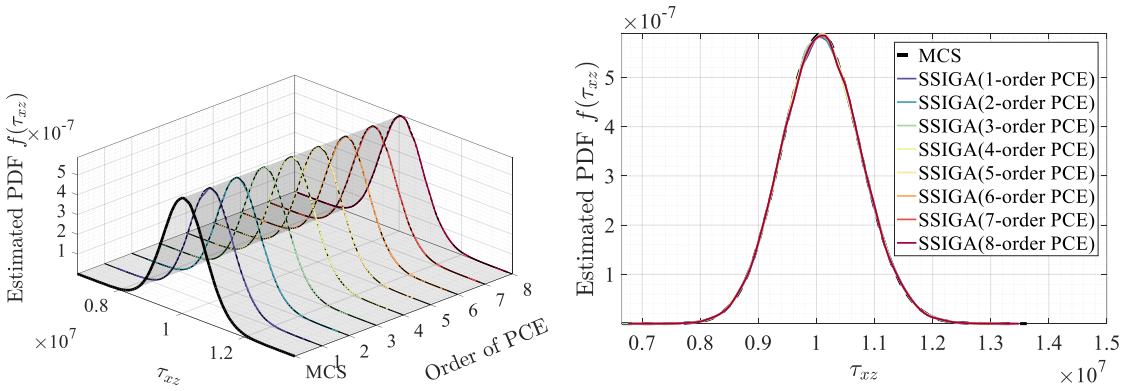

(a) (b)

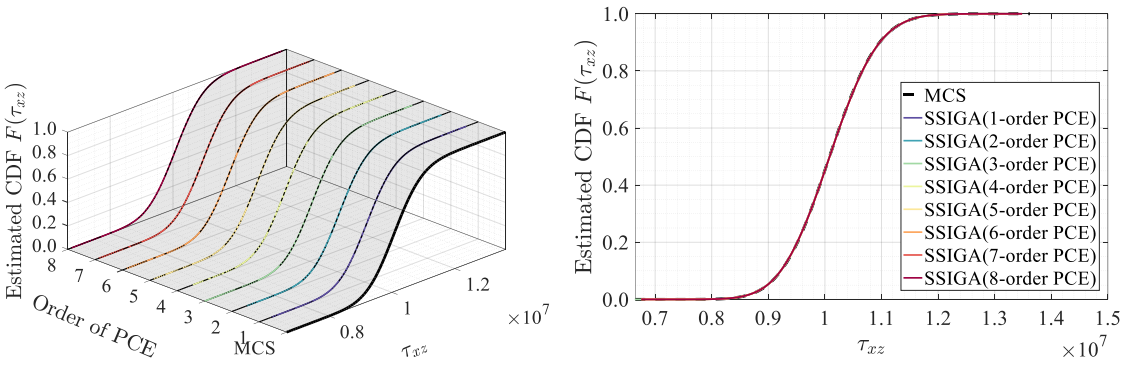

(c) (d)

Figure 4.7 Estimated (a) PDF(3D), (b) PDF(2D), (c) CDF(3D), and (d) CDF(2D) of τ_{xz} at x_0

Furthermore, the results of the MCS approach were obtained by running on one node of a cluster. The implemented node had 2×8 cores (Intel Xeon E5-2670 (Sandy Bridge) 2.6GHz), namely 16 processors in total. The MCS with 1,000,000 simulation cycles were executed by parallel computing with 16 workers on the cluster and costed 40 hours 30 mins 0 seconds as showed in Table 4.3.

Table 4.3 Comparison of computational time between SSIGA and MCS

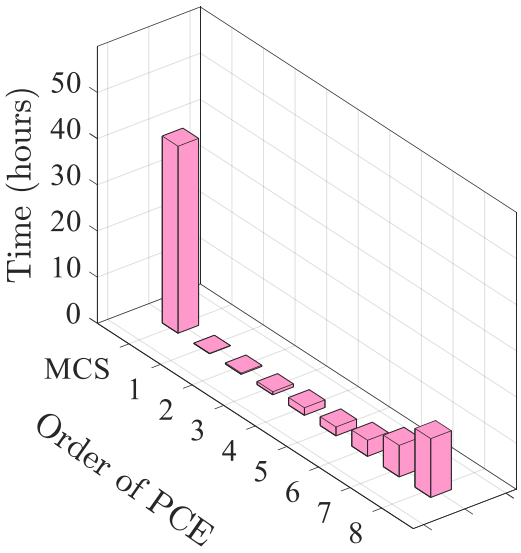

Method	Time (hh:mm:ss)
MCS	40:30:00
SSIGA(1-order PCE)	00:05::21
SSIGA(2-order PCE)	00:15:06
SSIGA(3-order PCE)	00:40:00
SSIGA(4-order PCE)	01:38:14
SSIGA(5-order PCE)	01:55:04
SSIGA(6-order PCE)	03:29:11
SSIGA(7-order PCE)	06:49:39
SSIGA(8-order PCE)	12:44:01

On the other hand, all the results of the SSIGA approach were obtained by running at a node on a cluster with 2×14 cores (Intel Xeon Broadwell technology, 2.6 GHz). However, parallel computing was not implemented in the calculation of the SSIGA approach. The computational time of the SSIGA approach are also reported in Table 4.3.

According to the results reported in Table 4.2, when the truncation order of the PCE is higher than 5, all the results obtained from the SSIGA are almost identical to the MCS approach but with much less computational time. Overall, based on the reported technical information, the proposed SSIGA approach certainly shows superior effectiveness and computational efficiency over the exhaustively simulative MCS approach for the dart shape FGM plate which suffers from both spatially dependent uncertainty and irregular geometry.

4.5.2 Numerical example: irregularly curved FGM plate

In the second numerical example, an irregularly curved ZrO_2-1/Al FGM plate involving spatially dependent uncertain Young's modulus is investigated to further explore the applicability of the proposed approach for system with complex geometry. The general structural layout and IGA refinement of the irregularly curved FGM plate is presented in Figure 8. The plate is subjected to a uniformly distributed load with magnitude of $q = 1\times10^3 kN/m^2$ along the z-axis. The considered FGM plate is fully clamped to the red column as illustrated in Figure 4.8. Once again, the Young's modulus of the FGM plate is modelled as a Gaussian random field as follows:

$$E^G(\mathbf{x}, z, \theta) = H^G(\mathbf{x}, \theta)\left(E_m + (E_c - E_m)(\frac{1}{2} + \frac{z}{h})^n \right) \tag{4.66}$$

where $H^G(\mathbf{x}, \theta)$ denote a Gaussian random field with mean $\mu = 1.0$, standard deviation $\sigma = 0.1$, and covariance function $C_{HH}(\mathbf{x}, \mathbf{x}') = \sigma^2 \exp\left(-\frac{|x_1 - x_2|}{2} - \frac{|y_1 - y_2|}{2} \right)$; $h = 0.2$ m denotes plate thickness; $n = 2$ denotes volume fraction exponent; E_c denotes Young's modulus of ZrO_2-1; E_m denotes Young's modulus of Al. Also, one possible realization of the random field of the Young's modulus is illustrated in Figure 4.9.

Within the proposed method, the Gaussian random field of the Young's modulus is decomposed by 4-terms NURBS-based K-L expansion, and 5-order PCE is implemented to estimate all concerned stochastic structural responses in this case. Once again, the MCS with 1,000,000 simulation cycles was employed for the purpose of partial result verification.

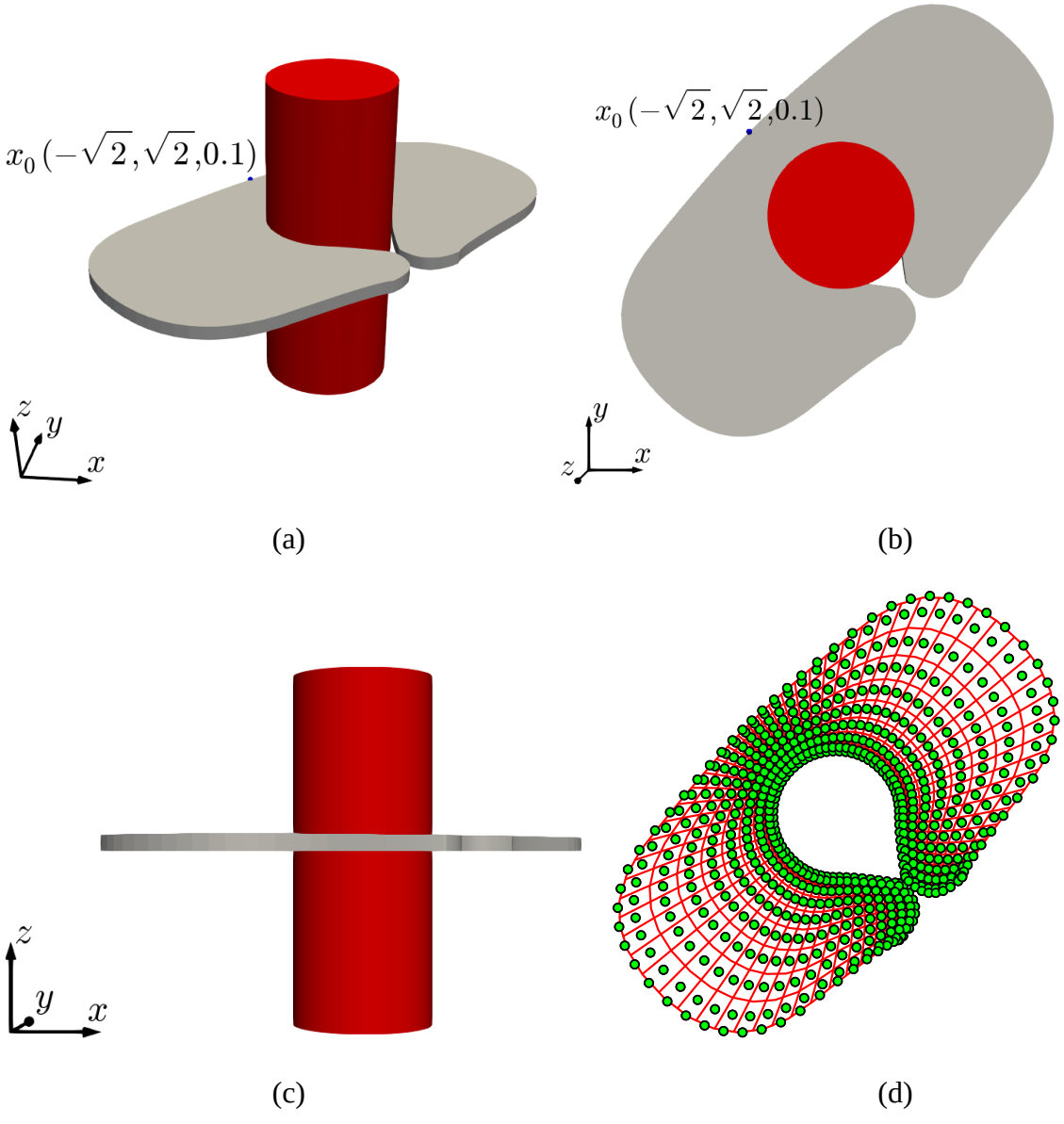

Figure 4.8 Irregularly curved FGM plate (a) 3D view; (b) top view; (c) front view; (d) IGA refinement

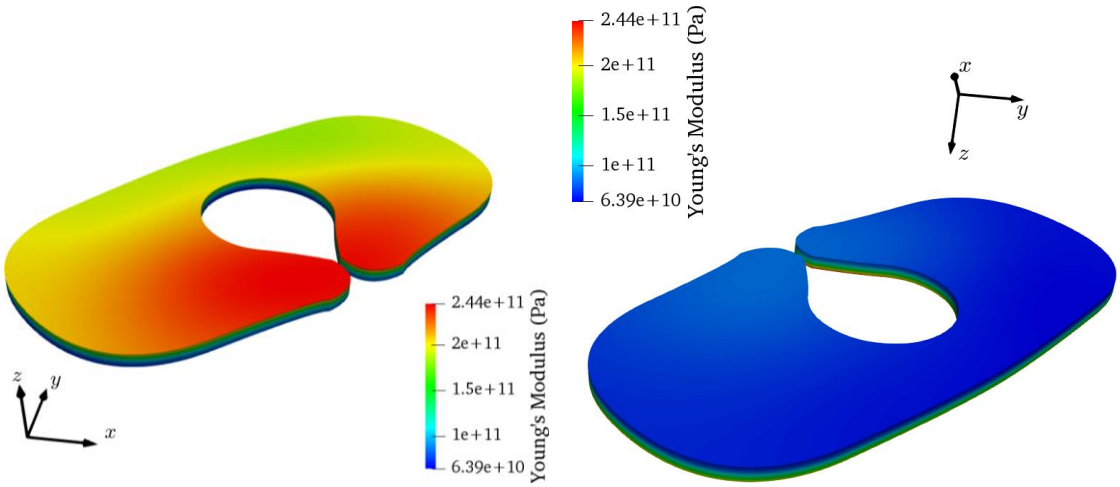

(a) (b)

Figure 4.9 Realization of the random field of the irregularly curved FGM plate (a) from top surface to bottom surface; (b) from bottom surface to top surface

In this example, a point x_0 on the top surface of the curved plate is analysed. The first two statistical moments of u_z, ε_{xx}, σ_{xx}, γ_{xz}, and τ_{xz} at x_0 are determined and the corresponding results are reported in Table 4.4. As evidently illustrated in Table 4.4, the means and standard deviations of the concerned structural response at x_0 obtained by the proposed method are having excellent agreement with the MCS approach.

Table 4.4 Statistical characteristics comparisons of u_z, ε_{xx}, σ_{xx}, γ_{xz}, and τ_{xz} at x_0 between SSIGA and MCS approaches

Method	Statistical characteristics	u_z	ε_{xx}	σ_{xx}	γ_{xz}	τ_{xz}
MCS	Mean	3.0927e-8	-3.1475e-7	-8.9545e+4	-1.1613e-9	-88.47
	Standard deviation	1.0066e-7	2.1591e-8	2.7570e+3	1.6016e-9	124.69

SSIGA (5-order PCE)	Mean	3.0750e-8	-3.1473e-7	-8.9548e+4	-1.1641e-9	-88.68
	Standard deviation	1.0064e-7	2.1538e-8	2.7485e+3	1.6026e-9	124.76

In addition to the determinations of the means and standard deviations of the concerned structural responses, the PDFs and CDFs of the concerned structural responses at point x_0 are established by utilizing the SSIGA and the results are also verified by comparing with the MCS results with 1,000,000 simulation cycles. The PDFs and CDFs of u_z, ε_{xx}, σ_{xx}, γ_{xz}, and τ_{xz} at x_0 are systematically established as shown in Figures 10-14. Particularly, the relative errors of the CDFs of the concerned structural responses are also reported in Figures 4.10-4.14.

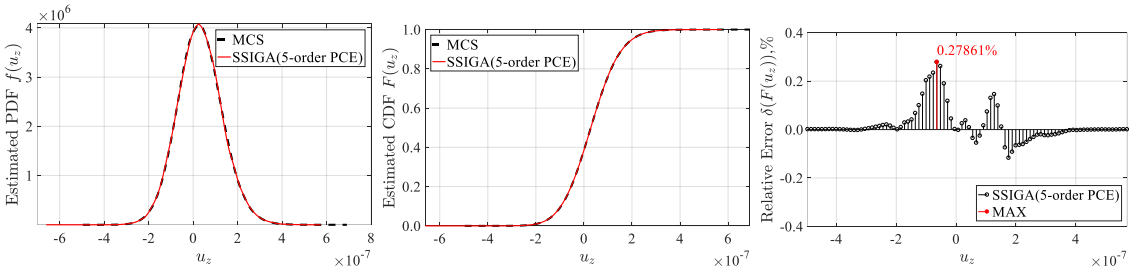

(a) (b) (c)

Figure 4.10 Estimated (a) PDF, (b) CDF and (c) relative errors of CDF of u_z at point x_0

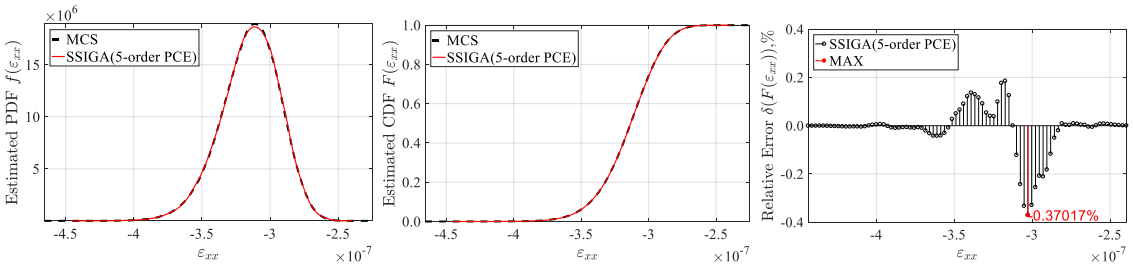

(a) (b) (c)

Figure 4.11 Estimated (a) PDF, (b) CDF and (c) relative errors of CDF of ε_{xx} at point x_0

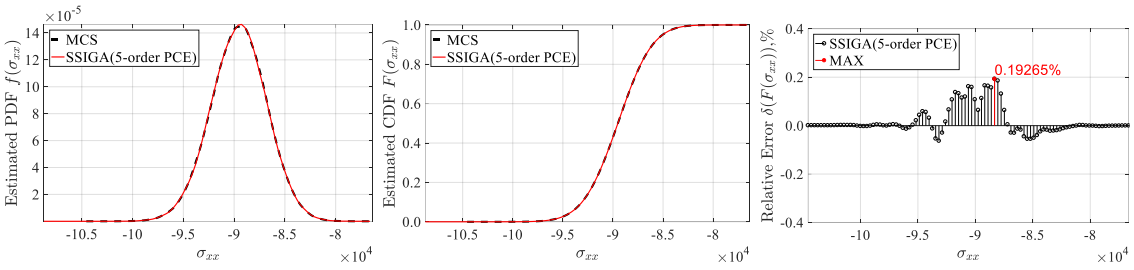

(a) (b) (c)

Figure 4.12 Estimated (a) PDF, (b) CDF and (c) relative errors of CDF of σ_{xx} at point x_0

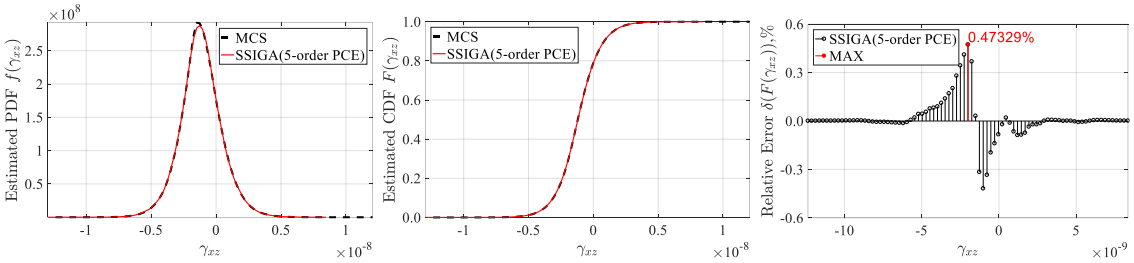

(a) (b) (c)

Figure 4.13 Estimated (a) PDF, (b) CDF and (c) relative errors of CDF of γ_{xz} at point x_0

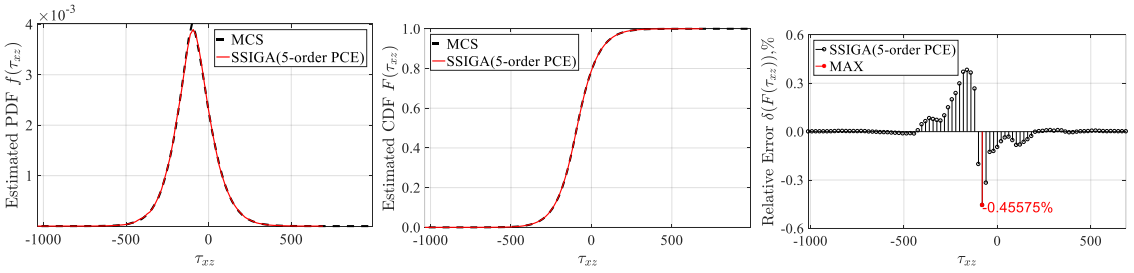

(a) (b) (c)

Figure 4.14 Estimated (a) PDF, (b) CDF and (c) relative errors of CDF of τ_{xz} at point x_0

From the quantitative assessment on the relative errors between SSIGA and MCS approaches, the maximum relative error between SSIGA results and MCS results are less than 0.5%, which is small enough to demonstrate the accuracy and applicability of the proposed SSIGA scheme for stochastic analysis of FGM plates with intricate geometries.

4.6 Conclusion

In this paper, a new computational stochastic analysis framework, namely spectral stochastic isogeometric analysis, is presented for stochastic static analysis of FGM plate through first-order shear deformation theory. The uncertain Young's modulus is modelled as a random field to incorporate the spatial variation effects of the uncertain system parameter. By implementing the NURBS as basis functions within the K-L expansion, a new random field discretization technique is presented which can effectively handle random fields defined within very complex geometry. After valid random field discretization, the means and standard deviations of structural displacement, strain, and stress of the FGM plate can be explicitly estimated through the PCE. In addition to the estimation to the estimation of the first two moments of statistics of the structural responses, the PDFs and CDFs of the concerned structural responses can also be established through the statistical inference techniques. Consequently, the serviceability and strength limits of the FGM plate can be effectively determined through the proposed SSIGA approach. The major advantage of the SSIGA analysis framework is that the proposed method is able to maintain the exact geometry of the structure as well as the

random field defined on the structure between the design model and the stochastic analysis model. Consequently, the quality of the uncertainty analysis (i.e., the quality of the PDFs and CDFs) can be improved.

In order to verify the applicability, accuracy and efficiency of the proposed methodology, two distinctive FGM plates with nonstandard geometries have been investigated. By closely examining the results against the MCS approach with large simulation cycles, all computational results of the SSIGA approach are satisfactory but with much higher computational efficiency. Therefore, the proposed SSIGA approach provides a quantitative assessment framework to evaluate the safety of practically motivated FGM plate with nonstandard geometry against static loadings and the physically inherent uncertainties.

Chapter 5

SPECTRAL STOCAHSTIC ISOGEOMETRIC ANALYSIS OF FREE VIBRATION

5.1 Summary

In Chapter 5, a novel spectral stochastic isogeometric analysis (SSIGA) is proposed for the free vibration analysis of engineering structures involving uncertainties. The stochastic Young's modulus and material density of the structure are modelled as random fields with Gaussian and non-Gaussian distributions.

The organization of Chapter 5 is briefed as follows. The stochastic free vibration analysis is briefly introduced in Section 5.3. Subsequently, the proposed SSIGA for stochastic free vibration analysis of engineering structures involving random fields is presented in Section 5.4. Particularly, the discretization of random field with non-Gaussian within SSIGA and the freshly introduced aPC approach are presented in subsections 5.4.1 and 5.4.2 respectively. Consequently, the proposed Galerkin-based method is formulated in subsection 5.4.3. To illustrate the accuracy, efficiency, and applicability of the proposed SSIGA for stochastic free vibration analysis, two different numerical examples are explored comprehensively in Section 5.5. Finally, some conclusions are drawn in Section 5.6.

The research work presented in Chapter 5 has produced one journal paper which has been published in *Computer Methods in Applied Mechanics and Engineering*, detailed as:

Li, K., Wu, D., Gao, W. and Song, C., 2019. Spectral stochastic isogeometric analysis of free vibration. *Computer Methods in Applied Mechanics and Engineering*. 350, pp.1-27

5.2 Introduction

To overcome the challenges and revamp the traditional stochastic analysis routine, a novel spectral stochastic isogeometric analysis (SSIGA) framework is proposed for the free vibration analysis considering spatially dependent stochastic uncertainties. In the novel SSIGA approach, the considered stochastic uncertainties, which are including Young's modulus and material density, are modelled as Gaussian and non-Gaussian random fields. Since the stochastic analysis model within SSIGA is exactly the same as the design model in CAD, the random fields are assuredly acting on the physical domain of the intentionally designed model. Therefore, the geometric errors can be eliminated in the Karhunen-Loève (K-L) expansion for the random field discretization (Li, Gao, *et al.*, 2018; Rahman, 2018). Meanwhile, global smoothness representations of random fields are accessible by taking the advantage of the higher-order continuity of the basis functions in CAD system (Li, Gao, *et al.*, 2018; Rahman, 2018). Such feature also promises a globally smooth K-L discretization for random fields. Arbitrary polynomial chaos (Witteveen and Bijl, 2006) (aPC) method is freshly adopted to investigate the stochastic generalized eigenvalue problems. In this paper, the aPC approach is implemented through Stieltjes procedure, which is more stable than the classical Gram-Schmidt algorithm in (Witteveen and Bijl, 2006). A Galerkin-based method is proposed to orthogonalize the approximation error with respect to the Hilbert space spanned by the truncated aPC. Such

approach can circumvent the dependence of the statistical solution on the quality and quantity of the underlying random number generator, and provides an approximation to the complete probabilistic description of the eigensolutions. Finally, the stochastic generalized eigenvalue problem can be transformed into a system of deterministic non-linear equations. The system is solved by the Newton-Raphson method in this paper. Different orders of statistical moments, the probability density function (PDF), and the cumulative distribution function (CDF) of the concerned stochastic eigensolutions will be obtained. Since the closed-form solutions for the stochastic eigenvalue problems are usually unavailable, thus, the Monte Carlo Simulation (MCS) approach is adopted for partially verifying all the computational results. The accuracy, efficiency, and applicability of the proposed method are comprehensively investigated through two numerical examples.

5.3 Stochastic free vibration analysis

In isogeometric analysis, given a linear multi-degree-of-freedom structural system, the governing equation for the free vibrations can be formulated as:

$$\mathbf{M}\ddot{\mathbf{u}}(t) + \mathbf{K}\mathbf{u}(t) = \mathbf{0} \tag{5.1}$$

where $\ddot{\mathbf{u}}(t) = d^2\mathbf{u}(t)/dt^2$ denotes the acceleration vector and $\mathbf{u}(t)$ denotes the displacement vector; $\mathbf{M}$ and $\mathbf{K}$ denote the global consistent mass and stiffness matrices respectively, and can be assembled by their corresponding elemental matrices $\mathbf{M}^e$ and $\mathbf{K}^e$ as follows,

$$\mathbf{M} = \sum_e \mathbf{M}^e \quad \mathbf{K} = \sum_e \mathbf{K}^e \tag{5.2}$$

and

$$\mathbf{K}^e = \int_{D_e} \mathbf{B}^T \mathbf{D}\mathbf{B} dD \quad \mathbf{M}^e = \int_{D_e} \rho \mathbf{N}^T \mathbf{N} dD \tag{5.3}$$

where e denotes the element index; ρ denotes the material density; $\mathbf{N}$ denotes the displacement interpolation matrix within an element; $\mathbf{B}$ denotes the compatibility matrix which relates strain vector to the displacement vector within an element; $\mathbf{D}$ denotes the elasticity matrix; D_e denotes the volume of the eth element.

The following formulation will be carried out for a single physical mode. Since the basis functions within IGA are pointwise non-negative, every component of the consistent mass matrix is non-negative. The normal mode, $\mathbf{\Phi}$ can be obtained by the separation of variables:

$$\mathbf{u}(t) = \mathbf{\Phi} e^{\mathrm{i}\omega t} \tag{5.4}$$

where ω denotes the natural frequency with unit rad/s . Combining Eq.(5.1) and Eq.(5.4) leads to the generalized eigenvalue problem (Cottrell *et al.*, 2006):

$$\mathbf{K}\mathbf{\Phi} = \lambda \mathbf{M}\mathbf{\Phi} \tag{5.5}$$

where λ denotes the eigenvalue, and $\mathbf{\Phi}$ denotes the corresponding eigenvector.

The normal modes are defined up to a multiplicative constant. Different ways of normalization have been proposed. One of the most widely used is

$$\mathbf{\Phi}^T \mathbf{M}\mathbf{\Phi} = 1 \tag{5.6}$$

When considering randomness in the parameters of the underlying physical system such as elastic and dynamic parameters, the stochastic generalized eigenvalue problem in Eq.(5.5) and the normalization condition Eq.(5.6) can be represented as follows,

$$\mathbf{K}(\theta)\mathbf{\Phi}(\theta) = \lambda(\theta)\mathbf{M}(\theta)\mathbf{\Phi}(\theta) \tag{5.7}$$

$$\mathbf{\Phi}^T(\theta)\mathbf{M}(\theta)\mathbf{\Phi}(\theta)=1 \tag{5.8}$$

where $\theta \in \Omega$ and (Ω, Σ, P) is the probability space associated with the underlying physical experiments. The space of square integrable random variables, $L_2(\Omega)$, forms a Hilbert pace, with the norm denoted by $\|\cdot\|_{L_2(\Omega)}$.

5.4 SSIGA for the generalized stochastic eigenvalue problem

5.4.1 Generalized isogeometric basis function based Karhunen-Loève expansion

Generally, random system parameters presented in Eqs.(5.7) and (5.8) can be modelled as random variables $\{\eta_i(\theta)\}_{i=1}^m$ or as random field $H(\mathbf{x},\theta)$. In this paper, all random parameters are modelled as random fields, which provides a more generalized stochastic analysis framework by incorporating both spatially dependent and independent uncertain parameters. Particularly, the homogeneous Gaussian and Lognormal random fields are implemented herein. Moreover, exponential and Bessel covariance functions are adopted to model the dependency of the uncertain parameters. The incorporated covariance functions have generalized forms as follows,

$$\begin{aligned} C_{HH}(\mathbf{x},\mathbf{x}') &= \sigma_H^2 \cdot e^{-\frac{\|x-x'\|}{l}} && \text{(Exponential)} \\ C_{HH}(\mathbf{x},\mathbf{x}') &= \sigma_H^2 \cdot \frac{\|x-x'\|}{l} \cdot K_1\left(\frac{\|x-x'\|}{l}\right) && \text{(Bessel)} \end{aligned} \tag{5.9}$$

where $\sigma_H \in \Re^+$ denotes the standard deviation of the random field; $\|\bullet\|$ denotes the norm of a vector in 1-, 2-, or 3-dimensional Euclidean space. $l \in \Re$ denotes the correlation lengths; K_1 is the modified second-kind Bessel function of order one.

For general engineering applications, the homogeneous Gaussian random fields can be represented with respect to some basis set in $L_2(\Omega,\Sigma,F)$ by the Karhunen-Loève expansion. The generalized isogeometric basis functions based K-L expansion within SSIGA has already been investigated in (Li, Gao, *et al.*, 2018; Rahman, 2018).

Given a random field $H(\mathbf{x},\theta)$ with spatial geometry represented as Eq.(3.9), by implementing the K-L expansion processes and formulations that have already presented in Chapter 3, the homogeneous Gaussian random field $H(\mathbf{x},\theta)$ can be approximated by $\hat{H}(\mathbf{x},\theta)$ with M terms as follows,

$$H(\mathbf{x},\theta)\approx\hat{H}(\mathbf{x},\theta)=\sum_{\mathbf{I}}^{\mathbf{N}_{cp}}\mu_{\mathbf{I}}^{H}R_{\mathbf{I}}^{\mathbf{P}}(\xi)+\sum_{i=1}^{M}\sqrt{\lambda_i}\eta_i(\theta)\left(\sum_{\mathbf{I}}^{\mathbf{N}_{cp}}\vartheta_{\mathbf{I}}^{i}R_{\mathbf{I}}^{\mathbf{P}}(\xi)\right) \tag{5.10}$$

The utilization of the Gaussian random field to model spatially dependent uncertainties is common practice in the context of stochastic analysis. However, Gaussian random fields are not well suited to modelling material properties (Young's modulus, material density), which are by their nature positive valued. In contrast, the lognormal field appears more suitable in engineering applications to model positive valued physical uncertain parameters. For a lognormal random field $H^L(\mathbf{x},\theta)$, which can be defined as a transformation of a Gaussian field $H^G(\mathbf{x},\theta)$ as

$$H^L(\mathbf{x},\theta)=\exp(H^G(\mathbf{x},\theta)) \tag{5.11}$$

In order to incorporate the lognormal random fields in the proposed SSIGA framework for stochastic free vibration analysis, the lognormal random field $H^L(\mathbf{x},\theta)$ can be approximated by the arbitrary polynomial chaos expansion as in (R. Ghanem, 1999b; Sudret and Kiureghian, 2000). The concept and formulation of arbitrary polynomial chaos expansion will be introduced in the following subsection.

5.4.2 The arbitrary polynomial chaos expansion (aPC)

When solving a stochastic generalized eigenvalue problem, which involves charactering the probabilistic measure of the specific eigenvalue λ and the corresponding eigenvectors $\mathbf{\Phi}$ with respect to random parameters, the polynomial chaos decompositions provide a rational framework for representing random variables and vectors with respect to a basis set of orthogonal polynomials. In order to provide a general analysis framework, the arbitrary polynomial chaos expansion (aPC) is adopted to represent the stochastic responses, i.e. $\lambda(\theta)$ and $\mathbf{\Phi}(\theta)$.

For achieving a more effective illustration, considering a stochastic system response $u(\mathbf{x},\theta)$, which can be expanded by a polynomial chaos expansion. That is,

$$u(\mathbf{x},\theta)=\sum_{j=0}^{\infty}u_j(\mathbf{x})\mathbf{\Psi}_j(\boldsymbol{\eta}(\theta)) \tag{5.12}$$

where $\{u_j(\mathbf{x})\}$ denotes the *j*th polynomial chaos expansion coefficient; $\mathbf{\Psi}_j(\boldsymbol{\eta}(\theta))$ denotes the *j*th multidimensional orthogonal polynomial in terms of an *m*-dimensional vector of random variables $\boldsymbol{\eta}(\theta)$, and *m* is the number of uncertain parameters. In typical numerical analysis, the infinite summation series involved in Eq.(5.12) is truncated at the *P*th degree, namely, $u(\mathbf{x},\theta)\approx\hat{u}(\mathbf{x},\theta)=\sum_{j=0}^{P-1}u_j(\mathbf{x})\mathbf{\Psi}_j(\boldsymbol{\eta}(\theta))$ with

$$P=\frac{(m+p)!}{m!\,p!} \tag{5.13}$$

where *p* is the highest order of the polynomials $\{\mathbf{\Psi}_j(\boldsymbol{\eta})\}_{j=0}^{P-1}$. The polynomials $\{\mathbf{\Psi}_j(\boldsymbol{\eta})\}_{j=0}^{P-1}$ satisfy the following orthogonality relation

$$\left\langle\mathbf{\Psi}_i(\boldsymbol{\eta})\mathbf{\Psi}_j(\boldsymbol{\eta})\right\rangle=\left\langle\mathbf{\Psi}_i^2(\boldsymbol{\eta})\right\rangle\delta_{ij},\qquad i,j=0,1,\ldots,P-1 \tag{5.14}$$

with δ_{ij} the Kronecker delta and $\langle \bullet \rangle$ denotes

$$\langle \bullet \rangle = \int_{S_{\boldsymbol{\eta}}} (\bullet)\mathbf{W}(\boldsymbol{\eta})d\boldsymbol{\eta} \tag{5.15}$$

where $\mathbf{W}(\boldsymbol{\eta})$ is the weighting function corresponding to the polynomial chaos $\{\boldsymbol{\Psi}_j(\boldsymbol{\eta})\}_{j=0}^{P-1}$ and $S_{\boldsymbol{\eta}}$ is the support of $\boldsymbol{\eta}$.

In the framework of aPC expansion, the multidimensional orthogonal polynomials $\{\boldsymbol{\Psi}_j(\boldsymbol{\eta})\}_{j=0}^{P-1}$ can be constructed using the tensor product of the one-dimensional polynomial $\{\Psi_j(\eta)\}_{j=0}^{P-1}$, which is constructed numerically with respect to the weight function by different algorithms, such as, the classical Gram-Schmidt procedure, the modified Gram-Schmidt procedure, the Stieltjes procedure, etc. In this chapter, the classical Gram-Schmidt procedure and the Stieltjes procedure are introduced briefly, but only the Stieltjes procedure is adopted in the numerical examples.

For the classical Gram-Schmidt procedure, a set of one-dimensional monic orthogonal polynomials $\{\Psi_j(\eta)\}_{j=0}^{P-1}$ can be generated recursively as follows,

$$\Psi_j(\eta) = e_j(\eta) - \sum_{k=0}^{j-1} c_{jk}\Psi_k(\eta), \qquad j = 1,2,...,P-1 \tag{5.16}$$

with $\Psi_0 = 1$ and

$$c_{jk} = \frac{\langle e_j(\eta)\Psi_k(\eta)\rangle}{\langle \Psi_k(\eta)\Psi_k(\eta)\rangle} \tag{5.17}$$

where the polynomials $e_j(\eta)$ are polynomials of exact degree *j*.

However, the classical Gram-Schmidt procedure, as well as the modified version, suffers from numerical instability. That is, the round-off errors can accumulate and destroy the orthogonality of the resulting polynomials, especially for the high-order orthogonal polynomials. Therefore, the Stieltjes procedure is also introduced briefly herein.

For the Stieltjes procedure in (Gautschi, 2008), a set of one-dimensional monic orthogonal polynomials $\{\Psi_j(\eta)\}_{j=0}^{P-1}$ can be generated by following the recurrence relation as follows,

$$\begin{aligned} &\Psi_{-1}(\eta)=0, \quad \Psi_0(\eta)=1, \\ &\Psi_{k+1}(\eta)=(\eta-a_k)\Psi_k(\eta)-b_k\Psi_{k-1}(\eta), \quad k=0,1,2,\ldots,P-1 \end{aligned} \tag{5.18}$$

where the coefficients a_k and b_k of the aPC expansion can be determined by

$$a_k=\frac{\langle \eta\Psi_k(\eta)\Psi_k(\eta)\rangle}{\langle \Psi_k(\eta)\Psi_k(\eta)\rangle}, \quad k=0,1,2,\ldots,P-1 \tag{5.19}$$

$$b_0=\int_{S_\eta} w(\eta)d\eta, \quad b_k=\frac{\langle \Psi_k(\eta)\Psi_k(\eta)\rangle}{\langle \Psi_{k-1}(\eta)\Psi_{k-1}(\eta)\rangle}, \quad k=1,2,\ldots,P-1 \tag{5.20}$$

As aforementioned, lognormal random field can be represented by aPC, and the detailed expansion process for a lognormal random field $H^L(\mathbf{x},\theta)$ through the aPC approach is presented herein.

Considering the following truncated Karhunen-Loève expansion of a homogeneous Gaussian random field $\hat{H}^G(\mathbf{x},\theta)$ within SSIGA framework as Eq.(5.10)

$$\hat{H}^G(\mathbf{x},\theta)=\bar{H}^G(\mathbf{x})+\tilde{H}^G(\mathbf{x},\theta)=\sum_{\mathbf{I}}^{\mathbf{N}_{cp}}\mu_{\mathbf{I}}^G R_{\mathbf{I}}^{\mathbf{P}}(\xi)+\sum_{i=1}^{M}\sqrt{\lambda_i}\eta_i(\theta)\left(\sum_{\mathbf{I}}^{\mathbf{N}_{cp}}\vartheta_{\mathbf{I}}^i R_{\mathbf{I}}^{\mathbf{P}}(\xi)\right) \tag{5.21}$$

Then, a lognormal random field transformed from $\hat{H}^G(\mathbf{x},\theta)$ can be defined as follows

$$H^L(\mathbf{x},\theta) = \exp(\hat{H}^G(\mathbf{x},\theta)) \tag{5.22}$$

Now, an arbitrary polynomial chaos expansion is adopted to represent the lognormal random field $\hat{H}^L(\mathbf{x},\theta)$ as follows,

$$H^L(\mathbf{x},\theta) \approx \hat{H}^L(\mathbf{x},\theta) = \sum_{i=0}^{P-1} L_i(\mathbf{x})\boldsymbol{\Psi}_i(\boldsymbol{\eta}(\theta)) \tag{5.23}$$

Finally, each coefficient corresponding to $L_i(\mathbf{x})$ can be obtained as follows,

$$L_i(\mathbf{x}) = \frac{\left\langle H^L(\mathbf{x},\theta)\cdot\boldsymbol{\Psi}_i(\boldsymbol{\eta}(\theta))\right\rangle}{\left\langle \boldsymbol{\Psi}_i^2(\boldsymbol{\eta}(\theta))\right\rangle} \tag{5.24}$$

5.4.3 Galerkin-based method within SSIGA for stochastic generalized eigenvalue problem

In this study, both Young's modulus $E(\mathbf{x})$ and material density $\rho(\mathbf{x})$ of the engineering structure are considered as random fields, i.e. $E(\mathbf{x},\theta)$ and $\rho(\mathbf{x},\theta)$. To achieve a generalized computational stochastic mechanics framework, two explicit cases of analysis are considered herein. The first case of analysis considers all random fields as homogeneous Gaussian random fields, whereas the second case investigates the situation when lognormal random fields are implemented to model the spatially dependent uncertain system parameters.

Firstly, considering the case when both $E(\mathbf{x},\theta)$ and $\rho(\mathbf{x},\theta)$ are modelled as homogeneous Gaussian random fields. By applying the K-L expansion within the

proposed SSIGA approach, $E^G(\mathbf{x},\theta)$ and $\rho^G(\mathbf{x},\theta)$ can be approximated by $\hat{E}^G(\mathbf{x},\theta)$ and $\hat{\rho}^G(\mathbf{x},\theta)$ respectively,

$$E^G(\mathbf{x},\theta) \approx \hat{E}^G(\mathbf{x},\theta) = \sum_{\mathbf{I}}^{\mathbf{N}_{cp}} \mu_{\mathbf{I}}^E R_{\mathbf{I}}^{\mathbf{P}}(\xi) + \sum_{i_1=1}^{M_1} \sqrt{\lambda_{i_1}}\,\eta_{i_1}(\theta) \left(\sum_{\mathbf{I}}^{\mathbf{N}_{cp}} \vartheta_{\mathbf{I}}^{i_1} R_{\mathbf{I}}^{\mathbf{P}}(\xi) \right) \tag{5.25}$$

$$\rho^G(\mathbf{x},\theta) \approx \hat{\rho}^G(\mathbf{x},\theta) = \sum_{\mathbf{I}}^{\mathbf{N}_{cp}} \mu_{\mathbf{I}}^\rho R_{\mathbf{I}}^{\mathbf{P}}(\xi) + \sum_{i_2=1}^{M_2} \sqrt{\lambda_{i_2}}\,\varsigma_{i_2}(\theta) \left(\sum_{\mathbf{I}}^{\mathbf{N}_{cp}} \phi_{\mathbf{I}}^{i_2} R_{\mathbf{I}}^{\mathbf{P}}(\xi) \right) \tag{5.26}$$

Substituting Eqs.(5.25) and (5.26) into Eq.(5.3),

$$\mathbf{K}^e(\theta) = \int_{D_e} \mathbf{B}^T \hat{E}^G(\mathbf{x},\theta) \mathbf{D}_0 \mathbf{B} dD \tag{5.27}$$

$$\mathbf{M}^e(\theta) = \int_{D_e} \hat{\rho}^G(\mathbf{x},\theta) \mathbf{N}^T \mathbf{N} dD \tag{5.28}$$

where $\mathbf{D}_0$ denotes the deterministic elasticity matrix.

Then, by expanding $\hat{E}^G(\mathbf{x},\theta)$, the stochastic elemental stiffness matrix $\mathbf{K}^e(\theta)$ .can be reformulated as:

$$\mathbf{K}^e(\theta) = \mathbf{K}_0^e + \sum_{i_1=1}^{M_1} \mathbf{K}_{i_1}^e \eta_{i_1}(\theta) \tag{5.29}$$

where $\mathbf{K}_0^e$ denotes the mean element stiffness matrix and $\mathbf{K}_i^e$ denotes deterministic element stiffness matrix. Specifically,

$$\mathbf{K}_0^e = \int_{D_e} \sum_{\mathbf{I}}^{\mathbf{N}_{cp}} \mu_{\mathbf{I}}^E R_{\mathbf{I}}^{\mathbf{P}}(\xi) \mathbf{B}^T \mathbf{D}_0 \mathbf{B} dD \tag{5.30}$$

$$\mathbf{K}_{i_1}^e = \sqrt{\lambda_{i_1}} \int_{D_e} \left(\sum_{\mathbf{I}}^{\mathbf{N}_{cp}} \vartheta_{\mathbf{I}}^{i_1} R_{\mathbf{I}}^{\mathbf{P}}(\xi) \right) \mathbf{B}^T \mathbf{D}_0 \mathbf{B} dD \tag{5.31}$$

Similarly, the stochastic elemental mass matrix can be reformulated as:

$$\mathbf{M}^e(\theta) = \mathbf{M}_0^e + \sum_{i_2=1}^{M_2} \mathbf{M}_{i_2}^e \varsigma_{i_2}(\theta) \tag{5.32}$$

where $\mathbf{M}_0^e$ denotes the mean element mass matrix and $\mathbf{M}_i^e$ denotes the deterministic element mass matrix. Specifically,

$$\mathbf{M}_0^e = \int_{D_e} \sum_{\mathbf{I}}^{\mathbf{N}_{cp}} \mu_{\mathbf{I}}^{\rho} R_{\mathbf{I}}^{\mathbf{P}}(\boldsymbol{\xi}) \mathbf{N}^T \mathbf{N} dD \tag{5.33}$$

$$\mathbf{M}_{i_2}^e = \sqrt{\lambda_{i_2}} \int_{D_e} \left(\sum_{\mathbf{I}}^{\mathbf{N}_{cp}} \phi_{\mathbf{I}}^{i_2} R_{\mathbf{I}}^{\mathbf{P}}(\boldsymbol{\xi}) \right) \mathbf{N}^T \mathbf{N} dD \tag{5.34}$$

Then, by supposing $\eta_0(\theta) \equiv 1$ and $\varsigma_0(\theta) \equiv 1$, the stochastic global stiffness and mass matrices $\mathbf{K}(\theta)$ and $\mathbf{M}(\theta)$ can be reformulated as follows

$$\mathbf{K}(\theta) = \sum_{i_1=0}^{M_1} \mathbf{K}_{i_1} \eta_{i_1}(\theta) \tag{5.35}$$

$$\mathbf{M}(\theta) = \sum_{i_2=0}^{M_1} \mathbf{M}_{i_2} \varsigma_{i_2}(\theta) \tag{5.36}$$

For the second case, both Young's modulus and material density are modelled as lognormal random fields, i.e. $E^L(\mathbf{x},\theta)$ and $\rho^L(\mathbf{x},\theta)$. By implementing the aPC approach, $E^L(\mathbf{x},\theta)$ and $\rho^L(\mathbf{x},\theta)$ can be approximated as:

$$E^L(\mathbf{x},\theta) \approx \hat{E}^L(\mathbf{x},\theta) = \sum_{i=0}^{P_1-1} E_i^L(\mathbf{x}) \boldsymbol{\Psi}_i(\boldsymbol{\eta}(\theta)) \tag{5.37}$$

$$\rho^L(\mathbf{x},\theta) \approx \hat{\rho}^L(\mathbf{x},\theta) = \sum_{m=0}^{P_2-1} \rho_m^L(\mathbf{x}) \boldsymbol{\Psi}_m(\boldsymbol{\varsigma}(\theta)) \tag{5.38}$$

By applying the same algorithm as mentioned in the previous section, the stochastic stiffness and mass matrices $\mathbf{K}(\theta)$ and $\mathbf{M}(\theta)$ can also be reformulated as,

$$\mathbf{K}(\theta) = \sum_{i=0}^{P_1-1} \mathbf{K}_i \boldsymbol{\Psi}_i(\boldsymbol{\eta}(\theta)) \tag{5.39}$$

$$\mathbf{M}(\theta) = \sum_{m=0}^{P_2-1} \mathbf{M}_m \boldsymbol{\Psi}_m(\boldsymbol{\varsigma}(\theta)) \tag{5.40}$$

Specifically, for each $\mathbf{K}_i$ and $\mathbf{M}_m$ of a specific element e, they can be represented as follows,

$$\mathbf{K}_i^e = \int_{D_e} E_i^L \mathbf{B}^T \mathbf{D}_0 \mathbf{B} dD \tag{5.41}$$

$$\mathbf{M}_m^e = \int_{D_e} \rho_m^L \mathbf{N}^T \mathbf{N} dD \tag{5.42}$$

Finally, in order to provide a unified formulation, the stochastic stiffness and mass matrices $\mathbf{K}(\theta)$ and $\mathbf{M}(\theta)$ are approximated by a finite decomposition in the following forms,

$$\mathbf{K}(\theta) = \sum_{i=0}^{L_1} \mathbf{K}_i \boldsymbol{\varphi}_i(\boldsymbol{\eta}(\theta)) \tag{5.43}$$

$$\mathbf{M}(\theta) = \sum_{m=0}^{L_2} \mathbf{M}_m \boldsymbol{\varphi}_m(\boldsymbol{\varsigma}(\theta)) \tag{5.44}$$

where all the terms are corresponding to Eq.(5.35), Eq.(5.36) or Eq.(5.39), Eq(5.40) respectively, which are depending on whether the Gaussian or lognormal random field is adopted to model $E(\mathbf{x}, \theta)$ and $\rho(\mathbf{x}, \theta)$.

For the stochastic responses $\lambda(\theta)$ and $\mathbf{\Phi}(\theta)$ that are formulated in Eq.(5.7), the aPC approach can be implemented to approximate them as $\hat{\lambda}(\theta)$ and $\hat{\mathbf{\Phi}}(\theta)$, respectively. Since $\{\eta_{i_1}(\theta)\}$ and $\{\varsigma_{i_2}(\theta)\}$ are random parameters of the stochastic eigenvalue problem, the aPC should be constructed with respect to a (M_1+M_2)-dimensional random vector $\{\eta_{i_1}(\theta),\varsigma_{i_2}(\theta)\}$. For the *P*th-order truncation, $\hat{\lambda}(\theta)$ and $\hat{\mathbf{\Phi}}(\theta)$ can be represented as follows,

$$\hat{\lambda}(\theta)=\sum_{l=0}^{P-1}\lambda_l\mathbf{\Psi}_l(\boldsymbol{\eta}(\theta),\boldsymbol{\varsigma}(\theta)) \tag{5.45}$$

$$\hat{\mathbf{\Phi}}(\theta)=\sum_{j=0}^{P-1}\mathbf{\Phi}_j\mathbf{\Psi}_j(\boldsymbol{\eta}(\theta),\boldsymbol{\varsigma}(\theta)) \tag{5.46}$$

Then, substituting Eqs.(5.43), (5.44), (5.45), and (5.46) into Eq.(5.7), the stochastic generalized eigenvalue problem can be reformulated as:

$$\sum_{j=0}^{P-1}\sum_{i=0}^{L_1}\mathbf{K}_i\mathbf{\Phi}_j\boldsymbol{\varphi}_i\mathbf{\Psi}_j=\sum_{j=0}^{P-1}\sum_{l=0}^{P-1}\sum_{m=0}^{L_2}\lambda_l\mathbf{M}_m\mathbf{\Phi}_j\boldsymbol{\varphi}_m\mathbf{\Psi}_l\mathbf{\Psi}_j+r \tag{5.47}$$

where r denotes a random residual vector due to the finite term approximation. The residual can be minimized by requiring it to be orthogonal to the approximation subspace spanned by $\{\mathbf{\Psi}_k(\boldsymbol{\eta}(\theta))\}_{k=0}^{P-1}$, resulting in

$$\sum_{j=0}^{P-1}\sum_{i=0}^{L_1}\mathbf{K}_i\mathbf{\Phi}_j\left\langle\boldsymbol{\varphi}_i\mathbf{\Psi}_j\mathbf{\Psi}_k\right\rangle=\sum_{j=0}^{P-1}\sum_{l=0}^{P-1}\sum_{m=0}^{L_2}\lambda_l\mathbf{M}_m\mathbf{\Phi}_j\left\langle\boldsymbol{\varphi}_m\mathbf{\Psi}_l\mathbf{\Psi}_j\mathbf{\Psi}_k\right\rangle,\qquad k=0,\ldots,P-1 \tag{5.48}$$

Similarly, the normalization condition in Eq.(5.8) can be expressed as follows

$$\sum_{i=0}^{P-1}\sum_{j=0}^{P-1}\sum_{m=0}^{L_2}\mathbf{\Phi}_i^T\mathbf{M}_m\mathbf{\Phi}_j\left\langle\boldsymbol{\varphi}_m\mathbf{\Psi}_i\mathbf{\Psi}_j\mathbf{\Psi}_k\right\rangle=\delta_{k0},\qquad k=0,\ldots,P-1 \tag{5.49}$$

Assuming $\mathbf{K}_i \in \Re^{N\times N}$, the stochastic generalized eigenvalue problem can be transformed into a set of $(NP+P)$ nonlinear deterministic equations for each physical mode of the structure with stochastic parameters. To solve the system of nonlinear equations, different algorithms can be adopted. In this paper, the Newton-Raphson (NR) method is adopted to solve the system of nonlinear equations.

Eqs.(5.48) and (5.49) can be written in the form of $\mathbf{R}(\mathbf{x})=0$ where $\mathbf{x}\in\Re^{(NP+P)}$ is a vector containing the set $\{\lambda_0,...,\lambda_{P-1},\boldsymbol{\Phi}_0,...,\boldsymbol{\Phi}_{P-1}\}$. Expanding $\mathbf{R}(\mathbf{x})$ by the Taylor series around $\mathbf{x}$ results

$$\mathbf{R}(\mathbf{x}+\Delta\mathbf{x})=\mathbf{R}(\mathbf{x})+\mathbf{J}\cdot\Delta\mathbf{x}+O(\Delta\mathbf{x}^2) \tag{5.50}$$

where

$$\mathbf{J}_{ij}=\frac{\partial\mathbf{R}_i}{\partial\mathbf{x}_j} \tag{5.51}$$

In order to search for the zeros of $\mathbf{R}(\mathbf{x})$, imposing $\mathbf{R}(\mathbf{x}+\Delta\mathbf{x})=\mathbf{0}$ and neglecting the higher-order terms results:

$$\mathbf{J}\cdot\Delta\mathbf{x}=-\mathbf{R} \tag{5.52}$$

which can compute $\Delta\mathbf{x}$, updating the estimate of $\mathbf{x}$ by

$$\mathbf{x}_{new}=\mathbf{x}_{old}+\Delta\mathbf{x} \tag{5.53}$$

For Eq.(5.48), these can be expressed as

$$\mathbf{R}_k=\sum_{j=0}^{P-1}\sum_{i=0}^{L_1}\mathbf{K}_i\boldsymbol{\Phi}_j\left\langle\boldsymbol{\varphi}_i\boldsymbol{\Psi}_j\boldsymbol{\Psi}_k\right\rangle-\sum_{j=0}^{P-1}\sum_{l=0}^{P-1}\sum_{m=0}^{L_2}\lambda_l\mathbf{M}_m\boldsymbol{\Phi}_j\left\langle\boldsymbol{\varphi}_m\boldsymbol{\Psi}_l\boldsymbol{\Psi}_j\boldsymbol{\Psi}_k\right\rangle,\quad k=0,...,P-1 \tag{5.54}$$

$$\frac{\partial \mathbf{R}_k}{\partial \mathbf{\Phi}_j} = \sum_{i=0}^{L_1} \mathbf{K}_i \left\langle \boldsymbol{\varphi}_i \boldsymbol{\Psi}_j \boldsymbol{\Psi}_k \right\rangle - \sum_{l=0}^{P-1} \sum_{m=0}^{L_2} \lambda_l \mathbf{M}_m \left\langle \boldsymbol{\varphi}_m \boldsymbol{\Psi}_l \boldsymbol{\Psi}_j \boldsymbol{\Psi}_k \right\rangle, \quad k = 0,...,P-1,\ j = 0,...,P-1 \tag{5.55}$$

$$\frac{\partial \mathbf{R}_k}{\partial \lambda_l} = -\sum_{j=0}^{P-1} \sum_{m=0}^{L_2} \mathbf{M}_m \mathbf{\Phi}_j \left\langle \boldsymbol{\varphi}_m \boldsymbol{\Psi}_l \boldsymbol{\Psi}_j \boldsymbol{\Psi}_k \right\rangle, \quad k = 0,...,P-1, l = 0,...,P-1 \tag{5.56}$$

where $\mathbf{R}_k$ denotes the set of N functions in Eq.(5.49) that is corresponding each k.

For Eq.(5.49), by denoting the lth term of the vector $\mathbf{\Phi}_j$ as $\mathbf{\Phi}_{jl}$, these can be expressed as

$$\mathbf{R}_k = \sum_{i=0}^{P-1} \sum_{j=0}^{P-1} \sum_{m=0}^{L_2} \mathbf{\Phi}_i^T \mathbf{M}_m \mathbf{\Phi}_j \left\langle \boldsymbol{\varphi}_m \boldsymbol{\Psi}_i \boldsymbol{\Psi}_j \boldsymbol{\Psi}_k \right\rangle - \delta_{k0}, \quad k = 0,...,P-1 \tag{5.57}$$

$$\frac{\partial \mathbf{R}_k}{\partial \mathbf{\Phi}_{jl}} = 2\sum_{i=0}^{P-1} \sum_{m=0}^{L_2} \mathbf{\Phi}_{in} (\mathbf{M}_m)_{nl} \left\langle \boldsymbol{\varphi}_m \boldsymbol{\Psi}_i \boldsymbol{\Psi}_j \boldsymbol{\Psi}_k \right\rangle - \delta_{k0}, \quad k = 0,...,P-1,\ j = 0,...,P-1 \tag{5.58}$$

$$\frac{\partial \mathbf{R}_k}{\partial \lambda_j} = 0, \quad k = 0,...,P-1,\ j = 0,...,P-1 \tag{5.59}$$

where $\mathbf{R}_k$ denotes the function in Eq.(5.49) that is corresponding to each k. Detailed derivations of Eqs.(5.58) and (5.59) are presented in Appendix 5A. The Jacobian matrix $\mathbf{J}$ is calculated from Eqs.(5.55), (5.56), (5.58), and (5.59). $\Delta\mathbf{x}$ can be obtained from Eq.(5.52). Finally, the updated result $\mathbf{x}_{new}$ can be obtained from Eq.(5.53). The whole procedure is iterated until a pre-defined tolerance is satisfied, which is imposed here using the quantity $\|\mathbf{R}\|$. In order to more effectively illustrate the proposed SSIGA approach for stochastic free vibration analysis, the following flowchart is presented in Figure 5.1.

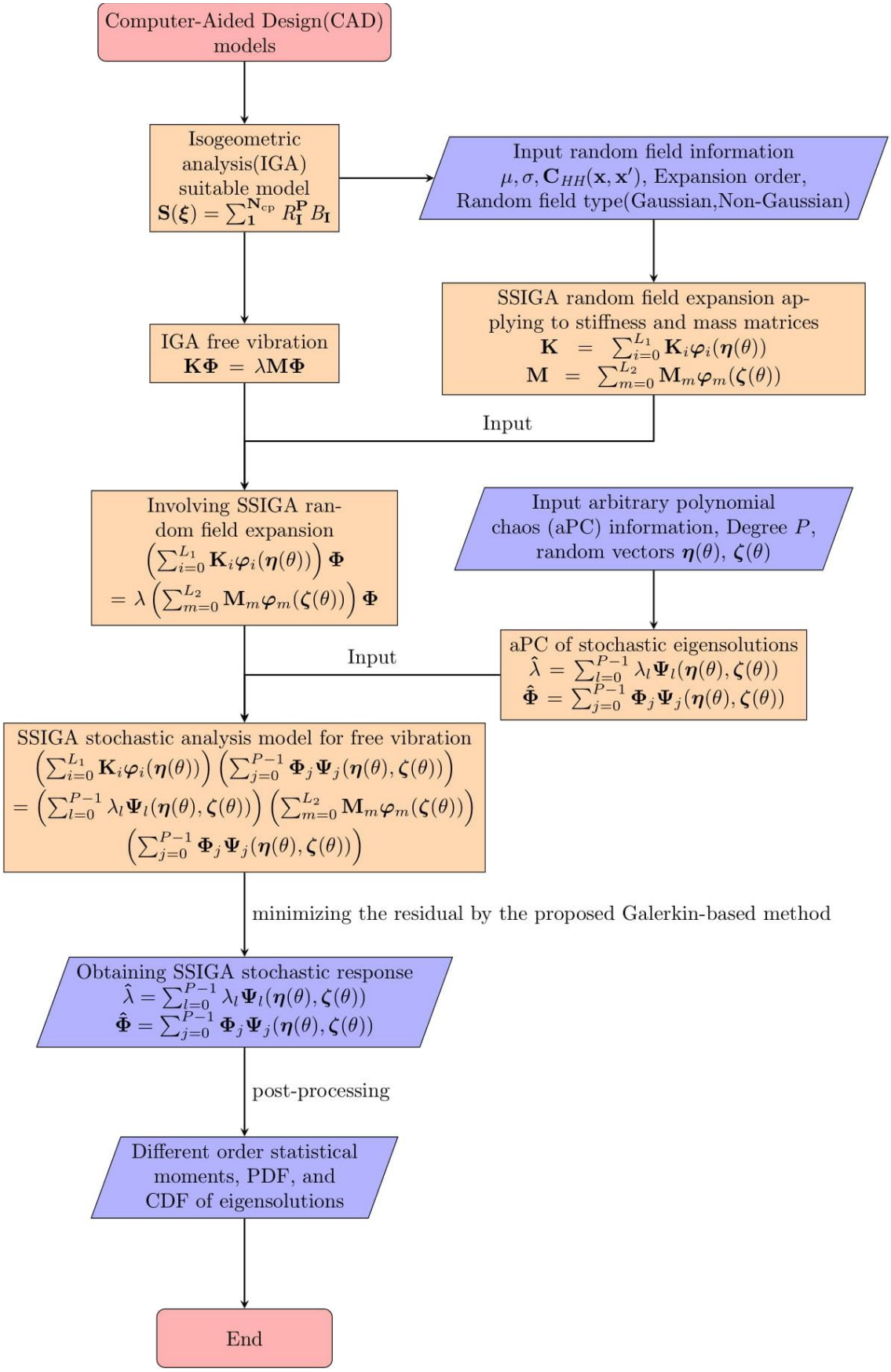

Figure 5.1 Flowchart of SSIGA approach for stochastic free vibration analysis

5.5 Numerical examples

To demonstrate the accuracy, efficiency and applicability of the proposed SSIGA framework for stochastic free vibration analysis of engineering structures with random fields, two numerical examples are thoroughly investigated in this section. For the first numerical example, the proposed method is implemented for a circular strip Mindlin plate. For the second numerical example, a flower-shape Kirchhoff-Love shell is investigated by the proposed method. Since the closed-form analytical solutions are absent for the two numerical examples, all the results obtained within SSIGA framework are partially compared with Monte Carlo Simulation method with large simulation size. The Monte Carlo Simulation adopted herein is achieved by repeatedly executing the deterministic IGA with one possible realization of the random field at each cycle until the predefined total number of simulations is reached. Within the context of the presented numerical examples, all random numbers are generated by employing the Statistics toolbox of MATLAB R2018a, also the evaluation of IGA basis functions is based on the technique presented in (V. P. Nguyen *et al.*, 2015).

5.5.1 Numerical example: circular strip Mindlin plate

In the first numerical example, a circular strip Mindlin plate involving spatially dependent uncertain Young's modulus and material density is investigated. The thickness of the plate is 0.1m. The general structural layout and the adopted IGA mesh of the investigated plate are shown in Figure 5.2. The plate is clamped at its inner edge. Both the Young's modulus and material density of the plate is modelled as homogeneous Gaussian random field for the purpose of demonstration only, and for a specific point $\mathbf{x}_0$, $\mu_{E^G(\mathbf{x}_0,\theta)} = 200\,\text{GPa}$, $\sigma_{E^G(\mathbf{x}_0,\theta)} = 20\,\text{GPa}$, $\mu_{\rho^G(\mathbf{x}_0,\theta)} = 5700\,\text{kg/m}^3$, and

$\sigma_{\rho^G(\mathbf{x}_0,\theta)} = 570\,\mathrm{kg/m^3}$. The exponential covariance function in Eq.(16) with $l = 5\mathrm{m}$ is adopted in two random field modellings.

Within the proposed SSIGA framework, the Young's modulus and material density are assumed as homogeneous Gaussian random fields, which are decomposed by the generalized isogeometric basis functions based K-L expansion approach with three terms. All the stochastic eigensolutions are estimated by different orders of aPC (i.e. 1-order aPC, 2-order aPC, 3-order aPC.). The proposed Galerkin-based method is applied to solve the coefficients of the aPCs, and the tolerance for the Newton-Raphson method is predefined as 10^{-7}. Moreover, the MCS approach with 1,000,000 simulation cycles was adopted for result verification.

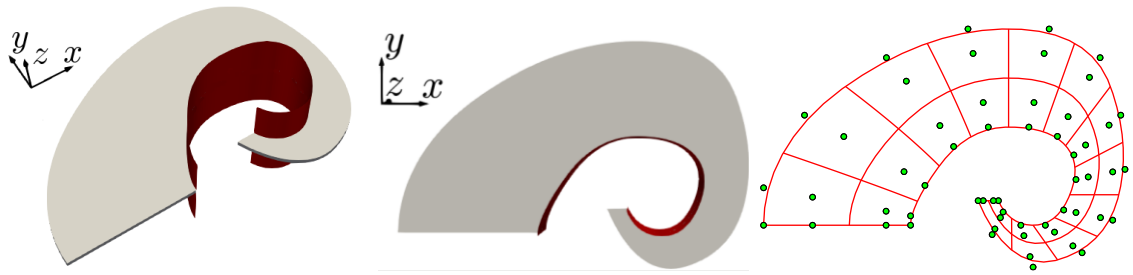

(a) (b) (c)

Figure 5.2 Circular stripe plate (a) 3D view; (b) top view; (c) IGA refinement

By utilizing the proposed SSIGA approach and MCS method with 1,000,000 simulations, the first two statistical moments (i.e., mean and standard deviation) of the first five eigenvalues represented by aPCs with different orders are reported in Table 1. As evidently illustrated in Table 5.1, the means and standard deviations of the considered eigenvalues obtained by the Galerkin method are having excellent agreement with the MCS approach. Moreover, when the order of the aPC is increased, both means and standard deviations of the considered eigenvalues are converged. Indeed, an aPC with

order 3 has illustrated the competence on providing excellent approximation of the eigenvalue in compassion with the MCS method in this numerical example. For each investigated eigenvalue, it can be observed that the mean and standard deviation obtained by the aPC approach are slightly larger than the MCS results. The reason for such phenomenon is that the proposed Galerkin method within the SSIGA provides an approximation to the complete probabilistic description of eigenvalues, whereas the MCS simulation heavily relies on the quality of underlying random number generator and the quantity of simulation cycles, which, in general, cannot provide an approximation to the complete probability space.

In addition to the validation of the proposed SSIGA for stochastic free vibration analysis through the Galerkin-based approach on the determination of the first two statistical moments of the concerned eigenvalues, the proposed approach is also implemented for the estimations of the PDFs and CDFs of the first five eigenvalues based on the same 1,000,000 realizations of the considered random fields implemented in the MCS approach. Within this part of investigation, all PDFs and CDFs of the concerned eigenvalues were established by implementing a non-parametric statistical inference technique known as the kernel density estimation approach. All the PDFs and CDFs of the first five eigenvalues are established and reported in Figures 5.3-5.7, respectively. From the information presented in Figures 5.3-5.7, it is evidently illustrated that the proposed SSIGA approach is competent for establishing the PDFs and CDFs of the concerned eigenvalues. From the quantitative assessment on the relative errors between the SSIGA approach and MCS approach, a crucial point can be realized from this investigation is that when the order of the aPC is increased, the quality of estimations on the PDFs and CDFs of the proposed SSIGA approach would be improved comparing to the MCS results. Also, the maximum relative error between the SSIGA approach with 3-

order aPC and the MCS results is less than 0.06%, which is small enough to evidently demonstrate the accuracy and applicability of the proposed SSIGA approach for the stochastic generalized eigenvalue problems.

Table 5.1 Comparison for the first five eigenvalues between SSIGA and MCS approaches

Statistical characteristics	Methods	λ_1	λ_2	λ_3	λ_4	λ_5
Mean	MCS	6.2314e+03	2.6405e+04	5.3217e+04	1.6624e+05	4.6167e+05
	SSIGA (1-order aPC)	6.2324e+03	2.6407e+04	5.3219e+04	1.6626e+05	4.6172e+05
	SSIGA (2-order aPC)	6.2328e+03	2.6408e+04	5.3221e+04	1.6626e+05	4.6173e+05
	SSIGA (3-order aPC)	6.2328e+03	2.6408e+04	5.3221e+04	1.6626e+05	4.6173e+05
Standard deviation	MCS	7.1930e+02	2.8692e+03	5.5443e+03	1.6297e+04	5.0021e+04
	SSIGA (1-order aPC)	7.1270e+02	2.8470e+03	5.4994e+03	1.6182e+04	4.9736e+04
	SSIGA (2-order aPC)	7.1999e+02	2.8715e+03	5.5496e+03	1.6319e+04	5.0133e+04
	SSIGA (3-order aPC)	7.2017e+02	2.8720e+03	5.5508e+03	1.6321e+04	5.1040e+04

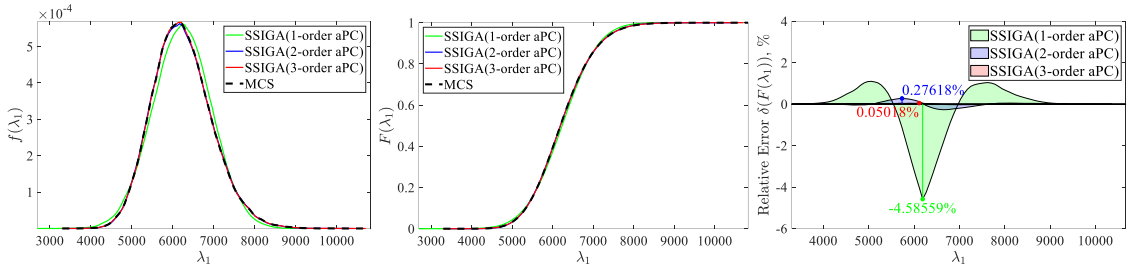

(a) (b) (c)

Figure 5.3 Esitimated (a) PDF, (b) CDF, (c) relative error of CDF of the 1st eigenvalue λ_1

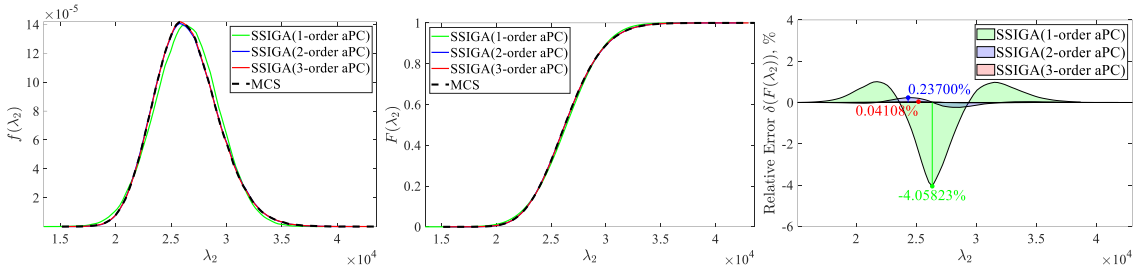

(a) (b) (c)

Figure 5.4 Esitimated (a) PDF, (b) CDF, (c) relative error of CDF of the 2nd eigenvalue λ_2

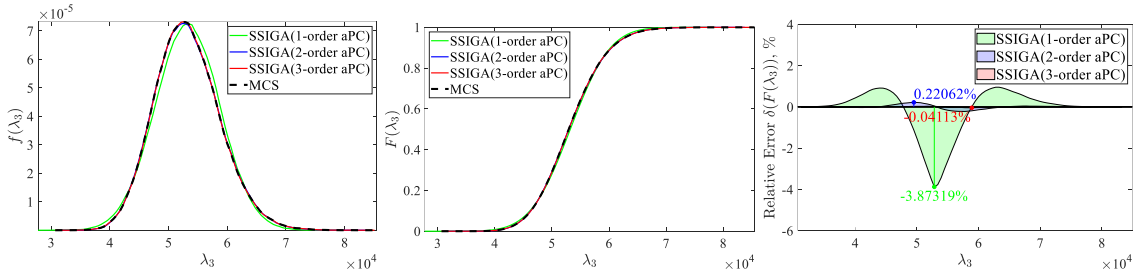

(a) (b) (c)

Figure 5.5 Esitimated (a) PDF, (b) CDF, (c) relative error of CDF of the 3rd eigenvalue λ_3

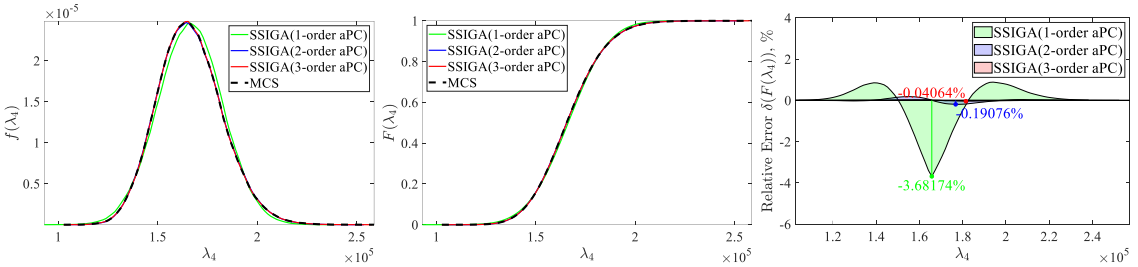

(a) (b) (c)

Figure 5.6 Esitimated (a) PDF, (b) CDF, (c) relative error of CDF of the 4th eigenvalue λ_4

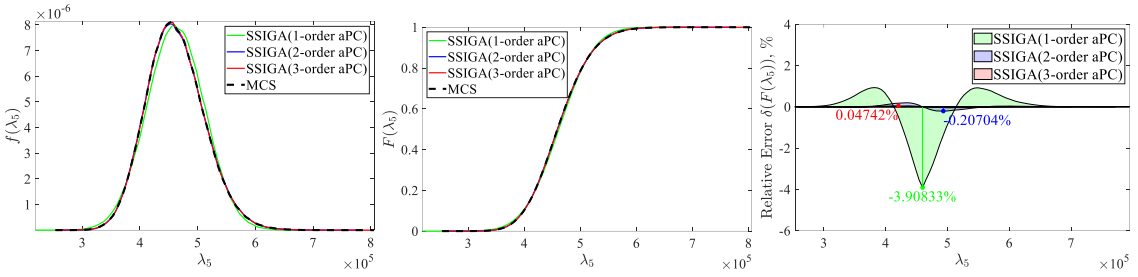

(a) (b) (c)

Figure 5.7 Esitimated (a) PDF, (b) CDF, (c) relative error of CDF of the 5th eigenvalue λ_5

Moreover, after assessing the quality of the aPC estimations on the eigenvalues through various compassions between the proposed method and the MCS approach, the first five physical modes and the eigenvalues that are corresponding to three specific events $\theta_0, \theta_1, \theta_2 \in \Omega$ are obtained by the proposed SSIGA approach. That is, for each event, all the random variables characterizing the system are obtained correspondingly and the eigenvectors are evaluated through the constructed aPCE. The physical modes obtained by the proposed SSIGA approach are compared with the corresponding MCS results. Figures 5.8-5.12 report the five physical modes and the corresponding

eigenvalues obtained by the MCS and the proposed SSIGA with 3-order aPC approaches. By closely examining these figures, different events can certainly result large variations on eigenvalues, but barely influence the corresponding physical mode shape of the original structure. That is, the considered uncertain material properties in this example does not influence the general shape of each physical mode of the structure.

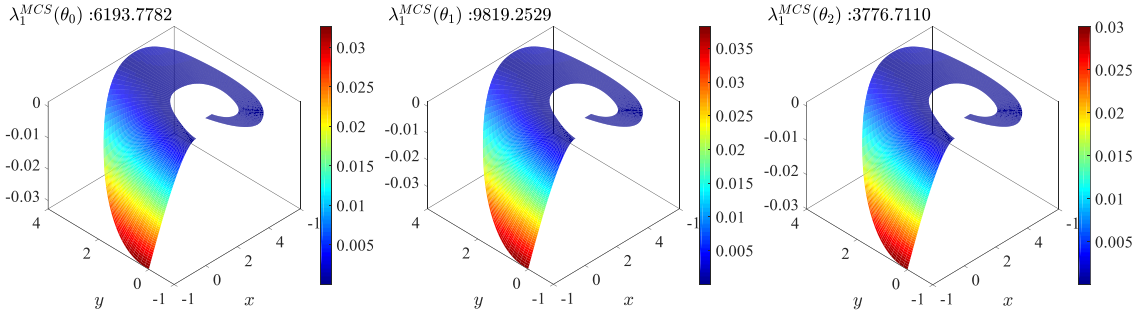

(a)

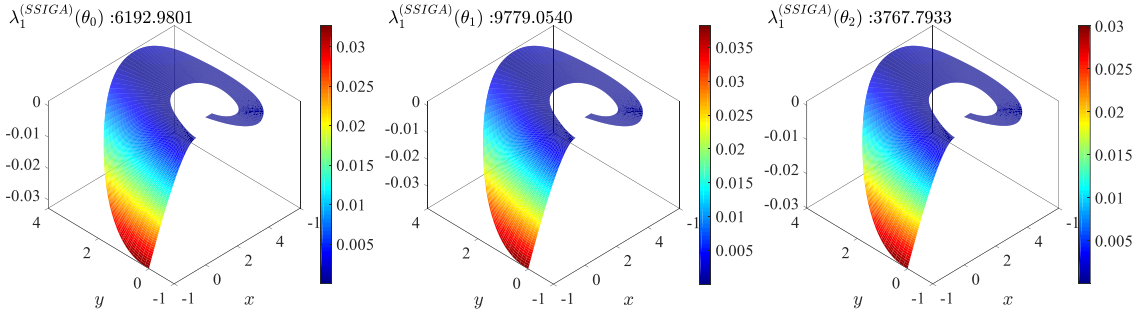

(b)

Figure 5.8 1st eigenvalue and eigenvector obtained by (a) the MCS and (b) the proposed SSIGA with 3-order aPC approaches at specific events θ_0, θ_1, and θ_2.

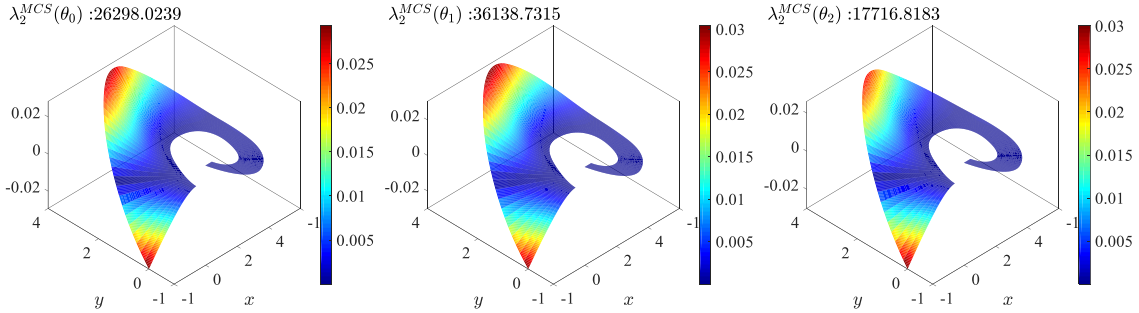

(a)

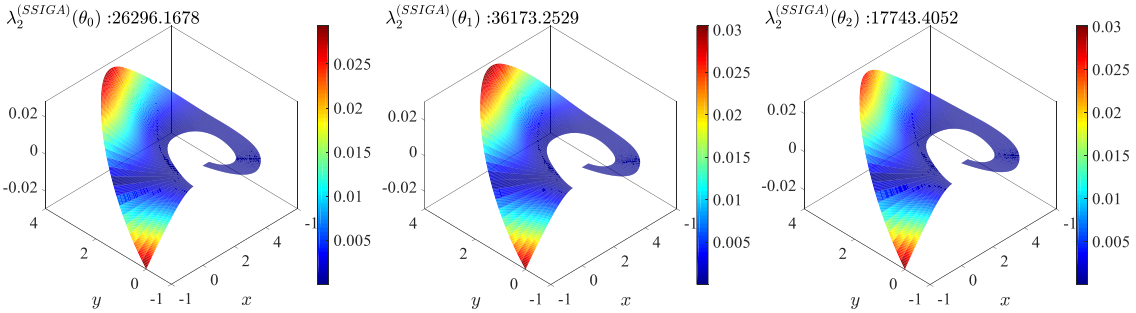

(b)

Figure 5.9 2nd eigenvalue and eigenvector obtained by (a) the MCS and (b) the proposed SSIGA with 3-order aPC approaches at specific events θ_0, θ_1, and θ_2.

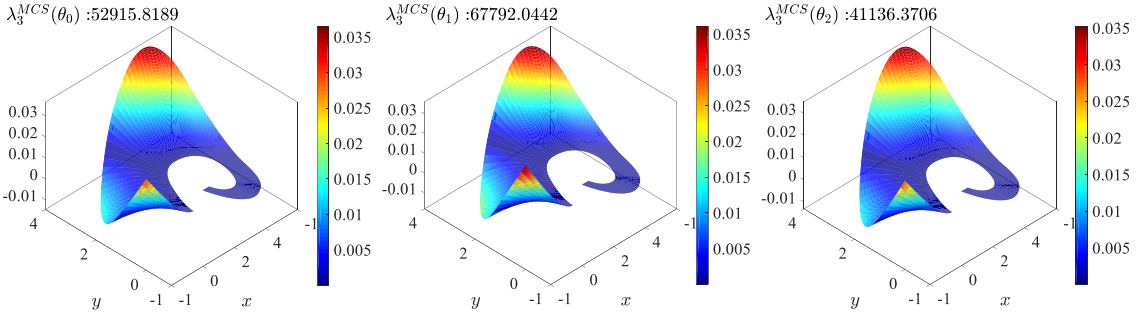

(a)

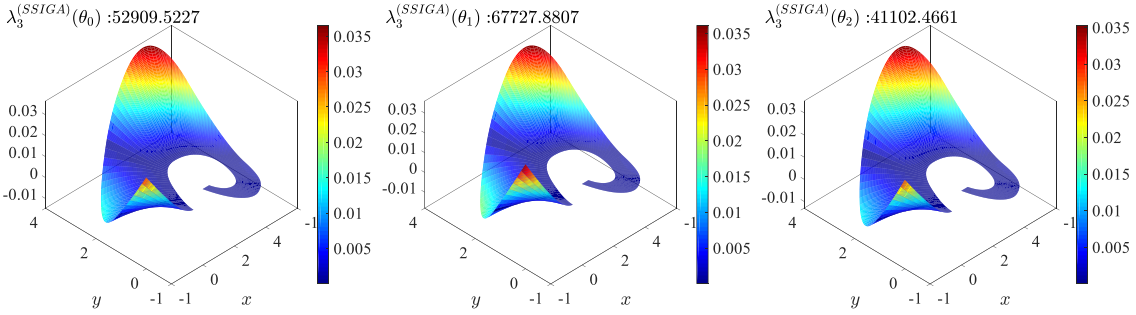

(b)

Figure 5.10 3rd eigenvalue and eigenvector obtained by (a) the MCS and (b) the proposed SSIGA with 3-order aPC approaches at specific events θ_0, θ_1, and θ_2.

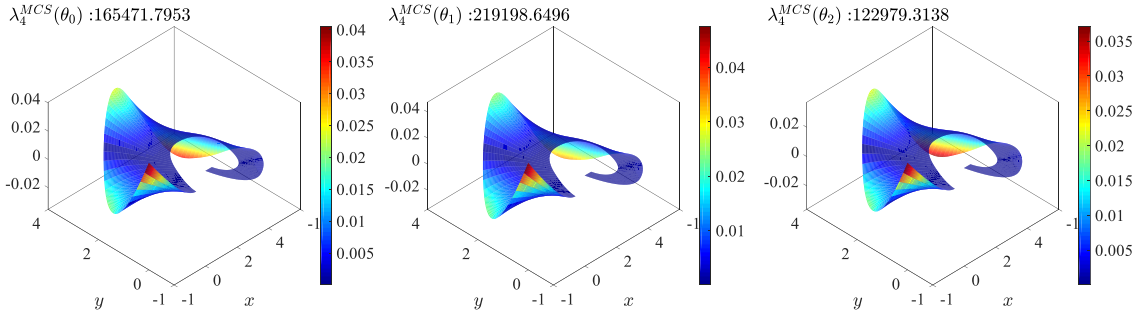

(a)

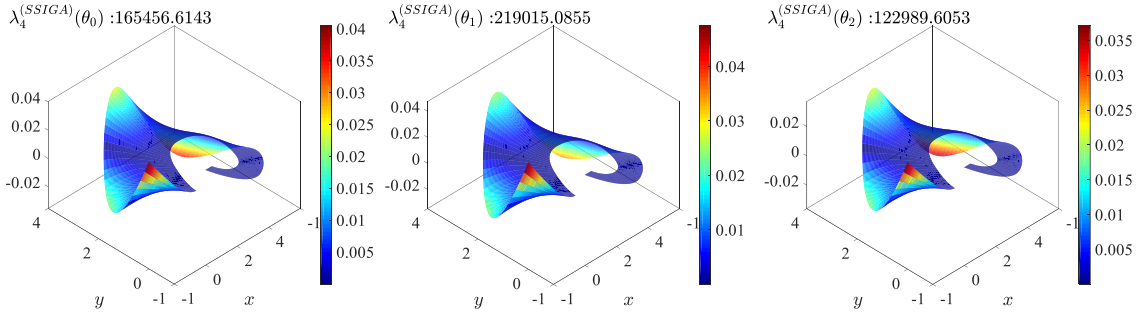

(b)

Figure 5.11 4th eigenvalue and eigenvector obtained by (a) the MCS and (b) the proposed SSIGA with 3-order aPC approaches at specific events θ_0 , θ_1, and θ_2 .

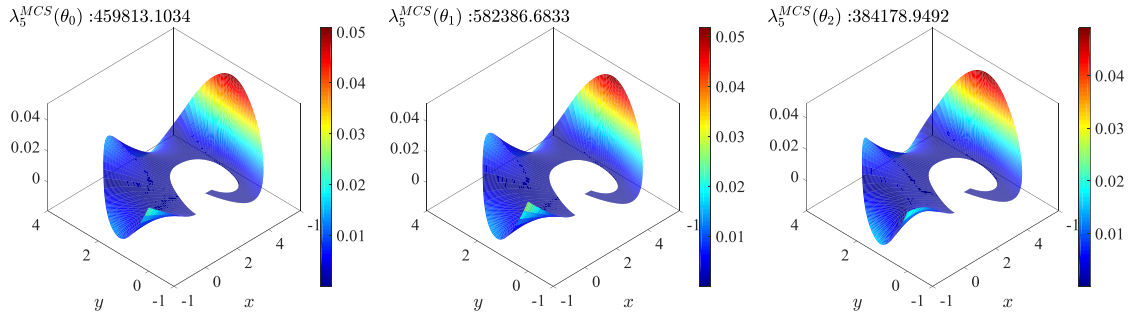

(a)

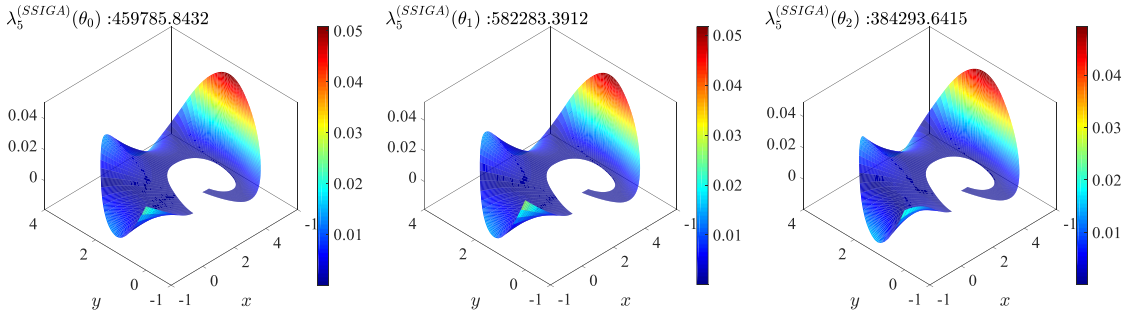

(b)

Figure 5.12 5th eigenvalue and eigenvector obtained by (a) the MCS and (b) the proposed SSIGA with 3-order aPC approaches at specific events θ_0, θ_1, and θ_2.

For this numerical example, the results of the MCS approach were obtained by running on a workstation with Intel Core i7-6700 3.4GHz and 16 GB RAM. For the first five physical modes and corresponding eigenvalues, the MCS with 1,000,000 simulation cycles were executed by parallel computing with 4 workers on this computer and costed 16 hours 9 minutes 21 seconds. On the other hand, for each physical mode, the SSIGA with 3-order aPC was obtained on the same computer without implementing parallel-computing. The computational time of the Galerkin approach for a single physical mode is 13 minutes 27 seconds, and it is about 68 minutes for the first five physical modes. Therefore, based on the reported technical information, the proposed SSIGA approach certainly shows superior computational efficiency over the exhaustively simulative MCS approach for the circular strip Mindlin plate.

5.5.2 Numerical example: flower Kirchhoff -Love shell

In the second numerical example, a flower shaped Kirchhoff-Love shell (Kiendl *et al.*, 2009) involving spatially dependent uncertain Young's modulus and material density is investigated to further explore the applicability of the SSIGA approach, especially for engineering structures with irregular and complex geometry. The thickness of the shell is

0.02m. The general structural layout and the adopted IGA refinement of the investigated flower shaped shell are shown in Figure 5.13. The shell is constrained at the two edges of the base of the shell with $u = 0, v = 0, w = 0$ as indicated in Figure 13(a). Both the Young's modulus and material density of the shell are modelled as homogeneous Lognormal random fields, and for a specific point $\mathbf{x}_0$, $\mu_{E^L(\mathbf{x}_0,\theta)} = 210\text{GPa}$, $\sigma_{E^L(\mathbf{x}_0,\theta)} = 21\text{GPa}$, $\mu_{\rho^L(\mathbf{x}_0,\theta)} = 7800\text{kg/m}^3$, and $\sigma_{\rho^L(\mathbf{x}_0,\theta)} = 780\text{kg/m}^3$. The Bessel covariance function expressed in Eq.(16) with $l = 5\text{m}$ is adopted for the two random fields modelling.

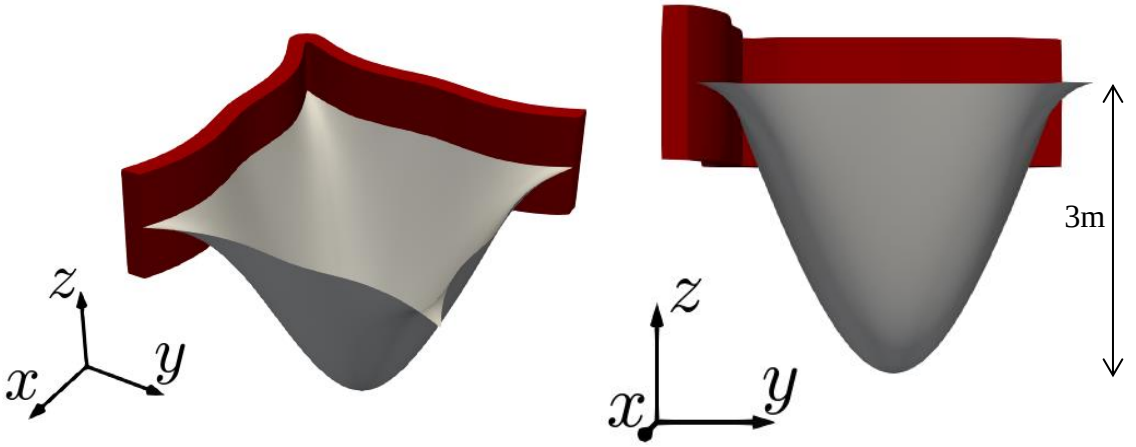

(a) (b)

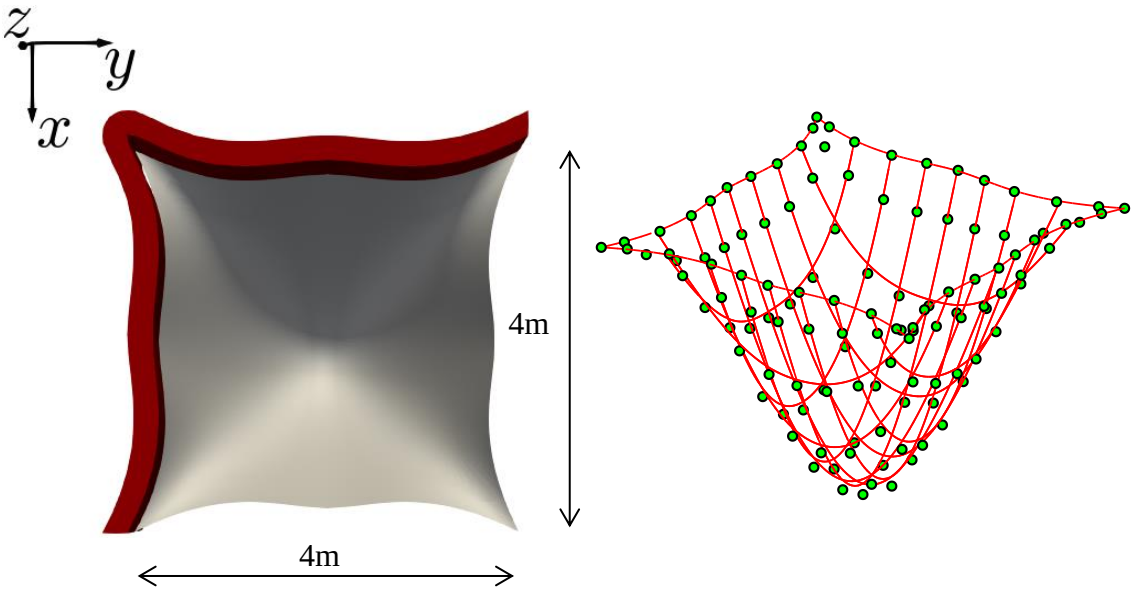

(c) (d)

Figure 5.13 Flower shell (a) 3D view; (b) front view; (c) top view; (d) IGA refinement

Within the proposed SSIGA framework, the underlying Gaussian random fields of the corresponding Lognormal random fields are both decomposed by the K-L expansion with three terms, and the Lognormal random fields are represented by the aPC with 4-order. All the stochastic eigensolutions are estimated by the aPC approach with three different orders of expansion (i.e. 1-order aPC, 2-order aPC, 3-order aPC.). The proposed Galerkin-based method is applied to solve the coefficients of the aPCs, and the tolerance for Newton-Raphson method is predefined as 10^{-7}. Moreover, the MCS approach with 1,000,000 simulation cycles was adopted for partially verifying the results.

In this example, the first two statistical moments of the first five eigenvalues obtained from the MCS and the proposed SSIGA approaches are reported in Table 2. By closely examining Table 5.2, an agreement of results between the SSIGA and MCS approaches can be observed for both the means and standard deviations of the first five eigenvalues.

In addition to the validation of the proposed method on the determination of the first two statistical moments of the concerned eigenvalues, the SSIGA approach is further implemented to estimate the PDFs and CDFs of the first five eigenvalues. All the PDFs and CDFs of the first five eigenvalues are established based on the SSIGA result and reported in Figure 5.14-5.18, respectively. From the quantitative assessment on the relative errors between the SSIGA and MCS approaches, higher order aPCs can always deliver a better approximation than the MCS approach. Also, the maximum relative error between the SSIGA with 3-order aPC and MCS methods is less than 0.04%, which is

small enough to prove the accuracy and applicability of the proposed SSIGA method for the stochastic free vibration analysis for shell structures with complex geometries.

Table 5.2 Comparison for the first five eigenvalues between the SSIGA and MCS approaches

Statistical characteristics	Methods	λ_1	λ_2	λ_3	λ_4	λ_5
Mean	MCS	6.7216e+03	2.9467e+04	8.6343e+04	1.2122e+05	1.8887e+05
	SSIGA (1-order aPC)	6.7219e+03	2.9468e+04	8.6346e+04	1.2123e+05	1.8888e+05
	SSIGA (2-order aPC)	6.7220e+03	2.9469e+04	8.6348e+04	1.2123e+04	1.8888e+05
	SSIGA (3-order aPC)	6.7220e+03	2.9469e+04	8.6348e+04	1.2123e+04	1.8888e+05
Standard deviation	MCS	8.9758e+02	3.8973+03	1.1311e+04	1.5874e+04	2.4681e+04
	SSIGA (1-order aPC)	8.9043e+02	3.8672e+03	1.1226e+04	1.5757e+04	2.4490e+04
	SSIGA (2-order aPC)	8.9824e+02	3.9005e+03	1.1320e+04	1.5887e+04	2.4701e+04
	SSIGA (3-order aPC)	8.9831e+02	3.9008e+03	1.1321e+04	1.5888e+04	2.4702e+04

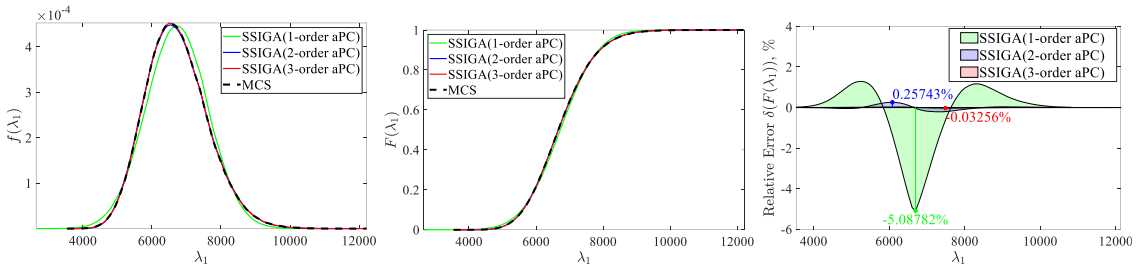

(a) (b) (c)

Figure 5.14 Esitimated (a) PDF, (b) CDF, (c) relative error of CDF of the 1st eigenvalue λ_1

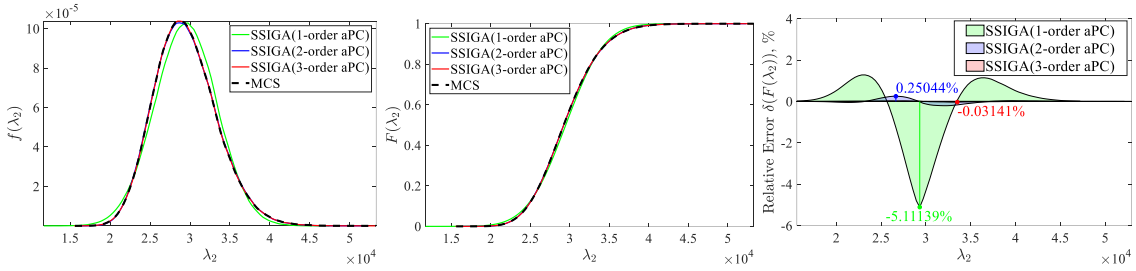

(a) (b) (c)

Figure 5.15 Esitimated (a) PDF, (b) CDF, (c) relative error of CDF of the 2nd eigenvalue λ_2

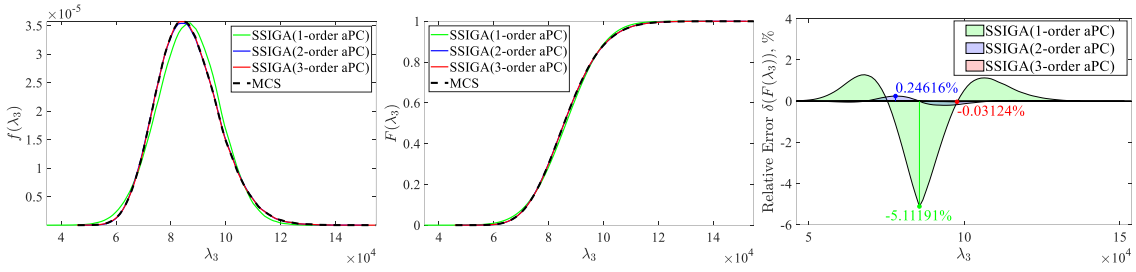

(a) (b) (c)

Figure 5.16 Esitimated (a) PDF, (b) CDF, (c) relative error of CDF of the 3rd eigenvalue λ_3

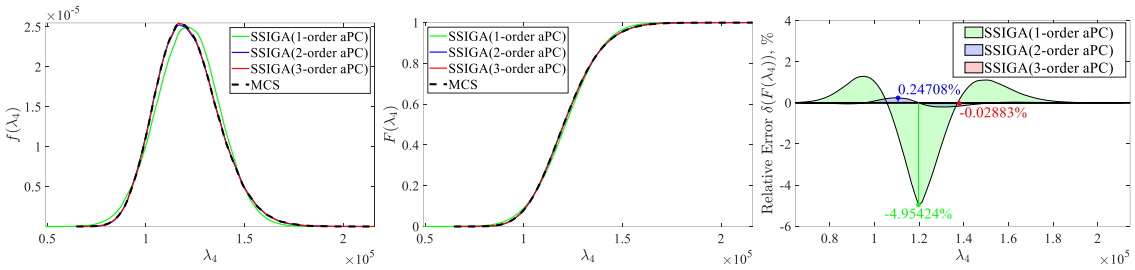

(a) (b) (c)

Figure 5.17 Esitimated (a) PDF, (b) CDF, (c) relative error of CDF of the 4th eigenvalue λ_4

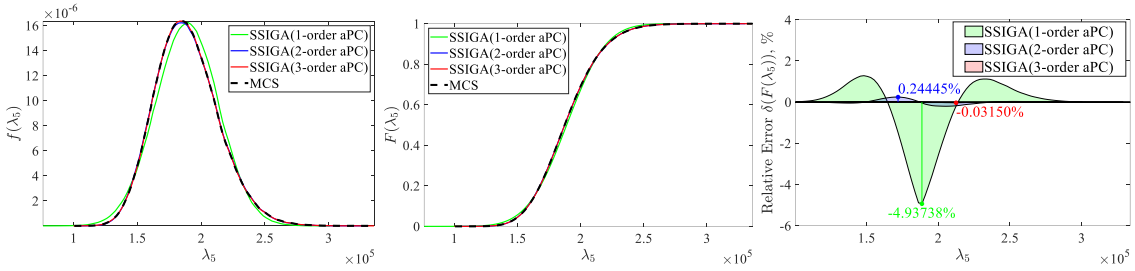

(a) (b) (c)

Figure 5.18 Esitimated (a) PDF, (b) CDF, (c) relative error of CDF of the 5th eigenvalue λ_5

Furthermore, after successfully establishing the aPC estimations of eigenvalues and eigenvectors by the proposed method, the first five physical modes and eigenvalues that are corresponding to three specific events $\theta_3, \theta_4, \theta_5 \in \Omega$ are obtained by the aPC approach with 3-order. Once again, the physical modes obtained from the SSIGA approach is compared with the results of the MCS method. Figures 5.19-5.23 report the five physical modes and the corresponding eigenvalues obtained by the MCS and the proposed SSIGA approaches with 3-order aPC. Once again, as illustrated in Figures 5.19-5.23, different events do result large variations on the eigenvalues, but still barely influence the corresponding physical mode shape.

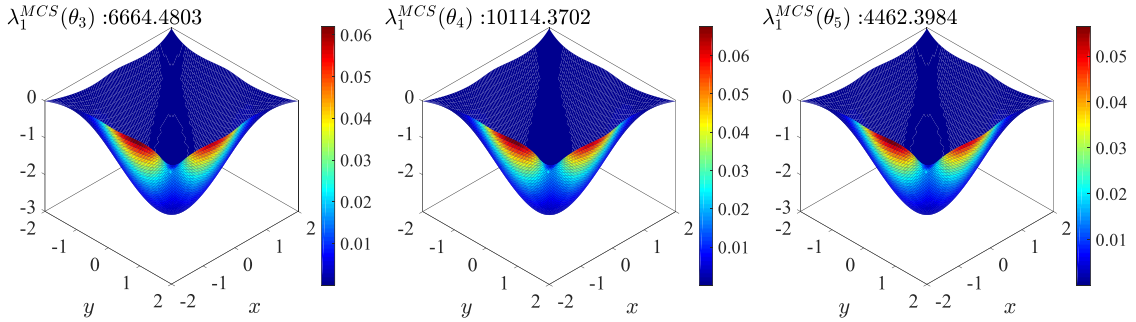

(a)

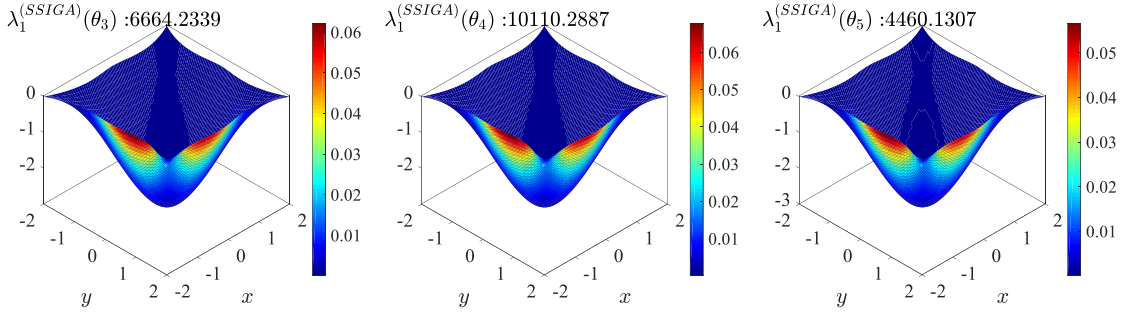

(b)

Figure 5.19 1st eigenvalue and eigenvector obtained by (a) the MCS and (b) the proposed SSIGA with 3-order aPC approaches at specific events θ_3, θ_4, and θ_5

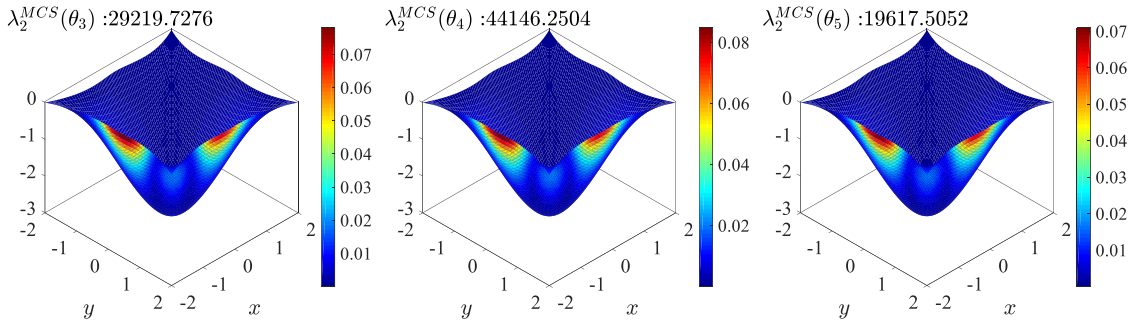

(a)

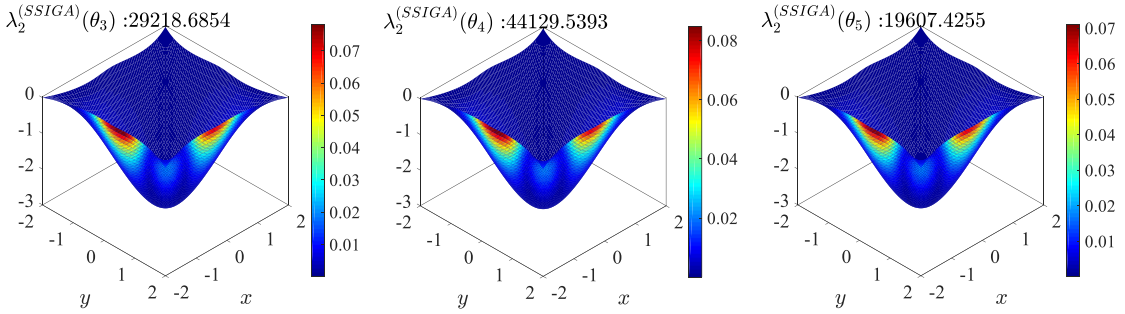

(b)

Figure 5.20 2nd eigenvalue and eigenvector obtained by (a) the MCS and (b) the proposed SSIGA with 3-order aPC approaches at specific events θ_3, θ_4, and θ_5.

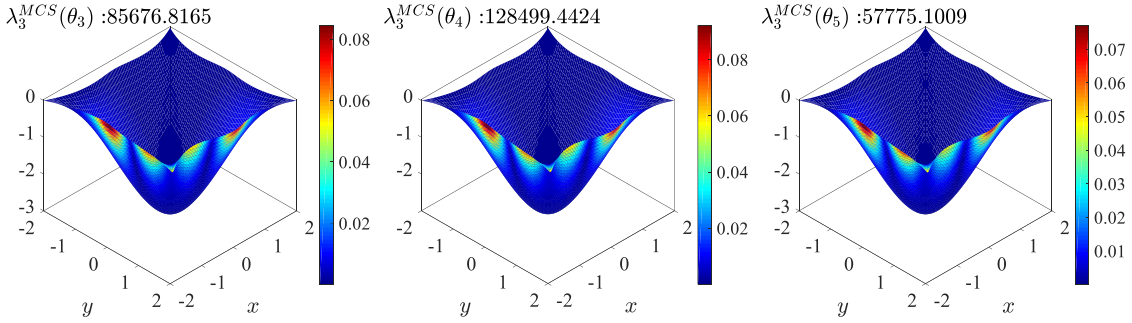

(a)

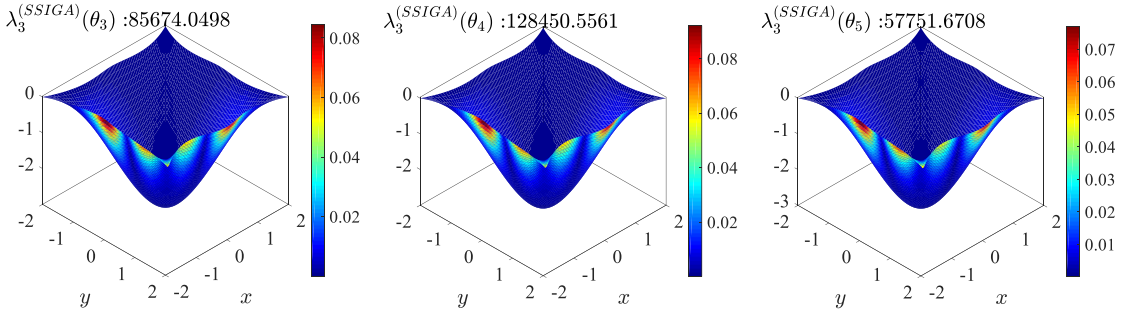

(b)

Figure 5.21 3rd eigenvalue and eigenvector obtained by (a) the MCS and (b) the proposed SSIGA with 3-order aPC approaches at specific events θ_3, θ_4, and θ_5.

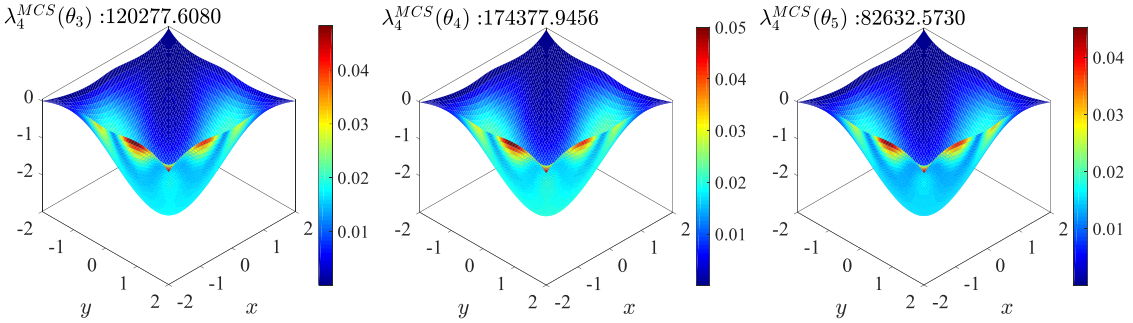

(a)

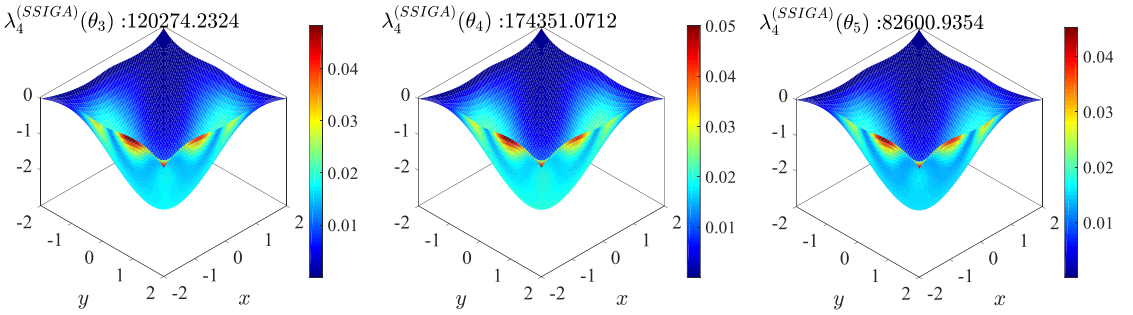

(b)

Figure 5.22 4th eigenvalue and eigenvector obtained by (a) the MCS and (b) the proposed SSIGA with 3-order aPC approaches at specific events θ_3, θ_4, and θ_5.

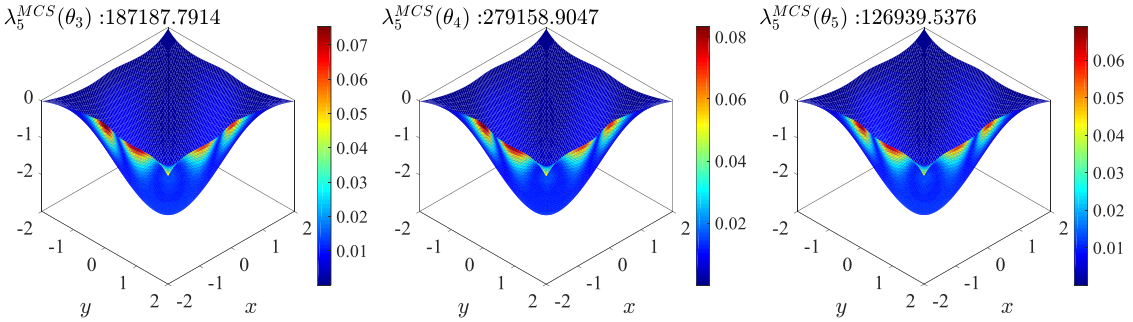

(a)

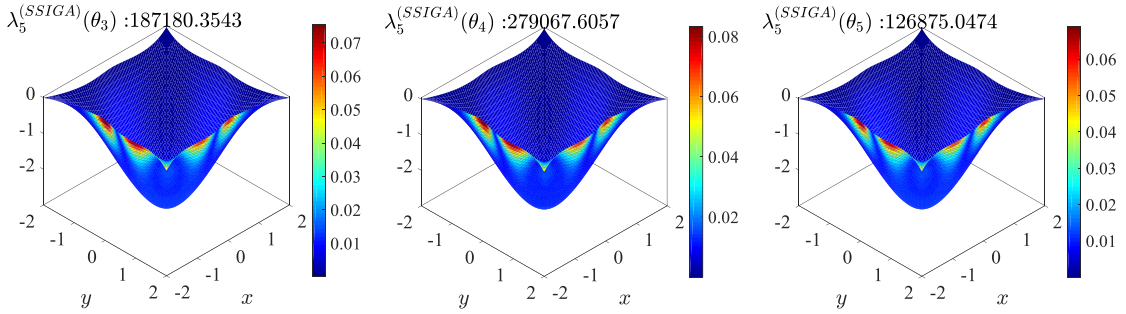

(b)

Figure 5.23 5th eigenvalue and eigenvector obtained by (a) the MCS and (b) the proposed SSIGA with 3-order aPC approaches at specific events θ_3, θ_4, and θ_5.

For the flower shaped Kirchhoff-Love shell example, the results of the MCS approach were obtained by running on a workstation with Intel Core i7-6700 3.4GHz and 16 GB RAM. For the first five physical modes and corresponding eigenvalues, the MCS with 1,000,000 simulation cycles were executed by parallel computing with 4 workers on this computer and costed 49 hours 51 minutes 33 seconds. On the other hand, for each physical mode, the SSIGA approach with 3-order aPC was executed on the same computer without implementing the parallel-computing techniques. The computational time of the SSIGA approach for a single physical mode was about 1 hour 5 minutes 26 seconds, and it was about 5 hour 27 minutes 10 seconds for the entire computation of the first five physical modes. Therefore, the proposed SSIGA approach certainly demonstrates much higher superiority on the computational efficiency over the exhaustively simulative MCS approach for the Kirchhoff-Love shell with complex geometry example.

5.6 Conclusion

In this chapter, a brand new SSIGA approach is proposed for the stochastic free vibration analysis for engineering structures involving random fields. The uncertain

Young's modulus and material density are modelled as Gaussian and non-Gaussian random fields to incorporate the spatial variation effects of the uncertain system parameters. The arbitrary polynomial chaos expansion is firstly introduced into SSIGA framework to investigate the stochastic generalized eigenvalues problems. A Galerkin-based computational approach is proposed to transform the stochastic generalized eigenvalue problem into a group of nonlinear equations, whose solution is the coefficients of the aPC for eigenvalues and eigenvectors. Newton-Raphson method is adopted to solve the nonlinear equations. Finally, statistical moments with different orders can be effectively obtained. In addition, PDFs and CDFs of the eigenvalues can also be established through statistical inference techniques. Two distinctive numerical examples are comprehensively investigated, so the accuracy, efficiency and applicability of the proposed SSIGA for stochastic free vibration of engineering structures can be evidently illustrated.

Appendix 5A. Detailed derivations of Eqs.(5.58) and (5.59)

The detailed formulation for the derivatives of Eq.(5.57), i.e. Eq.(5.58) and Eq.(5.59), are formulated in this section.

Firstly, the Eq.(5.57) is as follows

$$\mathbf{R}_k = \sum_{i=0}^{P-1}\sum_{j=0}^{P-1}\sum_{m=0}^{L_2} \mathbf{\Phi}_i^T \mathbf{M}_m \mathbf{\Phi}_j \left\langle \boldsymbol{\varphi}_m \boldsymbol{\Psi}_i \boldsymbol{\Psi}_j \boldsymbol{\Psi}_k \right\rangle - \delta_{k0}, \qquad k = 0,...,P-1 \quad (5A.1)$$

Obviously, this equation does not contain any terms containing λ_j, therefore, Eq.(5.59) can be obtained easily,

$$\frac{\partial \mathbf{R}_k}{\partial \lambda_j} = 0, \quad k = 0,...,P-1,\ j = 0,...,P-1 \qquad (5A.2)$$

Denoting $X_{mijk} = \left\langle \boldsymbol{\varphi}_m \boldsymbol{\Psi}_i \boldsymbol{\Psi}_j \boldsymbol{\Psi}_k \right\rangle$, and representing $\mathbf{R}_k$ in a tensor form as follows,

$$\mathbf{R}_k = \sum_{i=0}^{P-1} \sum_{j=0}^{P-1} \sum_{m=0}^{L_2} \boldsymbol{\Phi}_{in} (\mathbf{M}_m)_{nl} \boldsymbol{\Phi}_{jl} X_{mijk} - \delta_{k0} \tag{5A.3}$$

Expanding above expression

$$\begin{aligned}
\mathbf{R}_k &= \sum_{i=0}^{P-1} \sum_{m=0}^{L_2} [\boldsymbol{\Phi}_{in} (\mathbf{M}_m)_{nl} \boldsymbol{\Phi}_{0l} X_{mi0k} + \boldsymbol{\Phi}_{in} (\mathbf{M}_m)_{nl} \boldsymbol{\Phi}_{1l} X_{mi1k} \\
&\quad + \cdots + \boldsymbol{\Phi}_{in} (\mathbf{M}_m)_{nl} \boldsymbol{\Phi}_{(P-1)l} X_{mi(P-1)k}] - \delta_{k0} \\
&= \sum_{m=0}^{L_2} [\boldsymbol{\Phi}_{0n} (\mathbf{M}_m)_{nl} \boldsymbol{\Phi}_{0l} X_{m00k} + \boldsymbol{\Phi}_{0n} (\mathbf{M}_{im})_{nl} \boldsymbol{\Phi}_{1l} X_{m01k} \\
&\quad + \cdots + \boldsymbol{\Phi}_{0n} (\mathbf{M}_m)_{nl} \boldsymbol{\Phi}_{(P-1)l} X_{m0(P-1)k} \\
&\quad + \cdots + \boldsymbol{\Phi}_{(P-1)n} (\mathbf{M}_m)_{nl} \boldsymbol{\Phi}_{0l} X_{m(P-1)0k} + \boldsymbol{\Phi}_{(P-1)n} (\mathbf{M}_m)_{nl} \boldsymbol{\Phi}_{1l} X_{m(P-1)1k} \\
&\quad + \cdots + \boldsymbol{\Phi}_{(P-1)m} (\mathbf{M}_{i_2})_{ml} \boldsymbol{\Phi}_{(P-1)l} X_{i_2(P-1)(P-1)k}] - \delta_{k0}
\end{aligned} \tag{5A.4}$$

where $\boldsymbol{\Phi}_{jl}$ denotes the *l*th term of $\boldsymbol{\Phi}_j$.

The partial derivative of Eq.(5A.4) with respect to any element, for example $\boldsymbol{\Phi}_{0l}$, is

$$\begin{aligned}
\frac{\partial \mathbf{R}_k}{\partial \boldsymbol{\Phi}_{0l}} &= \sum_{i_2=0}^{M_2} [\boldsymbol{\Phi}_{0m} (\mathbf{M}_{i_2})_{ml} X_{i_2 00k} + \boldsymbol{\Phi}_{1m} (\mathbf{M}_{i_2})_{ml} X_{i_2 10k} + \cdots + \boldsymbol{\Phi}_{(P-1)m} (\mathbf{M}_{i_2})_{ml} X_{i_2(P-1)0k} \\
&\quad + (\mathbf{M}_{i_2})_{ml} \boldsymbol{\Phi}_{0l} X_{i_2 00k} + (\mathbf{M}_{i_2})_{ml} \boldsymbol{\Phi}_{1l} X_{i_2 01k} + \cdots + (\mathbf{M}_{i_2})_{ml} \boldsymbol{\Phi}_{(P-1)l} X_{i_2 0(P-1)k}]
\end{aligned} \tag{5A.5}$$

Because $X_{i_2ijk} = X_{i_2 jik}$, which can be easily proved by the definition, the above expression can be expressed as

$$\frac{\partial \mathbf{R}_k}{\partial \boldsymbol{\Phi}_{0l}} = \sum_{i=0}^{P-1} \sum_{i_2=0}^{M_2} 2\boldsymbol{\Phi}_{im} (\mathbf{M}_{i_2})_{ml} X_{i_2 i0k} \tag{5A.6}$$

Then, in general, Eq.(5.58) can be obtained

$$\frac{\partial \mathbf{R}_k}{\partial \boldsymbol{\Phi}_{jl}} = 2 \sum_{i=0}^{P-1} \sum_{i_2=0}^{M_2} \boldsymbol{\Phi}_{im} (\mathbf{M}_{i_2})_{ml} \left\langle \varsigma_{i_2} \boldsymbol{\Psi}_i \boldsymbol{\Psi}_j \boldsymbol{\Psi}_k \right\rangle - \delta_{k0}, \quad k = 0, ..., P-1, \; j = 0, ..., P-1 \tag{5A.7}$$

Chapter 6

SPECTRAL STOCHASTIC ISOGEOMETRIC ANALYSIS FOR LINEAR STABILITY ANALYSIS OF PLATE

6.1 Summary

Chapter 6 presents spectral stochastic isogeometric analysis (SSIGA) scheme for the stochastic linear stability analysis of plate with uncertain material properties. Within the proposed SSIGA scheme, the first-order shear deformation theory of plate is adopted for modelling the kinematic relationship.

The structure of Chapter 6 is briefed as follows. The concept of IGA and the linear stability analysis of FGM plate via IGA are briefly introduced in Section 6.3. Subsequently, the proposed SSIGA for the stochastic linear stability analysis of FGM plate is presented in Section 6.4. Two numerical examples are thoroughly investigated to illustrate the accuracy, efficiency and applicability of the proposed stochastic analysis framework in Section 6.5. Finally, some conclusions are drawn in Section 6.6.

The research work developed in Chapter 6 has produced one journal paper which has been published in *Computer Methods in Applied Mechanics and Engineering*, detailed as:

Li, K., Wu, D. and Gao, W., 2019. Spectral stochastic isogeometric analysis for linear stability analysis of plate. *Computer Methods in Applied Mechanics and Engineering*. 352, pp.1-31.

6.2 Introduction

A novel computational stochastic analysis framework, namely the spectral stochastic isogeometric analysis (SSIGA), is introduced for the stochastic linear stability analysis of plates with uncertain material properties and complex geometries. The proposed SSIGA scheme is applicable to different material models, for example homogeneous material, functionally graded material, and functionally graded porous material (Li, Wu, *et al.*, 2018), etc. Within the proposed stochastic linear stability analysis framework, both spatially independent (i.e. random variables, random vectors) and dependent (i.e. random fields) uncertain parameters are taken into consideration. Also, random fields with Gaussian and non-Gaussian distributions can be incorporated within this new computational stochastic analysis. Moreover, by adopting the geometric representation techniques of the CAD environment (e.g., NURBS, T-spline etc.), both the geometry of the engineering structure and the associated material uncertainties can be consistently represented within a single scheme. Consequently, the SSIGA approach can robustly maintain the precise geometric information of the engineering structure at both initial design and stochastic analysis stages (Li, Gao, *et al.*, 2018). Moreover, the basis functions within the CAD environment possess higher-order continuity over the whole physical domain. Such feature offers a globally smooth Karhunen-Loève (K-L) discretization for the considered random fields. In addition, since the geometric transformation between CAD and CAE is eliminated, the computational efficiency of the stochastic linear stability analysis of FGM plate can be dramatically improved. Furthermore, an extended support

vector regression (X-SVR) with a generalized Gegenbauer polynomial kernel is developed, and then implemented within the SSIGA approach for establishing the statistical characteristics (e.g., mean and standard deviation etc.) of the structural buckling load. Since the proposed X-SVR approach is a non-intrusive sampling scheme, both the probability density function (PDF) and cumulative distribution function (CDF) of the critical buckling load of the FGM plate can be effectively established with relatively small sampling size. Therefore, the computational efficiency can be significantly reduced when comparing with the crude full-scale Monte-Carlo simulation (MCS) technique. The accuracy, efficiency, and applicability of the proposed approach are illustrated through two numerical examples.

6.3 Stochastic linear stability analysis

6.3.1 The first-order shear deformation theory of plate

Let D denote a domain in $\Re^2$ occupied by the mid-plane of a plate with thickness h. According to the FSDT, the kinematic relationship of the plate is defined as:

$$\begin{cases} u(x,y,z) = u_0(x,y) - z\beta_x(x,y) \\ v(x,y,z) = v_0(x,y) - z\beta_y(x,y), \qquad -\dfrac{h}{2} \le z \le \dfrac{h}{2} \\ w(x,y.z) = w_0(x,y) \end{cases} \tag{6.1}$$

where u_0 and v_0 are the in-plane displacements of the mid-plane; w_0 is the out-of-plane displacement of the mid-plane; β_x and β_y are the rotations in the *x*-*z*, *y*-*z* planes, respectively. Thus, the displacement fields of the plate are:

$$\mathbf{u} = \{u, v, w, \beta_x, \beta_y\}^{\mathrm{T}} \tag{6.2}$$

Since the FSDT plate is well developed, the relevant formulation derivations are provided in Appendix A. Based on Appendix A, an eigenvalue problem for the pre-buckling equilibrium state based on load step t_n is obtained through Eq.(6A.9). The lowest eigenvalue is considered as an estimation of the critical load factor ${}^{cr}\zeta$. By neglecting the second-order term, the final eigenvalue problem can be formulated as

$$a^*({}^n\zeta\,{}^n\mathbf{u},\delta\mathbf{y},\mathbf{y}) = A({}^n\mathbf{u},\delta\mathbf{y},\mathbf{y}) + {}^n\zeta G_1({}^n\mathbf{u},\delta\mathbf{y},\mathbf{y}) = 0 \tag{6.3}$$

6.3.2 The linear stability analysis through IGA

By implementing the IGA basis functions to represent the mid-plane of the plate, the displacement fields of the plate, which is presented in Eq.(6.2), can be interpreted as follow,

$$\mathbf{u}(\xi) = \sum_{\mathbf{I}}^{\mathbf{N}_{cp}} R_{\mathbf{I}}^{\mathbf{P}}(\xi)\mathbf{u}_{\mathbf{I}} \tag{6.4}$$

where $R_{\mathbf{I}}^{\mathbf{P}}$ denotes the isogeometric basis function of the **I**th control point; $\mathbf{u}_{\mathbf{I}} = \{u_{0\mathbf{I}}, v_{0\mathbf{I}}, w_{0\mathbf{I}}, \beta_{x\mathbf{I}}, \beta_{y\mathbf{I}}\}^{\mathrm{T}}$ denotes the degrees of freedom of the **I**th control point

Therefore, the in-plane strains $\boldsymbol{\varepsilon}_i$, the bending strains $\boldsymbol{\varepsilon}_b$, and the shear strains $\boldsymbol{\varepsilon}_s$ are represented as follows,

$$\boldsymbol{\varepsilon}_i = \boldsymbol{\varepsilon}_i^L + \boldsymbol{\varepsilon}_i^{NL} = (\mathbf{B}_i^L + \frac{1}{2}\mathbf{B}_i^{NL})\mathbf{a}\,,\quad \boldsymbol{\varepsilon}_b = \mathbf{B}_b\mathbf{a}\,,\ \boldsymbol{\varepsilon}_s = \mathbf{B}_s\mathbf{a} \tag{6.5}$$

where $\mathbf{a} = \{\mathbf{u}_1, \mathbf{u}_2, \ldots, \mathbf{u}_{\mathbf{N}_{cp}}\}^{\mathrm{T}}$ denotes the degree of freedoms of the whole system; $\mathbf{B}_i^L = \{\mathbf{B}_{i1}^L, \mathbf{B}_{i2}^L, \ldots, \mathbf{B}_{i\mathbf{N}_{cp}}^L\}$, $\mathbf{B}_i^{NL} = \{\mathbf{B}_{i1}^{NL}, \mathbf{B}_{i2}^{NL}, \ldots, \mathbf{B}_{i\mathbf{N}_{cp}}^{NL}\}$, $\mathbf{B}_b = \{\mathbf{B}_{b1}, \mathbf{B}_{b2}, \ldots, \mathbf{B}_{b\mathbf{N}_{cp}}\}$, and

$\mathbf{B}_s = \{\mathbf{B}_{s1}, \mathbf{B}_{s2}, \ldots, \mathbf{B}_{s\mathbf{N}_{cp}}\}$ are kinematic matrices with $\mathbf{B}_{i\mathbf{I}}^L$, $\mathbf{B}_{i\mathbf{I}}^{NL}$, $\mathbf{B}_{b\mathbf{I}}$, and $\mathbf{B}_{s\mathbf{I}}$ are formulated as,

$$\mathbf{B}_{i\mathbf{I}}^L = \begin{bmatrix} R_{\mathbf{I},x}^{\mathbf{P}} & 0 & 0 & 0 & 0 \\ 0 & R_{\mathbf{I},y}^{\mathbf{P}} & 0 & 0 & 0 \\ R_{\mathbf{I},y}^{\mathbf{P}} & R_{\mathbf{I},x}^{\mathbf{P}} & 0 & 0 & 0 \end{bmatrix} \quad \mathbf{B}_{i\mathbf{I}}^{NL} = \begin{bmatrix} 0 & 0 & \partial w_0 / \partial x \cdot R_{\mathbf{I},x}^{\mathbf{P}} & 0 & 0 \\ 0 & 0 & \partial w_0 / \partial y \cdot R_{\mathbf{I},y}^{\mathbf{P}} & 0 & 0 \\ 0 & 0 & \partial w_0 / \partial y \cdot R_{\mathbf{I},x}^{\mathbf{P}} + \partial w_0 / \partial x \cdot R_{\mathbf{I},y}^{\mathbf{P}} & 0 & 0 \end{bmatrix}$$
$$\mathbf{B}_{b\mathbf{I}} = \begin{bmatrix} 0 & 0 & 0 & -R_{\mathbf{I},x}^{\mathbf{P}} & 0 \\ 0 & 0 & 0 & 0 & -R_{\mathbf{I},y}^{\mathbf{P}} \\ 0 & 0 & 0 & -R_{\mathbf{I},y}^{\mathbf{P}} & -R_{\mathbf{I},x}^{\mathbf{P}} \end{bmatrix} \quad \mathbf{B}_{s\mathbf{I}} = \begin{bmatrix} 0 & 0 & R_{\mathbf{I},x}^{\mathbf{P}} & -R_{\mathbf{I}}^{\mathbf{P}} & 0 \\ 0 & 0 & R_{\mathbf{I},y}^{\mathbf{P}} & 0 & -R_{\mathbf{I}}^{\mathbf{P}} \end{bmatrix} \tag{6.6}$$

Subsequently, the variations of the in-plane strains $\delta\boldsymbol{\varepsilon}_i$, the bending strains $\delta\boldsymbol{\varepsilon}_b$, and the shear strains $\delta\boldsymbol{\varepsilon}_s$ are represented as follows,

$$\delta\boldsymbol{\varepsilon}_i = \delta\boldsymbol{\varepsilon}_i^L + \delta\boldsymbol{\varepsilon}_i^{NL} = (\mathbf{B}_i^L + \mathbf{B}_i^{NL})\delta\mathbf{a}\ ,\ \delta\boldsymbol{\varepsilon}_b = \mathbf{B}_b\delta\mathbf{a}\ ,\ \delta\boldsymbol{\varepsilon}_s = \mathbf{B}_s\delta\mathbf{a} \tag{6.7}$$

And $\Delta\boldsymbol{\varepsilon}_i$, $\Delta\boldsymbol{\varepsilon}_b$, and $\Delta\boldsymbol{\varepsilon}_s$ are obtained as

$$\Delta\boldsymbol{\varepsilon}_i = \Delta\boldsymbol{\varepsilon}_i^L + \Delta\boldsymbol{\varepsilon}_i^{NL} = (\mathbf{B}_i^L + \mathbf{B}_i^{NL})\Delta\mathbf{a}\ ,\ \Delta\boldsymbol{\varepsilon}_b = \mathbf{B}_b\Delta\mathbf{a}\ ,\ \Delta\boldsymbol{\varepsilon}_s = \mathbf{B}_s\Delta\mathbf{a} \tag{6.8}$$

By adopting the IGA formulations, the linear stiffness matrix can be formulated as:

$$\mathbf{K} = \mathbf{K}_{ib} + \mathbf{K}_s \tag{6.9}$$

where $\mathbf{K}_{ib}$ denotes the linear in-plane-bending stiffness matrix

$$\mathbf{K}_{ib} = \int_D \begin{bmatrix} \mathbf{B}_i^L \\ \mathbf{B}_b \end{bmatrix}^{\mathrm{T}} \begin{bmatrix} \mathbf{A} & \mathbf{B} \\ \mathbf{B} & \mathbf{D}_\mathbf{b} \end{bmatrix} \begin{bmatrix} \mathbf{B}_i^L \\ \mathbf{B}_b \end{bmatrix} dD \tag{6.10}$$

and $\mathbf{K}_s$ denotes the shear stiffness matrix

$$\mathbf{K}_s = \int_D \mathbf{B}_s^{\mathrm{T}} \mathbf{D}_s \mathbf{B}_s dD \tag{6.11}$$

Moreover, the nonlinear in-plane stiffness matrix within the scheme of IGA is formulated as:

$$\mathbf{K}_i^{NL} = \int_D \left((\mathbf{B}_i^L)^{\mathrm{T}} \mathbf{A} \mathbf{B}_i^{NL} + (\mathbf{B}_i^{NL})^{\mathrm{T}} \mathbf{A} \mathbf{B}_i^L \right) dD \tag{6.12}$$

and the initial stress matrix can be formulated as:

$$\mathbf{K}_\sigma = \int_D \Delta\delta\boldsymbol{\varepsilon}_i^{\mathrm{T}} \hat{\boldsymbol{\sigma}}_i dD = \int_D \mathbf{S}^{\mathrm{T}} \bar{\boldsymbol{\sigma}} \mathbf{S} dD \tag{6.13}$$

where $\bar{\boldsymbol{\sigma}} = \begin{bmatrix} N_x & N_{xy} \\ N_{xy} & N_y \end{bmatrix}$ is composed of in-plane stress resultants $\hat{\boldsymbol{\sigma}}_i$ at load step t_n; $\mathbf{S}$ is defined as

$$\mathbf{S} = \begin{bmatrix} 0 & 0 & R_{1,x}^{\mathbf{P}} & 0 & 0 & \dots & 0 & 0 & R_{\mathbf{N}_{cp},x}^{\mathbf{P}} & 0 & 0 \\ 0 & 0 & R_{1,y}^{\mathbf{P}} & 0 & 0 & \dots & 0 & 0 & R_{\mathbf{N}_{cp},y}^{\mathbf{P}} & 0 & 0 \end{bmatrix} \tag{6.14}$$

Consequently, the linear stability of the plate through the analysis framework of IGA can be explicitly formulated as:

$$\left[(\mathbf{K}_{ib} + \mathbf{K}_s) + {}^n\zeta (\mathbf{K}_i^{NL} + \mathbf{K}_\sigma) \right] \mathbf{y} = \mathbf{0} \tag{6.15}$$

6.3.3 Stochastic linear stability analysis for the plate

The intrinsic randomness of a physical system has been widely acknowledged. By considering the uncertainties through the physical system parameters, i.e., Young's modulus $E(\theta)$, Poisson's ratio $\nu(\theta)$, and the gradient index of FGM $n(\theta)$, the stochastic linear stability analysis of plate is transformed into a stochastic eigenvalue problem,

$$\left[(\mathbf{K}_{ib}(\theta) + \mathbf{K}_s(\theta)) + {}^n\zeta(\theta) (\mathbf{K}_i^{NL}(\theta) + \mathbf{K}_\sigma(\theta)) \right] \mathbf{y}(\theta) = \mathbf{0} \tag{6.16}$$

where $\theta \in \Omega$ and (Ω, Σ, F) is the probability space associated with the underlying physical experiments.

The stochastic linear stability analysis aims to characterize the stochastic buckling load with the consideration of the whole sample space Ω, which represents all the possible events involved within the physical system. Such problem is very challenging to be solved by traditional uncertainty quantification methods. Firstly, the stochastic eigenvalue problem has always been a very complex problem in mathematics. Both generalized analytical and numerical solutions are unavailable for stochastic eigenvalue problem inspired from engineering practices. Moreover, compared with the stochastic linear elasticity analysis, the stochastic linear stability analysis is a stochastic eigenvalue problem coupled with a stochastic linear elasticity analysis. Two levels, yet coupled, of randomness have forged the stochastic linear stability analysis to become an intricate problem that is extremely difficult for the traditional non-sampling stochastic methods. However, the stochastic linear stability analysis is critical for engineering practices since the structure may fail before yielding. Therefore, it is necessary to develop an effective and efficient method to conquer such difficulty.

6.4 SSIGA for the stochastic linear stability analysis

6.4.1 The extended support vector regression (X-SVR)

6.4.1.1 The linear X-SVR

The Support Vector Machine (SVM) is a supervised learning algorithm which was initially introduced by Vapnik (Vapnik, 2013) for binary classification problem and subsequently, extended to regression (Drucker *et al.*, 1997) and multinomial classifications (Hsu and Lin, 2002). Among many established SVMs, the pq-SVM

(Dunbar *et al.*, 2010) is an excellent candidate for binary classification. By extending the pq-SVM, a decomposition process is firstly adopted to eliminate the L_1-norm $\|\mathbf{w}\|_1$ computation so a new X-SVR is developed.

Given a particular training dataset with input $\mathbf{x}_{train} = [\mathbf{x}_1, \mathbf{x}_2, ..., \mathbf{x}_i, ..., \mathbf{x}_m]^{\mathrm{T}} \in \Re^{m \times n}$ ($\mathbf{x}_i \in \Re^n, i = 1, 2, ..., m$) and output $\mathbf{y}_{train} = [y_1, y_2, \ldots, y_i, \ldots, y_m]^{\mathrm{T}} \in \Re^m$, the hyperplane that separating the two classes can be defined as $\hat{f}(\mathbf{x}) = \mathbf{w}^{\mathrm{T}}\mathbf{x} - \gamma$ where m denotes the number of training samples; n denotes the number of input variables; $\mathbf{w} = [w_1, w_1, \ldots, w_i, \ldots, w_n]^{\mathrm{T}} \in \Re^n$ denotes the normal vector of the hyperplane; and $\gamma \in \Re$ denotes the bias. A quadratic ε-insensitive loss function (i.e., l_2^{ε}) is implemented herein as:

$$l_2^{\varepsilon}(y_i - \hat{f}(\mathbf{x}_i)) = \left| y_i - \hat{f}(\mathbf{x}_i) \right|^2, i = 1, ..., m \tag{6.17}$$

to improve the numerical stability when solving the succeeding mathematical programs.

Consequently, the governing formulation for the proposed X-SVR can be explicitly expressed as:

$$\min_{\mathbf{p},\mathbf{q},\gamma,\xi,\hat{\xi}} : \frac{\hat{\lambda}_1}{2}\left(\|\mathbf{p}\|_2^2 + \|\mathbf{q}\|_2^2\right) + \hat{\lambda}_2 \mathbf{e}_n^T(\mathbf{p} + \mathbf{q}) + \frac{C}{2}\left(\boldsymbol{\beta}^T\boldsymbol{\beta} + \hat{\boldsymbol{\beta}}^T\hat{\boldsymbol{\beta}}\right) \tag{6.18a}$$

$$s.t. \quad \begin{cases} \mathbf{x}_{train}(\mathbf{p} - \mathbf{q}) - \gamma \mathbf{e}_m - \mathbf{y}_{train} \le \varepsilon \mathbf{e}_m + \boldsymbol{\beta} \\ \mathbf{y}_{train} - \mathbf{x}_{train}(\mathbf{p} - \mathbf{q}) + \gamma \mathbf{e}_m \le \varepsilon \mathbf{e}_m + \hat{\boldsymbol{\beta}} \\ \mathbf{p},\ \mathbf{q} \ge \mathbf{0}_n;\ \boldsymbol{\beta},\ \hat{\boldsymbol{\beta}} \ge \mathbf{0}_m \end{cases} \tag{6.18b}$$

where $\hat{\lambda}_1, \hat{\lambda}_2 \in \Re^+$ denote two toning parameters which balance the classification performance and feature selection; $\boldsymbol{\beta}, \hat{\boldsymbol{\beta}} \in \Re^m$ are two non-negative slack variable vectors;

$\mathbf{e}_m = [1,1,...,1]^{\mathrm{T}} \in \Re^m$ and $\mathbf{0}_n = [0,0,...,0]^T \in \Re^n$ denote unit vector and zeros vector in dimensions of n, respectively; $\mathbf{p},\mathbf{q} \in \Re^n$ are two non-negative variables such that:

$$p_\ell := (w_\ell)_+ = \begin{cases} 0, & w_\ell \le 0 \\ w_\ell, & w_\ell > 0 \end{cases} \text{ and } q_\ell := (w_\ell)_- = \begin{cases} -w_\ell, & w_\ell < 0 \\ 0, & w_\ell \ge 0 \end{cases}, \text{ for } \ell = 1,2,...,n \tag{6.19}$$

Therefore, for $\forall \ell$, $p_j q_j = 0$ is guaranteed. Thus,

$$\begin{cases} \|\mathbf{w}\|_1 = |w_1| + |w_2| + ... + |w_n| = p_1 + q_1 + p_2 + q_2 + ... + p_n + q_n = \mathbf{e}_n^T(\mathbf{p}+\mathbf{q}) \\ \|\mathbf{w}\|_2^2 = \|\mathbf{p}-\mathbf{q}\|_2^2 = \|\mathbf{p}\|_2^2 + \|\mathbf{q}\|_2^2 - 2\mathbf{p}^T\mathbf{q} = \|\mathbf{p}\|_2^2 + \|\mathbf{q}\|_2^2 \end{cases} \tag{6.20}$$

To achieve a more simplified formulation, Eq.(6.18) can be alternatively formulated as:

$$\min_{\mathbf{z},\gamma} : \frac{1}{2}\left(\mathbf{z}^T\hat{\mathbf{C}}\mathbf{z} + \gamma^2\right) + \hat{\lambda}_2\mathbf{b}^T\mathbf{z} \tag{6.21a}$$

$$s.t. \quad (\hat{\mathbf{A}} + \mathbf{I}_{(2m+2n)\times(2m+2n)})\mathbf{z} + (\varepsilon\mathbf{I}_{(2m+2n)\times(2m+2n)} + \gamma\hat{\mathbf{G}})\hat{\mathbf{e}} + \hat{\mathbf{d}} \ge \mathbf{0}_{2m+2n} \tag{6.21b}$$

where $\mathbf{I}_{(2m+2n)\times(2m+2n)} \in \Re^{(2m+2n)\times(2m+2n)}$ denotes an identity matrix. Also, the square of the bias parameter (i.e., γ^2) is added to the objective function, which provides the benefits of optimizing the orientation and location of the regression model simultaneously (Mangasarian and Musicant, 2000; Dunbar *et al.*, 2010).The matrices $\hat{\mathbf{C}}$, $\hat{\mathbf{G}}$ and $\hat{\mathbf{A}}$ are defined as:

$$\hat{\mathbf{C}} = \begin{bmatrix} \lambda_1\mathbf{I}_{2n\times 2n} & \mathbf{0}_{2n\times 2m} \\ \mathbf{0}_{2m\times 2n} & C\mathbf{I}_{2m\times 2m} \end{bmatrix}, \ \hat{\mathbf{G}} = \begin{bmatrix} \mathbf{0}_{2n\times 2n} & \mathbf{0}_{2n\times m} & \mathbf{0}_{2n\times m} \\ \mathbf{0}_{m\times 2n} & \mathbf{I}_{m\times m} & \mathbf{0}_{m\times m} \\ \mathbf{0}_{m\times 2n} & \mathbf{0}_{m\times m} & -\mathbf{I}_{m\times m} \end{bmatrix}, \ \hat{\mathbf{A}} = \begin{bmatrix} \mathbf{0}_{2n\times n} & \mathbf{0}_{2n\times n} & \mathbf{0}_{2n\times 2m} \\ -\mathbf{x}_{train} & \mathbf{x}_{train} & \mathbf{0}_{m\times 2m} \\ \mathbf{x}_{train} & -\mathbf{x}_{train} & \mathbf{0}_{m\times 2m} \end{bmatrix}$$

(6.22)

and the vectors $\mathbf{b}$, $\hat{\mathbf{e}}$, $\hat{\mathbf{d}}$ and $\mathbf{z} \in \Re^{(2m+2n)}$ are defined as:

$$\mathbf{b} = \begin{bmatrix} \mathbf{e}_{2n} \\ \mathbf{0}_{2m} \end{bmatrix},\ \hat{\mathbf{e}} = \begin{bmatrix} \mathbf{0}_{2n} \\ \mathbf{e}_{2m} \end{bmatrix},\ \hat{\mathbf{d}} = \begin{bmatrix} \mathbf{0}_{2n} \\ \mathbf{y}_{train} \\ -\mathbf{y}_{train} \end{bmatrix},\ \mathbf{z} = \begin{bmatrix} \mathbf{p} \\ \mathbf{q} \\ \boldsymbol{\beta} \\ \hat{\boldsymbol{\beta}} \end{bmatrix} \tag{6.23}$$

The constraints on **p** and **q** being non-negative have been reinforced by Eq.(6.21b).

Alternatively, Eq.(6.21) can be also solved through its dual formulation as follows,

$$\min_{\mathbf{u}} : \frac{1}{2}\mathbf{u}^T\mathbf{Q}\mathbf{u} - \mathbf{m}^T\mathbf{u} \tag{6.24a}$$

$$s.t. \quad \mathbf{u} \geq \mathbf{0}_{2m+2n} \tag{6.24b}$$

where $\mathbf{u} \in \Re^{2m+2n}$ denotes the Lagrange multiplier vector; $\mathbf{Q} \in \Re^{(2m+2n)\times(2m+2n)}$ and $\mathbf{m} \in \Re^{2m+2n}$ are defined as:

$$\begin{cases} \mathbf{Q} = (\hat{\mathbf{A}} + \mathbf{I}_{(2m+2n)\times(2m+2n)})\hat{\mathbf{C}}^{-1}(\hat{\mathbf{A}} + \mathbf{I}_{(2m+2n)\times(2m+2n)})^T + \hat{\mathbf{G}}\hat{\mathbf{e}}\hat{\mathbf{e}}^T\hat{\mathbf{G}} \\ \mathbf{m} = \lambda_2(\hat{\mathbf{A}} + \mathbf{I}_{(2m+2n)\times(2m+2n)})\hat{\mathbf{C}}^{-1}\mathbf{b} - \varepsilon\hat{\mathbf{e}} - \hat{\mathbf{d}} \end{cases} \tag{6.25}$$

Proposition 1. *Given the training dataset with input* $\mathbf{x}_{train} \in \Re^{m\times n}$ *and output* $\mathbf{y}_{train} \in \Re^{m}$, *with pre-defining the positive tuning parameters for X-SVR as* $\hat{\lambda}_1, \hat{\lambda}_2, c, \varepsilon \in \Re^{+}$, *the optimization problem defined in Eq. (6.24) is a convex quadratic programming problem.*

The proof of Proposition 1 is presented in Appendix 6B.

Subsequently, the global optimum of the proposed X-SVR approach can be efficiently determined by solving the associated dual problem by any available quadratic programming solvers. Let $\mathbf{u}^* \in \Re^{2m+2n}$ be the solution of the X-SVR, then the variables

$\mathbf{z}$ and γ can be calculated as $\mathbf{z} = \hat{\mathbf{C}}^{-1}\left[(\hat{\mathbf{A}} + \mathbf{I}_{(2m+2n)\times(2m+2n)})^T \mathbf{u}^* - \lambda_2 \mathbf{b}\right]$ and $\gamma = \hat{\mathbf{e}}^T \hat{\mathbf{G}} \mathbf{u}^*$, and $\mathbf{w}$ can be obtained as:

$$\mathbf{w} = \mathbf{p} - \mathbf{q} = \mathbf{z}(1:n) - \mathbf{z}(n+1:2n) \tag{6.26}$$

Consequently, the established linear regression function by the proposed X-SVR approach can be formulated as:

$$\hat{f}(\mathbf{x}) = (\mathbf{p} - \mathbf{q})^T \mathbf{x} - \hat{\mathbf{e}}^T \hat{\mathbf{G}} \mathbf{u}^* \tag{6.27}$$

6.4.1.2 The nonlinear X-SVR

The proposed X-SVR can also be extended to the nonlinear regression. To effectively transform the linear X-SVR to a kernelized learning approach, an alternative method, namely the empirical kernel map (Scholkopf *et al.*, 1999; Kung, 2014), is employed herein. The implemented empirical kernelization can be expressed as:

$$\mathbf{x}_i = [x_{i,1}, x_{i,2}, ..., x_{i,n}]^T \mapsto \hat{\mathbf{k}}(\mathbf{x}_i) = \begin{bmatrix} \bar{\mathbf{\Phi}}(\mathbf{x}_1)^T \bar{\mathbf{\Phi}}(\mathbf{x}_i) \\ \bar{\mathbf{\Phi}}(\mathbf{x}_2)^T \bar{\mathbf{\Phi}}(\mathbf{x}_i) \\ \vdots \\ \bar{\mathbf{\Phi}}(\mathbf{x}_m)^T \bar{\mathbf{\Phi}}(\mathbf{x}_i) \end{bmatrix} = \begin{bmatrix} K(\mathbf{x}_1, \mathbf{x}_i) \\ K(\mathbf{x}_2, \mathbf{x}_i) \\ \vdots \\ K(\mathbf{x}_m, \mathbf{x}_i) \end{bmatrix}, \text{for } i = 1, 2, ..., m \tag{6.28}$$

where $\bar{\mathbf{\Phi}}(\mathbf{x}_i)$ denotes the appropriate mapping function, implicitly mapping the *i*th input data $\mathbf{x}_i \in \Re^n$ into a higher-dimensional Euclidian space or even infinite dimensional Hilbert feature space; $\hat{\mathbf{k}}(\mathbf{x}_i)$ denotes the *i*th empirical feature vector with the empirical degree m which is equal to the number of training samples (Kung, 2014). Such m-dimensional vector space is defined as the empirical feature space (Xiong, Swamy and Ahmad, 2005). Then, the empirical feature vector $\hat{\mathbf{k}}(\mathbf{x}_i)$ is regarded as the *i*th training sample for constructing the learning model. The empirical feature space is finite-

dimensional and jointly defined by the employed kernel function and training samples (Kung, 2014). This kernel map approach has also been prevalently implemented in other kernelized learning methods, including the kernelized LASSO (Least Absolute Selection and Shrinkage Operator) (Gao, Kwan and Shi, 2010), the kernelized elastic net (Feng *et al.*, 2016), the linear programming SVR (Dai, Zhang and Wang, 2015) as well as the multiple empirical kernel learning machine (Fan *et al.*, 2017).

Thus, given the training dataset $\mathbf{x}_{train}$ and a specific kernel function $K(\bullet,\bullet)$, the initial training samples can be transferred through the kernel matrix $\mathbf{K}_{train} \in \Re^{m\times m}$ as:

$$\mathbf{K}_{train} = \begin{bmatrix} K(\mathbf{x}_1,\mathbf{x}_1) & K(\mathbf{x}_1,\mathbf{x}_2) & \cdots & K(\mathbf{x}_1,\mathbf{x}_m) \\ K(\mathbf{x}_2,\mathbf{x}_1) & K(\mathbf{x}_2,\mathbf{x}_2) & \cdots & K(\mathbf{x}_2,\mathbf{x}_m) \\ \vdots & \vdots & \cdots & \vdots \\ K(\mathbf{x}_m,\mathbf{x}_1) & K(\mathbf{x}_m,\mathbf{x}_2) & \cdots & K(\mathbf{x}_m,\mathbf{x}_m) \end{bmatrix} \tag{6.29}$$

and the kernel matrix $\mathbf{K}_{train}$ is utilized as the training dataset. Consequently, the nonlinear X-SVR problem can be formulated as:

$$\min_{\mathbf{p}_k,\mathbf{q}_k,\gamma,\xi,\hat{\xi}} : \frac{\hat{\lambda}_1}{2}(\|\mathbf{p}_k\|_2^2 + \|\mathbf{q}_k\|_2^2) + \hat{\lambda}_2\mathbf{e}_m^T(\mathbf{p}_k + \mathbf{q}_k) + \frac{C}{2}(\boldsymbol{\beta}^T\hat{\boldsymbol{\beta}} + \hat{\boldsymbol{\beta}}^T\hat{\boldsymbol{\beta}}) \tag{6.30a}$$

$$s.t. \quad \begin{cases} \mathbf{K}_{train}(\mathbf{p}_k - \mathbf{q}_k) - \gamma\mathbf{e}_m - \mathbf{y}_{train} \le \varepsilon\mathbf{e}_m + \boldsymbol{\beta} \\ \mathbf{y}_{train} - (\mathbf{K}_{train}(\mathbf{p}_k - \mathbf{q}_k) - \gamma\mathbf{e}_m) \le \varepsilon\mathbf{e}_m + \hat{\boldsymbol{\beta}} \\ \mathbf{p}_k, \mathbf{q}_k, \boldsymbol{\beta}, \hat{\boldsymbol{\beta}} \ge \mathbf{0}_m \end{cases} \tag{6.30b}$$

where $\mathbf{p}_k, \mathbf{q}_k \in \Re^m$ serve the same functions as $\mathbf{p}$ and $\mathbf{q}$ for the linear X-SVR; the subscript k indicates a kernelized learning model. Similarly to Eq.(6.18), the kernelized X-SVR can also be reformulated into:

$$\min_{\mathbf{z}_k,\gamma} : \frac{1}{2}(\mathbf{z}_k^T\hat{\mathbf{C}}\mathbf{z}_k + \gamma^2) + \lambda_2\mathbf{b}_k^T\mathbf{z}_k \tag{6.31a}$$

$$s.t. \quad (\hat{\mathbf{A}}_k + \mathbf{I}_{4m\times 4m})\mathbf{z}_k + (\varepsilon \mathbf{I}_{4m\times 4m} + \gamma \hat{\mathbf{G}}_k)\hat{\mathbf{e}}_k + \hat{\mathbf{d}}_k \geq \mathbf{0}_{4m} \tag{6.31b}$$

where the kernelized matrices $\hat{\mathbf{C}}_k$, $\hat{\mathbf{G}}_k$ and $\hat{\mathbf{A}}_k \in \Re^{4m\times 4m}$ are defined as:

$$\hat{\mathbf{C}}_k = \begin{bmatrix} \lambda_1 \mathbf{I}_{2m\times 2m} & \\ & c\mathbf{I}_{2m\times 2m} \end{bmatrix} \hat{\mathbf{G}}_k = \begin{bmatrix} \mathbf{0}_{2m\times 2m} & \mathbf{0}_{2m\times m} & \mathbf{0}_{2m\times m} \\ \mathbf{0}_{m\times 2m} & \mathbf{I}_{m\times m} & \mathbf{0}_{m\times m} \\ \mathbf{0}_{m\times 2m} & \mathbf{0}_{m\times m} & -\mathbf{I}_{m\times m} \end{bmatrix} \hat{\mathbf{A}}_k = \begin{bmatrix} \mathbf{0}_{2m\times m} & \mathbf{0}_{2m\times m} & \mathbf{0}_{2m\times 2m} \\ -\mathbf{K}_{train} & \mathbf{K}_{train} & \mathbf{0}_{m\times 2m} \\ \mathbf{K}_{train} & -\mathbf{K}_{train} & \mathbf{0}_{m\times 2m} \end{bmatrix}$$

(6.32)

and the kernelized vectors $\mathbf{b}_k$, $\hat{\mathbf{e}}_k$, $\hat{\mathbf{d}}_k$ and $\mathbf{z}_k \in \Re^{4m}$ are defined as:

$$\mathbf{b}_k = \begin{bmatrix} \mathbf{e}_{2m} \\ \mathbf{0}_{2m} \end{bmatrix}, \ \hat{\mathbf{e}}_k = \begin{bmatrix} \mathbf{0}_{2m} \\ \mathbf{e}_{2m} \end{bmatrix}, \ \hat{\mathbf{d}}_k = \begin{bmatrix} \mathbf{0}_{2m} \\ \mathbf{y}_{train} \\ -\mathbf{y}_{train} \end{bmatrix}, \ \mathbf{z}_k = \begin{bmatrix} \mathbf{p}_k \\ \mathbf{q}_k \\ \boldsymbol{\beta} \\ \hat{\boldsymbol{\beta}} \end{bmatrix} \tag{6.33}$$

Once again, the mathematical program defined in Eq.(6.31) can be equivalently solved through its dual formulation by using the Lagrange method with the KKT conditions. By introducing the non-negative Lagrange multiplier $\mathbf{u}_k \in \Re^{4m}$, the proposed kernelized X-SVR can be alternatively calculated through a quadratic program. That is,

$$\min_{\mathbf{u}_k} : \frac{1}{2}\mathbf{u}_k^T \mathbf{Q}_k \mathbf{u}_k - \mathbf{m}_k^T \mathbf{u}_k \tag{6.34a}$$

$$s.t. \quad \mathbf{u}_k \geq \mathbf{0}_{4m} \tag{6.34b}$$

where $\mathbf{Q}_k \in \Re^{4m\times 4m}$ and $\mathbf{m}_k \in \Re^{4m}$ are defined as:

$$\begin{cases} \mathbf{Q}_k = \mathbf{Q}_k = (\hat{\mathbf{A}}_k + \mathbf{I}_{4m\times 4m})\hat{\mathbf{C}}_k^{-1}(\hat{\mathbf{A}}_k + \mathbf{I}_{4m\times 4m})^T + \hat{\mathbf{G}}_k \hat{\mathbf{e}}_k \hat{\mathbf{e}}_k^T \hat{\mathbf{G}}_k \\ \mathbf{m}_k = \lambda_2 (\hat{\mathbf{A}}_k + \mathbf{I}_{4m\times 4m})\hat{\mathbf{C}}_k^{-1}\mathbf{b}_k - \varepsilon \hat{\mathbf{e}}_k - \hat{\mathbf{d}}_k \end{cases} \tag{6.35}$$

Let $\boldsymbol{\lambda}_k^* \in \Re^{4m}$ be the solution of Eq.(6.34), the variables $\mathbf{z}_k$ and γ_k can be determined as $\mathbf{z}_k = \hat{\mathbf{C}}_k^{-1}\left[(\hat{\mathbf{A}}_k + \mathbf{I}_{4m\times 4m})^T \mathbf{u}_k^* - \lambda_2 \mathbf{b}_k\right]$ and $\gamma = \hat{\mathbf{e}}_k^T \hat{\mathbf{G}}_k \mathbf{u}_k^*$. Then, the coefficient $\mathbf{w}$ can be obtained as:

$$\mathbf{w} = \mathbf{p}_k - \mathbf{q}_k = \mathbf{z}_k(1:m) - \mathbf{z}_k(m+1:2m) \tag{6.36}$$

Consequently, the nonlinear regression function obtained by the proposed kernelized X-SVR can be formulated as:

$$\hat{f}_k(\mathbf{x}) = (\mathbf{p}_k - \mathbf{q}_k)^T \mathbf{k}(\mathbf{x}) - \hat{\mathbf{e}}_k^T \hat{\mathbf{G}}_k \mathbf{u}_k^* \tag{6.37}$$

The difference between the linear and nonlinear X-SVR is that the input dataset has been mapped into an empirical space by utilizing the specified kernel function within the non-linear model. Subsequently, the kernelized X-SVR is equivalent to a linear X-SVR with a manipulated input samples and therefore, the convexity of the mathematical program is well preserved regardless of the type of kernel function.

6.4.1.3 The generalized Gegenbauer polynomial kernel

Inspired by the remarkable performance of the orthogonal polynomial based kernels for SVR/SVM, the Gegenbauer polynomial (San Kim, Kim and Rim, 2012) is implemented herein as a new type of kernel for X-SVR. The proposed orthogonal polynomial kernel is constructed by using the partial sum of the inner products of generalized Gegenbauer polynomials, namely the Generalized Gegenbauer Kernel (GGK). By adopting the strategy utilized for defining the generalized Chebyshev polynomial for vector inputs (Ozer, Chen and Cirpan, 2011), the generalized Gegenbauer polynomials are defined recursively as following:

$$\begin{cases} P_0^{\alpha}(\mathbf{x}) = 1 \\ P_1^{\alpha}(\mathbf{x}) = 2\alpha \mathbf{x}^T \\ P_d^{\alpha}(\mathbf{x}) = \dfrac{1}{d}[2\mathbf{x}^T(d+\alpha-1)P_{d-1}^{\alpha}(\mathbf{x}) - (d+2\alpha-2)P_{d-2}^{\alpha}(\mathbf{x})],\ d = 2,3,4,... \end{cases} \tag{6.38}$$

where $\mathbf{x} \in \Re^n$ denotes the column vector of input variables. It can be revealed from Eq. (6.38) that the generalized Gegenbauer polynomial $P_d^{\alpha}(\mathbf{x})$ yields a scalar value when the polynomial order d is an even number, otherwise it will yield a column vector.

Moreover, the Gaussian kernel function is implemented as the weighting function for the proposed GGK. Consequently, the proposed *n*th order Generalized Gegenbauer Kernel function $K_{GGK}(\mathbf{x}_i, \mathbf{x}_j)$ of two arbitrary input vectors $\mathbf{x}_i$ and $\mathbf{x}_j$ is defined as:

$$K_{GGK}(\mathbf{x}_i, \mathbf{x}_j) = \frac{\sum_{l=0}^{d} P_l^{\alpha}(\mathbf{x}_i)^T P_l^{\alpha}(\mathbf{x}_j)}{\exp(\sigma \left\| \mathbf{x}_i - \mathbf{x}_j \right\|_2^2)} \tag{6.39}$$

where each element of $\mathbf{x}_i$ and $\mathbf{x}_j$ is defined in $[-1,1]$. In this context, both α and σ are considered as the kernel scales or the so-called decaying parameters of the proposed kernel function.

It is emphasized that the proposed GGK satisfies the Mercer Theorem (Vapnik, 1998, 2013; Smola and Schölkopf, 2004; Campbell and Ying, 2011; Kung, 2014).

Proposition 2. *The proposed GGK expressed in Eq.(6.39) is a valid Mercer kernel.*

The detailed proof of Proposition 2 is presented in Appendix 6C.

6.4.1.4 The selection of the X-SVR model parameters

Within the proposed X-SVR with GGK, there are seven hyperparameters presented in this approach which are including the two regularization parameters λ_1 and λ_2, the

penalty parameter C, the insensitive tube width ε, the polynomial order d and two positive kernel scale parameters α and σ.

The k-fold cross-validation (CV) over the training samples is adopted herein to ensure the adequacy of the regression model for accurate prediction of the training dataset without overfitting into certain extent. Practically, k is commonly set between 5-10 as a trade-off of computational cost and prediction accuracy. In this paper, the k-fold CV error which denoted by Err_{kCV} is employed as the training error measure for X-SVR.

$$Err_{kCV} = \frac{1}{k}\sum_{i=1}^{k} err_i \tag{6.40}$$

where err_i denotes the mean squared error (MSE) between the predicted output $\hat{f}(\mathbf{x})$ obtained by the X-SVR model and the output of the true function $f(\mathbf{x})$ in each fold i. err_i is expressed as:

$$err_i = \frac{1}{m_i}\sum_{j=1}^{m_i}(y_j - \hat{f}(\mathbf{x}_j))^2 \tag{6.41}$$

where m_i denotes the number of training samples in the fold i. To minimize Err_{kCV}, the Bayesian optimization method is integrated within the proposed X-SVR with GGK for adaptively selecting the suitable learning parameters.

6.4.2 SSIGA for stochastic linear stability analysis of FGM plate

In this paper, the Young's modulus $E(z)$ and the Poisson's ratio $\nu(z)$ of the FGM plate are considered as random fields, whereas the gradient index of FGM n is modelled as a lognormal random variable as presented in Chapter 5.

For random field $E(\mathbf{x},z,\theta)$ and $\nu(\mathbf{x},z,\theta)$ with different distribution types, they are defined as

$$\begin{cases} E(\mathbf{x},z,\theta)=H_E^G(\mathbf{x},\theta)E(z,\theta)=H_E^G(\mathbf{x},\theta)\left[E_m+(E_c-E_m)(\frac{1}{2}+\frac{z}{h})^{\chi(\theta)}\right](\text{Gaussian}) \\ \nu(\mathbf{x},z,\theta)=H_\nu^G(\mathbf{x},\theta)\nu(z,\theta)=H_\nu^G(\mathbf{x},\theta)\left[\nu_m+(\nu_c-\nu_m)(\frac{1}{2}+\frac{z}{h})^{\chi(\theta)}\right](\text{Gaussian}) \\ E(\mathbf{x},z,\theta)=H_E^L(\mathbf{x},\theta)E(z,\theta)=H_E^L(\mathbf{x},\theta)\left[E_m+(E_c-E_m)(\frac{1}{2}+\frac{z}{h})^{\chi(\theta)}\right](\text{Lognormal}) \\ \nu(\mathbf{x},z,\theta)=H_\nu^L(\mathbf{x},\theta)\nu(z,\theta)=H_\nu^L(\mathbf{x},\theta)\left[\nu_m+(\nu_c-\nu_m)(\frac{1}{2}+\frac{z}{h})^{\chi(\theta)}\right](\text{Lognormal}) \end{cases} \tag{6.42}$$

where $H_E^G(\mathbf{x},\theta)$ and $H_\nu^G(\mathbf{x},\theta)$ are homogeneous Gaussian random fields with predefined means, standard deviations and covariance functions; $H_E^L(\mathbf{x},\theta)$ and $H_\nu^L(\mathbf{x},\theta)$ are homogeneous lognormal random fields with predefined means, standard deviations and covariance functions; $\chi(\theta)$ is a lognormal random variable with predefined mean and variance.

By implementing the K-L expansion, the discretization of the spatially dependent uncertain Young's modulus and Poisson's ratio of FGM plate, with M_1 and M_2 terms respectively, are explicitly formulated as,

$$\begin{cases} \hat{E}(\mathbf{x},z,\theta)=\left[\sum_{\mathbf{I}}^{\mathbf{N}_{cp}}\mu_{\mathbf{I}}^E R_{\mathbf{I}}^{\mathbf{P}}(\xi)+\sum_{i_1=1}^{M_1}\sqrt{\lambda_{i_1}}\zeta_{i_i}(\theta)\left(\sum_{\mathbf{I}}^{\mathbf{N}_{cp}}\vartheta_{\mathbf{I}}^{i_1}R_{\mathbf{I}}^{\mathbf{P}}(\xi)\right)\right]E(z,\theta)(\text{Gaussian}) \\ \hat{\nu}(\mathbf{x},z,\theta)=\left[\sum_{\mathbf{I}}^{\mathbf{N}_{cp}}\mu_{\mathbf{I}}^\nu R_{\mathbf{I}}^{\mathbf{P}}(\xi)+\sum_{i_2=1}^{M_2}\sqrt{\lambda_{i_2}}\varsigma_{i_2}(\theta)\left(\sum_{\mathbf{I}}^{\mathbf{N}_{cp}}\phi_{\mathbf{I}}^{i_2}R_{\mathbf{I}}^{\mathbf{P}}(\xi)\right)\right]\nu(z,\theta)(\text{Gaussian}) \\ \hat{E}(\mathbf{x},z,\theta)=\exp\left[\sum_{\mathbf{I}}^{\mathbf{N}_{cp}}\mu_{\mathbf{I}}^E R_{\mathbf{I}}^{\mathbf{P}}(\xi)+\sum_{i_1=1}^{M_1}\sqrt{\lambda_{i_1}}\zeta_{i_i}(\theta)\left(\sum_{\mathbf{I}}^{\mathbf{N}_{cp}}\vartheta_{\mathbf{I}}^{i_1}R_{\mathbf{I}}^{\mathbf{P}}(\xi)\right)\right]E(z,\theta)(\text{Lognormal}) \\ \hat{\nu}(\mathbf{x},z,\theta)=\exp\left[\sum_{\mathbf{I}}^{\mathbf{N}_{cp}}\mu_{\mathbf{I}}^\nu R_{\mathbf{I}}^{\mathbf{P}}(\xi)+\sum_{i_2=1}^{M_2}\sqrt{\lambda_{i_2}}\varsigma_{i_2}(\theta)\left(\sum_{\mathbf{I}}^{\mathbf{N}_{cp}}\phi_{\mathbf{I}}^{i_2}R_{\mathbf{I}}^{\mathbf{P}}(\xi)\right)\right]\nu(z,\theta)(\text{Lognormal}) \end{cases} \tag{6.43}$$

As aforementioned, the X-SVR model is proposed within the SSIGA for the stochastic linear stability analysis of plate. Subsequently, an X-SVR compatible SSIGA formulation is proposed herein. First of all, an experiment design algorithm is meticulously proposed to generate the training input samples for the X-SVR model. The algorithm is briefly introduced in Algorithm 1.

Input: m, n_{MCS}, M_1, M_2

Output: $\mathbf{x}_{train}$, $\mathbf{x}$

- Generate n_{MCS} realizations for M_1 independent Gaussian random variables, i.e., $\boldsymbol{\zeta} \in \Re^{n_{MCS} \times M_1}$, of the random field of the Young's modulus.
- Generate n_{MCS} realizations for M_2 independent Gaussian random variables, i.e., $\boldsymbol{\eta} \in \Re^{n_{MCS} \times M_2}$, of the random field of the Poisson's ratio.
- Generate n_{MCS} realizations for the random variable with the specific distribution, i.e., $\boldsymbol{\chi} \in \Re^{n_{MCS}}$
- Construct the inputs, i.e., $\mathbf{x} = (\boldsymbol{\zeta}, \boldsymbol{\eta}, \boldsymbol{\chi}) \in \Re^{n_{MCS} \times (M_1 + M_2 + 1)}$, for the Monte Carlo Simulation.
- Sort $\mathbf{x}$ in a descending order of the first column of $\mathbf{x}$.
- Divide $\mathbf{x}$ into m groups, select the midpoint of each group as the *i*th component (i.e., $\mathbf{x}_i$) of the training sample $\mathbf{x}_{train} = (\mathbf{x}_1, \mathbf{x}_2, \ldots, \mathbf{x}_i, \ldots \mathbf{x}_m)^T$

Algorithm 1. Experiment design algorithm of the SSIGA for linear stability analysis of plate

where n_{MCS} denotes the number of MCS simulation cycles. By following Algorithm 1, the training input $\mathbf{x}_{train} = (\mathbf{x}_1, \mathbf{x}_2, \ldots, \mathbf{x}_i, \ldots \mathbf{x}_m)^{\mathrm{T}}$ can be generated, where m denotes the size of training sample; $\mathbf{x}_i = \left\{ \{\zeta_{i_1}(\theta_i)\}_{i_1=1}^{M_1}, \{\varsigma_{i_2}(\theta_i)\}_{i_2=1}^{M_2}, \chi(\theta_i) \right\}$ denotes the random variables for the Young's modulus, Poisson's ratio and gradient index of the FGM corresponding to the event $\theta_i \in \Omega$. To construct the X-SVR model for the stochastic linear stability problem, the corresponding output y_i (i.e., the buckling load $P_i^{cr}(\theta_i)$, of

each $\mathbf{x}_i$ should be calculated in prior. The calculation for the output y_i of a specific event θ_i can be formulated as follows,

$$\left[(\mathbf{K}_{ib}(\theta_i)+\mathbf{K}_s(\theta_i))+{}^n\zeta(\theta_i)(\mathbf{K}_i^{NL}(\theta_i)+\mathbf{K}_\sigma(\theta_i))\right]\mathbf{y}(\theta_i)=\mathbf{0} \tag{6.44}$$

After solving the eigenvalue problem, the output y_i can be obtained as ${}^{cr}\zeta(\theta_i)^nP$. Subsequently, the proposed X-SVR model within the SSIGA scheme can be constructed.

To verify the accuracy of the proposed X-SVR model, the Monte-Carlo simulation (MCS) is implemented with large simulation cycles. In addition, the normalized mean-square error (NMSE), the normalized average absolute error (NAAE), and the normalized maximum absolute error (NMAE) are provided to assess the results.

$$\begin{cases} \text{NMSE}=\dfrac{\sum_{i=1}^{n_{MCS}}(\hat{y}_i-y_i)^2}{\sum_{i=1}^{n_{MCS}}(\mu_y-y_i)^2} \\ \text{NAAE}=\dfrac{\sum_{i=1}^{n_{MCS}}\left|\hat{y}_i-y_i\right|}{n_{MCS}\sigma_y} \\ \text{NMAE}=\dfrac{\max_{i=1}^{n_{MCS}}\left|\hat{y}_i-y_i\right|}{n_{MCS}\sigma_y} \end{cases} \tag{6.45}$$

where $\hat{y}_i$ and y_i denote the estimated and actual buckling load for the input $\mathbf{x}_i$, respectively; μ_y denotes the mean of the actual buckling load; and σ_y denotes the standard deviation of the actual buckling load. The first two error-metrices provide a global accuracy measure, whereas the third one relates to a local measure of accuracy. To enhance the understanding of the proposed SSIGA for stochastic linear stability analysis of plate, a flowchart is provided.

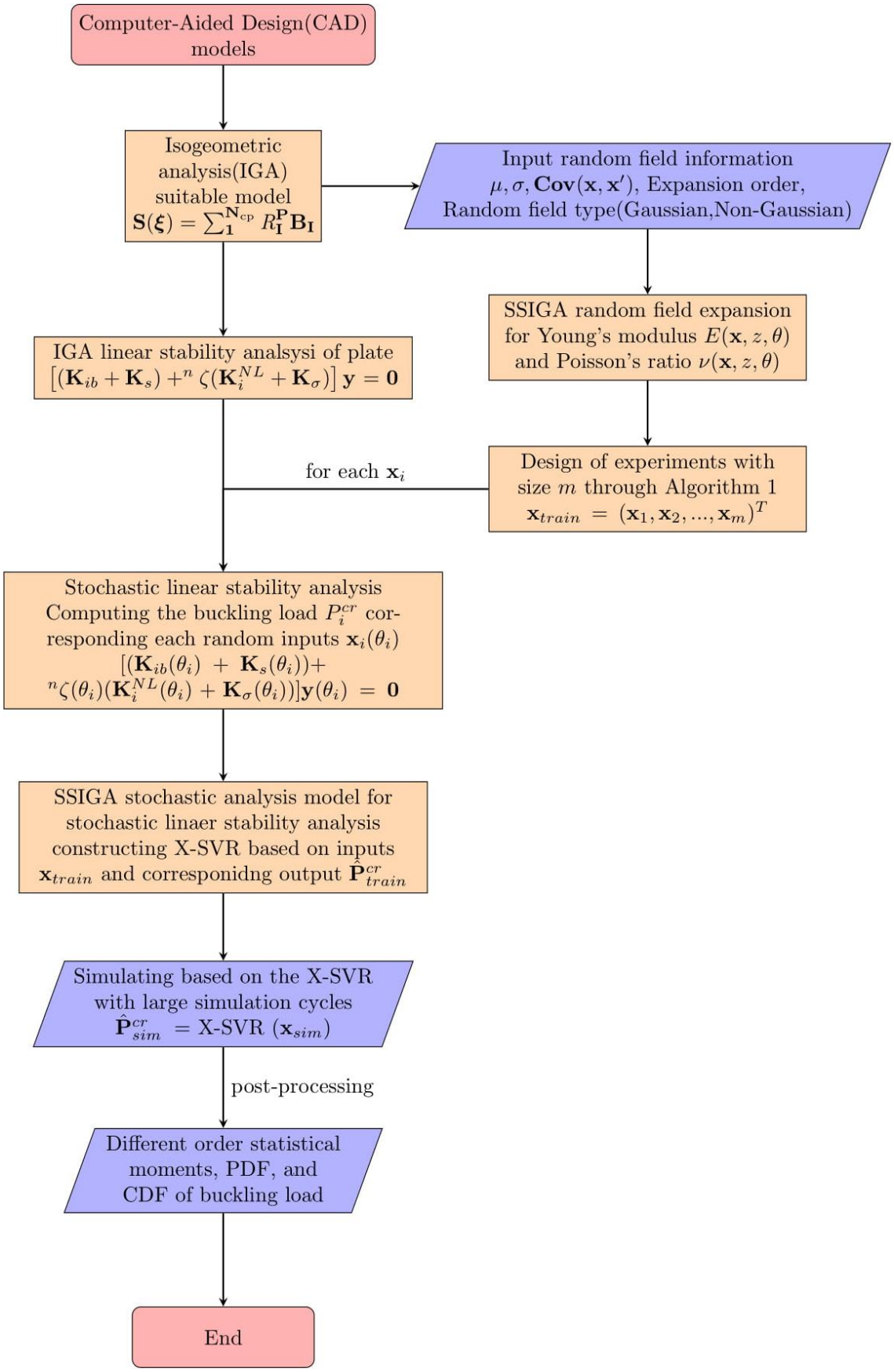

Figure 6.1 Flowchart of the SSIGA for stochastic linear stability analysis

6.5 Numerical examples

To demonstrate the accuracy, efficiency and applicability of the proposed SSIGA approach for stochastic linear stability analysis of FGM plate with the consideration of both spatially dependent and independent uncertain parameters, two numerical examples are thoroughly investigated in this section. For the first numerical example, the proposed method is implemented for a circular ring FGM plate with only spatially dependent uncertain parameters. For the second numerical example, the proposed method is implemented for an irregularly shaped FGM plate with both spatially dependent and independent uncertain parameters. Since the closed-form analytical solutions are absent for the two investigated numerical examples, all the results obtained by the proposed method are partially compared with the MCS method with large simulation size. The MCS approach is achieved by repeatedly executing the deterministic IGA with one possible realization of the randomness at each cycle until the predefined total number of the simulation is reached. Within the context of the presented numerical examples, all random numbers are generated by employing the Statistics toolbox of MATLAB R2018a, also the evaluation of IGA basis functions is based on the technique presented in (V. P. Nguyen *et al.*, 2015).

6.5.1 Numerical example: circular ring plate

In the first numerical example, a circular ring Al_2O_3/Al FGM plate is investigated with the consideration of spatially dependent uncertain Young's modulus and Poisson's ratio. The thickness of the plate is 0.1m. The general structural layout and the adopted IGA mesh of the investigated plate are shown in Figure 6.2. The adopted IGA mesh is obtained by refining the corresponding coarsest IGA mesh. The plate is clamped at the two horizontal edges and is under uniformly distributed compression along the normal

direction of the outer edge. The Young's modulus is modelled as a homogeneous Gaussian random field as follows,

$$E(\mathbf{x},z,\theta)=H_E^G(\mathbf{x},\theta)E(z)=H_E^G(\mathbf{x},\theta)\left[E_m+(E_c-E_m)(\frac{1}{2}+\frac{z}{h})^n\right] \quad (6.46)$$

where $H_E^G(\mathbf{x},\theta)$ denotes a homogeneous Gaussian random field with mean $\mu=1$ and standard deviation $\sigma=0.1$. The Poisson's ratio is modelled as a homogeneous lognormal random field as follows,

$$\nu(\mathbf{x},z,\theta)=H_\nu^L(\mathbf{x},\theta)\nu(z)=H_\nu^L(\mathbf{x},\theta)\left[\nu_m+(\nu_c-\nu_m)(\frac{1}{2}+\frac{z}{h})^n\right] \quad (6.47)$$

where $H_\nu^L(\mathbf{x},\theta)$ denotes a homogeneous lognormal random field with mean $\mu=1$ and standard deviation $\sigma=0.1$. The exponential covariance function Eq.(5.9) with $l=4m$ is adopted to consider the spatial dependency of both random fields. E_m and E_c denote the Young's modulus of Al and Al_2O_3 respectively. ν_m and ν_c denote the Poisson's ratio of Al and Al_2O_3 respectively. The magnitudes of E_m, E_c, ν_m, and ν_c are selected from Table 4.1.

Within the proposed SSIGA framework, the generalized isogeometric basis functions based K-L expansion with six terms is adopted to decompose both random fields. After that, the stochastic buckling loads of the circular ring plate with different gradient indices of FGM are estimated by the proposed X-SVR approach. The investigated gradient indices of the FGM are $n=0,5,10,50$. For each gradient index, two types of kernel functions (i.e., Gegenbauer polynomial and Gaussian) are implemented within the proposed X-SVR. Moreover, various sampling sizes (i.e., 20, 50, and 100) of the X-SVR are also testified. In addition, the MCS approach with 1 million simulation cycles is

implemented for each gradient index of FGM. The MCS results are regarded as the actual buckling loads in subsequent analyses.

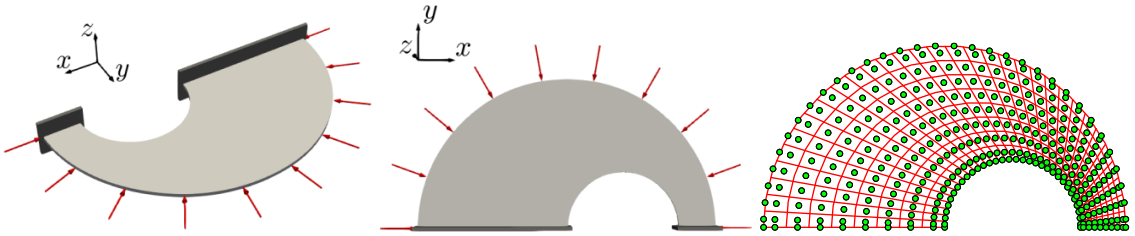

(a) (b) (c)

Figure 6.2 Circular ring FGM plate (a) 3D view; (b) front view; (c) IGA refinement

Three error-metrics, NMSE, NAAE, and NMAE, are adopted to assess the performance of the X-SVR model. Figures 6.3 reports the NMSE, NAAE, and NMAE of the X-SVR model for different gradient indices of FGM with different training sample sizes. By closely examining Figure 6.3, The increase of the training sample size can produce more accurate approximation al both global and local levels. In addition, the best X-SVR model with respect to the three metrics is established through the Gegenbauer polynomial kernel. Moreover, even with smaller training sample size, the Gegenbauer polynomial kernel is always superior over the Gaussian kernel with equal or larger training sample sizes. Figure 4 illustrates the estimated buckling loads by the X-SVR with Gegenbauer polynomial kernel against the MCS approach for different gradient indices of FGM with different training sample sizes. The three metrics and a reference line $\hat{P}_{cr} = P_{cr}$ are also provided in each plot. By closely inspecting Figure 6.4, the scatter plot with training sample size 20 is already very close to $\hat{P}_{cr} = P_{cr}$. By increasing the sample size, a more convergent training quality can be observed.

Moreover, the mean and the standard deviation of the buckling load obtained by different kernel functions with training sample size 100 are provided in Table 6.1 to

quantitatively validate the proposed method. According to the first two statistical moments, the X-SVRs with different kernel functions are all able to accurately predict the mean of the buckling load. However, only the X-SVRs with Gegenbauer polynomial kernel can accurately predict the standard deviation of the buckling load. Additionally, for all investigated gradient indices of the FGM, the X-SVR with Gegenbauer polynomial kernel has maximum relative error of 0.0199% and 0.4144% for the mean the standard deviation, respectively.

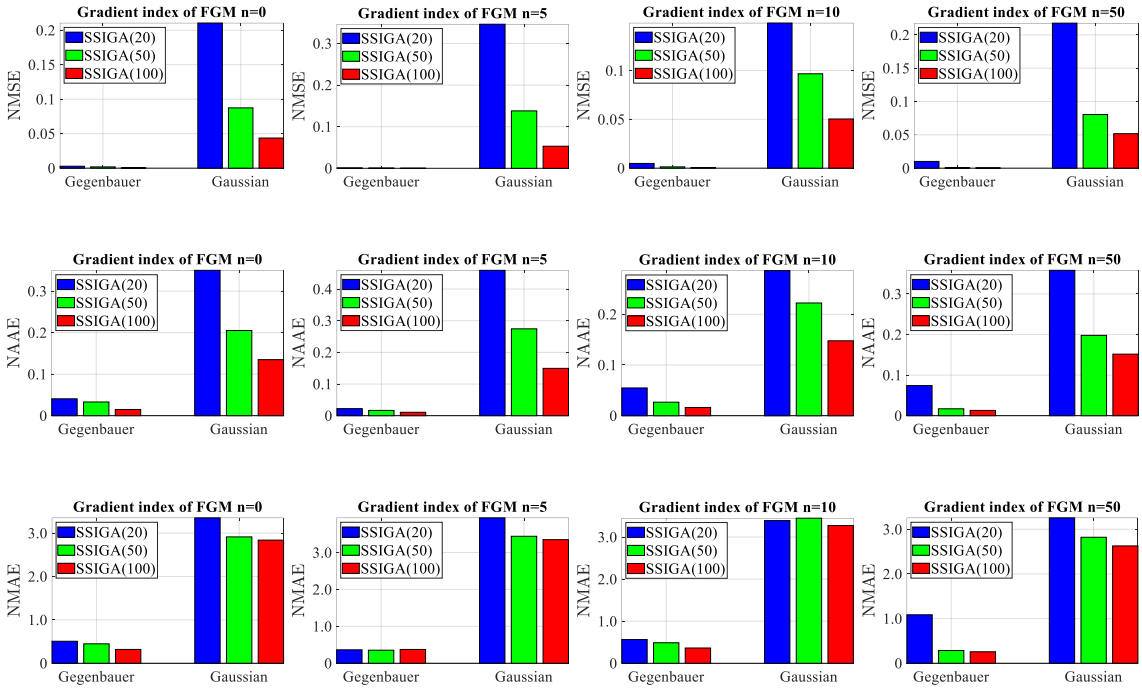

Figure 6.3 NMSE, NAAE, and NMAE of the X-SVR model for different gradient index of FGM with different training sample sizes

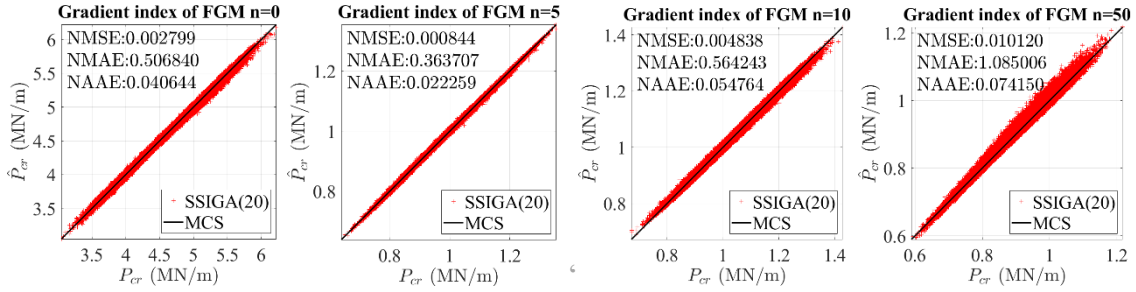

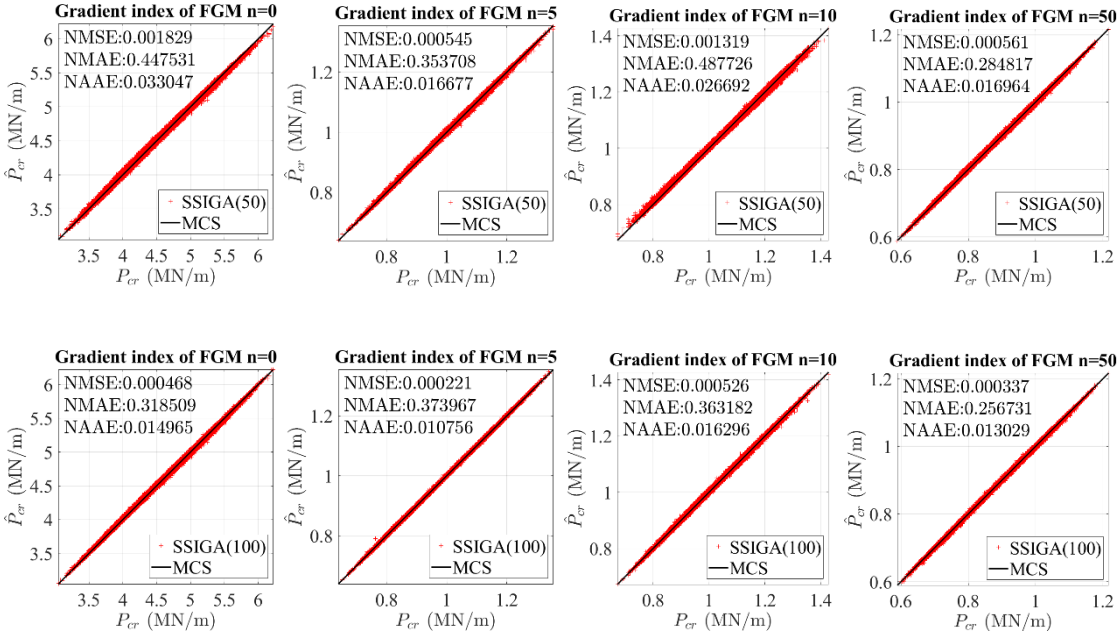

Figure 6.4 The quality of estimation of the X-SVR with Gegenbauer polynomials kernel for different gradient indexes of FGM with different sample sizes

Table 6.1 The mean and standard deviation of the buckling load obtained by different kernel functions with training sample size 100 (MN/m)

Statistical Moment	Gradient Index of FGM n	MCS	Gegenbauer	Gaussian
Mean	0	4.6158	4.6162	4.6153
	5	1.0037	1.0039	1.0054
	10	1.0487	1.0487	1.0496
	50	0.8873	0.8872	0.8862
Std	0	0.3378	0.3364	0.2963
	5	0.0744	0.0745	0.0632
	10	0.0774	0.0776	0.0663
	50	0.6491	0.6481	0.5543

In addition to the first two statistical moments of the buckling load, the PDF and CDF of the buckling load are also estimated through a non-parametric statistical inference technique known as the kernel density estimation approach. Figures 6.5-6.6, Figures 6.7-

6.8, Figures 6.9-6.10 and Figures 6.11-6.12 report the estimated PDFs and CDFs of the buckling load with different kernel functions for the gradient index of FGM 0, 5, 10, and 50, respectively. Evidently, the proposed X-SVR with Gegenbauer polynomial kernel is competent for establishing the PDF and CDF of the buckling load. From Figures 6.5-6.12, it is evidently illustrated that the proposed X-SVR of Gegenbauer kernel can produce higher quality results even at very small sampling size. However, with the same sampling size, the X-SVR with Gaussian kernel cannot provide the same level of quality. After assessing the performance of the proposed method on estimating the buckling load of the FGM plate, the buckling mode shapes corresponding to three specific events $\theta_1, \theta_2, \theta_3 \in \Omega$ for different gradient indices of FGM are presented in Figures 6.13-6.16.

In this numerical example, the results obtained by the MCS approach were executed on a cluster node with 2×14 cores Intel Xeon E5-2690v4 (Broadwell) 2.6 GHz), while the results obtained by the proposed SSIGA approach were executed on a workstation with 4 cores (Intel Core i7-6700 3.4GHz). For the buckling load of each gradient index of FGM, the MCS approach with 1 million simulation cycles were executed concurrently with 28 works on the cluster node and the total computational cost was 57h 15m 7s. Meanwhile, without parallel computation, the proposed X-SVR within SSIGA only consumed 1m 27s with training sample size 100. Moreover, by using the constructed X-SVR model, the prediction of the 1 million random samples with 4 cores on the workstation only consumed 4m 11s. Therefore, based on the reported information, the proposed method certainly shows superior computational efficiency over the exhaustively simulative MCS approach.

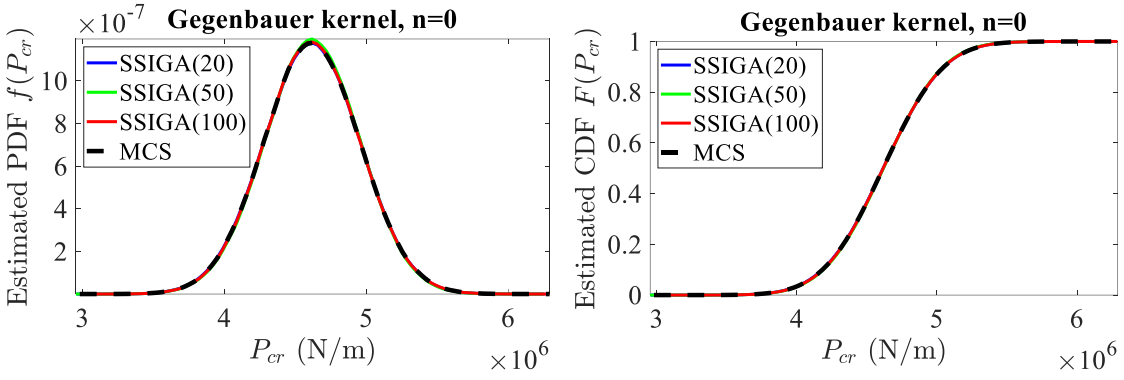

(a) (b)

Figure 6.5 The estimated (a) PDF and (b) CDF of the buckling load by Gegenbauer polynomial based X-SVR for $n = 0$

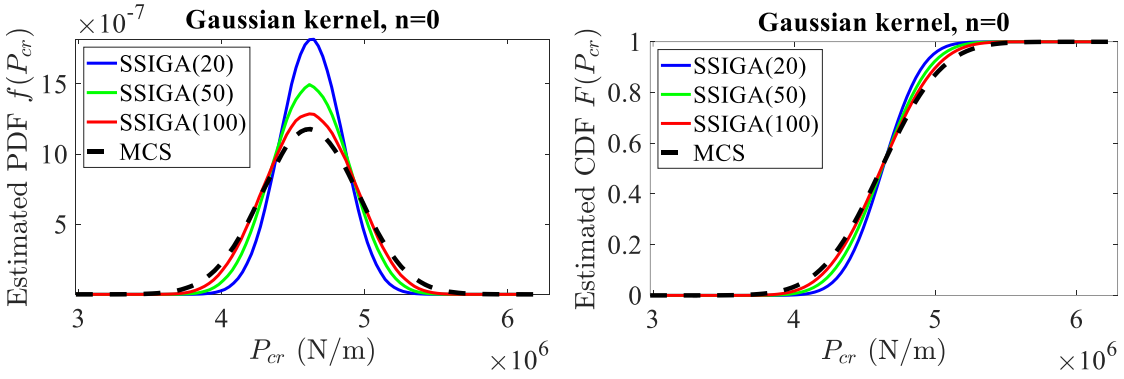

(a) (b)

Figure 6.6 The estimated (a) PDF and (b) CDF of the buckling load by Gaussian function based X-SVR for $n = 0$

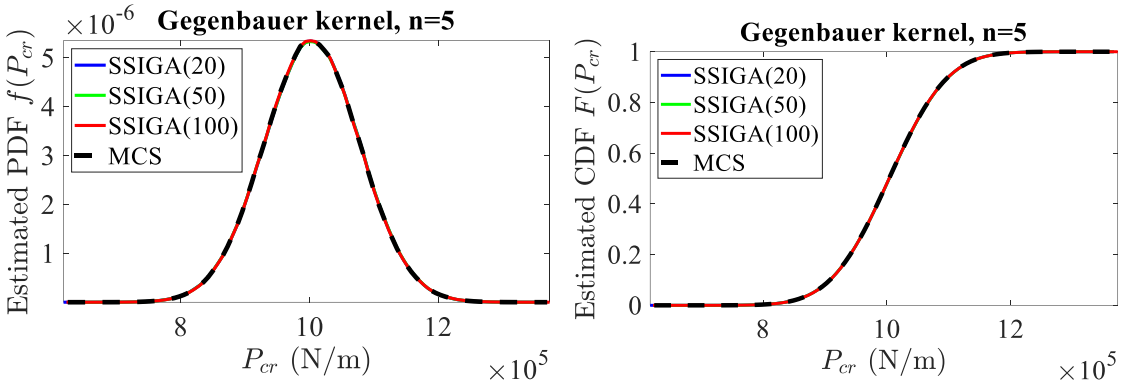

(a) (b)

Figure 6.7 The estimated (a) PDF and (b) CDF of the buckling load by Gegenbauer polynomial based X-SVR for $n=5$

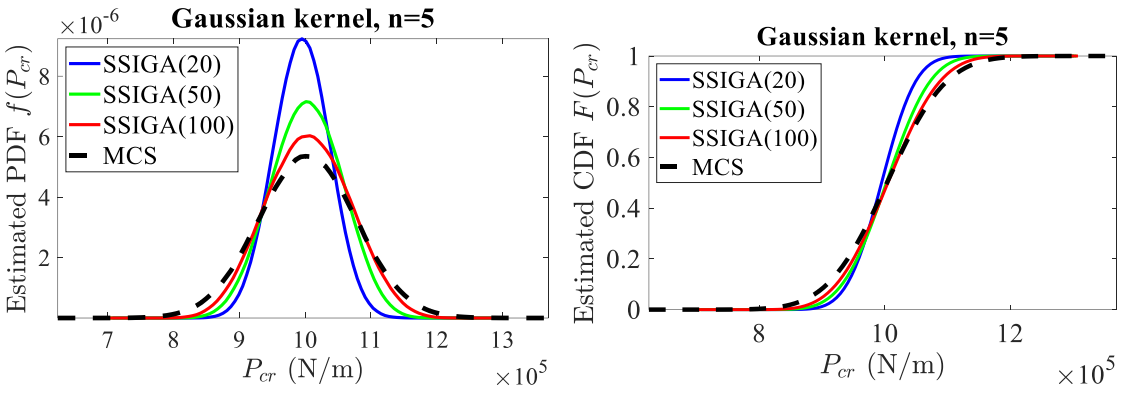

(a) (b)

Figure 6.8 The estimated (a) PDF and (b) CDF of the buckling load by Gaussian function based X-SVR for $n=5$

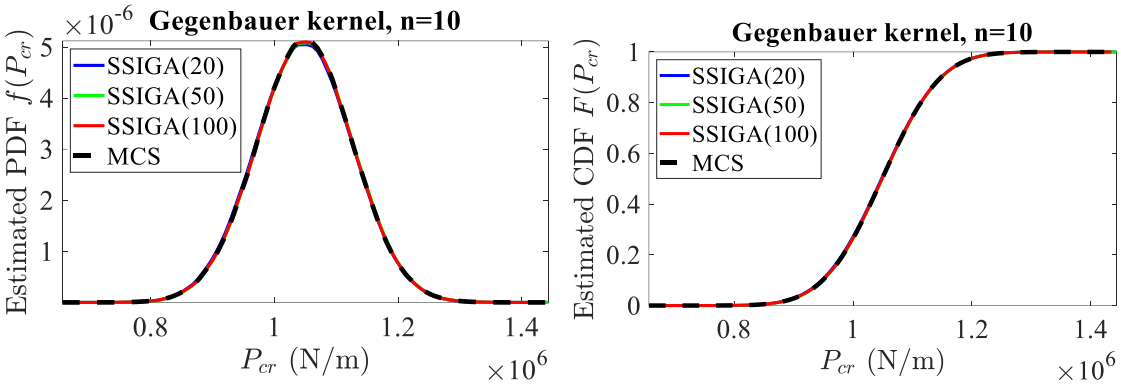

(a) (b)

Figure 6.9 The estimated (a) PDF and (b) CDF of the buckling load by Gegenbauer polynomial based X-SVR for $n=10$

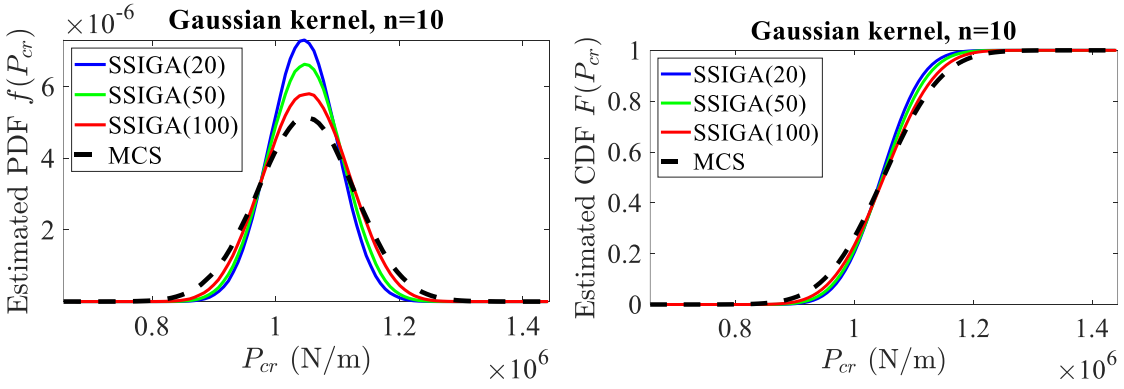

(a) (b)

Figure 6.10 The estimated (a) PDF and (b) CDF of the buckling load by Gaussian function based X-SVR for $n=10$

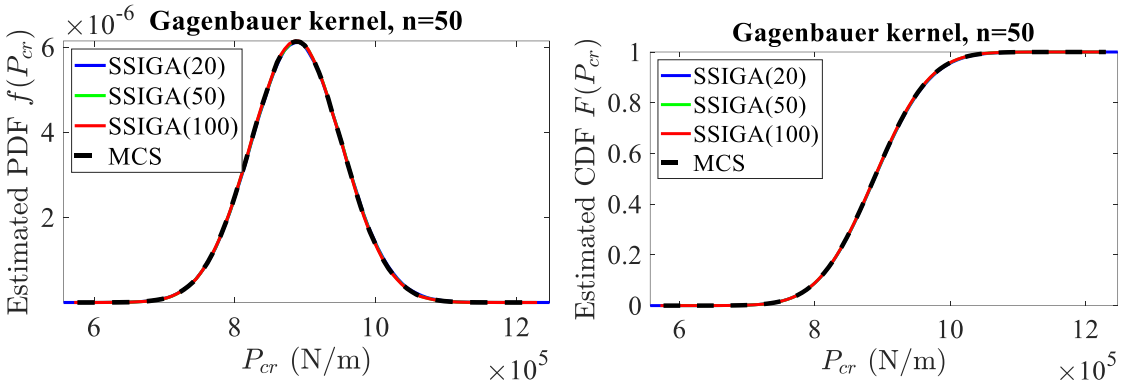

(a) (b)

Figure 6.11 The estimated (a) PDF and (b) CDF of the buckling load by Gegenbauer polynomial based X-SVR for $n=50$

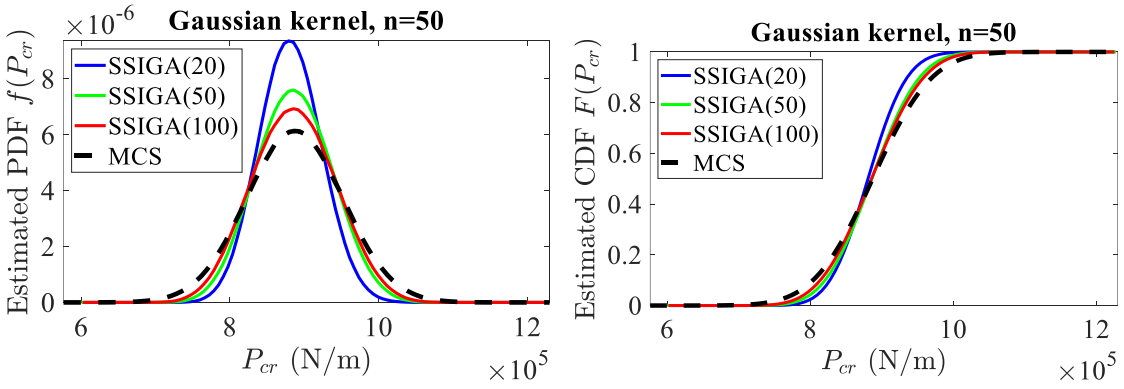

(a) (b)

Figure 6.12 The estimated (a) PDF and (b) CDF of the buckling load by Gaussian function based X-SVR for $n=50$

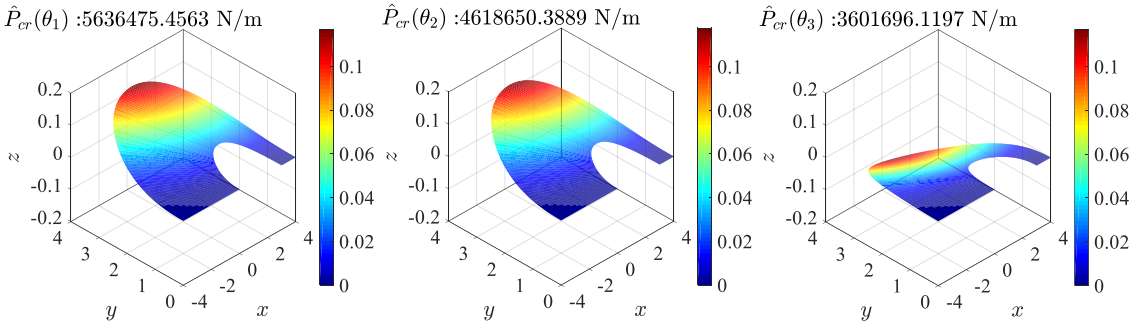

(a) (b) (c)

Figure 6.13 The buckling load and buckling mode shape of FGM plate with $n=0$ at specific event (a) θ_1; (b) θ_2; (c) θ_3

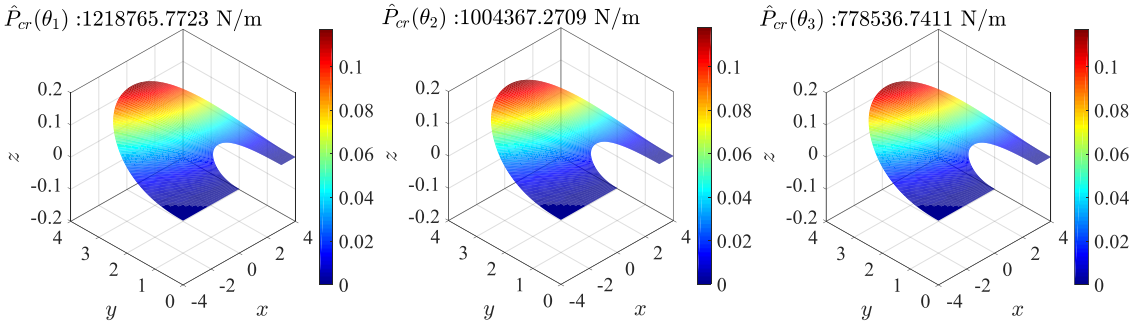

(a) (b) (c)

Figure 6.14 The buckling load and buckling mode shape of FGM plate with $n=5$ at specific event (a) θ_1; (b) θ_2; (c) θ_3

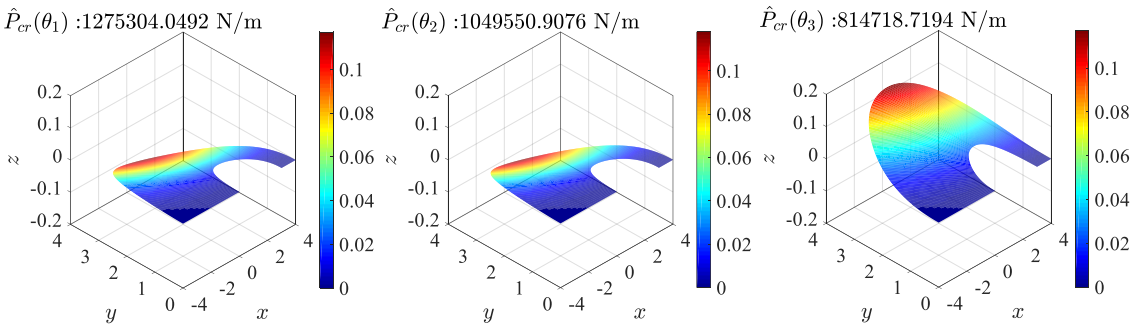

(a) (b) (c)

Figure 6.15 The buckling load and buckling mode shape of FGM plate with $n=10$ at specific event (a) θ_1; (b) θ_2; (c) θ_3

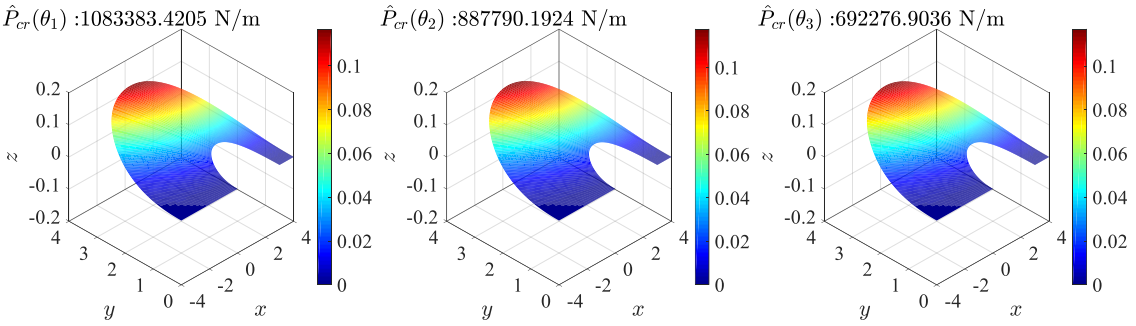

(a) (b) (c)

Figure 6.16 The buckling load and buckling mode shape of FGM plate with $n=50$ at specific event (a) θ_1; (b) θ_2; (c) θ_3

6.5.2 Numerical example: irregular plate

In the second numerical example, a ZrO_2-1/Al FGM plate with irregular geometry is investigated by considering not only the spatially dependent uncertain Young's modulus and Poisson's ratio, but also the spatially independent uncertain gradient index of the FGM. The thickness of the plate is 0.2m. The general structural layout and the adopted IGA mesh of the investigated plate are shown in Figure 6.17. The plate is fixed on the red column at the inner edge and is under uniformly distributed compression along the normal direction of the outer edge. The Young's modulus is modelled as a homogeneous lognormal random field as follows,

$$E(\mathbf{x},z,\theta)=H_E^L(\mathbf{x},\theta)E(z,\theta)=H_E^L(\mathbf{x},\theta)\left[E_m+(E_c-E_m)(\frac{1}{2}+\frac{z}{h})^{\chi(\theta)}\right] \quad (6.48)$$

where $H_E^L(\mathbf{x},\theta)$ denotes a homogeneous lognormal random field with mean $\mu=1$ and standard deviation $\sigma=0.1$; $\chi(\theta)$ denotes the random gradient index of the FGM, which

is a lognormal random variable with mean $\mu = 10$ and variance $\sigma^2 = 0.1$. The Poisson's ratio is modelled as a homogeneous lognormal random field as follows,

$$\nu(\mathbf{x}, z, \theta) = H_\nu^L(\mathbf{x}, \theta)\nu(z, \theta) = H_\nu^L(\mathbf{x}, \theta)\left[\nu_m + (\nu_c - \nu_m)(\frac{1}{2} + \frac{z}{h})^{\chi(\theta)} \right] \quad (6.49)$$

where $H_\nu^L(\mathbf{x}, \theta)$ denotes a homogeneous lognormal random field with mean $\mu = 1$ and standard deviation $\sigma = 0.1$; $\chi(\theta)$ denotes the random gradient index of the FGM, which is a lognormal random variable with mean $\mu = 10$ and variance $\sigma^2 = 0.1$. The Bessel covariance function Eq.(5.9) with $l = 4m$ is adopted to consider the spatial dependency of the Young's modulus random field, while the exponential covariance function present in Eq.(5.9) with $l = 4m$ is adopted for the Poisson's ratio random field. E_m and E_c denote the Young's moduli of Al and ZrO_2-1, respectively. ν_m and ν_c denote the Poisson's ratios of Al and ZrO_2-1, respectively. The magnitudes of E_m, E_c, ν_m, and ν_c are select from Table 4.1.

Within the proposed SSIGA framework, the homogeneous lognormal random fields are decomposed by the K-L expansion with six terms. Then, the stochastic buckling load of the plate is estimated by the proposed X-SVR model. Once again, both Gegenbauer polynomial and Gaussian function kernels are implemented to establish the X-SVR model. For each kernel function, different training sample sizes (i.e., 20, 50, and 100) are adopted. Additionally, the MCS approach with 1 million simulation cycles is also implemented, and the results are regarded as the actual buckling loads.

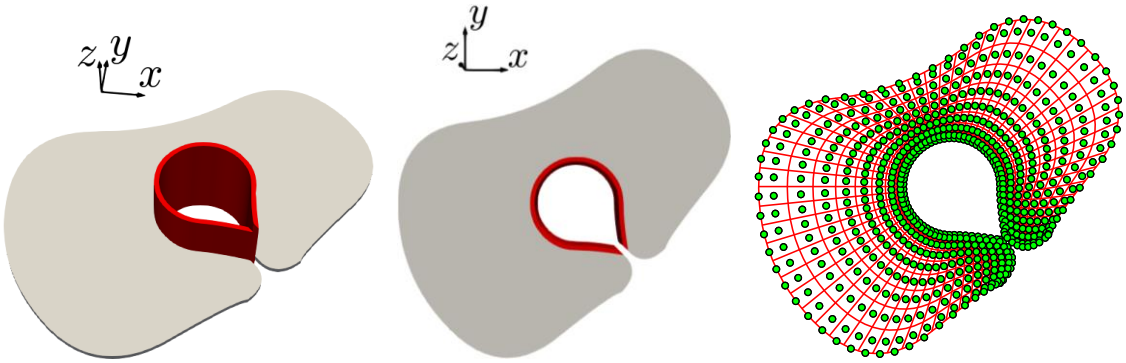

(a) (b) (c)

Figure 6.17 Irregular plate (a) 3D view; (b) top view; (c) IGA refinement

Three error-metrics, NMSE, NAAE, and NMAE, are also adopted to quantify the performance of the X-SVR model in this case. Figures 6.18 reports the NMSE, NAAE, and NMAE of the X-SVR model. Evidently, increasing the training sample size can improve the global and local accuracy of estimation. With respect to the three metrics, the best X-SVR model is obtained with the Gegenbauer polynomial kernel, while the worst one is obtained by using the Gaussian kernel function. Figures 6.19 shows the estimated buckling loads by the X-SVR with different kernels against the actual ones. Also, in each figure, the three metrics and a reference line $\hat{P}_{cr} = P_{cr}$ are provided. It is evidently illustrated that the more training samples are adopted, the better estimation can be anticipated.

Furthermore, the mean and the standard deviation of the buckling load obtained by different kernel functions with training sample size 100 are provided in Table 6.2. Based on the first two statistical moments, the X-SVRs with different kernel functions can accurately predict the mean of the buckling load, with maximum relative error of 0.28%. However, only the X-SVR with Gegenbauer polynomials kernel is able to provide an accurate estimation on the standard deviation.

Table 6.2 The mean and standard deviation of the buckling load obtained by different kernel functions with training sample size 100 (MN/m)

Statistical Moment	MCS	Gegenbauer	Gaussian
Mean	16.0684	16.0232	16.0676
Std	1.4897	1.4980	1.2570

Additionally, the estimated PDF and CDF of the buckling load based on the X-SVRs and the MCS approach are reported in Figures 6.20-6.21. Apparently, the proposed X-SVR with Gegenbauer polynomial kernel is able to estimate the PDF and CDF of the buckling load with 100 training samples. Similarly, the Gaussian function kernel clearly shows convergent behaviour as the training sample size increases, but the X-SVR based on this kernel is unable to estimate PDF and CDF very well. Finally, the buckling mode shapes corresponding to three specific events $\theta_4, \theta_5, \theta_6 \in \Omega$ are showed in Figures 6.22.

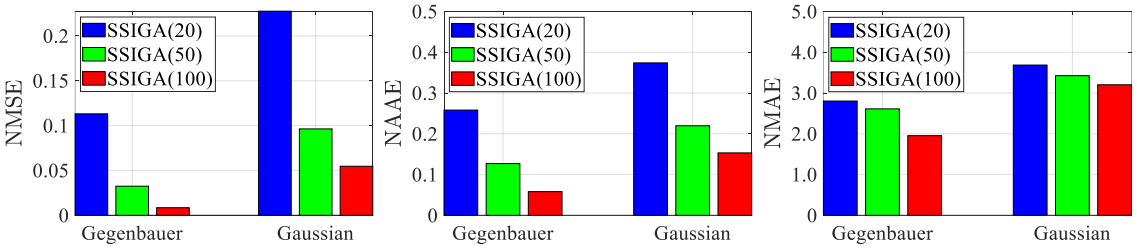

(a) (b) (c)

Figure 6.18 (a) NMSE, (b) NAAE, and (c) NMAE of the X-SVR model

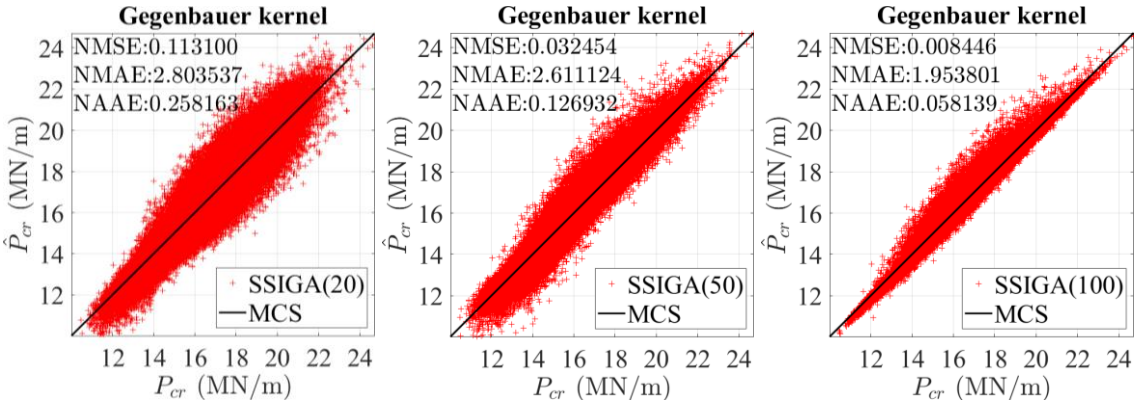

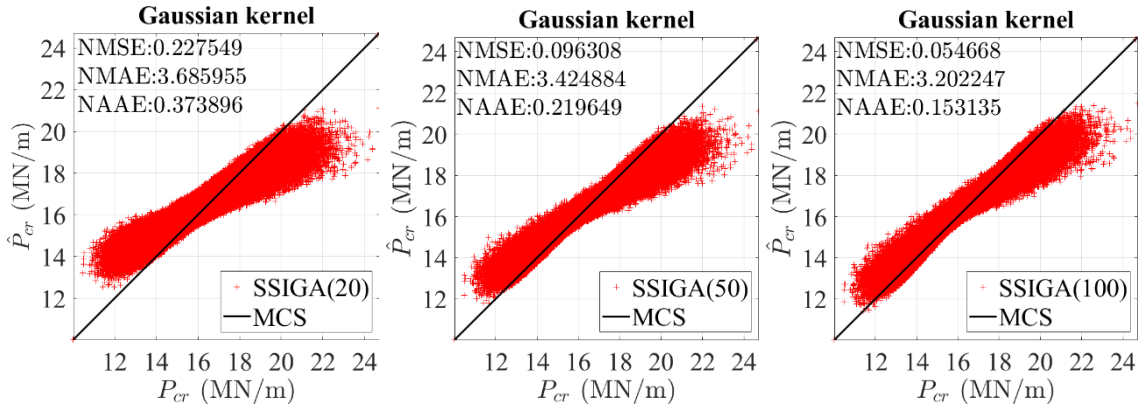

Figure 6.19 The estimated buckling loads by the X-SVR with different kernels and sample sizes against the actual ones by the MCS

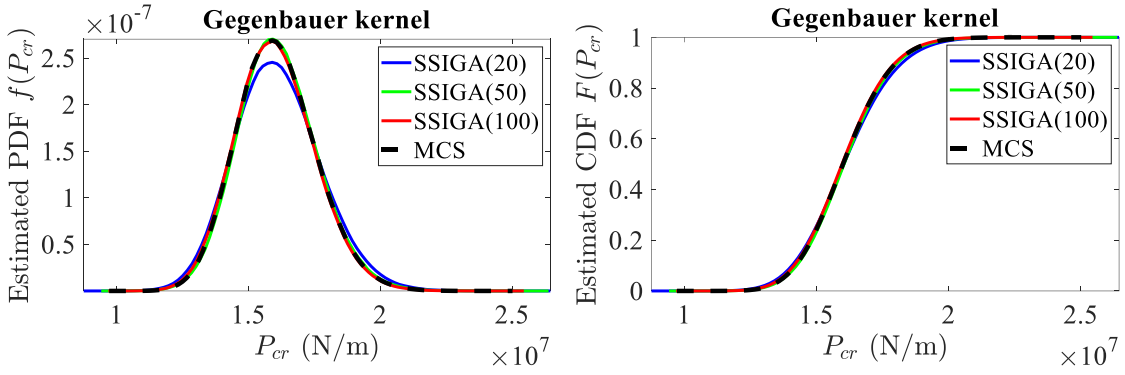

(a) (b)

Figure 6.20 The estimated (a) PDF and (b) CDF of the buckling load by Gegenbauer polynomial based X-SVR

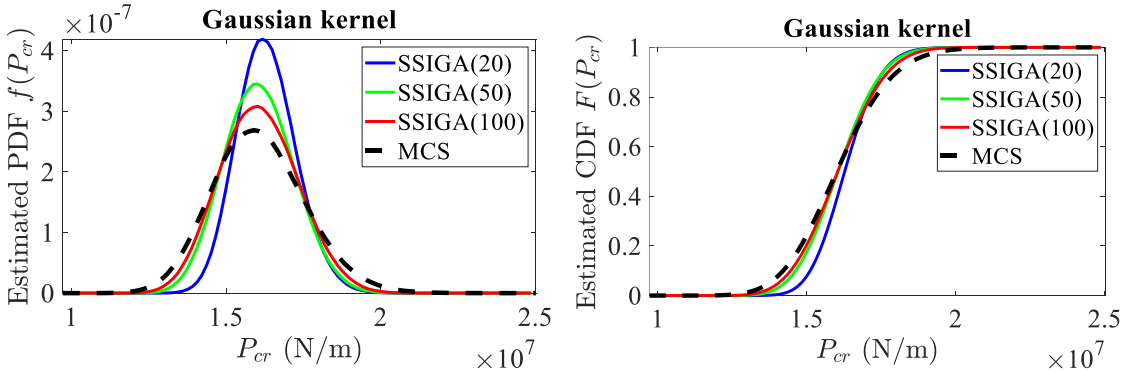

(a) (b)

Figure 6.21 The estimated (a) PDF and (b) CDF of the buckling load by Gaussian function based X-SVR

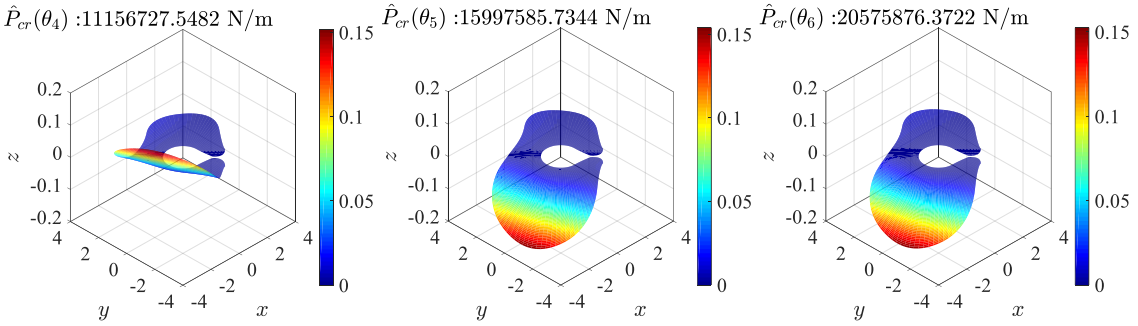

(a) (b) (c)

Figure 6.22 The buckling load and buckling mode shape of FGM plate at specific event (a) θ_4; (b) θ_5; (c) θ_6.

For this numerical example, the results obtained by the MCS approach were also run on a cluster node with 2×14 cores Intel Xeon E5-2690v4 (Broadwell) 2.6 GHz), while the results obtained by the proposed SSIGA approach were run on the same workstation as the first numerical example. The MCS approach with 1 million simulation cycles were executed concurrently with 28 works on the cluster node and costed 140h 7m 10s. Also, without parallel computation, the proposed X-SVR within the SSIGA scheme only consumed 3m 23s with training sample size 100. Subsequently, by using the constructed X-SVR model, the predictions of the same 1 million random samples with 4 cores on the workstation only took 10m 23s. Therefore, based on the technical information, the proposed method certainly shows superior computational efficiency over the exhaustively simulative MCS approach for the stochastic linear stability analysis with the consideration of both spatially dependent and independent uncertainties.

6.6 Conclusion

In this paper, a stochastic analysis framework, namely the spectral stochastic isogeometric analysis (SSIGA), is freshly developed for the stochastic linear stability analysis of plate through the first-order shear deformation theory. The SSIGA framework is applicable to different material models including homogeneous material, functionally graded material, functionally graded porous material, etc. The uncertain Young's modulus and Poisson's ratio are modelled as spatially dependent random fields with both Gaussian and lognormal distributions. The gradient index of the FGM is modelled as a spatially independent random variable. A generalized isogeometric basis functions based K-L expansion is adopted for the random field discretization. After successful discretisation the random fields, the X-SVR with a new Gegenbaur polynomial kernel is developed to establish the relationship between the uncertain system inputs and the stochastic buckling load. Finally, through the nonparametric statistical methods, the statistical moment up to second order, the PDF, and the CDF of the stochastic buckling load can be established. The major advantage of the proposed SSIGA approach is that an X-SVR can be effectively and efficiently established through a meticulously proposed experiments design algorithm without large simulation cycles and complicated formulations.

In order to verify the accuracy, efficiency, and the applicability of the proposed approach, two numerical examples with irregular geometries are thoroughly investigated. By closely examining the results against the MCS approach with large simulation cycles, all the computational results of the SSIGA approach are satisfactory but with much higher computational efficiency. Therefore, the proposed SSIGA provides a quantitative

assessment framework for stochastic linear stability analysis on plate with complex geometry and physically inherent uncertainties.

Appendix 6A: The linear stability analysis of plate based on FSDT

With the consideration of the geometric nonlinearity, the virtual work of the plate can be formulated as

$$\delta\Pi(\mathbf{u},\delta\mathbf{u}) = a(\mathbf{u},\delta\mathbf{u}) - \ell(\delta\mathbf{u}) = \int_D \delta\boldsymbol{\varepsilon}^{\mathrm{T}}\hat{\boldsymbol{\sigma}}dD - \int_D \delta\mathbf{u}^{\mathrm{T}}\mathbf{P}dD = 0 \qquad (6A.1)$$

where $\delta\boldsymbol{\varepsilon}$, $\hat{\boldsymbol{\sigma}}$, $\delta\mathbf{u}$ and $\mathbf{P}$ are the variations of the strain, the stress resultants, the variation of the displacement, and the external force vectors, respectively.

The strain vector $\boldsymbol{\varepsilon}$ is defined as

$$\boldsymbol{\varepsilon} = \begin{bmatrix} \varepsilon_x \\ \varepsilon_y \\ \gamma_{xy} \\ \gamma_{xz} \\ \gamma_{yz} \end{bmatrix} = \begin{bmatrix} \boldsymbol{\varepsilon}_i \\ \mathbf{0}_{2\times 1} \end{bmatrix} + \begin{bmatrix} z\boldsymbol{\varepsilon}_b \\ \boldsymbol{\varepsilon}_s \end{bmatrix} = \begin{bmatrix} \boldsymbol{\varepsilon}_i^L \\ \mathbf{0}_{2\times 1} \end{bmatrix} + \begin{bmatrix} \boldsymbol{\varepsilon}_i^{NL} \\ \mathbf{0}_{2\times 1} \end{bmatrix} + \begin{bmatrix} z\boldsymbol{\varepsilon}_b \\ \boldsymbol{\varepsilon}_s \end{bmatrix} \qquad (6A.2)$$

where $\mathbf{0}_{m\times n}$ is a zero matrix with dimension $m\times n$; $\boldsymbol{\varepsilon}_i^L$ and $\boldsymbol{\varepsilon}_i^{NL}$ are the linear and nonlinear parts of the in-plane strains $\boldsymbol{\varepsilon}_i$, respectively; $\boldsymbol{\varepsilon}_b$ and $\boldsymbol{\varepsilon}_s$ denotes the bending and shear strains, respectively.

Within the FSDT, the stress resultant vector $\hat{\boldsymbol{\sigma}}$ of the plate is defined as

$$\hat{\boldsymbol{\sigma}} = \begin{bmatrix} \hat{\boldsymbol{\sigma}}_i \\ \hat{\boldsymbol{\sigma}}_b \\ \hat{\boldsymbol{\sigma}}_s \end{bmatrix} = \begin{bmatrix} [N_x, N_y, N_{xy}]^{\mathrm{T}} \\ [M_x, M_y, M_{xy}]^{\mathrm{T}} \\ [Q_x, Q_y]^{\mathrm{T}} \end{bmatrix} = \begin{bmatrix} \left[\int_{-h/2}^{h/2} (\boldsymbol{\sigma}_x, \boldsymbol{\sigma}_y, \boldsymbol{\sigma}_{xy}) dz \right]^{\mathrm{T}} \\ \left[\int_{-h/2}^{h/2} (\boldsymbol{\sigma}_x, \boldsymbol{\sigma}_y, \boldsymbol{\sigma}_{xy}) z dz \right]^{\mathrm{T}} \\ \left[\int_{-h/2}^{h/2} (\boldsymbol{\tau}_{xz}, \boldsymbol{\tau}_{yz}) dz \right]^{\mathrm{T}} \end{bmatrix} \tag{6A.3}$$

where $\hat{\boldsymbol{\sigma}}_i$, $\hat{\boldsymbol{\sigma}}_b$, and $\hat{\boldsymbol{\sigma}}_s$ denote the in-plane stress resultants, the bending stress resultants, and the shear stress resultants, respectively.

Furthermore, the in-plane and bending stress resultants are represented by the in-plane and bending strains as follows,

$$\begin{bmatrix} \hat{\boldsymbol{\sigma}}_i \\ \hat{\boldsymbol{\sigma}}_b \end{bmatrix} = \begin{bmatrix} \mathbf{A} & \bar{\mathbf{B}} \\ \bar{\mathbf{B}} & \mathbf{D}_b \end{bmatrix} \begin{bmatrix} \boldsymbol{\varepsilon}_i \\ \boldsymbol{\varepsilon}_b \end{bmatrix} = \begin{bmatrix} \int_{-h/2}^{h/2} \begin{bmatrix} 1 & z \\ z & z^2 \end{bmatrix} \mathbf{Q}(z) dz \end{bmatrix} \begin{bmatrix} \boldsymbol{\varepsilon}_i \\ \boldsymbol{\varepsilon}_b \end{bmatrix} \tag{6A.4a}$$

$$\mathbf{Q}(z) = \frac{E(z)}{1-\nu^2(z)} \begin{bmatrix} 1 & \nu(z) & 0 \\ \nu(z) & 1 & 0 \\ 0 & 0 & [1-\nu(z)]/2 \end{bmatrix} \tag{6A.4b}$$

and the shear stress resultants are represented by the shear strain as follows,

$$\hat{\boldsymbol{\sigma}}_s = \mathbf{D}_s \boldsymbol{\varepsilon}_s = \left[\int_{-h/2}^{h/2} \mathbf{G}(z) dz \right] \boldsymbol{\varepsilon}_s \tag{6A.5a}$$

$$\mathbf{G}(z) = \frac{kE(z)}{2[1+\nu(z)]} \begin{bmatrix} 1 & 0 \\ 0 & 1 \end{bmatrix} \tag{6A.5b}$$

where $k = 5/6$ denotes the shear correction factor. $E(z)$ and $\nu(z)$ are the same as Chapter 4.

Subsequently, a residual $R(\mathbf{u}, \delta\mathbf{u})$ can be defined as the virtual work by

$$
\begin{aligned}
R(\mathbf{u},\delta\mathbf{u}) &= \int_D \begin{bmatrix} \delta\boldsymbol{\varepsilon}_i \\ \delta\boldsymbol{\varepsilon}_b \end{bmatrix}^{\mathrm{T}} \begin{bmatrix} \hat{\boldsymbol{\sigma}}_i \\ \hat{\boldsymbol{\sigma}}_b \end{bmatrix} dD + \int_D \delta\boldsymbol{\varepsilon}_s{}^{\mathrm{T}} \hat{\boldsymbol{\sigma}}_s dD - \int_D \delta\mathbf{u}^{\mathrm{T}} \mathbf{P} dD \\
&= \int_D \begin{bmatrix} \delta\boldsymbol{\varepsilon}_i^L \\ \delta\boldsymbol{\varepsilon}_b \end{bmatrix}^{\mathrm{T}} \begin{bmatrix} \mathbf{A} & \bar{\mathbf{B}} \\ \bar{\mathbf{B}} & \mathbf{D}_b \end{bmatrix} \begin{bmatrix} \boldsymbol{\varepsilon}_i^L \\ \boldsymbol{\varepsilon}_b \end{bmatrix} dD + \int_D \left(\delta\boldsymbol{\varepsilon}_i^L\right)^{\mathrm{T}} \mathbf{A}\delta\boldsymbol{\varepsilon}_i^{NL} dD \\
&+ \int_D \left(\delta\boldsymbol{\varepsilon}_i^{NL}\right)^{\mathrm{T}} \mathbf{A}\delta\boldsymbol{\varepsilon}_i^L dD + \int_D \left(\delta\boldsymbol{\varepsilon}_i^{NL}\right)^{\mathrm{T}} \mathbf{A}\delta\boldsymbol{\varepsilon}_i^{NL} dD \\
&+ \int_D \delta\boldsymbol{\varepsilon}_s{}^{\mathrm{T}} \mathbf{D}_s \boldsymbol{\varepsilon}_s dD - \int_D \delta\mathbf{u}^{\mathrm{T}} \mathbf{P} dD
\end{aligned}
\tag{6A.6}
$$

and, the linearization of the residual $R(\mathbf{u},\delta\mathbf{u})$ at $\mathbf{u}$ in the direction of $\Delta\mathbf{u}$ is represented as

$$
\begin{aligned}
L[R(\mathbf{u},\delta\mathbf{u})] = a^*(\mathbf{u},\delta\mathbf{u},\Delta\mathbf{u}) &= \int_D \begin{bmatrix} \delta\boldsymbol{\varepsilon}_i \\ \delta\boldsymbol{\varepsilon}_b \end{bmatrix}^{\mathrm{T}} \begin{bmatrix} \Delta\hat{\boldsymbol{\sigma}}_i \\ \Delta\hat{\boldsymbol{\sigma}}_b \end{bmatrix} dD + \int_D \delta\boldsymbol{\varepsilon}_s{}^{\mathrm{T}} \Delta\hat{\boldsymbol{\sigma}}_s dD \\
&+ \int_D \begin{bmatrix} \Delta\delta\boldsymbol{\varepsilon}_i \\ \Delta\delta\boldsymbol{\varepsilon}_b \end{bmatrix}^{\mathrm{T}} \begin{bmatrix} \hat{\boldsymbol{\sigma}}_i \\ \hat{\boldsymbol{\sigma}}_b \end{bmatrix} dD + \int_D \Delta\delta\boldsymbol{\varepsilon}_s{}^{\mathrm{T}} \hat{\boldsymbol{\sigma}}_s dD
\end{aligned}
\tag{6A.7}
$$

where $\Delta\hat{\boldsymbol{\sigma}}_i$, $\Delta\hat{\boldsymbol{\sigma}}_b$, and $\Delta\hat{\boldsymbol{\sigma}}_s$ are the linearization of the in-plane stress resultants, the bending stress resultants, and the shear stress resultants, respectively;

The stability analysis of plate aims to predict the maximum loading capacity of the structure against buckling failure, and such capacity is known as the critical buckling load. The structural tangent stiffness matrix becomes singular when the plate becomes unstable. For the ease of formulation derivation, Eq.(6A.7) can be divided into three parts:

$$
\begin{cases}
A(\mathbf{u},\delta\mathbf{u},\Delta\mathbf{u}) = \int_D \begin{bmatrix} \delta\boldsymbol{\varepsilon}_i^L \\ \delta\boldsymbol{\varepsilon}_b \end{bmatrix}^{\mathrm{T}} \begin{bmatrix} \mathbf{A} & \bar{\mathbf{B}} \\ \bar{\mathbf{B}} & \mathbf{D}_b \end{bmatrix} \begin{bmatrix} \Delta\boldsymbol{\varepsilon}_i^L \\ \Delta\boldsymbol{\varepsilon}_i^L \end{bmatrix} dD + \int_D \delta\boldsymbol{\varepsilon}_s{}^{\mathrm{T}} \mathbf{D}_s \Delta\boldsymbol{\varepsilon}_s dD \\
G_1(\mathbf{u},\delta\mathbf{u},\Delta\mathbf{u}) = \int_D (\delta\boldsymbol{\varepsilon}_i^L)^{\mathrm{T}} \mathbf{A}\Delta\boldsymbol{\varepsilon}_i^{NL} dD + \int_D (\delta\boldsymbol{\varepsilon}_i^{NL})^{\mathrm{T}} \mathbf{A}\Delta\boldsymbol{\varepsilon}_i^L dD + \int_D \left(\Delta\delta\boldsymbol{\varepsilon}_i^{NL}\right)^{\mathrm{T}} \hat{\boldsymbol{\sigma}}_i dD \\
G_2(\mathbf{u},\delta\mathbf{u},\Delta\mathbf{u}) = \int_D (\delta\boldsymbol{\varepsilon}_i^{NL})^{\mathrm{T}} \mathbf{A}\Delta\boldsymbol{\varepsilon}_i^{NL} dD
\end{cases}
\tag{6A.8}
$$

For a given critical displacement ${}^{cr}\mathbf{u}$ at the critical limit point $t_n = t_{cr}$, the governing equation of the stability analysis of the plate can be defined as,

$$a^*({}^{cr}\mathbf{u},\delta\mathbf{y},\mathbf{y}) = A({}^{cr}\mathbf{u},\delta\mathbf{y},\mathbf{y}) + G_1({}^{cr}\mathbf{u},\delta\mathbf{y},\mathbf{y}) + G_2({}^{cr}\mathbf{u},\delta\mathbf{y},\mathbf{y}) = 0 \quad (6A.9)$$

where the eigen-function $\mathbf{y}$ and its variation $\delta\mathbf{y}$ are implemented to replace the incremental displacement $\Delta\mathbf{u}$ and the variation of the displacement $\delta\mathbf{u}$.

The linear stability analysis of plate assumes that the plate becomes unstable at small elastic deformation state. Therefore, the pre-buckling equilibrium state can be obtained by linear elasticity analysis. That is, based on the load step t_n with a unit external load ${}^{n}P$,

$${}^{cr}\mathbf{u} = {}^{n}\zeta\,{}^{n}\mathbf{u},\ {}^{cr}\hat{\boldsymbol{\sigma}} = {}^{n}\zeta\,{}^{n}\hat{\boldsymbol{\sigma}},\ {}^{n}\mathbf{u} = \mathbf{K}^{-1}\mathbf{F} \quad (6A.10)$$

where $\mathbf{K}$ denotes the linear stiffness matrix; $\mathbf{F}$ denotes the force vector. ${}^{n}\mathbf{u}$ and ${}^{n}\hat{\boldsymbol{\sigma}}$ denote the displacement field and the stress resultants at load step t_n, respectively; they are obtained by linear elasticity analysis as Eq.(6A.10). ${}^{n}\zeta$ denotes the critical load factor.

Appendix 6B: Proof of Proposition 1

Proof. For quadratic programming expressed in Eq. (6.24), the proof of convexity is equivalent to proving that $\mathbf{Q} \succeq 0$. Moreover, considering that $\hat{\mathbf{C}}$ is a positive and diagonal matrix by definition, then $\hat{\mathbf{C}} \succ 0$, and also $\hat{\mathbf{C}}^{-1} \succ 0$. Let $\mathbf{v} \in \Re^{2m+2n}$ be a non-zero column vector, then:

$$\begin{aligned}\mathbf{v}^T\mathbf{Q}\mathbf{v} &= \mathbf{v}^T\left[(\hat{\mathbf{A}} + \mathbf{I}_{(2m+2n)\times(2m+2n)})\hat{\mathbf{C}}^{-1}(\hat{\mathbf{A}} + \mathbf{I}_{(2m+2n)\times(2m+2n)})^T + \hat{\mathbf{G}}\hat{\mathbf{e}}\hat{\mathbf{e}}^T\hat{\mathbf{G}}\right]\mathbf{v} \\ &= \left[(\hat{\mathbf{A}} + \mathbf{I}_{(2m+2n)\times(2m+2n)})^T\mathbf{v}\right]\hat{\mathbf{C}}^{-1}\left[(\hat{\mathbf{A}} + \mathbf{I}_{(2m+2n)\times(2m+2n)})^T\mathbf{v}\right] + (\hat{\mathbf{e}}^T\hat{\mathbf{G}}\mathbf{v})^2 \\ &\geq 0\end{aligned} \quad (6B.1)$$

Thus, $\mathbf{Q} \succeq 0$ is a Positive-definite matrix. Therefore, Eq.(6.24) is a convex optimization.

This concludes the proof. □

Appendix 6C: Proof of Proposition 2

Proof. The proposed GGK can be alternatively formulated as the product of two kernel functions $K_1(\mathbf{x}_i, \mathbf{x}_j) = \exp(-\sigma \left\| \mathbf{x}_i - \mathbf{x}_j \right\|_2^2)$ and $K_2(\mathbf{x}_i, \mathbf{x}_j) = \sum_{l=0}^{d} P_l^{\alpha}(\mathbf{x}_i)^T P_l^{\alpha}(\mathbf{x}_j)$ such that:

$$K_{GGK}(\mathbf{x}_i, \mathbf{x}_j) = K_1(\mathbf{x}_i, \mathbf{x}_j) K_2(\mathbf{x}_i, \mathbf{x}_j) \tag{6C.1}$$

According to (Vapnik, 1998, 2013), the multiplication of two valid Mercer kernels is also a valid kernel function. Since that $K_1(\mathbf{x}_i, \mathbf{x}_j)$ is the Gaussian kernel ($\sigma > 0$) which satisfies the Mercer Theorem, $K_{GGK}(\mathbf{x}_i, \mathbf{x}_j)$ can be proved as a valid kernel by verifying that $K_2(\mathbf{x}_i, \mathbf{x}_j)$ satisfies the Mercer Theorem.

Given an arbitrary squared integrable function $g(\mathbf{x})$ defined as $g: \Re^n \to \Re$ and assuming each element in $\mathbf{x}_i$ and $\mathbf{x}_j$ are independent with each other, then

$$\begin{aligned}
&\iint K_2(\mathbf{x}_i, \mathbf{x}_j) g(\mathbf{x}_i) g(\mathbf{x}_j) d\mathbf{x}_i d\mathbf{x}_j \\
&= \iint \sum_{l=0}^{d} P_l^{\alpha}(\mathbf{x}_i)^T P_l^{\alpha}(\mathbf{x}_j) g(\mathbf{x}_i) g(\mathbf{x}_j) d\mathbf{x}_i d\mathbf{x}_j \\
&= \sum_{l=0}^{d} \iint P_l^{\alpha}(\mathbf{x}_i)^T P_l^{\alpha}(\mathbf{x}_j) g(\mathbf{x}_i) g(\mathbf{x}_j) d\mathbf{x}_i d\mathbf{x}_j \\
&= \sum_{l=0}^{d} \left[\int P_l^{\alpha}(\mathbf{x}_i)^T g(\mathbf{x}_i) d\mathbf{x}_i \int P_l^{\alpha}(\mathbf{x}_j) g(\mathbf{x}_j) d\mathbf{x}_j \right] \\
&= \sum_{l=0}^{d} \left\{ \left[\int P_l^{\alpha}(\mathbf{x}_i)^T g(\mathbf{x}_i) d\mathbf{x}_i \right] \left[\int P_l^{\alpha}(\mathbf{x}_i) g(\mathbf{x}_i) d\mathbf{x}_i \right] \right\} \geq 0
\end{aligned} \tag{6C.2}$$

Thus, $K_2(\mathbf{x}_i, \mathbf{x}_j)$ is a valid Mercer kernel. Therefore, the proposed GGK $K_{GGK}(\mathbf{x}_i, \mathbf{x}_j)$ is an admissible Mercer kernel function.

This concludes the proof. □

Chapter 7

CONCLUSION AND FUTURE STUDIES

7.1 Conclusion

This thesis proposed and developed a CAD-CAE integrated stochastic analysis framework, namely, the spectral stochastic isogeometric analysis (SSIGA) framework, for modern engineering applications. By meticulously integrating uncertain quantification within the CAD system, a geometric consistency between intentionally designed model and stochastic analysis model can be achieved within the SSIGA framework. Consequently, the stochastic analysis within SSIGA framework is assuredly implemented on the intentionally designed model. Such rigor also provides advantages in computational efficiency by eliminating the communication process between the CAD and CAE environments, which inevitably exists in traditional stochastic analysis models. Moreover, the inherent higher order characteristics of basis functions within CAD system enables the SSIGA framework properly handle the higher accuracy requirements of contemporary engineering applications in modelling and analysis. Furthermore, the proposed approach is developed for several stochastic structural analysis problems involved with complex geometries. The accuracy, efficiency, and applicability of the proposed approach for each problem are comprehensively investigated thorough meticulously designed numerical examples.

In Chapter 3, the SSIGA framework is firstly proposed and developed by investigating the stochastic linear elasticity problem. The basis functions within CAD system are employed to represent the random fields, which can maintain the exact geometries of the structures and random fields between the CAD model and SSIGA stochastic analysis model. Unlike the traditional stochastic analysis methods, the random fields within SSIGA is certainly implemented on the same designed model. Moreover, the CAD basis function based Karhunen-Loève expansion approach is firstly proposed to spectrally decompose the input random fields. The influences of h- and k-refinement of CAD basis functions on K-L expansion is thoroughly investigated, and advantages in accuracy and efficiency are evidently illustrated. Subsequently, by employing the polynomial chaos expansion, the statistical characteristics of any concerned structural responses can be adequately estimated. Additionally, by adopting the non-parametric statistical inference techniques (e.g., the kernel density estimation approach), the PDFs and CDFs of any concerned structural responses can be robustly established. Consequently, the proposed SSIGA approach provides an integrated, yet physically valid, stochastic analysis framework for engineering structures that are suffering from both inevitable spatially dependent uncertainties and complex geometries. By comprehensively investigating three distinctive numerical examples, the applicability, accuracy and computational efficiency of the SSIGA approach are evidently illustrated.

Then, in Chapter 4, the novel SSIGA framework is further developed for the stochastic static analysis of FGM plate through first-order shear deformation theory. The uncertain Young's modulus is modelled as a random field. The CAD basis functions based K-L expansion is presented to effectively handle random fields of composite plates defined within complex geometry. Then, the means and standard deviations of structural displacement, strain, and stress of the FGM plate can be explicitly estimated through the

PCE. In addition to the estimation of the first two moments of statistics of the structural responses, the PDFs and CDFs of the concerned structural responses can also be established through the statistical inference techniques. Consequently, the serviceability and strength limits of the FGM plate can be effectively determined through the proposed SSIGA approach. The major advantage of the SSIGA analysis framework is that the proposed method is able to maintain the exact geometry of the structure as well as the random field defined on the structure between the design model and the stochastic analysis model. Consequently, the quality of the uncertainty analysis (i.e., the quality of the PDFs and CDFs) can be improved. The accuracy and efficiency of the proposed methodology are evidently demonstrated through two distinctive FGM plates with nonstandard geometries.

In Chapter 5, the SSIGA framework is proposed for the stochastic free vibration analysis of engineering structures. Both the Young's modulus and material density are considered and modelled as Gaussian or non-Gaussian (i.e., lognormal) random fields to incorporate the spatial variation effects of the uncertain material properties. Moreover, the arbitrary polynomial chaos (aPC) expansion is firstly incorporated into SSIGA framework to provide a more flexible and practical tool for structures confronting various complications. Then, a stochastic Galerkin-based computational approach is proposed to formulate the stochastic generalized eigenvalue problem into a system of nonlinear equations. After successfully solving the nonlinear system by classical Newton-Raphson method, the coefficients of the aPC for eigensolutions are efficiently obtained. Finally, statistical moments with different orders can be easily calculated. In addition, PDFs and CDFs of the eigenvalues can also be established through statistical inference techniques. In this chapter, two elaborately designed numerical examples, one Mindlin plate and another Kirchhoff-Love shell, are comprehensively investigated. Since the closed-form

solutions for the stochastic eigenvalue problems are not unavailable, the Monte Carlo Simulation (MCS) method is adopted to partially verify all the computational results.

In Chapter 6, the SSIGA framework is further developed for the stochastic linear stability analysis of plates through the first-order shear deformation theory. Different material models, including homogeneous model, functionally graded material, functionally graded porous material, etc., are incorporated into the SSIGA framework. Both Young's modulus and Poisson's ratio are considered and modelled as spatially dependent random fields with both Gaussian or lognormal distributions. Meanwhile, the gradient index is modelled as a spatially independent random variable. The CAD basis functions based K-L expansion is adopted for the random field discretization. Then, the X-SVR with a new Gegenbaur polynomial kernel is adopted to estimate the stochastic buckling load based on those uncertain parameters. Finally, through the nonparametric statistical methods, the second order statistical moments, the PDF, and the CDF of the stochastic buckling load are obtained. The main advantage of the proposed SSIGA approach is that an X-SVR can be easily and efficiently established through a meticulously proposed experiments design algorithm without large simulation cycles and complicated formulation. By closely examining the results against the MCS approach with large simulation cycles, all the computational results of the SSIGA approach are satisfactory but with much higher computational efficiency.

By the end of this study, the SSIGA framework is proposed and developed for three stochastic structural analysis problems, namely, the stochastic linear elasticity analysis problem, the stochastic free vibration analysis problem, and stochastic linear stability analysis problem. All the proposed approaches within SSIGA in this thesis possess well-preserved accuracy, high computational efficacy, and most importantly, strong applicability to modern engineering applications.

7.2 Future Studies

There are some potential extensions, developments and investigations which can be further conducted to enrich the capability of the SSIGA framework on stochastic analysis of modern engineering applications.

Possible future studies are including:

1. Extension of the SSIGA framework to linear stability of composite shell structures involving different uncertain material properties.
2. Development of new geometry modelling method for more complex geometries to enhance the capability of the SSIGA framework.
3. Development of new random field modelling methods for general and arbitrary non-Gaussian distribution.
4. Development of the SSIGA framework for structural dynamic analysis of continuous structures involving different uncertain material properties (i.e., Young's modulus, Poisson's ratio, and density)
5. Development of the SSIGA framework for stochastic material nonlinear analysis of continuous structures.
6. Development of the SSIGA framework for the uncertain analysis of 3D continuous solid structures.
7. Development of the SSIGA framework for contact problem involving different uncertain material properties.
8. Development of the SSIGA framework for the stochastic acoustic analysis.

REFERENCES

Adam, C., Bouabdallah, S., et al. (2015) ‘Improved numerical integration for locking treatment in isogeometric structural elements. Part II: Plates and shells’, Computer Methods in Applied Mechanics and Engineering, 284, pp. 106–137.

Adam, C., Hughes, T. J. R., et al. (2015) ‘Selective and reduced numerical integrations for NURBS-based isogeometric analysis’, Computer Methods in Applied Mechanics and Engineering, 284, pp. 732–761.

Adhikari, S. (2011) ‘Doubly Spectral Stochastic Finite-Element Method for Linear Structural Dynamics’, Journal of Aerospace Engineering, 24(3), pp. 264–276.

Akkerman, I. et al. (2007) ‘The role of continuity in residual-based variational multiscale modeling of turbulence’, Computational Mechanics, 41(3), pp. 371–378.

Anders, M. and Hori, M. (2001) ‘Three-dimensional stochastic finite element method for elasto-plastic bodies’, International Journal for Numerical Methods in Engineering, 51(4), pp. 449–478.

Apostolatos, A. et al. (2014) ‘A Nitsche-type formulation and comparison of the most common domain decomposition methods in isogeometric analysis’, International Journal for Numerical Methods in Engineering, 97(7), pp. 473–504.

Argyris, J., Papadrakakis, M. and Stefanou, G. (2002) ‘Stochastic finite element analysis of shells’, Computer Methods in Applied Mechanics and Engineering. North-Holland, 191(41–42), pp. 4781–4804.

Auricchio, F. et al. (2012) ‘A simple algorithm for obtaining nearly optimal quadrature

rules for NURBS-based isogeometric analysis', Computer Methods in Applied Mechanics and Engineering, 249–252, pp. 15–27.

Balobanov, V. et al. (2019) 'Kirchhoff–Love shells within strain gradient elasticity: Weak and strong formulations and an H3-conforming isogeometric implementation', Computer Methods in Applied Mechanics and Engineering. North-Holland, 344, pp. 837–857.

Bartezzaghi, A., Dedè, L. and Quarteroni, A. (2015) 'Isogeometric Analysis of high order Partial Differential Equations on surfaces', Computer Methods in Applied Mechanics and Engineering, 295, pp. 446–469.

Bazilevs, Y., Michler, C., et al. (2007) 'Weak Dirichlet boundary conditions for wall-bounded turbulent flows', Computer Methods in Applied Mechanics and Engineering, 196(49–52), pp. 4853–4862.

Bazilevs, Y., Calo, V. M., et al. (2007) 'YZβ discontinuity capturing for advection-dominated processes with application to arterial drug delivery', International Journal for Numerical Methods in Fluids, 54(6–8), pp. 593–608.

Bazilevs, Y. et al. (2009) 'Patient-specific isogeometric fluid–structure interaction analysis of thoracic aortic blood flow due to implantation of the Jarvik 2000 left ventricular assist device', Computer Methods in Applied Mechanics and Engineering, 198(45–46), pp. 3534–3550.

Bazilevs, Y., Calo, V. M., et al. (2010) 'Isogeometric analysis using T-splines', Computer Methods in Applied Mechanics and Engineering, 199(5–8), pp. 229–263.

Bazilevs, Y., Michler, C., et al. (2010) 'Isogeometric variational multiscale modeling of wall-bounded turbulent flows with weakly enforced boundary conditions on

unstretched meshes', Computer Methods in Applied Mechanics and Engineering, 199(13–16), pp. 780–790.

Bazilevs, Y. et al. (2013) 'Isogeometric analysis of Lagrangian hydrodynamics', Journal of Computational Physics, 243, pp. 224–243.

Bazilevs, Y. et al. (2014) 'Isogeometric analysis of Lagrangian hydrodynamics: Axisymmetric formulation in the rz-cylindrical coordinates', Journal of Computational Physics, 262, pp. 244–261.

BAZILEVS, Y. et al. (2006) 'ISOGEOMETRIC ANALYSIS: APPROXIMATION, STABILITY AND ERROR ESTIMATES FOR h-REFINED MESHES', Mathematical Models and Methods in Applied Sciences, 16(07), pp. 1031–1090.

Bazilevs, Y. and Akkerman, I. (2010) 'Large eddy simulation of turbulent Taylor–Couette flow using isogeometric analysis and the residual-based variational multiscale method', Journal of Computational Physics, 229(9), pp. 3402–3414.

Bazilevs, Y. and Hughes, T. J. R. (2007) 'Weak imposition of Dirichlet boundary conditions in fluid mechanics', Computers & Fluids, 36(1), pp. 12–26.

Beer, G., Marussig, B. and Zechner, J. (2015) 'A simple approach to the numerical simulation with trimmed CAD surfaces', Computer Methods in Applied Mechanics and Engineering, 285, pp. 776–790.

Beirão da Veiga, L. et al. (2011) 'Some estimates for h–p–k-refinement in Isogeometric Analysis', Numerische Mathematik, 118(2), pp. 271–305.

Beirão da Veiga, L. et al. (2012) 'An isogeometric method for the Reissner–Mindlin plate bending problem', Computer Methods in Applied Mechanics and Engineering.

North-Holland, 209–212, pp. 45–53.

Beirão Da Veiga, L. et al. (2015) ‘A locking-free model for Reissner–Mindlin plates: Analysis and isogeometric implementation via NURBS and triangular NURPS’, Mathematical Models and Methods in Applied Sciences. World Scientific Publishing Company, 25(08), pp. 1519–1551.

Beirão da Veiga, L., Cho, D. and Sangalli, G. (2012) ‘Anisotropic NURBS approximation in isogeometric analysis’, Computer Methods in Applied Mechanics and Engineering, 209–212, pp. 1–11.

Ben-Haim, Y. (1996) Robust Reliability in the Mechanical Sciences, Robust Reliability in the Mechanical Sciences. Berlin, Heidelberg: Springer Berlin Heidelberg.

Ben-Haim, Y. (2006) Information-Gap Decision Theory: Decisions Under Severe Uncertainty Academic Press, London.

Ben-Haim, Y. and Ben-Haim, Y. (2016) ‘Info-Gap Theory’, in Info-Gap Economics. London: Palgrave Macmillan UK, pp. 3–13.

Benson, D. J. et al. (2010) ‘A generalized finite element formulation for arbitrary basis functions: From isogeometric analysis to XFEM’, International Journal for Numerical Methods in Engineering.

Benson, D.J. et al. (2010) ‘Isogeometric shell analysis: The Reissner–Mindlin shell’, Computer Methods in Applied Mechanics and Engineering. North-Holland, 199(5–8), pp. 276–289.

Benson, D. J. et al. (2013) ‘Blended isogeometric shells’, Computer Methods in Applied Mechanics and Engineering. North-Holland, 255, pp. 133–146.

Berdinsky, D. et al. (2015) ‘Bases of T-meshes and the refinement of hierarchical B-splines’, Computer Methods in Applied Mechanics and Engineering, 283, pp. 841–855.

Bielewicz, E. and Górski, J. (2002) ‘Shells with random geometric imperfections simulation — based approach’, International Journal of Non-Linear Mechanics. Pergamon, 37(4–5), pp. 777–784.

Borden, M. J. et al. (2011) ‘Isogeometric finite element data structures based on Bézier extraction of NURBS’, International Journal for Numerical Methods in Engineering, 87(1–5), pp. 15–47.

Bornemann, P. B. and Cirak, F. (2013) ‘A subdivision-based implementation of the hierarchical b-spline finite element method’, Computer Methods in Applied Mechanics and Engineering, 253, pp. 584–598.

Breitenberger, M. et al. (2015) ‘Analysis in computer aided design: Nonlinear isogeometric B-Rep analysis of shell structures’, Computer Methods in Applied Mechanics and Engineering. North-Holland, 284, pp. 401–457.

Buchegger, F., Jüttler, B. and Mantzaflaris, A. (2016) ‘Adaptively refined multi-patch B-splines with enhanced smoothness’, Applied Mathematics and Computation, 272, pp. 159–172.

Buffa, A., Sangalli, G. and Vázquez, R. (2010) ‘Isogeometric analysis in electromagnetics: B-splines approximation’, Computer Methods in Applied Mechanics and Engineering, 199(17–20), pp. 1143–1152.

Buffa, A., Sangalli, G. and Vázquez, R. (2014) ‘Isogeometric methods for computational electromagnetics: B-spline and T-spline discretizations’, Journal of Computational

Physics, 257, pp. 1291–1320.

Cacciola, P. and Deodatis, G. (2011) ‘A method for generating fully non-stationary and spectrum-compatible ground motion vector processes’, Soil Dynamics and Earthquake Engineering. Elsevier, 31(3), pp. 351–360.

Campbell, C. and Ying, Y. (2011) ‘Learning with Support Vector Machines’, Synthesis Lectures on Artificial Intelligence and Machine Learning.

Casanova, C. F. and Gallego, A. (2013) ‘NURBS-based analysis of higher-order composite shells’, Composite Structures. Elsevier, 104, pp. 125–133.

Casquero, H. et al. (2017) ‘Arbitrary-degree T-splines for isogeometric analysis of fully nonlinear Kirchhoff–Love shells’, Computer-Aided Design. Elsevier, 82, pp. 140–153.

Cavdar, O. et al. (2008) ‘Perturbation Based Stochastic Finite Element Analysis of the Structural Systems with Composite Sections under Earthquake Forces’, Steel and Composite Structures. Techno-Press, 8(2), pp. 129–144.

Chen, J., Kong, F. and Peng, Y. (2017) ‘A stochastic harmonic function representation for non-stationary stochastic processes’, Mechanical Systems and Signal Processing. Academic Press, 96, pp. 31–44.

Chen, L. et al. (2014) ‘Explicit finite deformation analysis of isogeometric membranes’, Computer Methods in Applied Mechanics and Engineering. North-Holland, 277, pp. 104–130.

Chen, N.-Z. and Guedes Soares, C. (2008) ‘Spectral stochastic finite element analysis for laminated composite plates’, Computer Methods in Applied Mechanics and

Engineering. North-Holland, 197(51–52), pp. 4830–4839.

Chung, D. B. et al. (2005) ‘Efficient numerical strategies for spectral stochastic finite element models’, International Journal for Numerical Methods in Engineering, 64(10), pp. 1334–1349.

Coox, L. et al. (2016) ‘A performance study of NURBS-based isogeometric analysis for interior two-dimensional time-harmonic acoustics’, Computer Methods in Applied Mechanics and Engineering, 305, pp. 441–467.

Costantini, P. et al. (2010) ‘Quasi-interpolation in isogeometric analysis based on generalized B-splines’, Computer Aided Geometric Design, 27(8), pp. 656–668.

Cottrell, J. A. et al. (2006) ‘Isogeometric analysis of structural vibrations’, Computer Methods in Applied Mechanics and Engineering, 195(41–43), pp. 5257–5296.

Cottrell, J. A., Hughes, T. J. R. and Bazilevs, Y. (2009) Isogeometric Analysis: Toward Integration of CAD and FEA, Isogeometric Analysis: Toward Integration of CAD and FEA. Chichester, UK: John Wiley & Sons, Ltd.

Cottrell, J. A., Hughes, T. J. R. and Reali, A. (2007) ‘Studies of refinement and continuity in isogeometric structural analysis’, Computer Methods in Applied Mechanics and Engineering, 196(41–44), pp. 4160–4183.

Dai, H., Zhang, B. and Wang, W. (2015) ‘A multiwavelet support vector regression method for efficient reliability assessment’, Reliability Engineering and System Safety.

Dai, H., Zheng, Z. and Ma, H. (2019) ‘An explicit method for simulating non-Gaussian and non-stationary stochastic processes by Karhunen-Loève and polynomial chaos

expansion', Mechanical Systems and Signal Processing. Academic Press, 115, pp. 1–13.

Dalcin, L. et al. (2016) 'PetIGA: A framework for high-performance isogeometric analysis', Computer Methods in Applied Mechanics and Engineering, 308, pp. 151–181.

Dedè, L. and Santos, H. A. F. A. (2012) 'B-spline goal-oriented error estimators for geometrically nonlinear rods', Computational Mechanics, 49(1), pp. 35–52.

Deodatis, G. (1996a) 'Non-stationary stochastic vector processes: seismic ground motion applications', Probabilistic Engineering Mechanics, 11(3), pp. 149–167.

Deodatis, G. (1996b) 'Simulation of Ergodic Multivariate Stochastic Processes', Journal of Engineering Mechanics, 122(8), pp. 778–787.

Deodatis, G. and Micaletti, R. C. (2001) 'Simulation of Highly Skewed Non-Gaussian Stochastic Processes', Journal of Engineering Mechanics, 127(12), pp. 1284–1295.

Dimitri, R. et al. (2014) 'Isogeometric large deformation frictionless contact using T-splines', Computer Methods in Applied Mechanics and Engineering, 269, pp. 394–414.

Ding, C. et al. (2018) 'Modeling and simulation of steady heat transfer analysis with material uncertainty: Generalized n th order perturbation isogeometric stochastic method', Numerical Heat Transfer, Part A: Applications. Taylor & Francis, 74(9), pp. 1565–1582.

Ding, C. et al. (2019) 'Isogeometric generalized n th order perturbation-based stochastic method for exact geometric modeling of (composite) structures: Static and dynamic

analysis with random material parameters', Computer Methods in Applied Mechanics and Engineering. North-Holland, 346, pp. 1002–1024.

Do, D. M. et al. (2016) 'Interval spectral stochastic finite element analysis of structures with aggregation of random field and bounded parameters', International Journal for Numerical Methods in Engineering, 108(10), pp. 1198–1229.

Do, D. M. et al. (2017) 'The stochastic Galerkin scaled boundary finite element method on random domain', International Journal for Numerical Methods in Engineering. Elsevier, 110(3), pp. 248–278.

Do, D. M., Gao, W. and Song, C. (2016) 'Stochastic finite element analysis of structures in the presence of multiple imprecise random field parameters', Computer Methods in Applied Mechanics and Engineering, 300, pp. 657–688.

Doostan, A., Ghanem, R. G. and Red-Horse, J. (2007) 'Stochastic model reduction for chaos representations', Computer Methods in Applied Mechanics and Engineering, 196(37–40), pp. 3951–3966.

Dornisch, W. and Klinkel, S. (2014) 'Treatment of Reissner–Mindlin shells with kinks without the need for drilling rotation stabilization in an isogeometric framework', Computer Methods in Applied Mechanics and Engineering. North-Holland, 276, pp. 35–66.

Dornisch, W., Klinkel, S. and Simeon, B. (2013) 'Isogeometric Reissner–Mindlin shell analysis with exactly calculated director vectors', Computer Methods in Applied Mechanics and Engineering. North-Holland, 253, pp. 491–504.

Dornisch, W., Klinkel, S. and Simeon, Bernd (2013) 'Isogeometric Reissner–Mindlin shell analysis with exactly calculated director vectors', Computer Methods in

Applied Mechanics and Engineering, 253, pp. 491–504.

Dornisch, W., Vitucci, G. and Klinkel, S. (2015) ‘The weak substitution method - an application of the mortar method for patch coupling in NURBS-based isogeometric analysis’, International Journal for Numerical Methods in Engineering, 103(3), pp. 205–234.

Drucker, H. et al. (1997) ‘Support vector regression machines’, in Advances in Neural Information Processing Systems 9: Proceedings of the 1996 Conference.

Du, X., Sudjianto, A. and Huang, B. (2005) ‘Reliability-Based Design With the Mixture of Random and Interval Variables’, Journal of Mechanical Design. American Society of Mechanical Engineers, 127(6), p. 1068.

Du, X., Zhao, G. and Wang, W. (2015) ‘Nitsche method for isogeometric analysis of Reissner–Mindlin plate with non-conforming multi-patches’, Computer Aided Geometric Design, 35–36, pp. 121–136.

Dunbar, M. et al. (2010) ‘Simultaneous classification and feature selection via convex quadratic programming with application to HIV-associated neurocognitive disorder assessment’, European Journal of Operational Research.

Eiermann, M., Ernst, O. G. and Ullmann, E. (2007) ‘Computational aspects of the stochastic finite element method’, Computing and Visualization in Science. Springer-Verlag, 10(1), pp. 3–15.

Elishakoff, I. (1997) ‘Comment on “Fuzzy finite element approach for the analysis of imprecisely defined systems”’, AIAA Journal, 35, pp. 403–403.

Elishakoff, I. and Ren, Y. (1999) ‘The bird’s eye view on finite element method for

structures with large stochastic variations', Computer Methods in Applied Mechanics and Engineering. North-Holland, 168(1–4), pp. 51–61.

Embar, A., Dolbow, J. and Harari, I. (2010) 'Imposing Dirichlet boundary conditions with Nitsche's method and spline-based finite elements', International Journal for Numerical Methods in Engineering, p. n/a-n/a.

Evans, E. J. et al. (2015) 'Hierarchical T-splines: Analysis-suitability, Bézier extraction, and application as an adaptive basis for isogeometric analysis', Computer Methods in Applied Mechanics and Engineering, 284, pp. 1–20.

Evans, J. A. et al. (2009) 'n-Widths, sup–infs, and optimality ratios for the k-version of the isogeometric finite element method', Computer Methods in Applied Mechanics and Engineering, 198(21–26), pp. 1726–1741.

Evans, J. A. and Hughes, Thomas J. R. (2013) 'Explicit trace inequalities for isogeometric analysis and parametric hexahedral finite elements', Numerische Mathematik, 123(2), pp. 259–290.

Evans, J. A. and Hughes, Thomas J.R. (2013) 'Isogeometric divergence-conforming B-splines for the unsteady Navier–Stokes equations', Journal of Computational Physics, 241, pp. 141–167.

de Falco, C., Reali, A. and Vázquez, R. (2011) 'GeoPDEs: A research tool for Isogeometric Analysis of PDEs', Advances in Engineering Software, 42(12), pp. 1020–1034.

Falsone, G. and Ferro, G. (2007) 'An exact solution for the static and dynamic analysis of FE discretized uncertain structures', Computer Methods in Applied Mechanics and Engineering. North-Holland, 196(21–24), pp. 2390–2400.

Fan, Q. et al. (2017) ‘MREKLM: A fast multiple empirical kernel learning machine’, Pattern Recognition.

Feng, Y. et al. (2016) ‘Kernelized Elastic Net Regularization: Generalization Bounds, and Sparse Recovery’, Neural Computation, 28(3), pp. 525–562.

Foo, J., Yosibash, Z. and Karniadakis, G. E. (2007) ‘Stochastic simulation of riser-sections with uncertain measured pressure loads and/or uncertain material properties’, Computer Methods in Applied Mechanics and Engineering. North-Holland, 196(41–44), pp. 4250–4271.

Gao, J., Kwan, P. W. and Shi, D. (2010) ‘Sparse kernel learning with LASSO and Bayesian inference algorithm’, Neural Networks, 23(2), pp. 257–264.

Gao, W. (2007) ‘Random seismic response analysis of truss structures with uncertain parameters’, Engineering Structures. Elsevier, 29(7), pp. 1487–1498.

Gao, W. et al. (2011) ‘Hybrid probabilistic interval analysis of bar structures with uncertainty using a mixed perturbation Monte-Carlo method’, Finite Elements in Analysis and Design. Elsevier, 47(7), pp. 643–652.

Gao, W. and Kessissoglou, N. J. (2007) ‘Dynamic response analysis of stochastic truss structures under non-stationary random excitation using the random factor method’, Computer Methods in Applied Mechanics and Engineering. North-Holland, 196(25–28), pp. 2765–2773.

Gao, W., Song, C. and Tin-Loi, F. (2010) ‘Probabilistic interval analysis for structures with uncertainty’, Structural Safety. Elsevier, 32(3), pp. 191–199.

Gautschi, W. (2008) Orthogonal Polynomials Computation and Approximation,

Orthogonal Polynomials Computation and Approximation.

Ge, J. et al. (2016) ‘Blending isogeometric and Lagrangian elements in three-dimensional analysis’, Finite Elements in Analysis and Design, 112, pp. 50–63.

Ghaffari Motlagh, Y. et al. (2013) ‘Simulation of laminar and turbulent concentric pipe flows with the isogeometric variational multiscale method’, Computers & Fluids, 71, pp. 146–155.

Ghanem, Roger (1999) ‘Ingredients for a general purpose stochastic finite elements implementation’, Computer Methods in Applied Mechanics and Engineering. North-Holland, 168(1–4), pp. 19–34.

Ghanem, R. (1999a) ‘The Nonlinear Gaussian Spectrum of Log-Normal Stochastic Processes and Variables’, Journal of Applied Mechanics. American Society of Mechanical Engineers, 66(4), p. 964.

Ghanem, R. (1999b) ‘The Nonlinear Gaussian Spectrum of Log-Normal Stochastic Processes and Variables’, Journal of Applied Mechanics, 66(4), p. 964.

Ghanem, R. G. and Kruger, R. M. (1996a) ‘Numerical solution of spectral stochastic finite element systems’, Computer Methods in Applied Mechanics and Engineering. North-Holland, 129(3), pp. 289–303.

Ghanem, R. G. and Kruger, R. M. (1996b) ‘Numerical solution of spectral stochastic finite element systems’, Computer Methods in Applied Mechanics and Engineering, 129(3), pp. 289–303.

Ghanem, R. G. and Spanos, P. D. (1991) Stochastic Finite Elements: A Spectral Approach, Stochastic Finite Elements: A Spectral Approach. New York, NY: Springer New

York.

Ghanem, R. and Spanos, P. D. (1990) ‘Polynomial Chaos in Stochastic Finite Elements’, Journal of Applied Mechanics, 57(1), p. 197.

Ghosh, D. and Farhat, C. (2008) ‘Strain and stress computations in stochastic finite element methods’, International Journal for Numerical Methods in Engineering, 74(8), pp. 1219–1239.

Giannelli, C. et al. (2016) ‘THB-splines: An effective mathematical technology for adaptive refinement in geometric design and isogeometric analysis’, Computer Methods in Applied Mechanics and Engineering, 299, pp. 337–365.

Giannelli, C., Jüttler, B. and Speleers, H. (2012) ‘THB-splines: The truncated basis for hierarchical splines’, Computer Aided Geometric Design, 29(7), pp. 485–498.

Giovanis, D. G., Papadopoulos, V. and Stavroulakis, G. (2015) ‘An adaptive spectral Galerkin stochastic finite element method using variability response functions’, International Journal for Numerical Methods in Engineering.

Goyal, A. and Simeon, B. (2017) ‘On penalty-free formulations for multipatch isogeometric Kirchhoff–Love shells’, Mathematics and Computers in Simulation. North-Holland, 136, pp. 78–103.

Graham-Brady, L. and Xu, X. F. (2008) ‘Stochastic Morphological Modeling of Random Multiphase Materials’, Journal of Applied Mechanics, 75(6), p. 061001.

Greco, L. and Cuomo, M. (2014) ‘An implicit multi patch B-spline interpolation for Kirchhoff–Love space rod’, Computer Methods in Applied Mechanics and Engineering, 269, pp. 173–197.

Grigoriu, M. (1984) ‘Crossings of Non-Gaussian Translation Processes’, Journal of Engineering Mechanics, 110(4), pp. 610–620.

Grigoriu, M. (1995) Applied Non-Gaussian Processes: Examples, Theory, Simulation, Linear Random Vibration, And Matlab Solutions, PTR Prentice Hall. PTR Prentice Hall.

Grigoriu, M. (1998) ‘Simulation of Stationary Non-Gaussian Translation Processes’, Journal of Engineering Mechanics, 124(2), pp. 121–126.

Grigoriu, M. (2006) ‘Evaluation of Karhunen–Loève, Spectral, and Sampling Representations for Stochastic Processes’, Journal of Engineering Mechanics, 132(2), pp. 179–189.

Guo, J. and Du, X. (2009) ‘Reliability sensitivity analysis with random and interval variables’, International Journal for Numerical Methods in Engineering. John Wiley & Sons, Ltd, 78(13), pp. 1585–1617.

Guo, Y. and Ruess, M. (2015) ‘Nitsche’s method for a coupling of isogeometric thin shells and blended shell structures’, Computer Methods in Applied Mechanics and Engineering. North-Holland, 284, pp. 881–905.

Gurley, K. R., Kareem, A. and Tognarelli, M. A. (1996) ‘Simulation of a class of non-normal random processes’, International Journal of Non-Linear Mechanics. Pergamon, 31(5), pp. 601–617.

Gurley, K. R., Tognarelli, M. A. and Kareem, A. (1997) ‘Analysis and simulation tools for wind engineering’, Probabilistic Engineering Mechanics. Elsevier, 12(1), pp. 9–31.

Haldar, A. and Reddy, R. K. (1992) ‘A random-fuzzy analysis of existing structures’, Fuzzy Sets and Systems. North-Holland, 48(2), pp. 201–210.

Hassani, B., Ganjali, A. and Tavakkoli, M. (2012) ‘An isogeometrical approach to error estimation and stress recovery’, European Journal of Mechanics - A/Solids, 31(1), pp. 101–109.

Hennig, P., Müller, S. and Kästner, M. (2016) ‘Bézier extraction and adaptive refinement of truncated hierarchical NURBS’, Computer Methods in Applied Mechanics and Engineering, 305, pp. 316–339.

Hesch, C. and Betsch, P. (2012) ‘Isogeometric analysis and domain decomposition methods’, Computer Methods in Applied Mechanics and Engineering, 213–216, pp. 104–112.

Hien, T. D. and Noh, H.-C. (2017) ‘Stochastic isogeometric analysis of free vibration of functionally graded plates considering material randomness’, Computer Methods in Applied Mechanics and Engineering. North-Holland, 318, pp. 845–863.

Hillman, M., Chen, J. S. and Bazilevs, Y. (2015) ‘Variationally consistent domain integration for isogeometric analysis’, Computer Methods in Applied Mechanics and Engineering, 284, pp. 521–540.

Hsu, C. W. and Lin, C. J. (2002) ‘A comparison of methods for multiclass support vector machines’, IEEE Transactions on Neural Networks.

Hsu, M.-C. et al. (2015) ‘An interactive geometry modeling and parametric design platform for isogeometric analysis’, Computers & Mathematics with Applications, 70(7), pp. 1481–1500.

Huang, J., Nguyen-Thanh, N. and Zhou, K. (2017) ‘Extended isogeometric analysis based on Bézier extraction for the buckling analysis of Mindlin–Reissner plates’, Acta Mechanica. Springer Vienna, 228(9), pp. 3077–3093.

Huang, S. P., Quek, S. T. and Phoon, K. K. (2001a) ‘Convergence study of the truncated Karhunen–Loeve expansion for simulation of stochastic processes’, International Journal for Numerical Methods in Engineering. John Wiley & Sons, Ltd, 52(9), pp. 1029–1043.

Huang, S. P., Quek, S. T. and Phoon, K. K. (2001b) ‘Convergence study of the truncated Karhunen–Loeve expansion for simulation of stochastic processes’, International Journal for Numerical Methods in Engineering, 52(9), pp. 1029–1043.

Hughes, T. J. R. (2012) The finite element method: linear static and dynamic finite element analysis. Courier Corporation.

Hughes, T. J. R., Cottrell, J. A. and Bazilevs, Y. (2005) ‘Isogeometric analysis: CAD, finite elements, NURBS, exact geometry and mesh refinement’, Computer Methods in Applied Mechanics and Engineering, 194(39–41), pp. 4135–4195.

Hughes, T. J. R., Evans, J. A. and Reali, A. (2014) ‘Finite element and NURBS approximations of eigenvalue, boundary-value, and initial-value problems’, Computer Methods in Applied Mechanics and Engineering, 272, pp. 290–320.

Hughes, T. J. R., Reali, A. and Sangalli, G. (2008) ‘Duality and unified analysis of discrete approximations in structural dynamics and wave propagation: Comparison of p-method finite elements with k-method NURBS’, Computer Methods in Applied Mechanics and Engineering, 197(49–50), pp. 4104–4124.

Hurtado, J. E. and Alvarez, D. A. (2012) ‘The encounter of interval and probabilistic

approaches to structural reliability at the design point', Computer Methods in Applied Mechanics and Engineering. North-Holland, 225–228, pp. 74–94.

Irzal, F. et al. (2014) 'An isogeometric analysis Bézier interface element for mechanical and poromechanical fracture problems', International Journal for Numerical Methods in Engineering, 97(8), pp. 608–628.

Jari, H., Atri, H. R. and Shojaee, S. (2015) 'Nonlinear thermal analysis of functionally graded material plates using a NURBS based isogeometric approach', Composite Structures. Elsevier, 119, pp. 333–345.

Jiang, C., Long, X. Y., et al. (2013) 'Probability-interval hybrid reliability analysis for cracked structures existing epistemic uncertainty', Engineering Fracture Mechanics. Pergamon, 112–113, pp. 148–164.

Jiang, C., Bi, R. G., et al. (2013) 'Structural reliability analysis using non-probabilistic convex model', Computer Methods in Applied Mechanics and Engineering. North-Holland, 254, pp. 83–98.

Jiang, W. and Dolbow, J. E. (2015) 'Adaptive refinement of hierarchical B-spline finite elements with an efficient data transfer algorithm', International Journal for Numerical Methods in Engineering, 102(3–4), pp. 233–256.

Johannessen, K. A., Kvamsdal, T. and Dokken, T. (2014) 'Isogeometric analysis using LR B-splines', Computer Methods in Applied Mechanics and Engineering, 269, pp. 471–514.

Johannessen, K. A., Remonato, F. and Kvamsdal, T. (2015) 'On the similarities and differences between Classical Hierarchical, Truncated Hierarchical and LR B-splines', Computer Methods in Applied Mechanics and Engineering, 291, pp. 64–

101.

Kang, P. and Youn, S.-K. (2015) ‘Isogeometric analysis of topologically complex shell structures’, Finite Elements in Analysis and Design. Elsevier, 99, pp. 68–81.

Kang, Z. and Luo, Y. (2009) ‘Non-probabilistic reliability-based topology optimization of geometrically nonlinear structures using convex models’, Computer Methods in Applied Mechanics and Engineering. North-Holland, 198(41–44), pp. 3228–3238.

Kang, Z., Luo, Y. and Li, A. (2011) ‘On non-probabilistic reliability-based design optimization of structures with uncertain-but-bounded parameters’, Structural Safety. Elsevier, 33(3), pp. 196–205.

Kapl, M. et al. (2015) ‘Isogeometric analysis with geometrically continuous functions on two-patch geometries’, Computers & Mathematics with Applications. Pergamon, 70(7), pp. 1518–1538.

Kapoor, H. and Kapania, R. K. (2012) ‘Geometrically nonlinear NURBS isogeometric finite element analysis of laminated composite plates’, Composite Structures. Elsevier, 94(12), pp. 3434–3447.

Kapoor, H., Kapania, R. K. and Soni, S. R. (2013) ‘Interlaminar stress calculation in composite and sandwich plates in NURBS Isogeometric finite element analysis’, Composite Structures. Elsevier, 106, pp. 537–548.

Kardara, A., Bucher, C. G. and Shinozuka, M. (1989) ‘Structural Response Variability III’, Journal of Engineering Mechanics, 115(8), pp. 1726–1747.

Katafygiotis, L. S., Zerva, A. and Malyarenko, A. A. (1999) ‘Simulation of Homogeneous and Partially Isotropic Random Fields’, Journal of Engineering Mechanics, 125(10),

pp. 1180–1189.

Kiendl, J. et al. (2009) ‘Isogeometric shell analysis with Kirchhoff–Love elements’, Computer Methods in Applied Mechanics and Engineering, 198(49–52), pp. 3902–3914.

Kiendl, J. et al. (2010) ‘The bending strip method for isogeometric analysis of Kirchhoff–Love shell structures comprised of multiple patches’, Computer Methods in Applied Mechanics and Engineering. North-Holland, 199(37–40), pp. 2403–2416.

Kiendl, J. et al. (2015) ‘Isogeometric Kirchhoff–Love shell formulations for general hyperelastic materials’, Computer Methods in Applied Mechanics and Engineering. North-Holland, 291, pp. 280–303.

Kiendl, J., Marino, E. and De Lorenzis, L. (2017) ‘Isogeometric collocation for the Reissner–Mindlin shell problem’, Computer Methods in Applied Mechanics and Engineering. North-Holland, 325, pp. 645–665.

Kim, H.-J., Seo, Y.-D. and Youn, S.-K. (2009) ‘Isogeometric analysis for trimmed CAD surfaces’, Computer Methods in Applied Mechanics and Engineering, 198(37–40), pp. 2982–2995.

Kim, H.-J., Seo, Y.-D. and Youn, S.-K. (2010) ‘Isogeometric analysis with trimming technique for problems of arbitrary complex topology’, Computer Methods in Applied Mechanics and Engineering, 199(45–48), pp. 2796–2812.

Kleiber., M. and Hien, T. D. (1994) ‘The stochastic finite element method (basic perturbation technique and computer implementation)’, Applied Stochastic Models and Data Analysis, 10(4), pp. 297–297.

Kleiss, S. K. et al. (2012) ‘IETI – Isogeometric Tearing and Interconnecting’, Computer Methods in Applied Mechanics and Engineering, 247–248, pp. 201–215.

Kleiss, S. K. and Tomar, S. K. (2015) ‘Guaranteed and sharp a posteriori error estimates in isogeometric analysis’, Computers & Mathematics with Applications, 70(3), pp. 167–190.

Kumar, M., Kvamsdal, T. and Johannessen, K. A. (2017) ‘Superconvergent patch recovery and a posteriori error estimation technique in adaptive isogeometric analysis’, Computer Methods in Applied Mechanics and Engineering, 316, pp. 1086–1156.

Kung, S. Y. (2014) Kernel methods and machine learning, Kernel Methods and Machine Learning.

Le-Manh, T. and Lee, J. (2014) ‘Postbuckling of laminated composite plates using NURBS-based isogeometric analysis’, Composite Structures. Elsevier, 109, pp. 286–293.

Li, C. and Der Kiureghian, A. (1993) ‘Optimal Discretization of Random Fields’, Journal of Engineering Mechanics, 119(6), pp. 1136–1154.

Li, K., Wu, D., et al. (2018) ‘Isogeometric Analysis of functionally graded porous plates reinforced by graphene platelets’, Composite Structures. Elsevier, 204, pp. 114–130.

Li, K., Gao, W., et al. (2018) ‘Spectral stochastic isogeometric analysis of linear elasticity’, Computer Methods in Applied Mechanics and Engineering, 332, pp. 157–190.

Li, L. B., Phoon, K. K. and Quek, S. T. (2007) ‘Comparison between Karhunen–Loève expansion and translation-based simulation of non-Gaussian processes’, Computers & Structures. Pergamon, 85(5–6), pp. 264–276.

Li, Y. and Kareem, A. (1991) ‘Simulation of Multivariate Nonstationary Random Processes by FFT’, Journal of Engineering Mechanics, 117(5), pp. 1037–1058.

Liu, L. et al. (2014) ‘Volumetric T-spline construction using Boolean operations’, Engineering with Computers, 30(4), pp. 425–439.

Liu, W. K., Belytschko, T. and Mani, A. (1986) ‘Probabilistic finite elements for nonlinear structural dynamics’, Computer Methods in Applied Mechanics and Engineering. North-Holland, 56(1), pp. 61–81.

Liu, Z., Liu, W. and Peng, Y. (2016) ‘Random function based spectral representation of stationary and non-stationary stochastic processes’, Probabilistic Engineering Mechanics. Elsevier, 45, pp. 115–126.

Liu, Zhangjun, Liu, Zenghui and Peng, Y. (2018) ‘Simulation of multivariate stationary stochastic processes using dimension-reduction representation methods’, Journal of Sound and Vibration. Academic Press, 418, pp. 144–162.

Liu, Zhangjun, Liu, Zixin and Peng, Y. (2017) ‘Dimension reduction of Karhunen-Loeve expansion for simulation of stochastic processes’, Journal of Sound and Vibration. Academic Press, 408, pp. 168–189.

Long, X. Y. et al. (2015) ‘Stochastic response analysis of the scaled boundary finite element method and application to probabilistic fracture mechanics’, Computers & Structures. Pergamon, 153, pp. 185–200.

De Lorenzis, L. et al. (2011) ‘A large deformation frictional contact formulation using NURBS-based isogeometric analysis’, International Journal for Numerical Methods in Engineering, p. n/a-n/a.

De Lorenzis, L., Wriggers, P. and Hughes, T. J. R. (2014) ‘Isogeometric contact: a review’, GAMM-Mitteilungen, 37(1), pp. 85–123.

De Lorenzis, L., Wriggers, P. and Zavarise, G. (2012) ‘A mortar formulation for 3D large deformation contact using NURBS-based isogeometric analysis and the augmented Lagrangian method’, Computational Mechanics, 49(1), pp. 1–20.

Lu, J., Yang, G. and Ge, J. (2013) ‘Blending NURBS and Lagrangian representations in isogeometric analysis’, Computer Methods in Applied Mechanics and Engineering, 257, pp. 117–125.

Lucor, D., Su, C.-H. and Karniadakis, G. E. (2004) ‘Generalized polynomial chaos and random oscillators’, International Journal for Numerical Methods in Engineering. John Wiley & Sons, Ltd, 60(3), pp. 571–596.

De Luycker, E. et al. (2011) ‘X-FEM in isogeometric analysis for linear fracture mechanics’, International Journal for Numerical Methods in Engineering, 87(6), pp. 541–565.

Mangasarian, O. L. and Musicant, D. R. (2000) ‘Lagrangian support vector machines’, The Journal of Machine Learning Research, 1.

Manni, C., Pelosi, F. and Lucia Sampoli, M. (2011) ‘Generalized B-splines as a tool in isogeometric analysis’, Computer Methods in Applied Mechanics and Engineering, 200(5–8), pp. 867–881.

Martin, T. and Cohen, E. (2010) ‘Volumetric parameterization of complex objects by respecting multiple materials’, Computers & Graphics, 34(3), pp. 187–197.

Martin, T., Cohen, E. and Kirby, R. M. (2009) ‘Volumetric parameterization and trivariate B-spline fitting using harmonic functions’, Computer Aided Geometric Design, 26(6), pp. 648–664.

Marussig, B. and Hughes, T. J. R. (2018) ‘A Review of Trimming in Isogeometric Analysis: Challenges, Data Exchange and Simulation Aspects’, Archives of Computational Methods in Engineering, 25(4), pp. 1059–1127.

Matthies, H. G. et al. (1997) ‘Uncertainties in probabilistic numerical analysis of structures and solids-Stochastic finite elements’, Structural Safety. Elsevier, 19(3), pp. 283–336.

Maurin, F. et al. (2018) ‘Isogeometric collocation for Kirchhoff–Love plates and shells’, Computer Methods in Applied Mechanics and Engineering. North-Holland, 329, pp. 396–420.

Michel, L. (1977) Probability Theory. Springer-Verlag. Springer.

Mirzaei, M. and Kiani, Y. (2017) ‘Isogeometric thermal buckling analysis of temperature dependent FG graphene reinforced laminated plates using NURBS formulation’, Composite Structures. Elsevier, 180, pp. 606–616.

Möller, B. et al. (2009) ‘Fuzzy random processes and their application to dynamic analysis of structures’, Mathematical and Computer Modelling of Dynamical Systems. Taylor & Francis, 15(6), pp. 515–534.

Nagy, A. P. and Benson, D. J. (2015) ‘On the numerical integration of trimmed

isogeometric elements', Computer Methods in Applied Mechanics and Engineering, 284, pp. 165–185.

Nair, P. B. and Keane, A. J. (2002) 'Stochastic reduced basis methods', AIAA Journal, 40(8), pp. 1653–1664.

Ngah, M. F. and Young, A. (2007) 'Application of the spectral stochastic finite element method for performance prediction of composite structures', Composite Structures, 78(3), pp. 447–456.

Nguyen-Thanh, N. et al. (2011) 'Rotation free isogeometric thin shell analysis using PHT-splines', Computer Methods in Applied Mechanics and Engineering. North-Holland, 200(47–48), pp. 3410–3424.

Nguyen-Thanh, N. et al. (2015) 'An extended isogeometric thin shell analysis based on Kirchhoff–Love theory', Computer Methods in Applied Mechanics and Engineering. North-Holland, 284, pp. 265–291.

Nguyen-Xuan, H. et al. (2014) 'Isogeometric analysis of functionally graded plates using a refined plate theory', Composites Part B: Engineering. Elsevier, 64, pp. 222–234.

Nguyen-Xuan, H., Thai, C. H. and Nguyen-Thoi, T. (2013) 'Isogeometric finite element analysis of composite sandwich plates using a higher order shear deformation theory', Composites Part B: Engineering. Elsevier, 55, pp. 558–574.

Nguyen, H. X. et al. (2017) 'Geometrically nonlinear isogeometric analysis of functionally graded microplates with the modified couple stress theory', Computers & Structures. Pergamon, 193, pp. 110–127.

Nguyen, L. B. et al. (2019) 'An isogeometric Bézier finite element analysis for

piezoelectric FG porous plates reinforced by graphene platelets', Composite Structures. Elsevier, 214, pp. 227–245.

Nguyen, N.-T. et al. (2015) 'An efficient computational approach for size-dependent analysis of functionally graded nanoplates', Computer Methods in Applied Mechanics and Engineering. North-Holland, 297, pp. 191–218.

Nguyen, V.-H. et al. (2014) 'A new inverse trigonometric shear deformation theory for isotropic and functionally graded sandwich plates', Composites Part B: Engineering. Elsevier, 66, pp. 233–246.

Nguyen, V. P. et al. (2014) 'Nitsche's method for two and three dimensional NURBS patch coupling', Computational Mechanics, 53(6), pp. 1163–1182.

Nguyen, V. P. et al. (2015) 'Isogeometric analysis: An overview and computer implementation aspects', Mathematics and Computers in Simulation, 117, pp. 89–116.

Oden, J. T. et al. (2003) 'Research directions in computational mechanics', Computer Methods in Applied Mechanics and Engineering. North-Holland, 192(7–8), pp. 913–922.

Ozer, S., Chen, C. H. and Cirpan, H. A. (2011) 'A set of new Chebyshev kernel functions for support vector machine pattern classification', Pattern Recognition, 44(7), pp. 1435–1447.

Di Paola, M. (1998) 'Digital simulation of wind field velocity', Journal of Wind Engineering and Industrial Aerodynamics. Elsevier, 74–76, pp. 91–109.

Di Paola, M. and Gullo, I. (2001) 'Digital generation of multivariate wind field processes',

Probabilistic Engineering Mechanics. Elsevier, 16(1), pp. 1–10.

Papadopoulos, V., Deodatis, G. and Papadrakakis, M. (2005) ‘Flexibility-based upper bounds on the response variability of simple beams’, Computer Methods in Applied Mechanics and Engineering. North-Holland, 194(12–16), pp. 1385–1404.

Papadopoulos, V. and Papadrakakis, M. (2005) ‘The effect of material and thickness variability on the buckling load of shells with random initial imperfections’, Computer Methods in Applied Mechanics and Engineering. North-Holland, 194(12–16), pp. 1405–1426.

Papadrakakis, M. and Papadopoulos, V. (1996) ‘Robust and efficient methods for stochastic finite element analysis using Monte Carlo simulation’, Computer Methods in Applied Mechanics and Engineering. North-Holland, 134(3–4), pp. 325–340.

Papadrakakis, M., Papadopoulos, V. and Lagaros, N. D. (1996) ‘Structural reliability analyis of elastic-plastic structures using neural networks and Monte Carlo simulation’, Computer Methods in Applied Mechanics and Engineering. North-Holland, 136(1–2), pp. 145–163.

Pauletti, M. S. et al. (2015) ‘Igatools: An Isogeometric Analysis Library’, SIAM Journal on Scientific Computing, 37(4), pp. C465–C496.

Pellissetti, M. . and Ghanem, R. . (2000) ‘Iterative solution of systems of linear equations arising in the context of stochastic finite elements’, Advances in Engineering Software. Elsevier, 31(8–9), pp. 607–616.

Peng, L. et al. (2017) ‘Simulation of Multivariate Nonstationary Random Processes: Hybrid Stochastic Wave and Proper Orthogonal Decomposition Approach’, Journal

of Engineering Mechanics, 143(9), p. 04017064.

Phoon, K.-K., Quek, S.-T. and Huang, H. (2004) ‘Simulation of non-Gaussian processes using fractile correlation’, Probabilistic Engineering Mechanics. Elsevier, 19(4), pp. 287–292.

Phoon, K. ., Huang, S. . and Quek, S. . (2002) ‘Implementation of Karhunen–Loeve expansion for simulation using a wavelet-Galerkin scheme’, Probabilistic Engineering Mechanics. Elsevier, 17(3), pp. 293–303.

Phoon, K. K., Huang, H. W. and Quek, S. T. (2005) ‘Simulation of strongly non-Gaussian processes using Karhunen–Loeve expansion’, Probabilistic Engineering Mechanics. Elsevier, 20(2), pp. 188–198.

Phoon, K. K., Huang, S. P. and Quek, S. T. (2002) ‘Simulation of second-order processes using Karhunen–Loeve expansion’, Computers & Structures. Pergamon, 80(12), pp. 1049–1060.

Phung-Van, P., De Lorenzis, L., et al. (2015) ‘Analysis of laminated composite plates integrated with piezoelectric sensors and actuators using higher-order shear deformation theory and isogeometric finite elements’, Computational Materials Science. Elsevier, 96, pp. 495–505.

Phung-Van, P., Abdel-Wahab, M., et al. (2015) ‘Isogeometric analysis of functionally graded carbon nanotube-reinforced composite plates using higher-order shear deformation theory’, Composite Structures. Elsevier, 123, pp. 137–149.

Piegl, L. and Tiller, W. (1997) ‘The NURBS book, 2nd edition’, Springer-Verleg.

Pigazzini, M. S. et al. (2019) ‘Gradient-enhanced damage modeling in Kirchhoff–Love

shells: Application to isogeometric analysis of composite laminates', Computer Methods in Applied Mechanics and Engineering. North-Holland, 346, pp. 152–179.

Puig, B., Poirion, F. and Soize, C. (2002) 'Non-Gaussian simulation using Hermite polynomial expansion: Convergences and algorithms', Probabilistic Engineering Mechanics. Elsevier, 17(3), pp. 253–264.

Rahman, S. (2018) 'A Galerkin isogeometric method for Karhunen–Loève approximation of random fields', Computer Methods in Applied Mechanics and Engineering, 338, pp. 533–561.

Ratnani, A. and Sonnendrücker, E. (2012) 'An Arbitrary High-Order Spline Finite Element Solver for the Time Domain Maxwell Equations', Journal of Scientific Computing, 51(1), pp. 87–106.

Rice, S. O. (1945) 'Mathematical Analysis of Random Noise', Bell System Technical Journal, 24(1), pp. 46–156.

Riffnaller-Schiefer, A., Augsdörfer, U. H. and Fellner, D. W. (2016) 'Isogeometric shell analysis with NURBS compatible subdivision surfaces', Applied Mathematics and Computation. Elsevier, 272, pp. 139–147.

Rogers, D. F. (2001) 'An introduction to NURBS: with historical perspective', in.

Ruess, M. et al. (2014) 'Weak coupling for isogeometric analysis of non-matching and trimmed multi-patch geometries', Computer Methods in Applied Mechanics and Engineering, 269, pp. 46–71.

Rypl, D. and Patzák, B. (2012) 'From the finite element analysis to the isogeometric analysis in an object oriented computing environment', Advances in Engineering

Software, 44(1), pp. 116–125.

Sachdeva, S. K., Nair, P. B. and Keane, A. J. (2006) ‘Comparative study of projection schemes for stochastic finite element analysis’, Computer Methods in Applied Mechanics and Engineering. North-Holland, 195(19–22), pp. 2371–2392.

Sakamoto, S. and Ghanem, R. (2002) ‘Polynomial Chaos Decomposition for the Simulation of Non-Gaussian Nonstationary Stochastic Processes’, Journal of Engineering Mechanics, 128(2), pp. 190–201.

San Kim, D., Kim, T. and Rim, S.-H. (2012) ‘Some identities involving Gegenbauer polynomials’, Advances in Difference Equations. Springer, 2012(1), p. 219.

Sauer, R. A., Duong, T. X. and Corbett, C. J. (2014) ‘A computational formulation for constrained solid and liquid membranes considering isogeometric finite elements’, Computer Methods in Applied Mechanics and Engineering. North-Holland, 271, pp. 48–68.

Schellekens, J. C. J. and De Borst, R. (1993) ‘On the numerical integration of interface elements’, International Journal for Numerical Methods in Engineering, 36(1), pp. 43–66.

Schillinger, D., Hossain, S. J. and Hughes, T. J. R. (2014) ‘Reduced Bézier element quadrature rules for quadratic and cubic splines in isogeometric analysis’, Computer Methods in Applied Mechanics and Engineering, 277, pp. 1–45.

Schmidt, R., Wüchner, R. and Bletzinger, K.-U. (2012) ‘Isogeometric analysis of trimmed NURBS geometries’, Computer Methods in Applied Mechanics and Engineering, 241–244, pp. 93–111.

Scholkopf, B. et al. (1999) ‘Input space versus feature space in kernel-based methods’, IEEE Transactions on Neural Networks, 10(5), pp. 1000–1017.

Schuëller, G. I. (2006) ‘Developments in stochastic structural mechanics’, Archive of Applied Mechanics. Springer-Verlag, 75(10–12), pp. 755–773.

Scott, M. A. et al. (2011) ‘Isogeometric finite element data structures based on Bézier extraction of T-splines’, International Journal for Numerical Methods in Engineering, 88(2), pp. 126–156.

Scott, M. A. et al. (2012) ‘Local refinement of analysis-suitable T-splines’, Computer Methods in Applied Mechanics and Engineering. North-Holland, 213–216, pp. 206–222.

Sederberg, T. W. et al. (2003) ‘T-splines and T-NURCCs’, ACM Transactions on Graphics, 22(3), p. 477.

Seo, Y.-D., Kim, H.-J. and Youn, S.-K. (2010a) ‘Isogeometric topology optimization using trimmed spline surfaces’, Computer Methods in Applied Mechanics and Engineering, 199(49–52), pp. 3270–3296.

Seo, Y.-D., Kim, H.-J. and Youn, S.-K. (2010b) ‘Shape optimization and its extension to topological design based on isogeometric analysis’, International Journal of Solids and Structures, 47(11–12), pp. 1618–1640.

Shi, Y. and Koutsourelakis, S. (2006) ‘A Novel Approach for Simulation of Non-Gaussian Fields: Application in Estimating Wire Strengths From Experimental Data’, in 9th ASCE Specialty Conference on Probabilistic Mechanics and Structural Reliability.

Shields, M. D. and Kim, H. (2017) ‘Simulation of higher-order stochastic processes by spectral representation’, Probabilistic Engineering Mechanics. Elsevier, 47, pp. 1–15.

Shinozuka, M. (1971) ‘Simulation of Multivariate and Multidimensional Random Processes’, The Journal of the Acoustical Society of America, 49(1B), pp. 357–368.

Shinozuka, M. and Deodatis, G. (1991) ‘Simulation of Stochastic Processes by Spectral Representation’, Applied Mechanics Reviews. American Society of Mechanical Engineers, 44(4), p. 191.

Shinozuka, M. and Deodatis, G. (1996) ‘Simulation of Multi-Dimensional Gaussian Stochastic Fields by Spectral Representation’, Applied Mechanics Reviews. American Society of Mechanical Engineers, 49(1), p. 29.

Shinozuka, M. and Jan, C.-M. (1972) ‘Digital simulation of random processes and its applications’, Journal of Sound and Vibration. Academic Press, 25(1), pp. 111–128.

Shojaee, S. et al. (2012) ‘Free vibration analysis of thin plates by using a NURBS-based isogeometric approach’, Finite Elements in Analysis and Design. Elsevier, 61, pp. 23–34.

Shojaee, S., Izadpenah, E. and Haeri, A. (2012) ‘Imposition of Essential Boundary Conditions in Isogeometric Analysis Using the Lagrange Multiplier Method’, Iran University of Science \& Technology.

Silverman, B. W. (2018) Density Estimation for Statistics and Data Analysis, Density Estimation: For Statistics and Data Analysis. Routledge.

Smola, A. J. and Schölkopf, B. (2004) ‘A tutorial on support vector regression’, Statistics

and Computing, 14(3), pp. 199–222.

Spanos, P. D. and Zeldin, B. A. (1998) ‘Monte Carlo Treatment of Random Fields: A Broad Perspective’, Applied Mechanics Reviews. American Society of Mechanical Engineers, 51(3), p. 219.

Stavroulakis, G. et al. (2017) ‘A GPU domain decomposition solution for spectral stochastic finite element method’, Computer Methods in Applied Mechanics and Engineering. North-Holland, 327, pp. 392–410.

Stefanou, G. (2009) ‘The stochastic finite element method: Past, present and future’, Computer Methods in Applied Mechanics and Engineering. North-Holland, 198(9–12), pp. 1031–1051.

Stefanou, G. and Papadrakakis, M. (2004) ‘Stochastic finite element analysis of shells with combined random material and geometric properties’, Computer Methods in Applied Mechanics and Engineering. North-Holland, 193(1–2), pp. 139–160.

Stefanou, G. and Papadrakakis, M. (2007) ‘Assessment of spectral representation and Karhunen–Loève expansion methods for the simulation of Gaussian stochastic fields’, Computer Methods in Applied Mechanics and Engineering. North-Holland, 196(21–24), pp. 2465–2477.

Sudret, B., Defaux, G. and Pendola, M. (2005) ‘Time-variant finite element reliability analysis – application to the durability of cooling towers’, Structural Safety. Elsevier, 27(2), pp. 93–112.

Sudret, B. and Der Kiureghian, A. (2002) ‘Comparison of finite element reliability methods’, Probabilistic Engineering Mechanics. Elsevier, 17(4), pp. 337–348.

Sudret, B. and Kiureghian, D. (2000) ‘Stochastic Finite Element Methods and Reliability: A State-of-the-Art Report’, University of California Berkeley.

Surya Mohan, P., Nair, P. B. and Keane, A. J. (2008) ‘Multi-element stochastic reduced basis methods’, Computer Methods in Applied Mechanics and Engineering, 197(17–18), pp. 1495–1506.

Tagliabue, A., Dedè, L. and Quarteroni, A. (2014) ‘Isogeometric Analysis and error estimates for high order partial differential equations in fluid dynamics’, Computers & Fluids, 102, pp. 277–303.

Tan, P., Nguyen-Thanh, N. and Zhou, K. (2017) ‘Extended isogeometric analysis based on Bézier extraction for an FGM plate by using the two-variable refined plate theory’, Theoretical and Applied Fracture Mechanics. Elsevier, 89, pp. 127–138.

Tartakovsky, D. M. and Xiu, D. (2006) ‘Stochastic analysis of transport in tubes with rough walls’, Journal of Computational Physics. Academic Press, 217(1), pp. 248–259.

Temizer, İ., Wriggers, P. and Hughes, T. J. R. (2011) ‘Contact treatment in isogeometric analysis with NURBS’, Computer Methods in Applied Mechanics and Engineering, 200(9–12), pp. 1100–1112.

Temizer, İ., Wriggers, P. and Hughes, T. J. R. (2012) ‘Three-dimensional mortar-based frictional contact treatment in isogeometric analysis with NURBS’, Computer Methods in Applied Mechanics and Engineering, 209–212, pp. 115–128.

Tepole, A. B. et al. (2015) ‘Isogeometric Kirchhoff–Love shell formulations for biological membranes’, Computer Methods in Applied Mechanics and Engineering. North-Holland, 293, pp. 328–347.

Thai, C. H. et al. (2012) ‘Static, free vibration, and buckling analysis of laminated composite Reissner-Mindlin plates using NURBS-based isogeometric approach’, International Journal for Numerical Methods in Engineering. John Wiley & Sons, Ltd, 91(6), pp. 571–603.

Thai, C. H. et al. (2013) ‘Isogeometric analysis of laminated composite and sandwich plates using a layerwise deformation theory’, Composite Structures. Elsevier, 104, pp. 196–214.

Thai, C. H. et al. (2014) ‘Isogeometric analysis of laminated composite and sandwich plates using a new inverse trigonometric shear deformation theory’, European Journal of Mechanics - A/Solids. Elsevier Masson, 43, pp. 89–108.

Thai, C. H. et al. (2015) ‘Isogeometric Analysis of Laminated Composite Plates Using the Higher-Order Shear Deformation Theory’, Mechanics of Advanced Materials and Structures. Taylor & Francis, 22(6), pp. 451–469.

Thomas, D. C. et al. (2015) ‘Bézier projection: A unified approach for local projection and quadrature-free refinement and coarsening of NURBS and T-splines with particular application to isogeometric design and analysis’, Computer Methods in Applied Mechanics and Engineering, 284, pp. 55–105.

Tran, L. V. et al. (2014) ‘Isogeometric analysis of laminated composite plates based on a four-variable refined plate theory’, Engineering Analysis with Boundary Elements. Elsevier, 47, pp. 68–81.

Tran, L. V., Lee, J., et al. (2015) ‘Geometrically nonlinear isogeometric analysis of laminated composite plates based on higher-order shear deformation theory’, International Journal of Non-Linear Mechanics. Pergamon, 72, pp. 42–52.

Tran, L. V., Ly, H. A., et al. (2015) ‘Vibration analysis of cracked FGM plates using higher-order shear deformation theory and extended isogeometric approach’, International Journal of Mechanical Sciences. Pergamon, 96–97, pp. 65–78.

Tran, L. V., Ferreira, A. J. M. and Nguyen-Xuan, H. (2013) ‘Isogeometric analysis of functionally graded plates using higher-order shear deformation theory’, Composites Part B: Engineering. Elsevier, 51, pp. 368–383.

Tran, L. V. and Kim, S.-E. (2018) ‘Static and free vibration analyses of multilayered plates by a higher-order shear and normal deformation theory and isogeometric analysis’, Thin-Walled Structures. Elsevier, 130, pp. 622–640.

Tran, L. V., Thai, C. H. and Nguyen-Xuan, H. (2013) ‘An isogeometric finite element formulation for thermal buckling analysis of functionally graded plates’, Finite Elements in Analysis and Design. Elsevier, 73, pp. 65–76.

Valizadeh, N. et al. (2013) ‘NURBS-based finite element analysis of functionally graded plates: Static bending, vibration, buckling and flutter’, Composite Structures. Elsevier, 99, pp. 309–326.

VALIZADEH, N. et al. (2013) ‘ISOGEOMETRIC SIMULATION FOR BUCKLING, FREE AND FORCED VIBRATION OF ORTHOTROPIC PLATES’, International Journal of Applied Mechanics. Imperial College Press, 05(02), p. 1350017.

Vanmarcke, E. and Grigoriu, M. (1983) ‘Stochastic Finite Element Analysis of Simple Beams’, Journal of Engineering Mechanics, 109(5), pp. 1203–1214.

Vapnik, V. (1998) Statistical learning theory. 1998, New York John Wiley and Sons.

Vapnik, V. (2013) The nature of statistical learning theory. Springer science & business

media.

da Veiga, L. B. et al. (2014) ‘Mathematical analysis of variational isogeometric methods’, Acta Numerica, 23, pp. 157–287.

Wang, C. et al. (2014) ‘Stochastic interval analysis of natural frequency and mode shape of structures with uncertainties’, Journal of Sound and Vibration. Academic Press, 333(9), pp. 2483–2503.

Wang, D. and Xuan, J. (2010) ‘An improved NURBS-based isogeometric analysis with enhanced treatment of essential boundary conditions’, Computer Methods in Applied Mechanics and Engineering, 199(37–40), pp. 2425–2436.

Wang, P. et al. (2011) ‘Adaptive isogeometric analysis using rational PHT-splines’, Computer-Aided Design, 43(11), pp. 1438–1448.

Wang, W. et al. (2011) ‘Converting an unstructured quadrilateral mesh to a standard T-spline surface’, Computational Mechanics, 48(4), pp. 477–498.

Wang, W. et al. (2013) ‘Trivariate solid T-spline construction from boundary triangulations with arbitrary genus topology’, Computer-Aided Design, 45(2), pp. 351–360.

Wang, Y.-W. et al. (2013) ‘Isogeometric analysis for compound B-spline surfaces’, Computer Methods in Applied Mechanics and Engineering, 261–262, pp. 1–15.

Willberg, C. et al. (2012) ‘Comparison of different higher order finite element schemes for the simulation of Lamb waves’, Computer Methods in Applied Mechanics and Engineering, 241–244, pp. 246–261.

Witteveen, J. A. S. and Bijl, H. (2006) ‘Modeling Arbitrary Uncertainties Using Gram-

Schmidt Polynomial Chaos', in 44th AIAA Aerospace Sciences Meeting and Exhibit. Reston, Virigina: American Institute of Aeronautics and Astronautics.

Wu, D., Gao, W., Tin-Loi, F., et al. (2016) 'Probabilistic interval limit analysis for structures with hybrid uncertainty', Engineering Structures. Elsevier, 114, pp. 195–208.

Wu, D., Gao, W., Song, C., et al. (2016) 'Probabilistic interval stability assessment for structures with mixed uncertainty', Structural Safety. Elsevier, 58, pp. 105–118.

Wu, D., Gao, W., Wang, C., et al. (2016) 'Robust fuzzy structural safety assessment using mathematical programming approach', Fuzzy Sets and Systems. North-Holland, 293, pp. 30–49.

Wu, D. et al. (2017) 'Robust safety assessment of functionally graded structures with interval uncertainties', Composite Structures. Elsevier, 180, pp. 664–685.

Wu, D. and Gao, W. (2017a) 'Hybrid uncertain static analysis with random and interval fields', Computer Methods in Applied Mechanics and Engineering. North-Holland, 315, pp. 222–246.

Wu, D. and Gao, W. (2017b) 'Uncertain static plane stress analysis with interval fields', International Journal for Numerical Methods in Engineering. John Wiley & Sons, Ltd, 110(13), pp. 1272–1300.

Wu, D., Gao, W. and Tangaramvong, S. (2017) 'Time-Dependent Buckling Analysis of Concrete-Filled Steel Tubular Arch with Interval Viscoelastic Effects', Journal of Structural Engineering, 143(7), p. 04017055.

Xia, B., Yu, D. and Liu, J. (2013) 'Hybrid uncertain analysis of acoustic field with interval

random parameters', Computer Methods in Applied Mechanics and Engineering. North-Holland, 256, pp. 56–69.

Xiong, H., Swamy, M. N. S. and Ahmad, M. O. (2005) 'Optimizing the Kernel in the Empirical Feature Space', IEEE Transactions on Neural Networks, 16(2), pp. 460–474.

Xiu, D. and Karniadakis, G. E. (2003) 'The Wiener--Askey Polynomial Chaos for Stochastic Differential Equations', SIAM Journal on Scientific Computing, 24(2), pp. 619–644.

Xu, G. et al. (2012) 'A New Error Assessment Method in Isogeometric Analysis of 2D Heat Conduction Problems', Advanced Science Letters, 10(1), pp. 508–512.

Xu, G. et al. (2013a) 'Analysis-suitable volume parameterization of multi-block computational domain in isogeometric applications', Computer-Aided Design, 45(2), pp. 395–404.

Xu, G. et al. (2013b) 'Constructing analysis-suitable parameterization of computational domain from CAD boundary by variational harmonic method', Journal of Computational Physics, 252, pp. 275–289.

Xu, G. et al. (2013c) 'Optimal analysis-aware parameterization of computational domain in 3D isogeometric analysis', Computer-Aided Design, 45(4), pp. 812–821.

Yamazaki, F. and Shinozuka, M. (1988) 'Digital Generation of Non-Gaussian Stochastic Fields', Journal of Engineering Mechanics, 114(7), pp. 1183–1197.

Yin, S. et al. (2014) 'Isogeometric locking-free plate element: A simple first order shear deformation theory for functionally graded plates', Composite Structures. Elsevier,

118, pp. 121–138.

Yin, S., Yu, T. and Liu, P. (2013) ‘Free Vibration Analyses of FGM Thin Plates by Isogeometric Analysis Based on Classical Plate Theory and Physical Neutral Surface’, Advances in Mechanical Engineering. SAGE PublicationsSage UK: London, England, 5, p. 634584.

Yu, T. et al. (2016) ‘NURBS-based isogeometric analysis of buckling and free vibration problems for laminated composites plates with complicated cutouts using a new simple FSDT theory and level set method’, Thin-Walled Structures. Elsevier, 101, pp. 141–156.

Yu, T. T. et al. (2015) ‘A simple FSDT-based isogeometric analysis for geometrically nonlinear analysis of functionally graded plates’, Finite Elements in Analysis and Design. Elsevier, 96, pp. 1–10.

Zareh, M. and Qian, X. (2019) ‘Kirchhoff–Love shell formulation based on triangular isogeometric analysis’, Computer Methods in Applied Mechanics and Engineering. North-Holland, 347, pp. 853–873.

van der Zee, K. G. and Verhoosel, C. V. (2011) ‘Isogeometric analysis-based goal-oriented error estimation for free-boundary problems’, Finite Elements in Analysis and Design, 47(6), pp. 600–609.

Zentner, I. et al. (2016) ‘A biorthogonal decomposition for the identification and simulation of non-stationary and non-Gaussian random fields’, Journal of Computational Physics. Academic Press, 314, pp. 1–13.

Zhang, H. (2012) ‘Interval importance sampling method for finite element-based structural reliability assessment under parameter uncertainties’, Structural Safety.

Elsevier, 38, pp. 1–10.

Zhang, J. and Ellingwood, B. (1994) ‘Orthogonal Series Expansions of Random Fields in Reliability Analysis’, Journal of Engineering Mechanics, 120(12), pp. 2660–2677.

Zhang, X., Liu, Q. and Huang, H. (2019) ‘Numerical simulation of random fields with a high-order polynomial based Ritz–Galerkin approach’, Probabilistic Engineering Mechanics. Elsevier, 55, pp. 17–27.

Zhang, Y. et al. (2006) ‘Patient-Specific Vascular NURBS Modeling for Isogeometric Analysis of Blood Flow’, in Proceedings of the 15th International Meshing Roundtable. Berlin, Heidelberg: Springer Berlin Heidelberg, pp. 73–92.

Zhang, Y., Wang, W. and Hughes, T. J. R. (2012) ‘Solid T-spline construction from boundary representations for genus-zero geometry’, Computer Methods in Applied Mechanics and Engineering, 249–252, pp. 185–197.

Zhang, Y., Wang, W. and Hughes, T. J. R. (2013) ‘Conformal solid T-spline construction from boundary T-spline representations’, Computational Mechanics, 51(6), pp. 1051–1059.

Zheng, Z. and Dai, H. (2017) ‘Simulation of multi-dimensional random fields by Karhunen–Loève expansion’, Computer Methods in Applied Mechanics and Engineering. North-Holland, 324, pp. 221–247.

Zou, Z. et al. (2017) ‘A Geometrically Exact Isogeometric Blended Shell: Formulation, Benchmarking, and Automotive Application’, SAE International Journal of Passenger Cars - Mechanical Systems, 10(2), pp. 2017-01–1329.